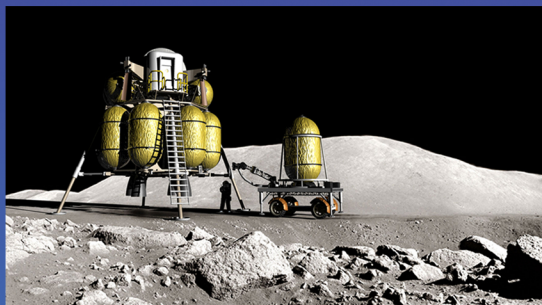




John F. Kennedy Space Center's 2006–2007 Report



technology development and application

Technology Development and Application 2006 – 2007 Report

John F. Kennedy Space Center

Foreword

Successful technology development and application projects are critical to maintaining and enhancing KSC capabilities. Advanced technologies are required in order to solve technical problems, resolve operational issues, and optimize designs of flight and ground systems. When new technologies are infused in KSC systems and processes, the outcomes are safer, more efficient, and more responsive spaceport and range operations for our customers.

The KSC technology development team includes a wide variety of partnerships among civil servants, contractors, academic institutions, and commercial industries. KSC focuses its advanced technology activities on a list of KSC high-priority technology needs defined by our primary stakeholders, including current operational programs, future programs, and institutional technical programs. We focus and align our technology investments, personnel investments, new project proposals, and strategic partnerships with the technology needs most important to the programs supporting our Nation's exploration mission.

This report highlights the results of KSC's applied technology efforts during 2006–2007. If you have questions or comments about applied technology at KSC, please contact me at 321-867-7069 or <David.E.Bartine@nasa.gov>.



David E. Bartine

David E. Bartine
Director, Applied Technology
John F. Kennedy Space Center

Contents

Spaceport Structures and Materials.....	1
Reversible Chemochromic Hydrogen Detectors.....	2
Determining Trajectory of Triboelectrically Charged Particles, Using Discrete Element Modeling.....	4
Using Indium Tin Oxide To Mitigate Dust on Viewing Ports *2007	6
High-Performance Polyimide Powder Coatings.....	8
Controlled-Release Microcapsules for Smart Coatings for Corrosion Applications *2006	10
Aerocoat 7 Replacement Coatings.....	12
Photocatalytic Coatings for Exploration and Spaceport Design *2006	14
New Materials for the Repair of Polyimide Electrical Wire Insulation	16
Commodity-Free Calibration *2006	18
Novel Ice Mitigation Methods *2006	20
Crack Offset Measurement With the Projected Laser Target Device.....	22
New Materials for Structural Composites and Protective Coatings *2007	24
Fire Chemistry Testing of Spray-On Foam Insulation (SOFI)	26
Using Aerogel-Based Insulation Material To Prevent Foam Loss on the Liquid-Hydrogen Intertank	28
Particle Ejection and Levitation Technology (PELT)	30
Electrostatic Characterization of Lunar Dust *2006	32
Numerical Analysis of Rocket Exhaust Cratering *2007	34
RESOLVE Projects: Lunar Water Resource Demonstration and Regolith Volatile Characterization	36
Tribocharging Lunar Soil for Electrostatic Beneficiation *2006	38
Numerically Modeling the Erosion of Lunar Soil by Rocket Exhaust Plumes *2006	40
Trajectory Model of Lunar Dust Particles.....	42
Using Lunar Module Shadows To Scale the Effects of Rocket Exhaust Plumes.....	44
Predicting the Acoustic Environment Induced by the Launch of the Ares I Vehicle.....	46
Measuring Ultrasonic Acoustic Velocity in a Thin Sheet of Graphite Epoxy Composite	48

* 2006, 2007 Center Director's Discretionary Fund Project

Contents (continued)

Range Technologies.....	51
Hail Size Distribution Mapping.....	52
Launch Pad 39 Hail Monitor Array System.....	54
Autonomous Flight Safety System – Phase III.....	56
The Photogrammetry Cube.....	58
Bird Vision System.....	60
Automating Range Surveillance Through Radio Interferometry and Field Strength Mapping Techniques.....	62
Next-Generation Telemetry Workstation.....	64
GPS Metric Tracking Unit.....	66
Space-Based Range.....	68
Fluid System Technologies	71
Calibrating the Helium Pressurization System for the Space Shuttle Liquid-Hydrogen Tank.....	72
Composite Materials for Low-Temperature Applications *2006.....	74
Mitigating Problems in Measuring Hypergolic Fuels.....	76
Cryogenic Moisture Analysis of Spray-On Foam Insulation (SOFI).....	78
Thermal Performance of Aged and Weathered Spray-On Foam Insulation (SOFI) Materials Under Cryogenic Vacuum Conditions (Cryostat-4).....	80
Automated Method for Estimating Nutation Time Constant Model Parameters for Spacecraft Spinning on Axis.....	82
Parameter Estimation of Lateral Spacecraft Fuel Slosh.....	84
Modeling of Slosh Dynamics in Cryogenic Propellant Tanks in Microgravity Environments.....	86
Biological Sciences.....	89
Countermeasure for Radiation Protection and Repair.....	90
Focused Metabolite Profiling for Dissecting Cellular and Molecular Processes of Living Organisms in Space Environments *2006.....	92

* 2006, 2007 Center Director's Discretionary Fund Project

Contents (continued)

Process and Human Factors Engineering Technologies	95
Distributed Observer Network	96
Influence Map Methodology for Evaluating Systemic Safety Issues	98
Simulation and Analysis of Launch Teams (SALT)	100
Solid-State Lighting Module (SSLM)	102
Systems Maintenance Automated Repair Tasks (SMART)	104
Launch and Landing Effects Ground Operations (LLEGO) Model	106
Exploration Supply Chain Simulation	107
Command, Control, and Monitoring Technologies	109
Nanosensors for Evaluating Hazardous Environments	110
Sixty-four-Channel Inline Cable Tester	112
Wireless Inclinometer Calibration System	114
Generating Safety-Critical PLC Code From a High-Level Application Software Specification	116
Spacecraft Electrostatic Radiation Shielding	118
Ion Beam Propulsion Study	120
RT-MATRIX: Measuring Total Organic Carbon by Photocatalytic Oxidation of Volatile Organic Compounds	122
Appendix A: KSC High-Priority Technology Needs	125
Appendix B: Innovative Partnership Program	129
Appendix C: Export Control and Interagency Liaison Division	135

Introduction

John F. Kennedy Space Center (KSC) technology development efforts support NASA's goals of increased safety, reduced cost of space access, and expansion of commercial markets by applying new technologies in current and future Space Transportation Systems.

KSC's role as the nation's premier launch site creates requirements for new spaceport and range technologies. KSC's people use our unique institutional resources to provide technologies to NASA program customers, including designers and operators of spaceports on Earth, lunar bases, and Mars bases. KSC has extensive expertise in designing, building, and operating a spaceport, with all its complex technologies and systems.

KSC technology development efforts are categorized by six Spaceport Technology and Science Product Lines: Spaceport Structures and Materials; Range Technologies; Fluid System Technologies; Biological Sciences; Process and Human Factors Engineering Technologies; and Command, Control, and Monitoring Technologies. This report is organized accordingly.

The primary stakeholders for spaceport and range technologies are current operational programs, future programs, and institutional technical programs. These stakeholders are illustrated on pages viii and ix. KSC focuses and aligns its technology investments, personnel investments, new project proposals, and strategic partnerships with the technology needs most important to our stakeholders in order to maximize benefits for the Agency and the Nation. The specific need addressed by the technology is identified next to the High-Priority Technology (HPT) icon in each report of results and progress.

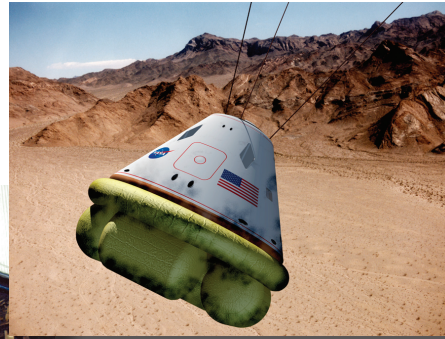
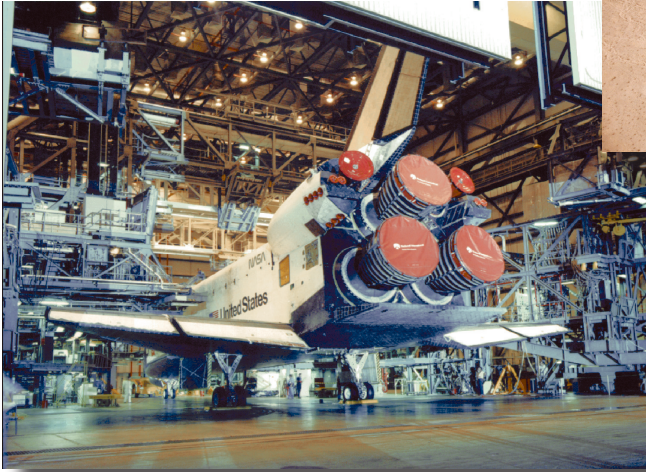
Through its Innovative Partnership Program, KSC seeks industry participation and collaboration in its technology development initiatives. Additional information on the Innovative Partnership Program is included in Appendix B. KSC reaches out to transfer expertise and technologies to the commercial sector and academic community. Programs and commercialization opportunities available to American industries and other organizations are described in the KSC Technology Transfer Office Internet Web site at <http://ksc.nasatechnology.com/>. University faculty and postdoctoral fellowship opportunities are described in the KSC University Programs Internet Web site at <http://education.ksc.nasa.gov/educators/faculty.htm>.

The U.S. Government controls exports of sensitive equipment, software, and technology as a means of promoting our national-security interests and foreign-policy objectives. This document has been reviewed for export control and intellectual property. Additional information on KSC's export control function appears in Appendix C.

An electronic version of this report is available at <http://rtreport.ksc.nasa.gov>.

Primary Stakeholders for KSC Technology Development and Application Efforts

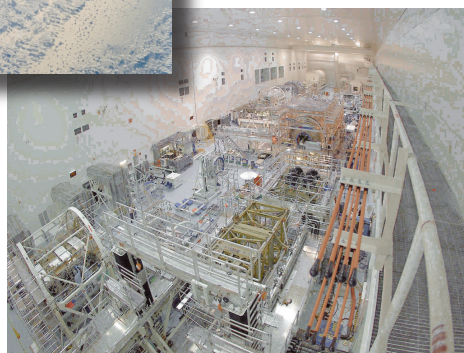
Launch Vehicle Processing

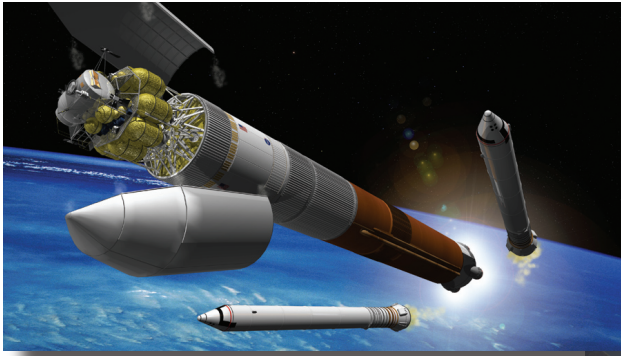


Launch Services Program

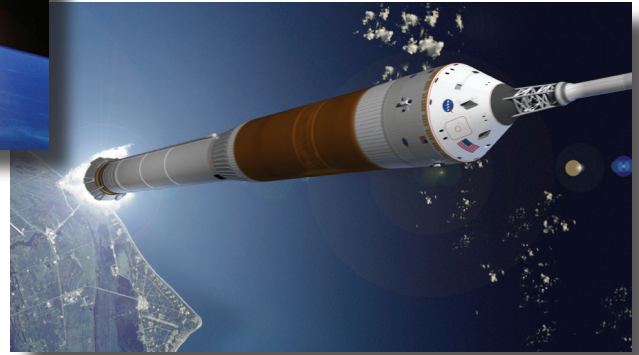


International Space Station/ Payload Processing

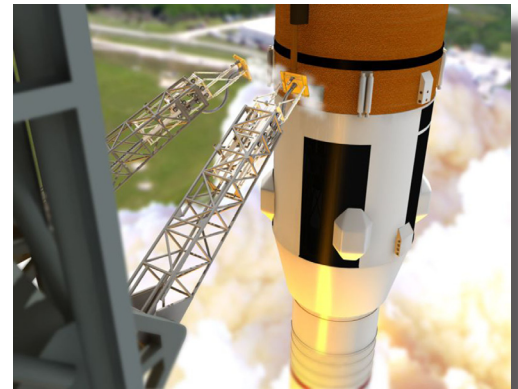




Constellation Systems



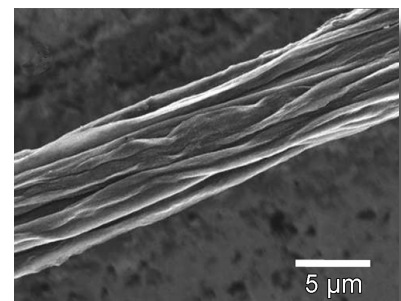
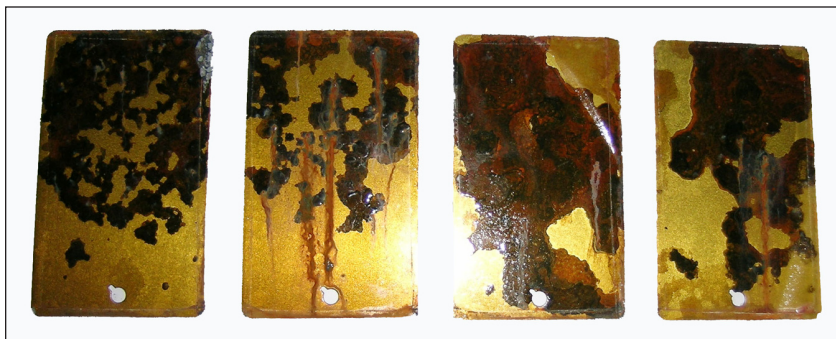
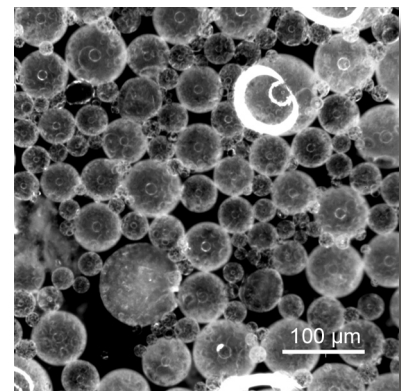
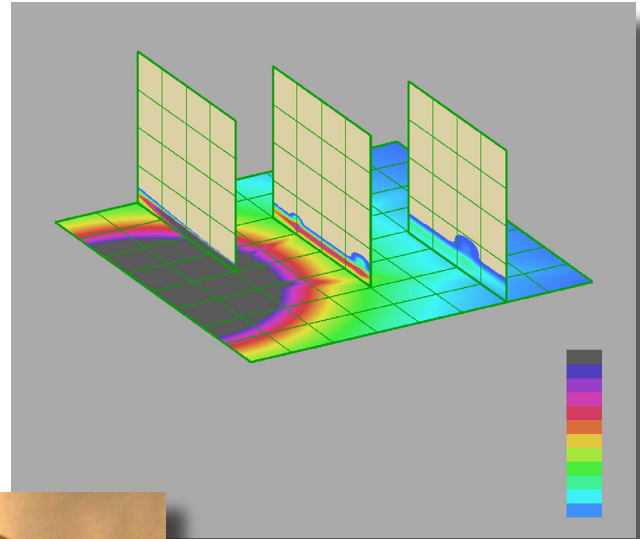
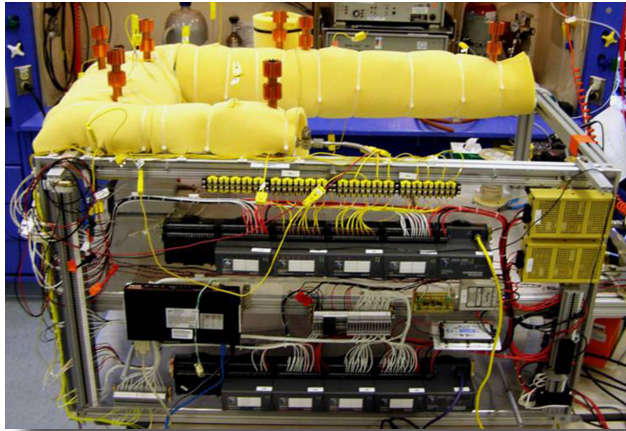
Surface Systems



Institutional Technical Programs

- Safety and Mission Assurance
- Center Operations
- Information Technology and Communication Services

Spaceport Structures and Materials



Reversible Chemochromic Hydrogen Detectors



Hazardous-Leak
Detection and
Isolation

The Florida Solar Energy Center (FSEC), affiliated with the University of Central Florida, has invented a reversible pigment that changes from light beige to blue when exposed to hydrogen and back to light beige when exposed to atmospheric oxygen.

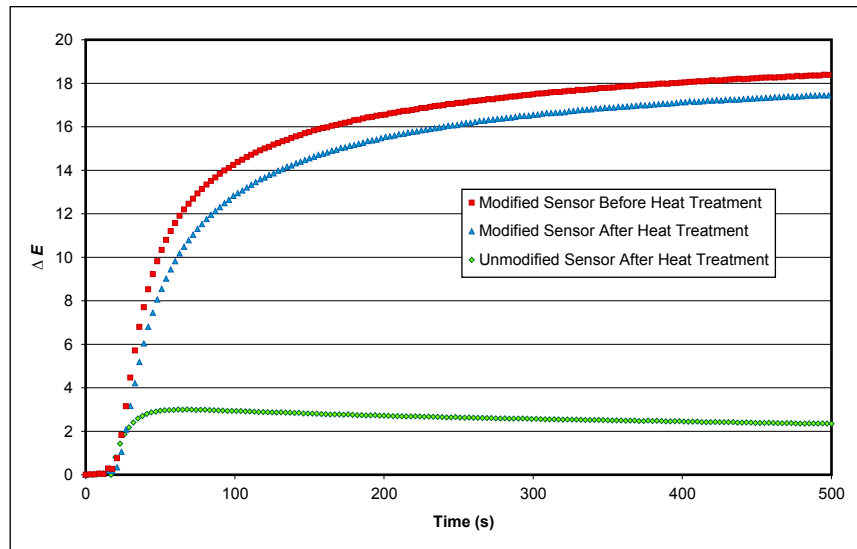
In laboratory and environmental studies, the FSEC pigment in its tape form failed to change color adequately when exposed to hydrogen after one day of exposure at Kennedy Space Center's Beach Corrosion Test Facility. The reversible hydrogen-detecting tape also lost its ability to change color after being placed in an environmental chamber at 45 °C for one day. The first attempts at extruding the reversible pigment into various polymers were unsuccessful because of the pigment's poor thermal stability. The goal of this project was to formulate a pigment with improved thermal and environmental stability for extrusion into a variety of appropriate polymer matrices.

The formulation of the reversible hydrogen-detecting pigment was modified by removing one reagent and chemically modifying the hydrogen sensitive ingredient. This was intended to improve the hydrophobicity of the pigment and alter the thermal degradation mechanism. A sensor with the new pigment was placed in an oven at 45 °C for 3 days. The figure shows how the newly formulated pigment changed color (ΔE) as it was exposed to 100 percent hydrogen. A larger ΔE indicates a greater color difference. The maximum ΔE for the modified sensor decreases by less than 2 following heat treatment when compared to an unheated sample. With a similar heat treatment, the original reversible pigment lost its sensitivity to hydrogen, since the maximum ΔE attained is less than 3. After changing color when heated to 45°C, the modified pigment was extruded at high temperatures into a tape. The extruded tape retained its color-changing ability.

Preliminary results show that the hydrophobicity of the FSEC pigment increases after the pigment has been modified; however, further testing is required to validate long-term results in a relevant environment.

Contacts: Dr. Janine E. Captain <Janine.E.Captain@nasa.gov>, NASA-KSC, (321) 867-6970; and Dr. Luke B. Roberson <Luke.B.Roberson@nasa.gov>, NASA-KSC, (321) 867-1543

Participating Organizations: NASA-KSC (Dr. Robert C. Youngquist), Florida Solar Energy Center (Dr. Gary Bokerman, Jessica Macpherson, Dr. Nahid Mohajeri, Dr. Nazim Muradov, and Dr. Ali T-Raissi), ASRC Aerospace (Barbara V. Peterson), and University of Central Florida (Cristina M. Berger and Dr. Mary C. Whitten)



Comparison of the detection performance sensors in 100 percent hydrogen.

Determining Trajectory of Triboelectrically Charged Particles, Using Discrete Element Modeling



Contamination
Control

The Kennedy Space Center (KSC) Electrostatics and Surface Physics Laboratory is participating in an Innovative Partnership Program (IPP) project with an industry partner to modify a commercial off-the-shelf simulation software product to treat the electrodynamics of particulate systems. The industry partner, DEM Solutions, Inc., has developed EDEM, a program that can calculate the dynamics of particles. Discrete element modeling (DEM) is a numerical technique that can track the dynamics of particle systems. This technique, which was introduced in 1979 for analysis of rock mechanics, was recently refined to include the contact force interaction of particles with arbitrary surfaces and moving machinery. In our work, we endeavor to incorporate electrostatic forces into the DEM calculations to enhance the fidelity of the software and its applicability to (1) particle processes, such as electrophotography, that are greatly affected by electrostatic forces, (2) grain and dust transport, and (3) the study of lunar and Martian regoliths [1].

After contact force is calculated, additional body forces acting on each particle are calculated. In this step, any desired force can be added to the simulation. After the forces on each particle are calculated, the linear and angular accelerations of each particle are updated according to Newton's second law. Then the positions and orientations of each particle are updated with an explicit time-marching algorithm.

The introduction of electrostatic forces into the current EDEM configuration requires the addition of a long-range model that works in conjunction with the existing dynamic calculations. This long-range force model is based on a version of Coulomb's law [2] that takes into account the electrostatic screening of adjacent particles. The electrostatic force, F , is given by

$$F = - \frac{dU_e}{dr} = \frac{q_1 q_2}{4\pi\epsilon_0} \left(\frac{\kappa}{r} + \frac{1}{r^2} \right) \quad (1)$$

where q_1 and q_2 are the charges of two particles, r is the distance between their centers, ϵ_0 is the permittivity of free space (8.854×10^{-12} F/m), U_e is the electrostatic potential, and κ is the inverse of the Debye length, λ_D , and is based on the local charge concentration.

For charge generation, we modify a charge generation equation [3] to model many particles.

$$Q(t) = Nq_s (1 - e^{-\alpha t}) \quad (2)$$

where N is the number of particles, $Q(t)$ is the total charge on the particles, q_s is the saturation charge, and α is the charge generation constant.

We developed a simple inclined-plane apparatus to compare theoretical results with experimental data (Figure 1). The inclined plane allowed 500 2.0-mm-diameter glass spheres to roll down over various polymer and metal surfaces and into a Faraday cup, where total charge on the spheres was measured. By timing the roll of the spheres down the plane and knowing the total charge, $Q(t)$, we were able to calculate the charge generation constant for the materials under test. The inclined-plane materials tested were low-density polyethylene (LDPE), polyvinyl chloride (PVC), nylon 6/6, polytetrafluoroethylene (PTFE), aluminum, and copper.

Initial results of the EDEM model of the inclined plane show good comparison to values of $Q(t)$ and α calculated from experimental data. Figure 2 compares the EDEM simulation output and example $Q(t)$ data.

The EDEM modeling tool can be applied to systems of charged particles that are of interest to NASA, for example, charged lunar and Martian regoliths. Proposed future work includes the addition of dielectrophoretic force and Van der Waals forces, electrodynamic forces from charged surfaces, and the modeling of nonspherical particles.

References:

- [1] C.I. Calle, J.G. Mantovani, E.E. Groop, C.R. Buhler, A.W. Nowicki, M.G. Buehler, and M.D. Hogue, "Electrostatic charging of polymers by particle impact at Martian atmospheric pressures," *Proceedings ESA-IEJ Joint Meeting*, NW University, Laplacian Press, Morgan Hill, California, 2002, pp. 106–117.
- [2] F.J. Bueche, *Introduction to Physics for Scientists and Engineers*, 3rd ed., McGraw-Hill, Inc., 1980, p. 343.
- [3] W.D. Greason, "Investigation of a test methodology for triboelectrification," *Journal of Electrostatics*, Vol. 49, Issue 3–4, August 2000, pp. 245–256.

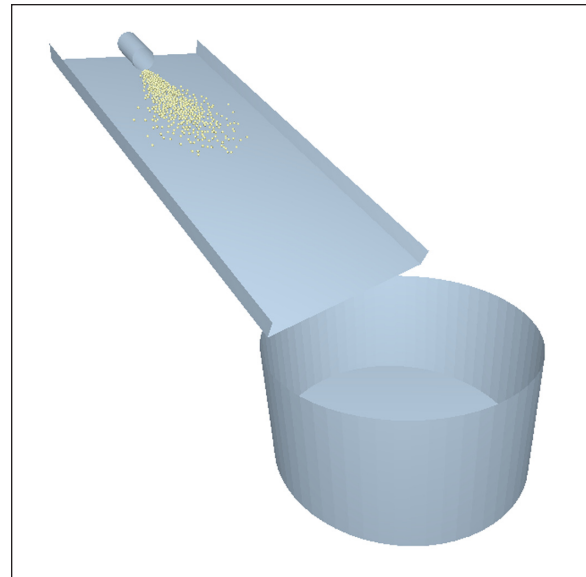


Figure 1. EDEM simulation of spheres rolling down the inclined plane.

Contacts: Dr. Michael D. Hogue <Michael.D.Hogue@nasa.gov>, NASA-KSC, (321) 867-7549; and Dr. Carlos I. Calle <Carlos.I.Calle@nasa.gov>, NASA-KSC, (321) 867-3274

Participating Organization: DEM Solutions, Inc. (Dr. Peter Weitzman and Dr. David R. Curry)

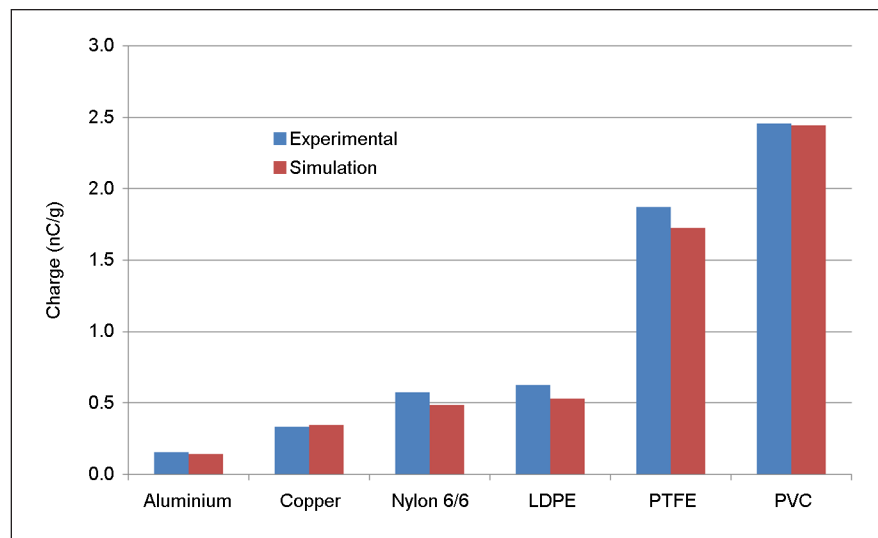


Figure 2. Charge-to-mass ratio for 15-degree experiment compared with simulation results for the six plane materials.

Using Indium Tin Oxide To Mitigate Dust on Viewing Ports

2007 Center Director's Discretionary Fund Project



Contamination
Control

NASA plans to use a number of onboard viewing ports to measure lunar regolith *in situ* and to monitor robotic and human activities on the lunar or Martian surface. Because of the size and abundance of dust particles on these bodies, the potential for dust to occlude viewing ports and windows is high enough to threaten system lifetime and reliability, especially when activities rely on relaying video to either a habitat module or controllers on Earth.

This project uses a technology being developed by KSC's Electrostatics and Surface Physics Laboratory to remove dust from windowlike surfaces. The technology applies an alternating electric potential to interlaced electrodes. In this application, we use indium tin oxide (ITO) to create various electrode patterns in order to determine the most reliable pattern for dust removal. This technology has application to systems where optical clarity is important. Specifically, this project considers the *in situ* resource utilization (ISRU) application of a viewing port for Raman spectroscopy, where the electrode pattern on glass would be coated with a scratch-resistant sapphire film (Al_2O_3).

Electrode patterns were tested in ambient and dry air. These patterns included a single-phase square, single-phase circle, single-phase comb, three-phase square, three-phase circle, and three-phase comb. The voltage, frequency, and waveform applied to each screen were varied in search of the best way to remove dust.

Of the patterns tested, the three-phase circular spiral was the most efficient at removing dust. The circular pattern minimizes the number of abrupt endings to the electrodes, thereby minimizing the points where high electric fields could lead to breakdown and sparking. The screen was tested with JSC-1 lunar simulant particles of less than 25 μm in diameter. A majority of the dust was removed within 10 s under ambient conditions and within 5 min under dry-air conditions (near 0 percent relative humidity).

We continued screen testing under vacuum conditions to demonstrate proof of concept in a more relevant environment. Test parameters were varied in a manner similar to the tests performed under ambient and dry-air conditions on a glass screen with a spiral ITO pattern coated with a thin film of sapphire. The clearing of the dust was similar to the clearing demonstrated under dry-air conditions.

An additional test successfully demonstrated the use of the screen on and near metal surfaces. The proximity of the metal surface did not appear to affect how well the screen removed dust. Applications for using the technology on metals range from dust transport mechanisms to clearing dust from seals and mechanical joints.

Key accomplishments were

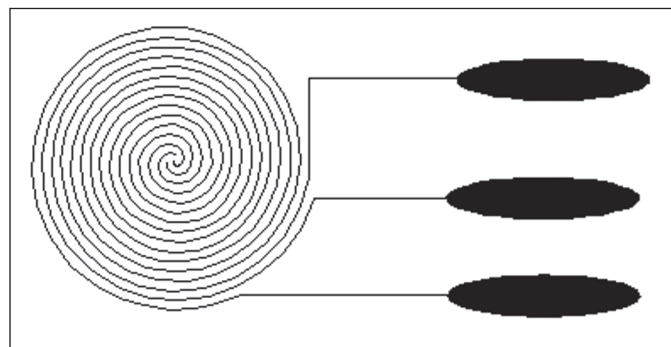
- developing a technique to apply electrode patterns to ITO-coated glass slides up to 0.7 mm thick,
- developing a processing technique to remove the uncoated ITO from the glass slides and coat the slides with an insulating material to prevent sparking, and
- optimizing test parameters (voltage, waveform, frequency).

Key milestones were

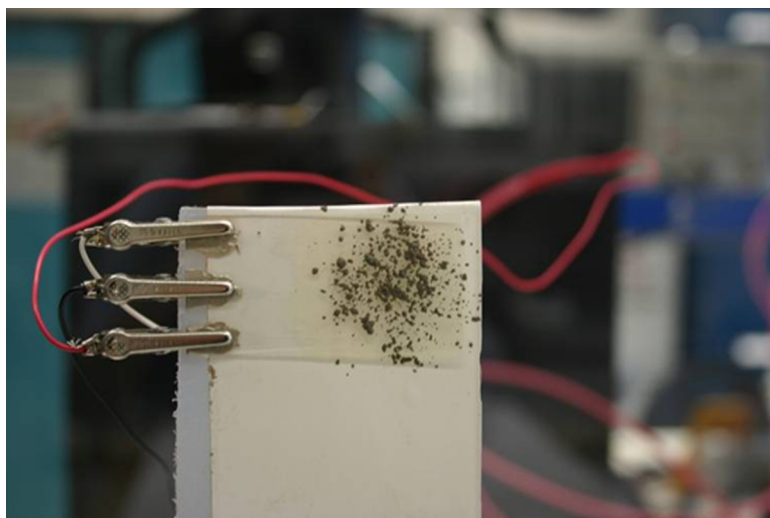
- determining an efficient pattern for dust removal,
- demonstrating the capability of ITO screens to remove dust under high-vacuum conditions, and
- demonstrating the capability of ITO screens to remove dust when backed with grounded and ungrounded metal plates.

Contacts: Dr. Carlos I. Calle <Carlos.I.Calle@nasa.gov>, NASA-KSC, (321) 867-3274; and Dr. Jacqueline W. Quinn <Jacqueline.W.Quinn@nasa.gov>, NASA-KSC, (321) 867-8410

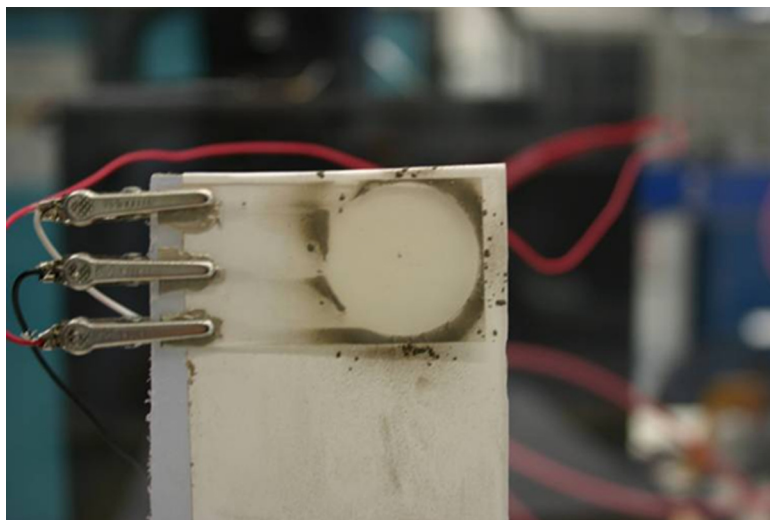
Participating Organizations: ASRC Aerospace (Dr. Charles R. Buhler, Judith L. McFall, and Mindy L. Ritz) and Appalachian State University (Dr. Sid Clements)



Screen pattern design.



A 2.3-cm circular spiral on ITO-coated glass at $T = 0$ s under dry/ambient conditions.



A 2.3-cm circular spiral on ITO-coated glass at $T = 8$ s under dry/ambient conditions.

High-Performance Polyimide Powder Coatings



Corrosion Control

Much of the infrastructure at Kennedy Space Center and other NASA sites has been subjected to outside weathering effects for more than 40 years. Because much of this infrastructure has metallic surfaces, considerable effort is continually devoted to developing methods to minimize the effects of corrosion on these surfaces. These efforts are especially intense at KSC, where offshore salt spray and exhaust from Solid Rocket Boosters accelerate corrosion. Coatings of various types have traditionally been the choice for minimizing corrosion, and improved corrosion control methods are constantly being researched.

Recent work at KSC on developing an improved method for repairing Kapton (polyimide)-based electrical wire insulation has identified polyimides with much lower melting points than traditional polyimides used for insulation. These lower melting points and the many other outstanding physical properties of polyimides (thermal stability, chemical resistance, and electrical properties) led us to investigate whether they could be used in powder coatings. In Phase 1 of our research, we found that polyimides have the potential to perform effectively as coatings. Physical-property testing of panels coated with an experimental polyimide formulation indicated that the resulting surfaces were hard and durable, with excellent impact resistance, adhesion, and flexibility. Salt fog corrosion testing revealed that this formulation performed very well on aluminum substrates but exhibited corrosion and lost adhesion on steel panels. All panels coated with this formulation developed, upon baking, a number of small craters or pin holes, randomly distributed across the coated surface, which we concluded reduced the formulation's corrosion performance on steel.

In Phase 2, we worked toward developing an effective polyimide powder coating resin. Research began with the goal of significantly improving the soak test adhesion and wetting of a polyimide-based powder coating. To soak-test the coating in the laboratory, we immersed the coated coupon in a 3-percent sodium chloride solution and observed the progress of delamination and corrosion over time. We identified significant improvements in polyimide powder coating resin performance through this screen test. The table shows one powder control and six polyimide formulations tested. Items 5 through 7 showed improved adhesion over the controls, and Item 2 was the best formulation identified through Phase 1 research.

A 1,000-hr salt fog test of Items 5 through 7 revealed significant corrosion resistance over the Phase 1 polyimide formula. Figures 1 and 2 highlight this improvement.

Results of adhesion and wetting tests.

Item	Formulation	Adhesion	Wetting	Comments
1	DuPont Clear Epoxy	3.5	5.0	
2	Phase 1 Polyimide Formula	2.0	4.5	Phase 1 Salt Fog Delamination begins > 14 days
3	Phase 2 Polyimide Resin A	5.0	3.0	
4	Phase 2 Polyimide Crosslinker	1.0	4.0	
5	3/4/Epoxy resin/PL 545 (8:1:0.7:0.3)w	5.0	4.5	"Formula 1"
6	3/4/PL 545 (9:0.7:0.3)w 3/polyester resin/PL 545	5.0	4.5	"Formula 2," all polyimide
7	(9.2:0.5:0.3)w	4.5	4.5	"Formula 3"; no methylacrylic acid (MAA)
0: Very poor; 5: Excellent		PL 545: flow/leveling aid		

Close examination of the corrosion spots on steel panels, shown in Figure 2, revealed that these corrosion spots began where small craters existed after coating. No corrosion was found where these craters were not present. No corrosion was noted on aluminum, even with the presence of small craters.

In conclusion, this research developed polyimide resins with good melt properties suitable for coatings. The results of a 1,000-hr salt fog test for 1-mil polyimide on steel coatings were encouraging, and excellent salt fog results were achieved on aluminum panels. This novel technology led to the submission of two NASA New Technology Reports.

Contacts: Dr. Luz Marina Calle <Luz.M.Calle@nasa.gov>, NASA-KSC, (321) 867-3278; and Dr. David Trejo <Trejo@civilmail.tamu.edu>, Texas A&M University, (979) 845-2416

Participating Organizations: ASRC Aerospace (Dr. Scott T. Jolley and Lilliana Fitzpatrick) and University of Central Florida (Dr. Mary C. Whitten)

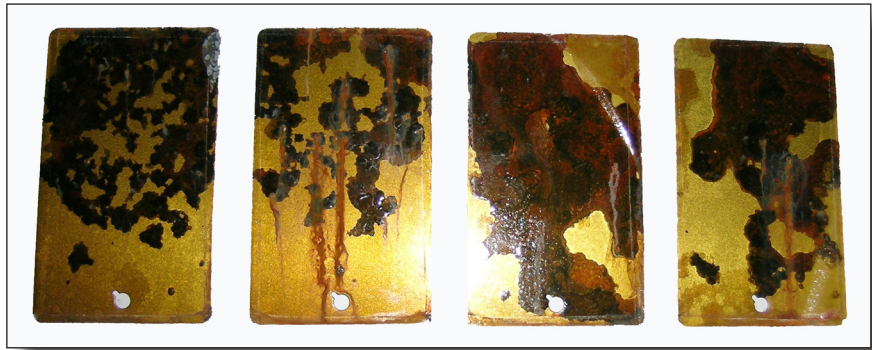


Figure 1. Steel, Item 4, Phase 1: 525-hour salt fog test.

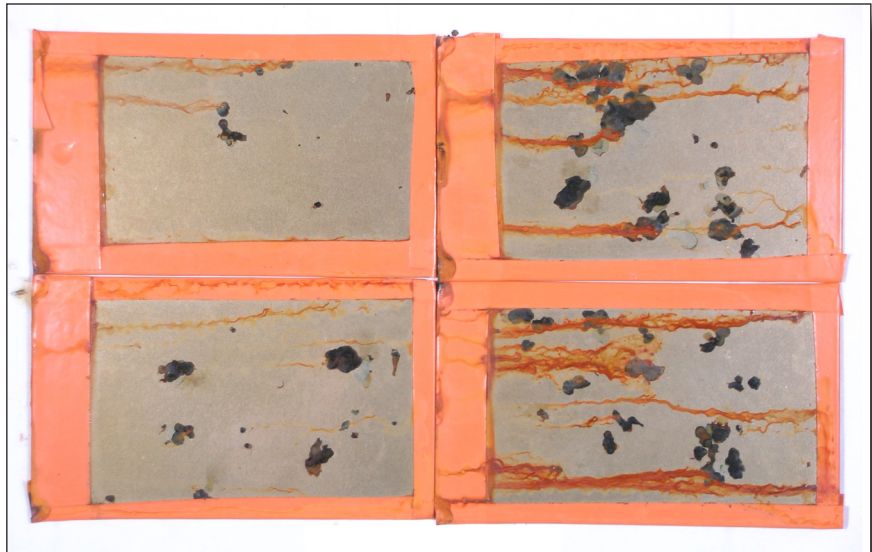


Figure 2. Steel, Item 7, Phase 2: 1,000-hour salt fog test.

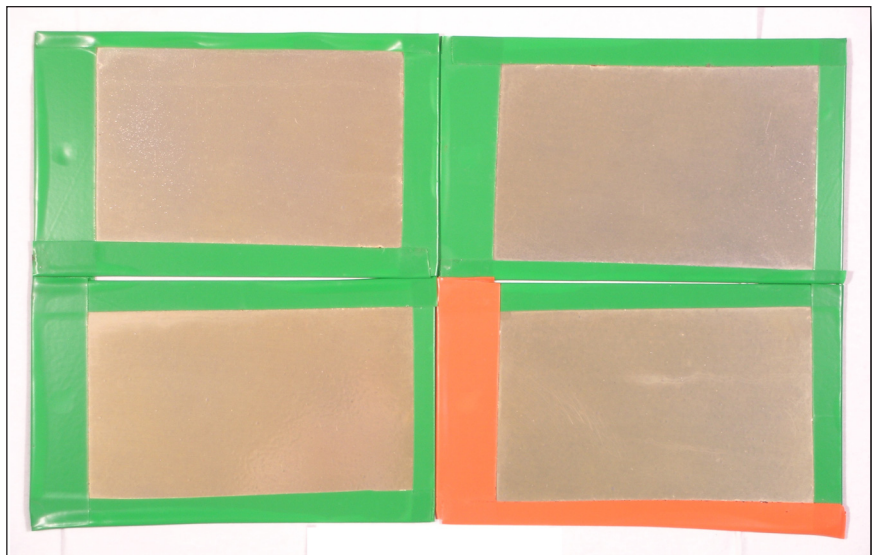


Figure 3. Aluminum, Item 4, Phase 2: 1,000-hour salt fog test.

Controlled-Release Microcapsules for Smart Coatings for Corrosion Applications

2006 Center Director's Discretionary Fund Project



Corrosion Control

Corrosion is a serious problem that has enormous costs and serious safety implications. Localized corrosion, such as pitting, is very dangerous and can cause catastrophic failures. The NASA Corrosion Technology Laboratory at Kennedy Space Center is developing a smart coating based on pH-sensitive microcapsules for corrosion applications. These versatile microcapsules are designed to be incorporated into a smart coating and deliver their core content when corrosion starts. Corrosion indication was the first function incorporated into the microcapsules. Current efforts are focused on incorporating the corrosion inhibition function through the encapsulation of corrosion inhibitors into water core and oil core microcapsules. Scanning electron microscopy (SEM) images of encapsulated corrosion inhibitors are shown in Figure 1.

Different formulations and conditions have been used to achieve the desired microcapsule size and size distribution. Though a homogenous size distribution is normally preferred, different sizes might be required for different applications. For example, a size of about 20 to 40 μm is suitable for corrosion indication, whereas a smaller size might be better for inhibitor delivery. Figure 2 shows microcapsules of various sizes ranging from 2 to 100 μm .

A common concern about incorporating microcapsules into paint systems is that their interaction with paint constituents could lower the adhesive and protective properties of the paint. The effect of the microcapsules on several paint properties of interest was tested by incorporating microcapsules into four representative paint systems (acrylic, epoxy, polyurethane, and siloxane) and applying the paint to sandblasted carbon steel test panels ($6 \times 4 \text{ in}^2$). The test results showed that, in most cases, incorporating these microcapsules into the representative paint systems had no significant effect (more than 15 percent) on the paint adhesion properties. These results are shown in Figure 3.

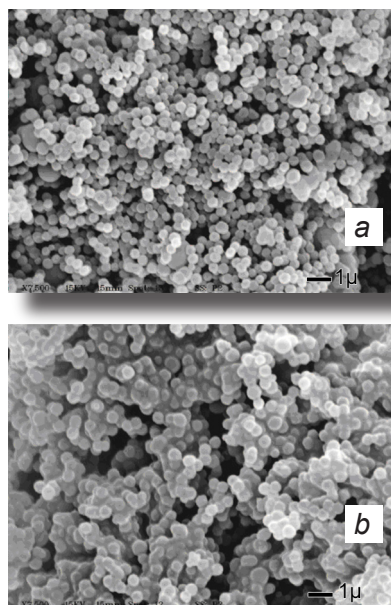


Figure 1. SEM images of dried microcapsules: (a) water core with corrosion inhibitor $\text{Ce}(\text{NO}_3)_3$ and (b) water core with corrosion inhibitor Na_2MoO_4 .

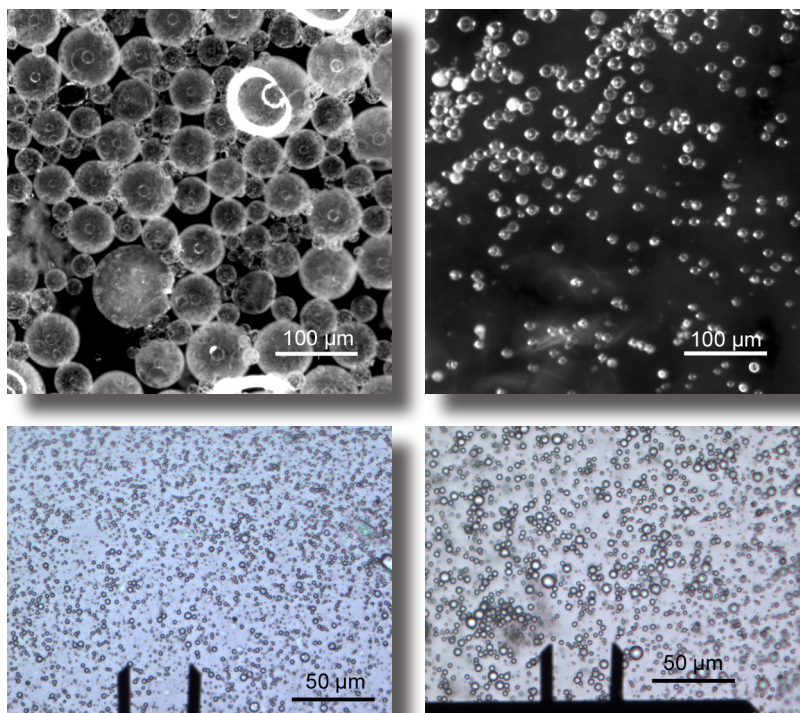


Figure 2. Microcapsules of various sizes.

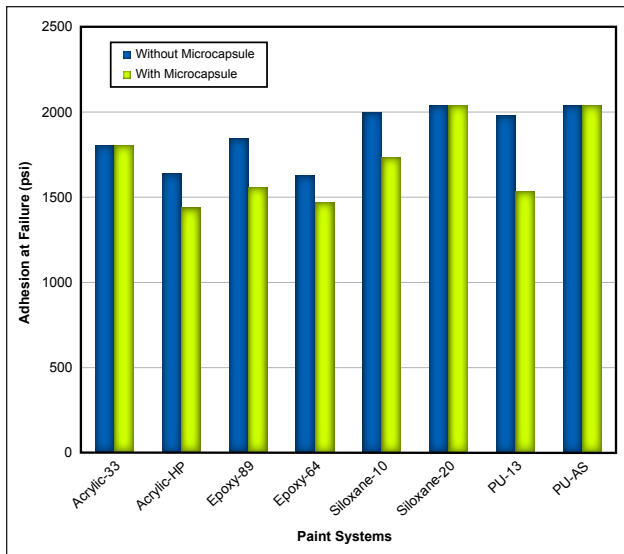


Figure 3. Adhesion test results.

A second concern is that the microcapsules might not survive the coating process, so the stability of the microcapsules in the coatings was examined by means of SEM. Figure 4 shows SEM images of well-dispersed microcapsules. The microcapsules appear to be intact and perfectly spherical, thus proving satisfactory survivability with no signs of rupturing.

A third concern is that the microcapsules might not keep the same functionality they exhibited in the colloid system or dried-powder form in dried paint. This concern was investigated through tests the pH sensitivity of the microcapsules in dry paint. Figure 5 shows the vivid color changes observed when the microcapsules in the dry paint were exposed to basic pH conditions.

Contacts: Dr. Luz Marina Calle <Luz.M.Calle@nasa.gov>, NASA-KSC, (321) 867-3278; and Dr. Wenyan Li <Wenyan.Li@nasa.gov>, ASRC Aerospace, (321) 867-3819

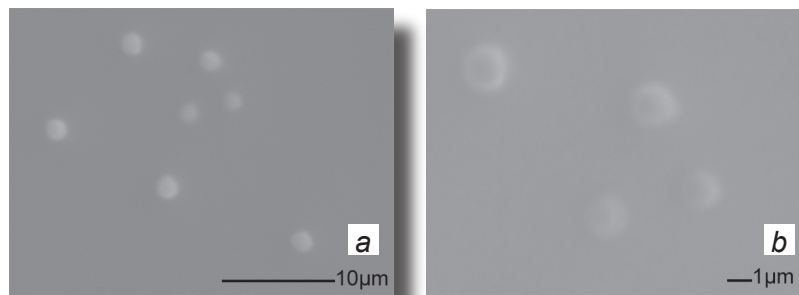


Figure 4. SEM images of epoxy coating with microcapsules captured at (a) 3,500 \times and (b) 7,500 \times magnification.

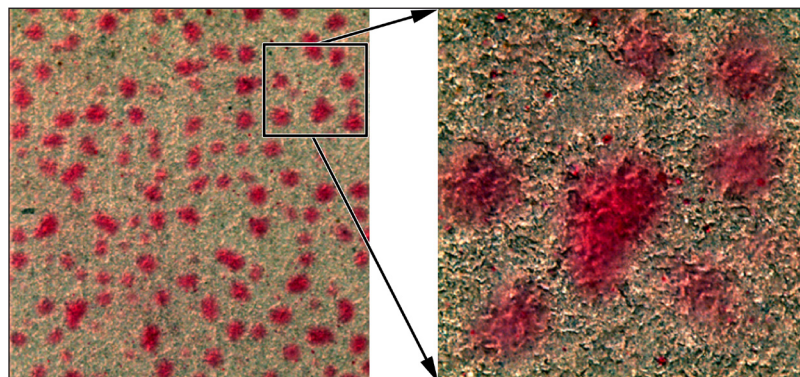


Figure 5. Color change observed when microcapsules in dried paint were exposed to basic pH conditions.

Aerocoat 7 Replacement Coatings



Corrosion
Control

Kennedy Space Center has used Aerocoat 7 (AR-7) to protect stainless-steel flex hoses at Launch Complex (LC-39) and hydraulic lines of the Mobile Launcher Platform (MLP) because it provides excellent corrosion protection in low-temperature applications. The Sovereign Company produced AR-7 exclusively for NASA but discontinued production because the coating released high levels of volatile organic compounds (VOCs) and had a significant environmental impact. The purpose of this project was to select and evaluate potential replacement coatings for AR-7 that would be more environmentally sound.

The physical and mechanical properties of commercially available coatings were investigated through the Internet. The ideal coating would be fluid enough to penetrate the outer mesh of a stainless-steel flex hose and coat the inner hose, and flexible enough to withstand the movement of the hose, as well as the expansion and contraction of its metal caused by changes in temperature. It would also be easy to apply and prepare samples for testing. Ideally, only a single coat would be necessary, applied by brushing, spraying, or dipping.

Forty-one coatings were initially selected. After evaluating the candidates against information obtained from the Internet and coating manufacturers, we narrowed the list to 15 coatings. After the coatings were applied, six were removed from consideration because of their reactivity, short pot life, or long curing time.

Accelerated corrosion tests were performed in the salt fog chamber of the NASA Corrosion Technology Laboratory, according to the guidelines of ASTM B117. After 500 hours of exposure, five coatings performed as well as or better than AR-7 and two others were eliminated from the study. Figure 1 shows coatings that performed worse than AR-7, the same as AR-7 (AR-7 was the control), and better than AR-7. Sample (a) was one of the coatings eliminated from the study.

After 1,000 hours in the chamber, even the best-performing coatings had blisters or creepage along the scribe. Only two of the unscribed coatings had no blisters or corrosion spots. The four best performers were selected for long-term exposure testing, and scribed samples of these coatings are shown in Figure 2. After 1,500 hours of exposure, none of the coatings performed as well as the control.

This study will continue through FY 2008 with further atmospheric exposure and cryogenic testing. Before being included in the list of qualified products in NASA-STD-5008, the replacement for AR-7 must demonstrate that it provides acceptable corrosion protection after exposure for 18 months at the NASA Corrosion Technology Laboratory beachside atmospheric-exposure test site.

Contact: Dr. Luz Marina Calle <Luz.M.Calle@nasa.gov>, NASA-KSC, (321) 867-3278

Participating Organizations: NASA-KSC (Janice K. Lomness) and ASRC Aerospace (Rubiela D. Vinje and Jerome P. Curran)

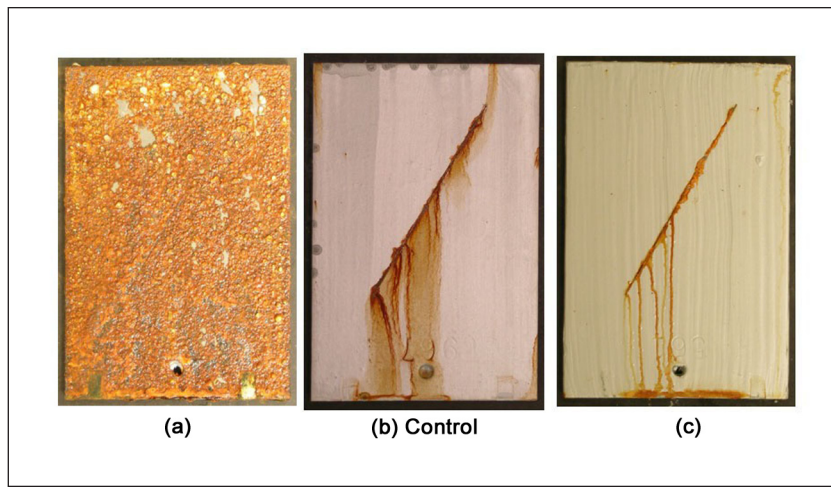


Figure 1. After 500 hours of salt fog exposure, coatings performed (a) worse than AR-7 (the control coating) and (c) better than AR-7.

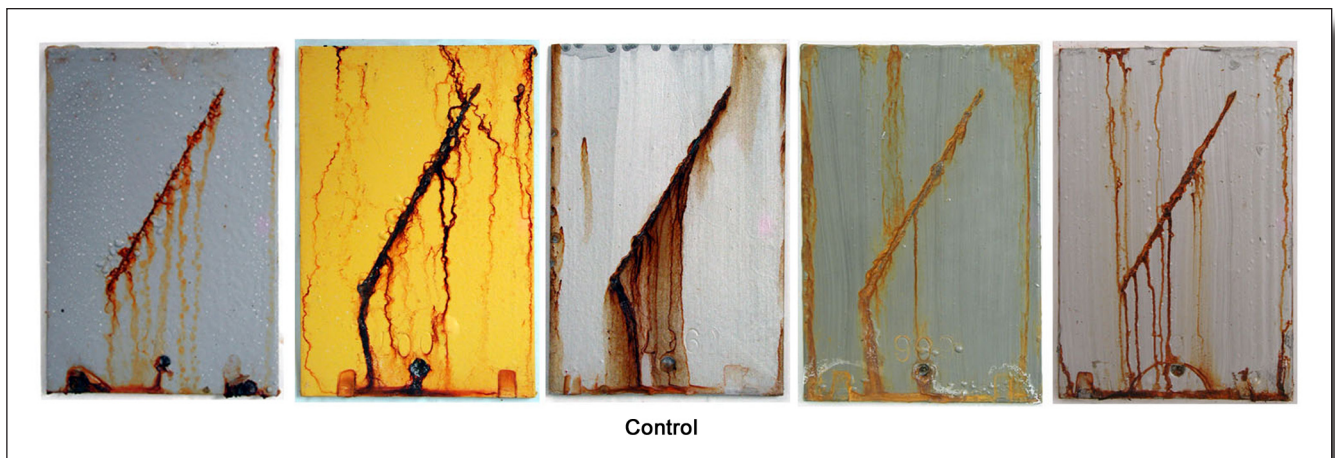


Figure 2. After 1,000 hours of salt fog exposure, all of the coatings showed degradation.

Photocatalytic Coatings for Exploration and Spaceport Design

2006 Center Director's Discretionary Fund Project



Corrosion
Control

This project developed self-cleaning photocatalytic coatings that remove contamination without human intervention. The coatings chemically remove organic contaminants and leave no residue. The photocatalyst will not negatively affect other coating properties, especially corrosion resistance.

Titanium dioxide, TiO_2 , is an extremely popular photocatalyst because of its chemical stability, nontoxicity, and low cost. TiO_2 is commonly used in the photocatalytic oxidation of organic matter or pollutants in the gas and liquid phases. However, TiO_2 does have some drawbacks. It has limited light absorption because of its large band-gap and suffers from a photonic efficiency of less than 10 percent for organic degradation. Dopants can lower the band-gap and improve efficiency. Since the photocatalytically active form of TiO_2 is a nanocrystalline powder, it can be difficult to make a robust coating with enough catalyst loading to be effective.

Photocatalysts become active when certain light energy is absorbed. When photons with an energy greater than the band-gap, E_g , (wavelengths shorter than 400 nm) impinge upon the surface of the TiO_2 , an electron-hole pair is formed (Figure 1). The electron-hole pair oxidizes adsorbed substances either directly or via reactive intermediates that form on the surface, such as hydroxyl radicals ($\text{OH}\cdot$) or superoxide ions (O_2^-).

Several factors can influence the band-gap energy of TiO_2 , two of which are crystal structure and impurities. TiO_2 exists as three crystal structures—brookite, anatase, and rutile—that can be controlled via heat treatment. Anatase is the most photocatalytically active crystal form of TiO_2 . Doping TiO_2 with impurities can alter its band-gap energy, as well as its effectiveness as a catalyst. Depending on their size, dopant atoms can occupy either the substitutional or interstitial lattice positions. Atoms that are relatively large will assume the interstitial positions and create a much greater energy disturbance in the crystal than will smaller atoms that take on the substitutional positions. This energy disturbance narrows the band-gap and thus allows photons with longer wavelengths and smaller energies (such as those in the visible-light spectrum) to create electron-hole pairs.

Raman spectroscopy was performed for the purpose of determining the crystal structure and the degree of crystallinity of the TiO_2 particles. Reflectance measurements indicated the wavelengths of light absorbed by the different catalysts. Reflectance is inversely proportional to absorbance and can help approximate the band-gap. The wavelength where the percentage of reflectance begins to decrease approximates the band-gap. For pure TiO_2 , only the sample heated to 600 °C exhibits different spectral behavior from the others. Its rutile crystal structure ended its absorbance near a wavelength of 460 nm instead of the 435-nm wavelength characteristic of the other samples in the anatase phase.

For the catalysis evaluation, 20 μL of 0.2-mg/mL Rhodamine B dye in ethanol was added to 10-mg samples of the catalyst. Half of the prepared samples were exposed to ultraviolet (UV) radiation (from an F8T5/BLB fluorescent light with peak emission at 365 nm) for 24 hours, while the other half were kept in the dark. Upon completion of the UV test, the addition of 5 mL of water dissolved the remaining dye. The absorbance of the dye, measured with an HP spectrophotometer, between 450 nm and 615 nm, revealed the amount of dye remaining after exposure. The effectiveness of each catalyst was determined by the comparison of the amount of absorbance of the dye remaining in the samples with the initial absorbance of the dye alone. All measurements were made in triplicate. Figure 2 shows results for the cleaning efficiency of pure TiO_2 made with three different procedures and different heat treatments. Procedure 3 with a heat treatment at 400 °C performed the best. In general for all the doped catalysts, Procedure 3 with the same heat treatment performed the best.

Contacts: Dr. Paul E. Hintze <Paul.E.Hintze@nasa.gov>, NASA-KSC, (321) 867-3751; and Dr. Luz Marina Calle <Luz.M.Calle@nasa.gov>, NASA-KSC, (321) 867-3278

Participating Organizations: NASA-KSC (Amanda B. Napier) and ASRC Aerospace (Jerome P. Curran)

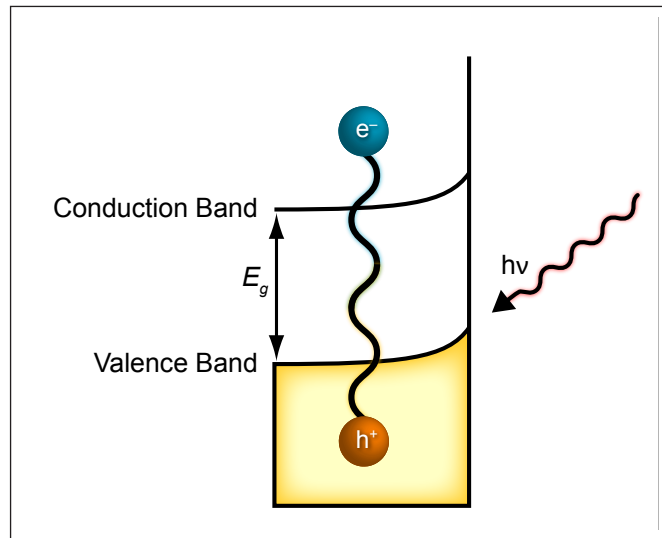


Figure 1. Electronic band structure of a semiconductor showing the electron-hole pair formed after it absorbs a photon of light.

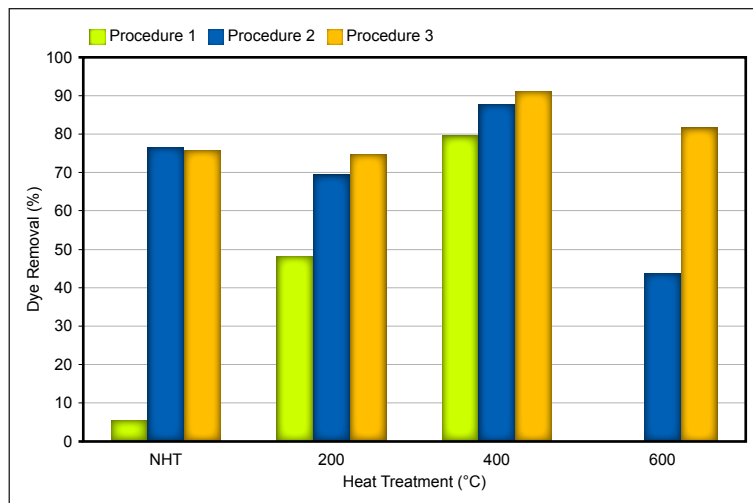


Figure 2. Dye reduction after the catalyst was exposed to UV light for 24 hours. The catalyst was pure TiO_2 made in three ways with different heat treatments. The high percentage reduction indicates that the catalyst oxidized nearly all the dye in contact with the surface. NHT indicates no heat treatment.

New Materials for the Repair of Polyimide Electrical Wire Insulation



Wire/Cable
Inspection
and Repair

Two viable polyimide backbone materials have been identified that will allow the repair of polyimide electrical wire insulation found on the Space Shuttle and other aging aircraft. This identification is the outcome of ongoing efforts to assess the viability of using such polyimides and polyimide precursors (polyamic acids [PAAs]) as repair materials for aging polyimide electrical wire insulation. These repair materials were selected because they match the chemical makeup of the underlying wire insulation as closely as possible. This similarity allows for maximum compatibility, coupled with the outstanding physical properties of polyimides. The two polyimide backbone materials allow the polymer to be extremely flexible and to melt at low temperatures. A polymer chain end capping group that allows the polymer to crosslink into a nonflowable repair upon curing at around 200 °C was also identified. The table highlights two repair materials prepared from each of the two backbone materials identified. Two films, one from each backbone, are soft, flexible films suitable for manually wrapping damaged wire. The other two are stiffer, more rigid films to be formed into “sleeves” that can easily be slipped onto a wire. Both of the wire repair materials achieved excellent results. Figure 1 shows that the repairs (on 12-gauge polyimide insulated wire) are small and compact, exhibiting excellent flexibility. Methods have also been established to repair electrical wire insulation based on fluoropolymers (polytetrafluoroethylene materials [Figure 2]). In addition, a heater was developed to melt and flow the materials, which enables the curing process required for repairs. A portable soldering iron was modified with a custom head designed to accommodate a wire wrapped with repair film. Figure 3 shows the wire holders that were modified for repairing wires.

Characteristics of repair materials prepared from two viable polyimide backbone materials.

Polymer	Type	Film Forming Ability	Wire Repair Results	Comments
A-1	Imide	Excellent	Good	Soft for wrapping; very good on voltage breakdown
A-2	Imide	Excellent	Good	Stiff for sleeve type repair
B-1	Imide	Excellent	Good	Soft for wrapping; v. good adhesion
B-2	Imide	Excellent	Good	Stiff for sleeves

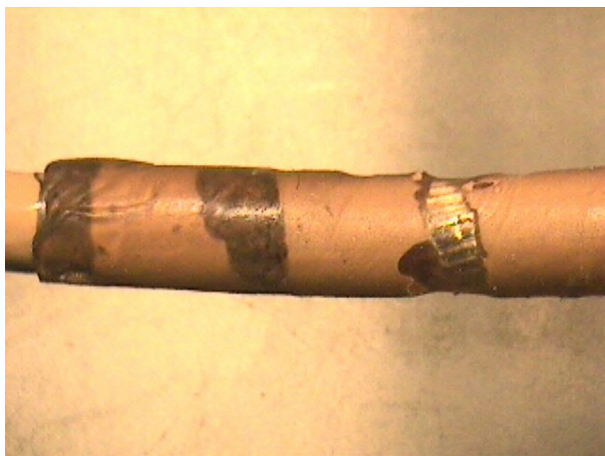


Figure 1. Small, compact repairs on 12-gauge insulated wires exhibit excellent flexibility.

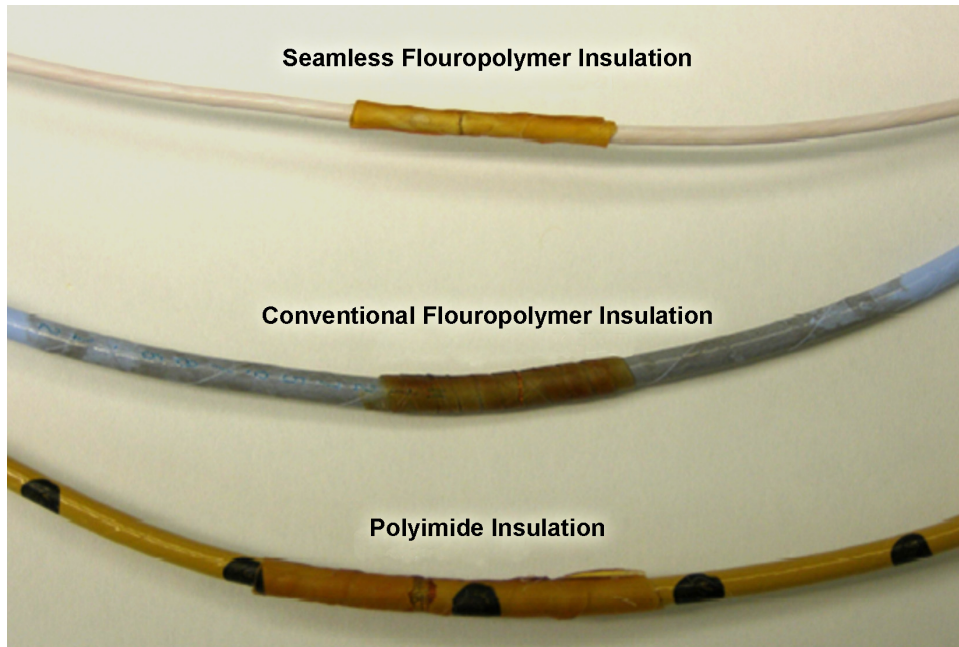


Figure 2. Repairs to various types of wire insulation materials.

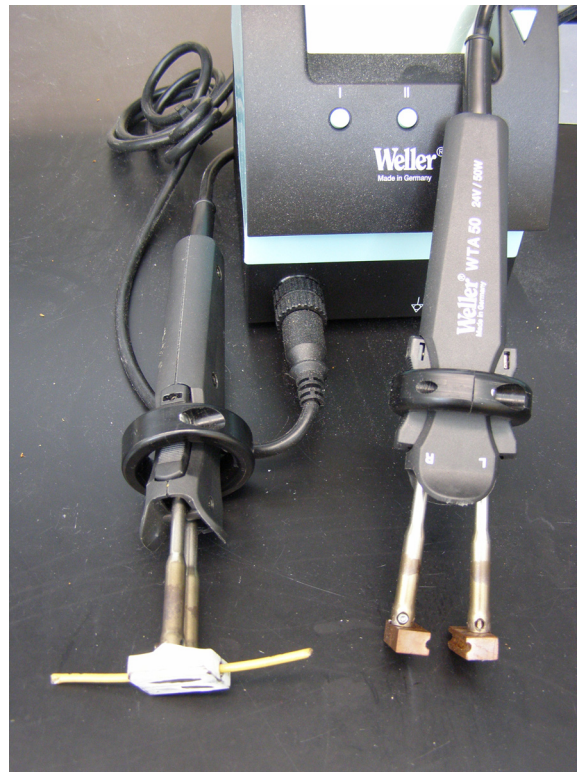


Figure 3. Wire holders modified for repairing wires.

Contacts: Dr. Tracy L. Gibson <Tracy.L.Gibson@nasa.gov>, (321) 867-7572, and Dr. Scott T. Jolley <Scott.T.Jolley@nasa.gov> (321) 867-7568, ASRC Aerospace; and Dr. Martha K. Williams <Martha.K.Williams@nasa.gov>, NASA-KSC, (321) 867-4554

Participating Organizations: NASA-KSC (Dr. LaNetra C. Tate, Trent M. Smith, and Dr. Luke B. Roberson) and ASRC Aerospace (Lilliana Fitzpatrick, Rubiela D. Vinje, and Steven L. Parks)

Commodity-Free Calibration

2006 Center Director's Discretionary Fund Project



Propellant Loading/
Servicing/Storage

Commodity-free calibration is a reaction rate calibration technique that does not require the addition of any commodities. This technique is a specific form of the reaction rate technique, where all of the necessary reactants, other than the sample being analyzed, are either inherent in the analyzing system or specifically added or provided to the system for a reason other than calibration.

After introduction, the component of interest is exposed to other reactants or flow paths already present in the system. The instrument detector records one of the following to determine the rate of reaction: the increase in the response of the reaction product, a decrease in the signal of the analyte response, or a decrease in the signal from the inherent reactant. With this data, the initial concentration of the analyte is calculated.

This type of system can analyze and calibrate simultaneously, reduce the risk of false positives and exposure to toxic vapors, and improve accuracy. Moreover, having an excess of the reactant already present in the system eliminates the need to add commodities, which further reduces cost, logistic problems, and potential contamination. Also, the calculations involved can be simplified by comparison to those of the reaction rate technique.

We conducted tests with hypergols as an initial investigation into the feasibility of the technique. Hypergols are prime candidates for commodity-free calibration because they are highly toxic and exceptionally reactive. Consequently, these vapors present considerable challenges in handling and quantification. After characterization, nitrogen tetroxide (NTO) vapors were collected at low concentrations (about 10 ppm) in a fixed-volume gas collection tube. At $t = 0$, immediately after vapor collection, an acidic N-(1-naphthyl)ethylenediamine dihydrochloride (“diamine”) solution was injected through a septum into the collection tube containing the trapped vapors. The NTO vapors were allowed to react with the absorbing solution for a reaction time, t . At the given t , the contents of the collection tube were emptied into a cuvette and absorbance was measured with a UV-Vis spectrophotometer. We conducted separate experiments with t ranging from 1 to 15 min and plotted the resulting data to generate a reaction profile of instrument response versus time for this reaction (Figure 1). The resultant curve merely approximates the actual reaction profile because

its data reflects a series of reactions rather than a single reaction monitored over time. However, these results do look promising in that the reaction proceeds at a rate reasonable for use in analysis.

To monitor the kinetics of a single reaction, we designed a custom UV-Vis cuvette (Figure 2) that could be placed in the spectrophotometer, with a gas sample being introduced at $t = 0$. Time-based absorbance measurements would monitor the formation of the product, and from the resulting data, the concentration of the NTO vapors could be calculated. Reaction reversibility is crucial in order for this procedure to fit the commodity-free requirement. If the reaction were not reversible, the commodity expended during operation would need to be replenished. For demonstration, NTO vapors were reacted with a diamine solution. Time-based absorbance measurements were taken during the process, and the results are plotted in Figure 3. The spherical bubble

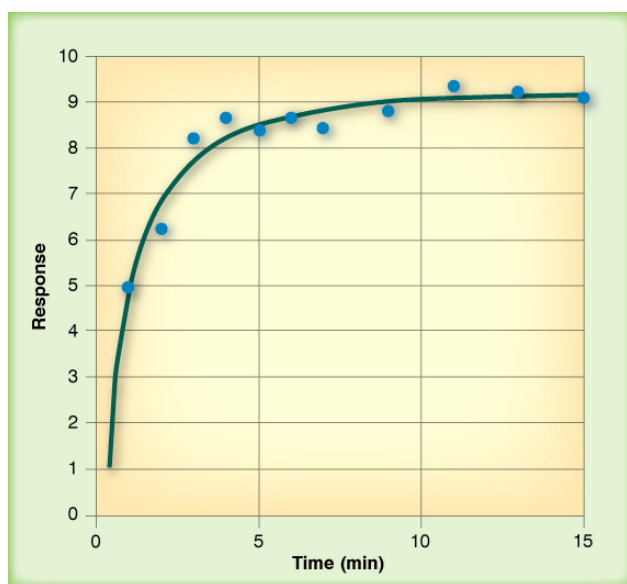


Figure 1. Reaction rate profile.

on top of the cuvette contains the NTO vapors and maximizes the solution-vapor interaction under these restricted reaction conditions. Upon delivery of the cuvette, reaction profiles from singular reactions over time can be generated. The plot of the log of the absorbance intensity (which is proportional to the product concentration) versus reaction time should be linear, with a slope that represents the reaction rate constant, k .

We studied the feasibility of using reaction time to calibrate a wide range of sensors and tested color-indicating chemistry as a way to track the reaction progress. We also developed systems using computer control, rather than color, to ensure the results are consistent. Our tests of these systems are showing promise for refining the technique. Future work includes finishing studies using the thermal desorption system to demonstrate if the technology is feasible for NASA's goals. Other reaction techniques could also be examined to determine the best approach.

Contacts: Dr. Timothy P. Griffin <Timothy.P.Griffin@nasa.gov>, NASA-KSC, (321) 867-6755; and Dr. C Richard Arkin <Richard.Arkin-1@ksc.nasa.gov>, ASRC Aerospace, (321) 867-6757

Participating Organization: ASRC Aerospace (Cristina M. Berger)

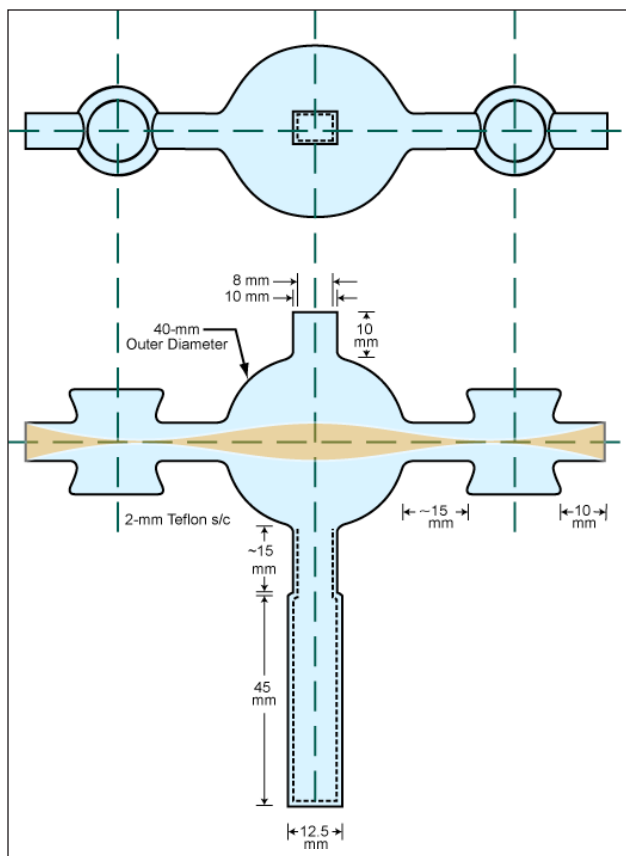


Figure 2. Custom-built UV-Vis cuvette.

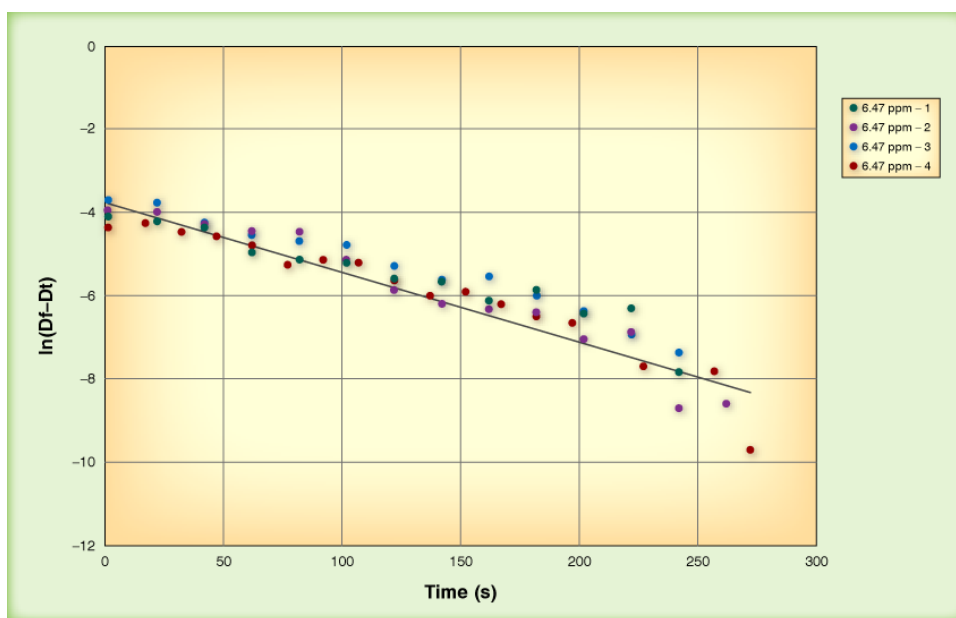


Figure 3. Time-based absorbance of NTO.

Novel Ice Mitigation Methods

2006 Center Director's Discretionary Fund Project



Propellant Loading/
Servicing/Storage

After the loss of Columbia, there was great concern in the Space Shuttle program for the impact of debris against the leading edges of the Orbiter wings. It was quickly recognized that, in addition to impacts by foam, ice that formed on the liquid-oxygen bellows running down the outside of the External Tank could break free during launch and hit this sensitive area. A number of possible solutions were considered, and eventually heaters were installed in this area. This allowed Shuttle launches to resume, but adding heat to the cryogenic flow system was not an optimal solution. Consequently, the Shuttle program requested that a Center Director's Discretionary Fund (CDDF) project explore possible alternatives.

Previously both the Shuttle program and the NASA Engineering and Safety Center had funded extensive efforts for ice mitigation. Many concepts were examined in detail, such as encapsulating the area, projecting heat, using flexible insulation, and applying innovative coatings, but all had drawbacks that prevented them from being used. So it was decided that the CDDF project would not devote resources to concepts that had already been heavily explored, and instead would concentrate on novel ideas that were potentially applicable. Patent and literature searches, as well as brainstorming sessions, resulted in a number of interesting concepts to be considered.

The resulting list of ideas was further filtered to remove ones that, while not considered for Discovery's return to flight, were already well developed and understood (for example, electro-expulsive ice removal). In the end, four concepts were chosen for testing and possible development: (1) adding compounds to the ice to affect its hardness, (2) using dark coatings to increase infrared absorption, (3) using shape memory alloys to break ice free, and (4) applying a high electric field with low-adherence coatings to repel ice.

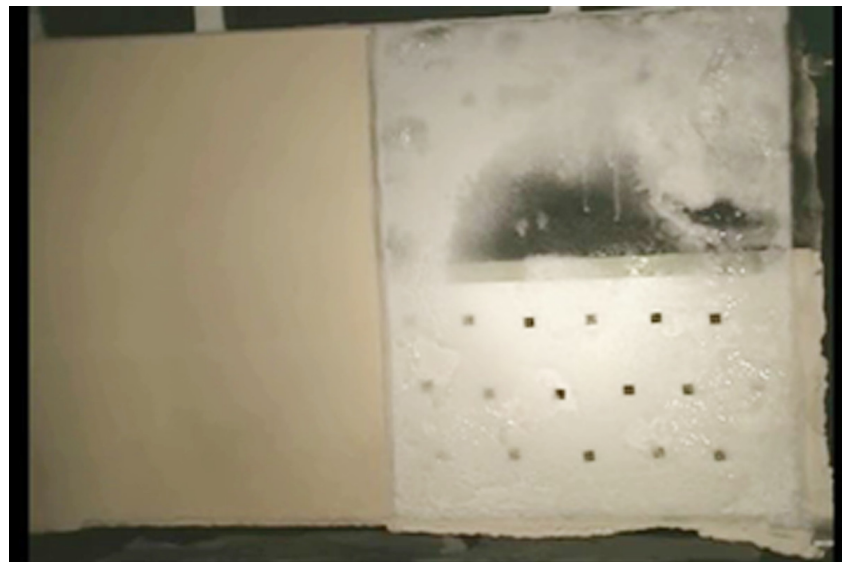


Figure 1. Ice sheet construction involved clamping a sheet of aluminum to a flat, liquid-nitrogen dewar and then spraying the surface with a water mist. The aluminum sheet had both white and dark surfaces, the idea being that the dark surfaces would absorb more radiation and melt the ice more quickly. In the picture, radiative heat has been applied to the panel for some time, warming the center region of the panel and melting the ice.

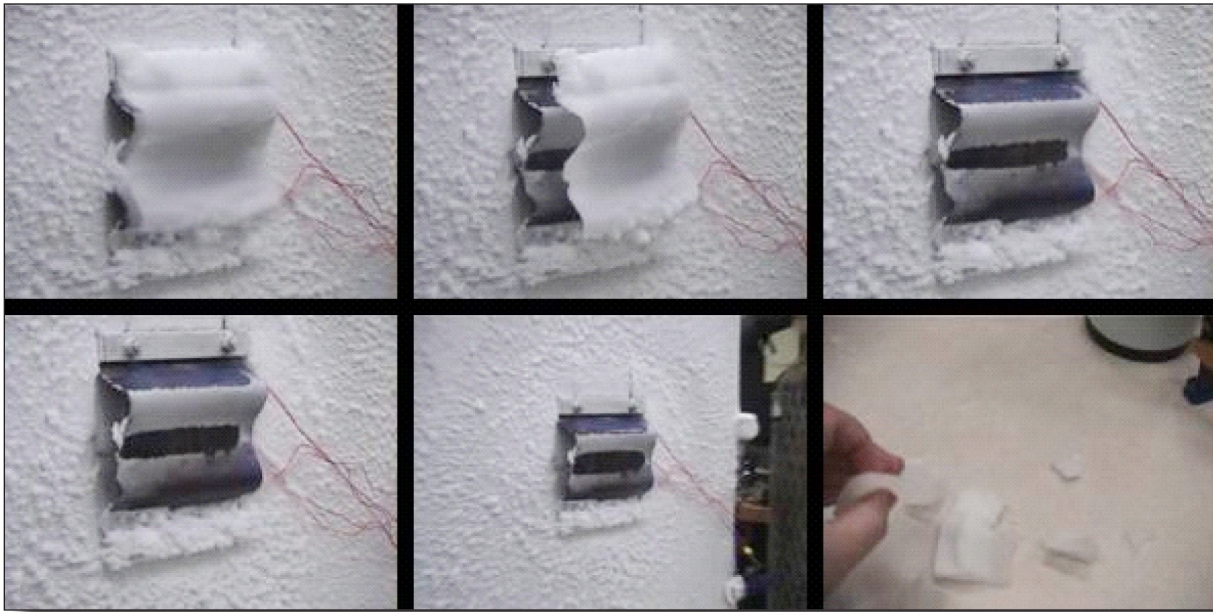


Figure 2. A corrugated NiTi sheet exhibiting a shape metal alloy effect was used in this experiment. As the timeline evolution from the upper left to the lower right shows, heating causes the corrugated pattern to return back to its bowed shape, ejecting the ice. The thick ice chunks shown in the last frame demonstrate the enormous stress force that the NiTi can exert.

Adding compounds to affect the hardness of ice could proceed in two directions; one idea was to form weak ice, which fractures easily and into small pieces, whereas a second idea recommended forming strong ice, thus minimizing ice shedding during launch. Various additives were shown to affect ice hardness, but significant amounts of these additives were required to achieve the desired goals, precluding this as a viable approach.

Infrared radiation tests were performed on 2-ft-square aluminum sheets on which ice had been grown (Figure 1). These sheets were painted with white and black regions so that the dark areas would absorb more heat from the radiation and melt the ice more quickly. In testing, though, this did not happen, probably because the ice itself reflected and absorbed much of the radiation before it reached the underlying coating.

The most successful of the new concepts for ice mitigation involved shape memory alloy materials. These materials can be bent into a given shape and, when heated, will return to their original shape. Figure 2 shows a piece of nickel titanium (NiTi) bent into a corrugated pattern and then chilled until a thick layer of ice formed on it. Then, after being heated, it returns to its original shape, throwing off the ice. This approach proved repeatable and, if further development were requested, would be our primary recommendation.

Our final concept explored how to use very high-voltage electric fields to eject ice as it is being formed. Very high-voltage fields were observed to cause ice to form in fine fingerlike structures and fly off. Special coatings minimized the attachment of the ice to a surface, and then high voltages were applied to see if they could repel the ice from the surface. This approach did not work consistently and, after several tries, was dropped.

Contacts: Trent M. Smith <Trent.M.Smith@nasa.gov>, NASA-KSC, (321) 867-7492; and Dr. Robert C. Youngquist <Robert.C.Youngquist@nasa.gov>, NASA-KSC, (321) 867-1829

Participating Organization: ASRC Aerospace (Dr. Tracy L. Gibson, Dr. Christopher D. Immer, and Dr. John E. Lane)

Crack Offset Measurement With the Projected Laser Target Device



Defect/Damage
Location

The device and associated analysis methodology summarized in this report were developed for the purpose of estimating the size of discontinuities in the surface of the foam that covers the Space Shuttle External Tank. These surface offsets are thought to be due to subsurface cracks in the foam insulation. The mathematical analysis and procedure described here provide a method to quantify the dimensions of the crack offset in a direction perpendicular to the surface, making use of the projected laser target device (PLTD) tool and a laser line projector.

The keys to the construction and use of the PLTD are the following geometrical design requirements:

- Laser dots are on a square grid: length α on a side.
- Laser beams are perpendicular to projected surface.
- Beams are parallel out to the distance being projected.

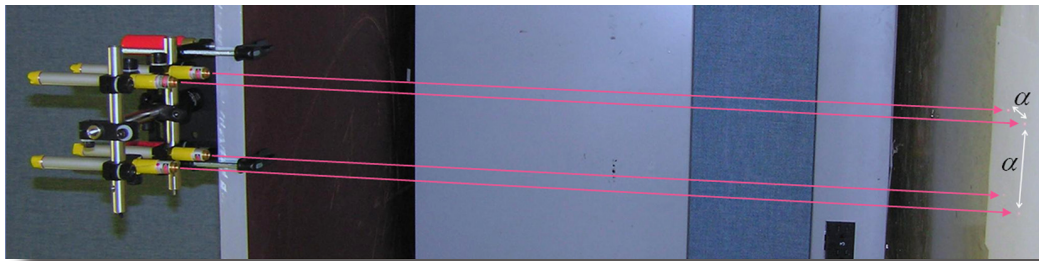


Figure 1. The projected laser target device (PLTD).

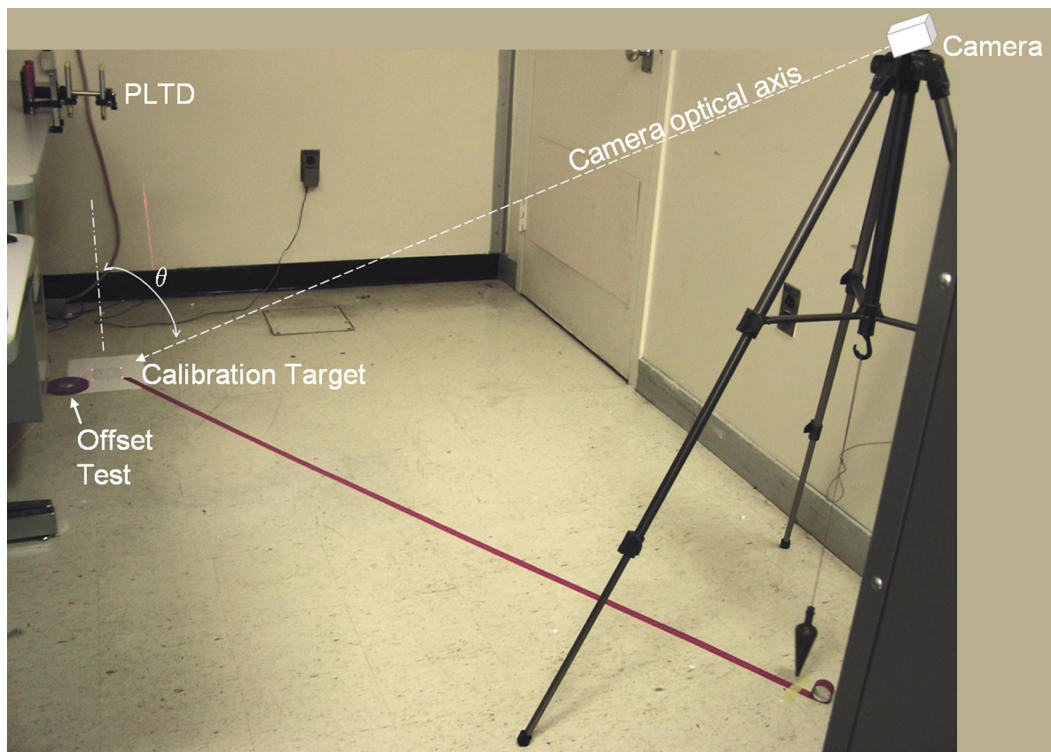


Figure 2. Test setup, with a camera, PLTD, and a laser line projector.

The PLTD can be used to (1) calibrate fixed cameras of unknown magnification and orientation (far-field solution); (2) provide equivalent calibration to multiple cameras, previously achieved only by the use of known target points, for example, in 3-D foreign-object debris tracking on a fixed launch platform; (3) compute scaling for conventional 2-D images, and depth of field for 3-D images (near-field solution); and (4) in conjunction with a laser line projector, achieve accurate measurements of surface discontinuity (cracks) in a direction perpendicular to the surface.

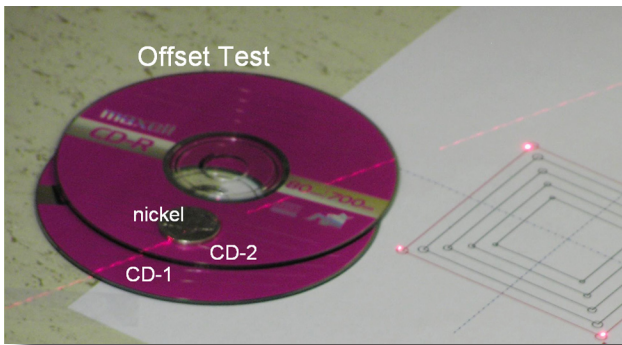


Figure 3. Setup for measuring vertical offset of test objects.

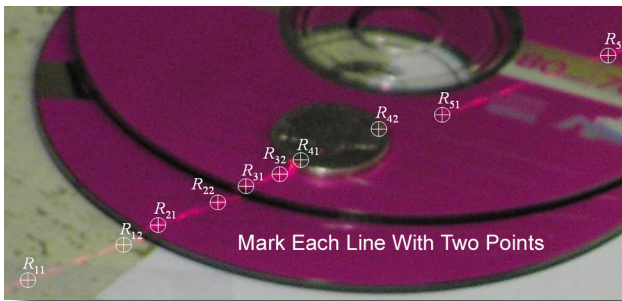


Figure 4. Image analysis of test in Figure 3.

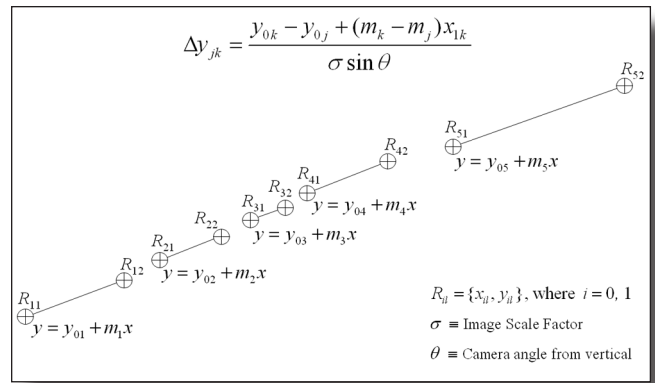


Figure 5. Data extracted from image analysis (Figure 4) for offset measurement.

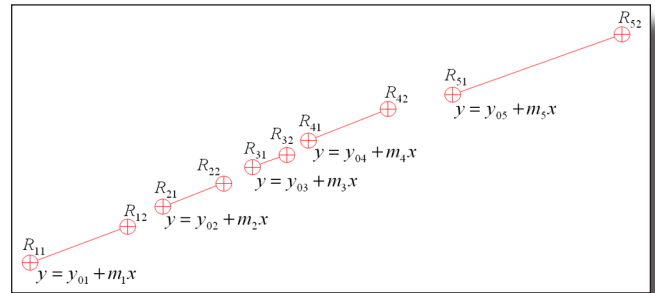


Figure 6. Analysis of data from Figure 5.

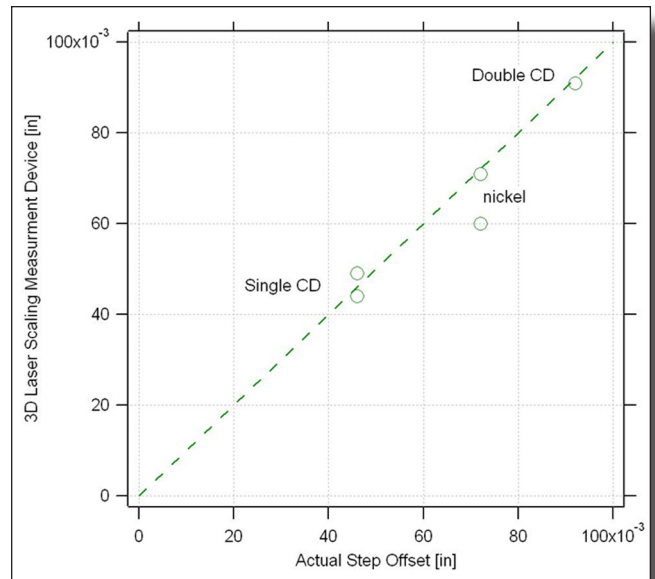


Figure 7. Plot of test data, showing measured offsets compared to actual offsets.

Contact: Dr. Robert C. Youngquist <Robert.C.Youngquist@nasa.gov>, NASA-KSC, (321) 867-1829

Participating Organizations: NASA-KSC (Charles G. Stevenson) and ASRC Aerospace (Dr. John E. Lane)

New Materials for Structural Composites and Protective Coatings

2007 Center Director's Discretionary Fund Project



Defect/Damage
Location

The objective of this Phase I project was to create novel conductive materials that are lightweight and strong enough for multiple ground support equipment and Exploration applications. The long-term goal is to combine these materials within specially designed devices to create composites or coatings with diagnostic capabilities, increased strength, and tunable properties such as transparency, electroluminescence, and fire resistance. One such technology application is a “smart windows” system. In such a system, the transmission of light through a window is controlled by electrical power. In the future, these materials may also be able to absorb sunlight and convert it into electrical energy to produce light, thereby creating a self-sufficient lighting system.

This experiment, conducted in collaboration with the Georgia Institute of Technology, demonstrated enhancements in fabricating fiber materials from carbon nanotubes (CNT). These nanotubes were grown as forests in an ultra-high-purity chemical vapor deposition (CVD) furnace and then drawn, using novel processing techniques, into fibers and yarns that would be turned into filaments. This work was submitted to the *Journal of Advanced Functional Materials*.

The CNT fibers were initially tested as filament materials at atmospheric pressure; however, even under high current loads, the filaments produced only random sparking. The CNT fibers were also converted into transparent, hydrophobic, and conductive sheets. Filament testing at low vacuum pressures is in progress, and the technology will be enhanced in 2008.

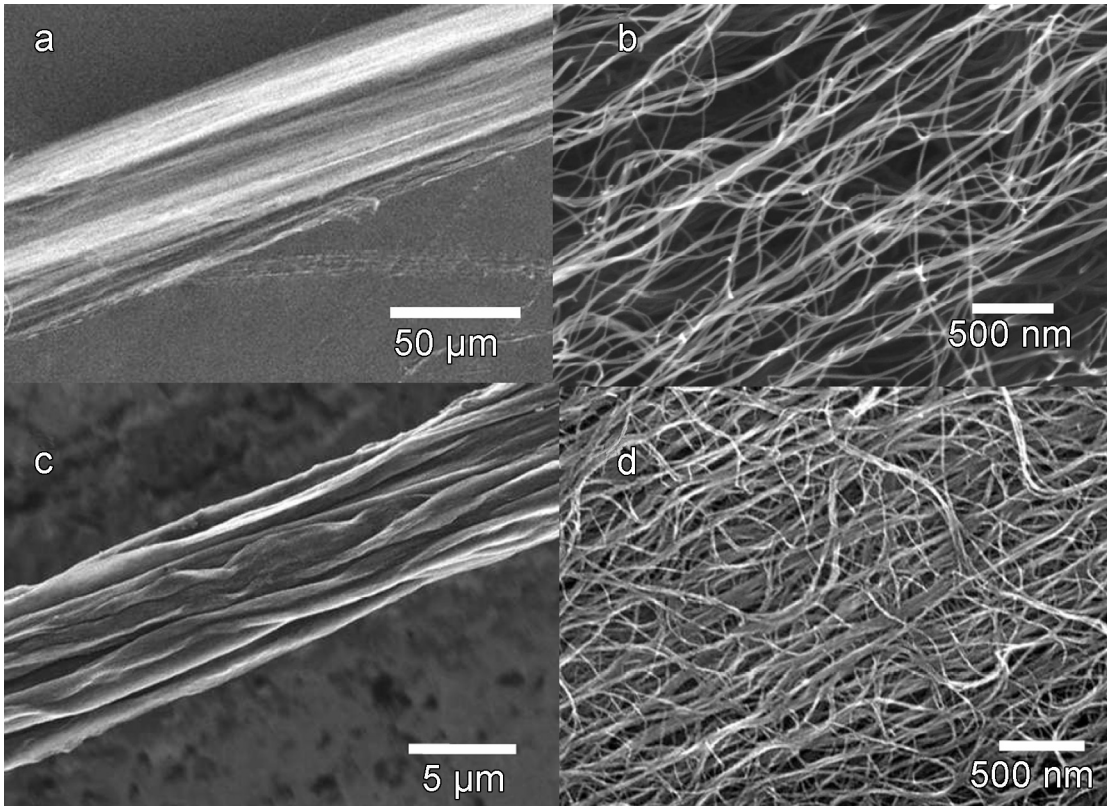
As initial proof of the smart-windows application concept, the use of CNT sheets as composites/ protective coatings was demonstrated in collaboration with Nanocomp Technologies of Concord, New Hampshire. CNT sheets were thermally welded between layers of high-performance polymer sheets with high thermal conductivity. The electrical conductivity of the sheets provided an ample flow of current to detect damage.

Enhancements to the fabrication process and performance of this type of system will be addressed in FY 2008. In Phase II, we intend to further address conductive composites, fabrication processes, and various applications. We will apply these next-generation composites and coatings to various hardware systems and analyze their mechanical properties, conductivity for detection, and thermal conductivity for thermal management in Lunar Architecture Team and Exploration applications.

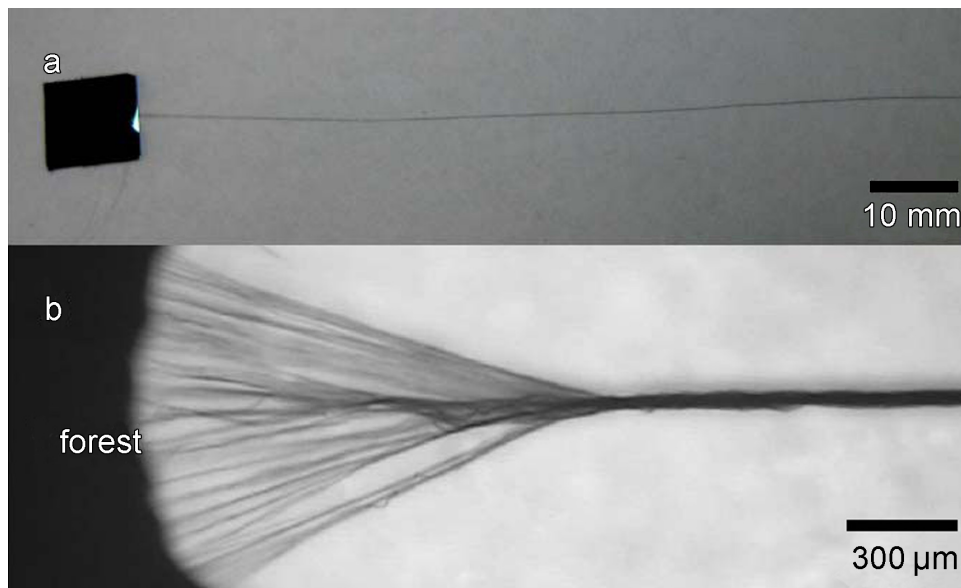
Key accomplishments included fabricating CNT filaments and evaluating them under atmospheric conditions, fabricating CNT sheet fabrication, and fabricating a structural conductive composite with ample current for damage detection.

Contacts: Dr. Luke B. Roberson <Luke.B.Roberson@nasa.gov>, NASA-KSC, (321) 867-1542; Dr. LaNetra C. Tate <LaNetra.C.Tate@nasa.gov>, NASA-KSC, (321) 867-3789; and Dr. Martha K. Williams <Martha.K.Williams@nasa.gov>, NASA-KSC, (321) 867-4554

Participating Organizations: NASA-KSC (Trent M. Smith and Dr. Robert C. Youngquist), Georgia Institute of Technology (Dr. Satish Kumar, Dr. Jud Ready, and Dr. Janusz Kowalik), Nanocomp Technologies, Inc. (Dr. David Lashmore), and ASRC Aerospace (Dr. Barry J. Meneghelli and Dr. Christopher D. Immer)



SEM images of neat MWNT fibers: (a) as-drawn aerogel fiber, (b) nanotube arrangements in the as-drawn fiber, (c) densified fiber, and (d) nanotube arrangement in the densified fiber.



Spinning continuous MWNT fibers from the forest: (a) fiber in the process of being drawn from the 10- by 10-mm² wafer scale forest and (b) optical image showing the nanotubes being pulled from the forest wall into a fiber.

Fire Chemistry Testing of Spray-On Foam Insulation (SOFI)



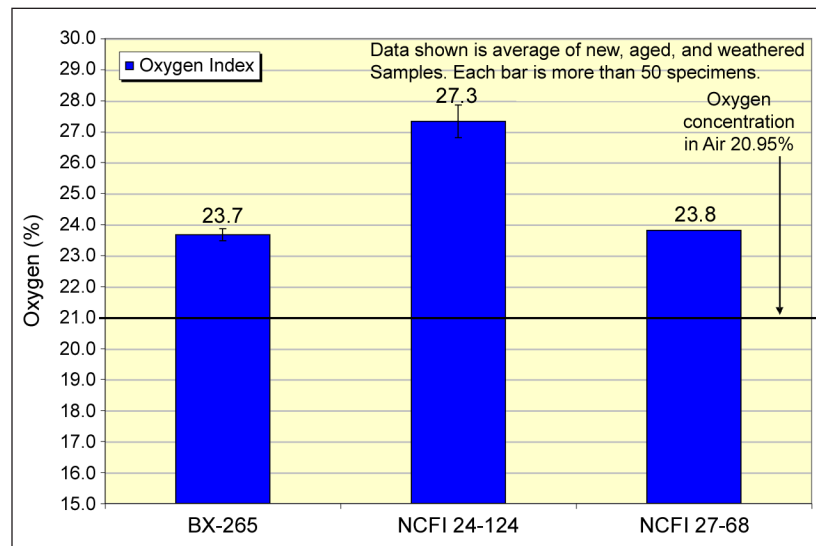
Flight Environment
Measurement

An experimental study was initiated that included the long-term testing of the following SOFI materials, which make up the majority of the Thermal Protection System of the Shuttle External Tank: NCFI 24-124 (acrage foam) and BX-265 (close-out foam, including the intertank flange and bipod areas). A potential alternate material, NCFI 27-68 (acrage foam with flame retardant removed), was also tested. Specimens of all three foam materials were placed at two locations: an aging site (Vehicle Assembly Building [VAB]) and a weathering site (Atmospheric Exposure Test Site, [beach site]). Fire chemistry testing was completed on samples that were retrieved after aging/weathering at intervals of 3, 6, and 12 months. The testing included three standard test methods: limiting oxygen index (ASTM G125), radiant panel (ASTM E162), and cone calorimeter (ASTM E1354).

During the 12-month weathering period, all foams showed little to no change in the limiting oxygen index (LOI). The LOI test, which measures the ease with which a flame is extinguished, indicated that NCFI 24-124 is an inherently flame-retardant material, whereas BX-125 and NCFI 27-68 are not. In essence, all foams tested will burn in an enriched-oxygen atmosphere (i.e., oxygen leak). Figure 1 shows the results of the LOI test.

The results of radiant-panel testing, which measures the critical ignition energy for a sample (flame spread factor) along with heat evolution, showed that the flame spread was quite high for NCFI 27-68 and BX-265 and that the flame spread rate increased with aged samples. A rind surface burns hotter, but slower (downward) than a machined surface for NCFI 27-68. The rind surface is also more susceptible to upward flash fire, according to the flame spread index. Both aging and weathering of SOFI samples increased the flame spread index.

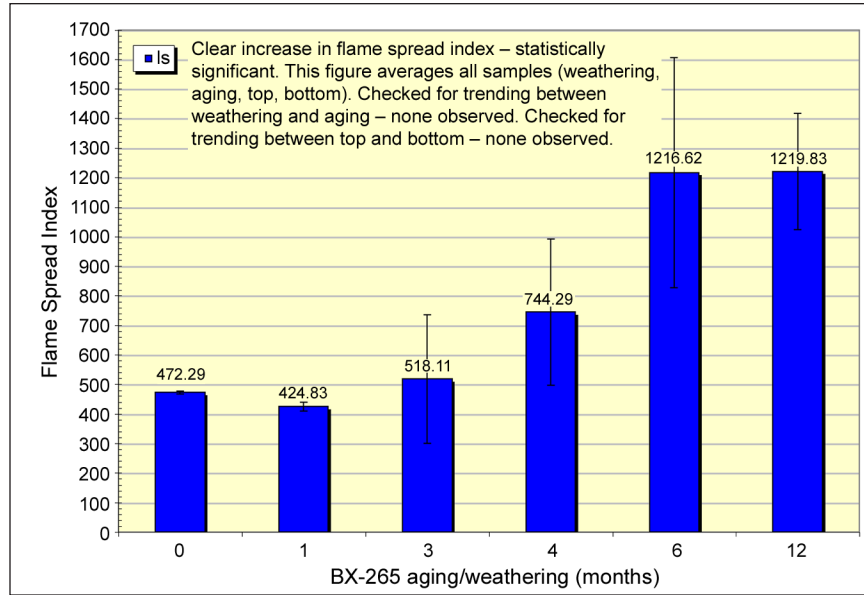
Cone calorimetry measures the peak heat release of a sample, along with the heat release rate, time to ignition, and smoke density. The heat release rates of BX-265 and NCFI 27-68 were not affected by the aging or weathering of these materials as measured by cone calorimetry. However, weathering did reduce the heat release rate of NCFI 24-124 as measured by cone calorimetry. The flame spread index and heat evolution factor were higher for samples with a rind, which reached the peak heat release rate faster. Samples with a rind also burned faster and hotter. The order of heat release rate based on machined data was BX-265 > NCFI 27-68 > NCFI 24-124. Additional samples will be tested to confirm these preliminary results.



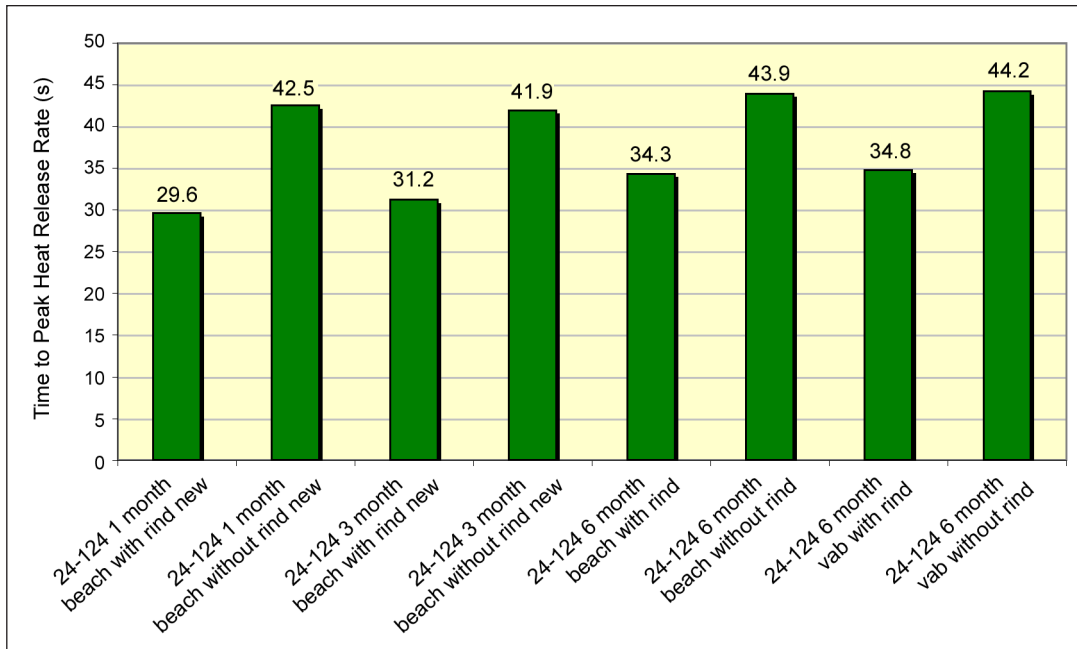
LOI test results for SOFI foam samples (3-, 6-, and 12-month composites).

Contacts: Trent M. Smith <Trent.M.Smith@nasa.gov>, NASA-KSC, (321) 867-7492; and Dr. Martha K. Williams <Martha.K.Williams@nasa.gov>, NASA-KSC, (321) 867-4554

Participating Organization: ASRC Aerospace (Dr. Barry J. Meneghelli)



Radiant panel test results for BX-265.



Core calorimetry test results for NCFI 24-124.

Using Aerogel-Based Insulation Material To Prevent Foam Loss on the Liquid-Hydrogen Intertank



Flight Environment
Measurement

Uninsulated areas on cryogenic propellant tanks and feedlines cause moisture in the air to condense or ice to form. Flange joints, bracket supports, expansion bellows, and other cavities are uninsulated by design. These areas cannot be sealed because conventional thermal insulation materials would restrict mechanical articulations.

Aerogel-based thermal insulation systems are able to seal critical locations such as the liquid-oxygen (LO₂) feedline bellows.

A new thermal insulation system was also necessary between the intertank wall, flange, and the liquid-hydrogen (LH₂) tank dome, where there is a cavity (or crevice) with an exposed 20-K surface. When nitrogen gas is used for purging within the intertank volume, it condenses on this cold surface. Some solid nitrogen may also form on the colder side of the crevice. Voids or discontinuities within the foam can pressurize and cause areas of foam to weaken and break off, reducing thermal efficiency and creating potentially dangerous debris.

To prevent this foam loss, we developed a thermal insulation system using bulk-fill aerogel material and demonstrated it with a one-tenth-scale model of the LH₂ intertank flange area (Figure 1). Temperature sensors were placed in the crevice, in the intertank barrel section, and on the foam surfaces (Figure 2). Cold helium gas sprayed onto the underside of the tank dome helped to maintain a cold-boundary temperature of 20 K ±5 K, and two electric tape-heaters on the lid helped to maintain a warm-boundary temperature of 300 K ±2 K. The intertank volume was purged with nitrogen gas at a controlled flow rate to maintain a thermal balance within the system, with the hot-side lid at 300 K and the cold-side tank dome at 20 K. The aerogel insulation dramatically reduced nitrogen cryopumping and generally increased temperatures throughout the intertank. Only a thin layer of aerogel insulation was required in order to prevent liquid nitrogen (LN₂) from forming. The aerogel material remained completely dry and friable (no free LN₂) in all cases.

These aerogel bulk-fill materials and other aerogel-based insulation systems are viable new options for the design and safe operation of cryogenic propellant tanks.

Contacts: Jared P. Sass <Jared.P.Sass@nasa.gov>, NASA-KSC, (321) 867-0694; and James E. Fesmire <James.E.Fesmire@nasa.gov>, NASA-KSC, (321) 867-7557

Participating Organization: ASRC Aerospace (Dr. Barry J. Meneghelli, Philip A. D'Andreamatteo, and Gary L. Wall)

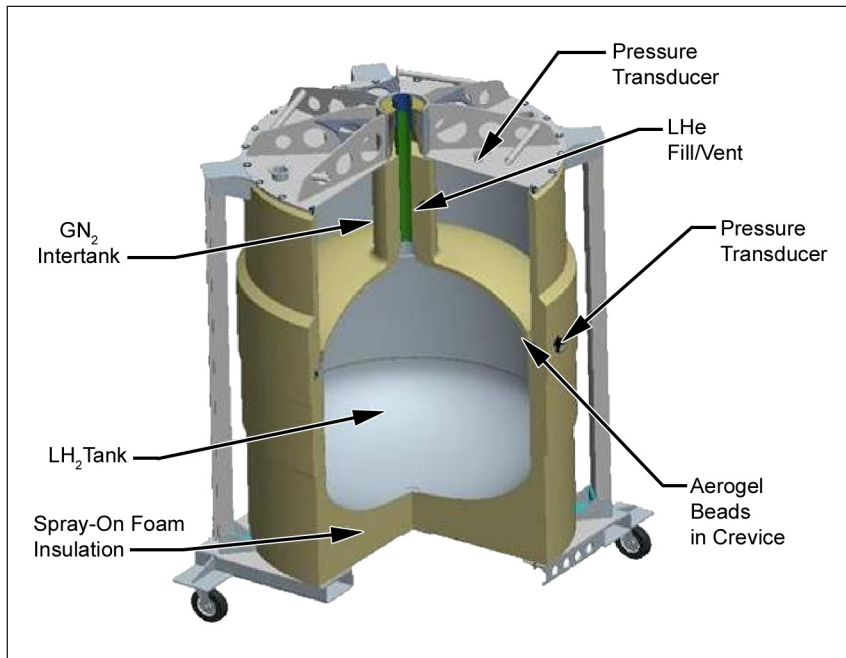


Figure 1. An isometric cutaway view of the LH₂ intertank demonstration test unit, showing main features.

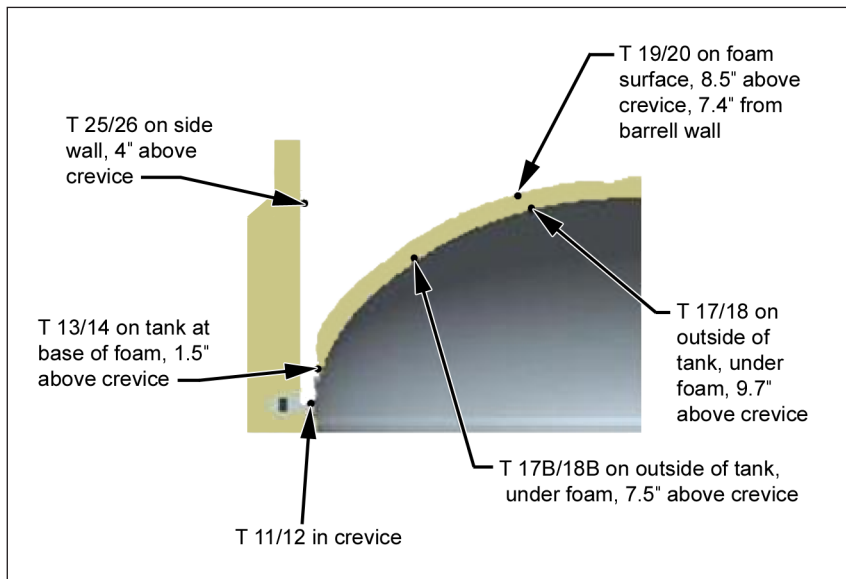


Figure 2. Section view of one-tenth-scale demonstration test unit, showing temperature sensor.

Particle Ejection and Levitation Technology (PELT)



Lunar Launch/
Landing Site
Ejecta Mitigation

Each of the six Apollo landers touched down at unique sites on the lunar surface. Aside from the Apollo 12 landing site located 180 meters from the Surveyor III lander, plume impingement effects on ground hardware during the landings were not a problem. The planned return to the Moon requires numerous landings at the same site. Since the top few centimeters of lunar soil are loosely packed regolith, plume impingement from the lander will eject the granular material at high velocities. Figure 1 shows what the astronauts viewed from the window of the Apollo 14 lander. There was tremendous dust excavation beneath the vehicle. With high-vacuum conditions on the Moon (10^{-14} to 10^{-12} torr), motion of all particles is completely ballistic. Estimates derived from damage to Surveyor III caused by the Apollo 12 lander show that the speed of the ejected regolith particles varies from 100 m/s to 2,000 m/s. It is imperative to understand the physics of plume impingement to safely design landing sites for future Moon missions.

Aerospace scientists and engineers have examined and analyzed images from Apollo video extensively in an effort to determine the theoretical effects of rocket exhaust impingement. KSC has joined the University of Central Florida (UCF) to develop an instrument that will measure the 3-D vector of dust flow caused by plume impingement during descent of landers. The data collected from the instrument will augment the theoretical studies and analysis of the Apollo videos.

Instrumentation designs and concepts were tested in a custom-designed wind tunnel that allows a bed of granular material to be eroded. The material erosion can be measured from altitudes similar to those at which the lunar erosion first begins: up to 30 m. The wind tunnel chamber operates at atmospheric pressure; however, ρV^2 (one of the important scaling parameters) is approximately the same as those for the lander cases on the Moon. Figure 2 shows yellow quartz sand flowing in a section of the wind tunnel. Figure 3 shows 2-D flow calculations of a scene similar to that shown in Figure 2.

The instrument can also measure other lunar surface dust effects, such as dust levitated by solar charging. Though most of the effort for the current instrument has been focused toward lunar applications, the instrument is quite general and could easily be adapted to other applications such as Martian landings.



Figure 1. Example view taken during descent of Apollo lander. The dust is eroding from the lower left to the upper right.



Figure 2. Quartz sand flowing in the wind tunnel used to test the PELT instrumentation designs.

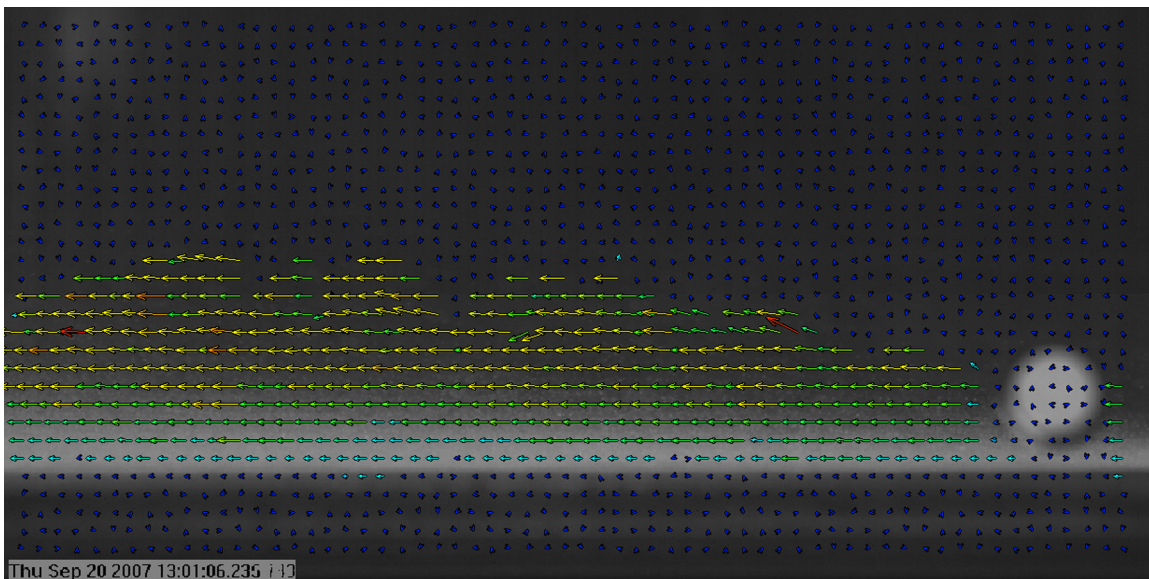


Figure 3. Example flow pattern of a scene similar to that shown in Figure 2.

Contact: Dr. Philip T. Metzger <Philip.T.Metzger@nasa.gov>, NASA-KSC, (321) 867-6052

Participating Organizations: ASRC Aerospace (Dr. Christopher D. Immer) and University of Central Florida (Dr. Jannick Rolland)

Electrostatic Characterization of Lunar Dust

2006 Center Director's Discretionary Fund Project



Lunar Launch/
Landing Site
Ejecta Mitigation

To ensure the safety and success of future lunar exploration missions, it is important to measure the toxicity of the lunar dust and its electrostatic properties. The electrostatic properties of lunar dust govern its behavior, from how the dust is deposited in an astronaut's lungs to how it contaminates equipment surfaces. Astronaut Harry Schmidt said, "Dust is going to be the environmental problem for future missions, both inside and outside the habitats." NASA has identified the threat caused by lunar dust as one of the top two problems that need to be solved before returning to the Moon.

The main reason lunar dust adheres to surfaces is its electrical charge, and the dry conditions on the Moon increase those adhesive properties. The Apollo 12 Mission Briefing report stated that "the cohesive properties of the lunar dust in vacuum, augmented by electrostatic properties, tend to make it adhere to anything it contacts."

To understand the electrostatic nature of lunar dust, NASA must answer the following questions: (1) how much charge can accumulate on the dust? (2) how long will the charge remain? and (3) can the dust be removed? These questions can be answered by measuring the electrostatic properties of the dust: its volume resistivity, charge decay, charge-to-mass ratio or chargeability, and dielectric properties. The volume resistivity of a material indicates the likelihood that the particles will acquire a charge and their ability to dissipate the charge. Charge decay measurements give the time it takes for samples to dissipate the applied charge. The charge-to-mass ratio (chargeability) measurements indicate the amount of charge the dust is likely to acquire during specific processes. The dielectric properties of the dust give a measure of the dust's ability to polarize.

All lunar dust samples that were returned to Earth have been contaminated by air. This contamination most likely affected the electrostatic properties of the material through oxidation. The addition of oxygen atoms to the surface changes the surface chemistry, lowers the surface free energy, and changes the work function of the material. In many cases, these properties influence the magnitude and sign of the charges exchanged between materials, which in turn influences the electrostatic properties. These relationships illustrate the importance of measuring the electrostatic

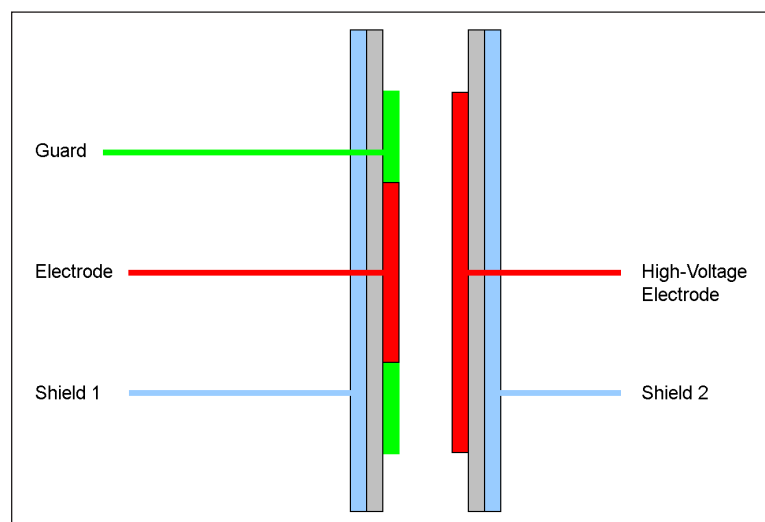


Figure 1. Schematic of the side profile of the design of the test cell used throughout the experiments.

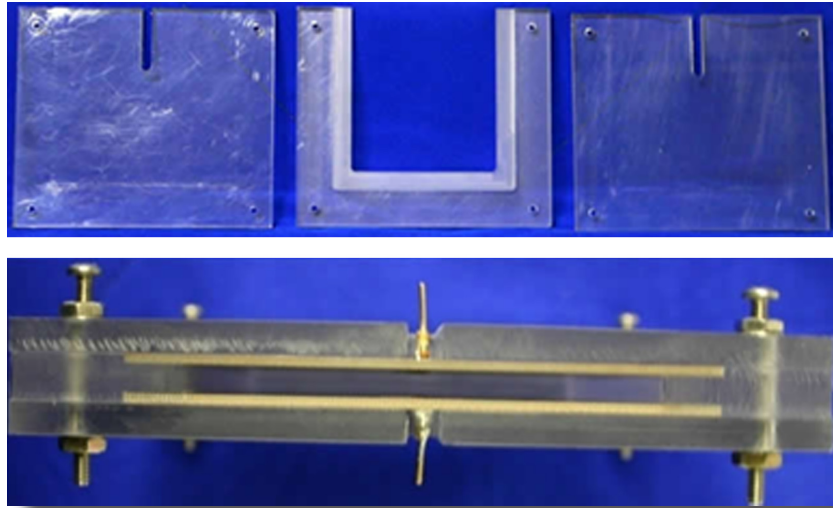


Figure 2. Top images show how the electrodes are sandwiched between a polycarbonate spacer and two backsides to form the cell. Bottom image is a top view of the test cell.

properties of lunar regolith *in situ*. Research performed in the Electrostatics and Surface Physics Laboratory at KSC has led to the development of a device that can be incorporated onto a lander or a rover for measuring all four electrostatic properties during future lunar missions.

A test cell was developed for experimentation with this device before using it on a lander or rover. This test cell compiled with standards in ASTM D 150 as well as British Standard (BS) 5958 in measuring the volume resistivity of powders. Figures 1 and 2 shows the test cell construction: a guard, a guarded electrode, and a shield on one plate; and a high-voltage electrode and a shield on the other plate. All tests with this test cell were performed in vacuum with Minnesota Lunar Simulant (MLS)-1. Because of its mineralogical composition, MLS-1 is believed to be a good lunar soil simulant, even though it does not contain glass or agglutinates. Once the material was delivered to the test cell, it was not disturbed. To measure the four different electrostatic properties, we only needed to change the electrical connections in test setup. This was done outside the test cell without disturbing the regolith.

The experiment mimicked how soils on the lunar surface may one day be handled. They would most likely be collected with a metal scoop or container and poured onto or into a sensitive device that could be damaged by the electrostatic fields produced by highly charged dust. Results of the chargeability test showed relatively high charge-to-mass ratios when the dust was poured onto the test cell. The results were not unexpected in the high-vacuum conditions used during the test. Dielectric measurements of the soil showed no fluctuation of the dielectric constant with frequency, which suggested the absence of moisture, and gave a dielectric constant of about 4. Volume resistivity measurements were made after the soil stabilized for several minutes. The values fell within the appropriate range for highly insulating silicate materials and were consistent with the literature on lunar fines. The charge decay measurements, made by induction-charging the soil, were also consistent with the literature and the previously measured electrostatic properties.

Contact: Dr. Carlos I. Calle <Carlos.I.Calle@nasa.gov>, NASA-KSC, (321) 867-3274

Participating Organizations: ASRC Aerospace (Dr. Charles R. Buhler and Mindy L. Ritz) and Appalachian State University (Dr. Sid Clements)

Numerical Analysis of Rocket Exhaust Cratering

2007 Center Director's Discretionary Fund Project



Lunar Launch/
Landing Site
Ejecta Mitigation

Supersonic jet exhaust impinging onto a flat surface is a fundamental flow encountered in space or with a missile launch vehicle system. The flow is important because it can endanger launch operations. The purpose of this study is to evaluate the effect of a landing rocket's exhaust on soils. From numerical simulations and analysis, we developed characteristic expressions and curves, which we can use, along with rocket nozzle performance, to predict cratering effects during a soft-soil landing.

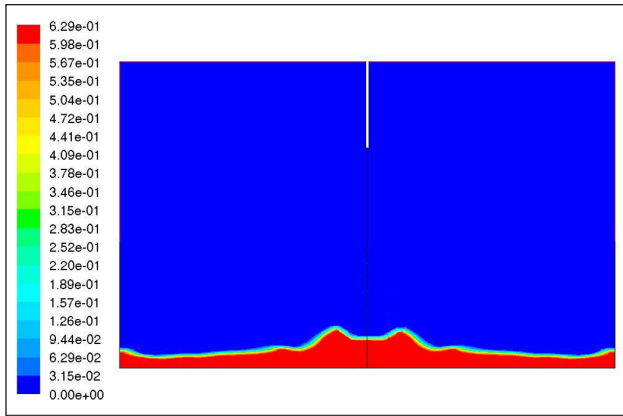
We conducted a series of multiphase flow simulations with two phases: exhaust gas and sand particles. The gas expanded from the nozzle exit with a prescribed velocity profile and impinged onto the sand surface. The interaction between those two phases formed the erosion on the sand bed. The results enabled use to describe the basic effects of gas jets impinging on sand and to relate crater dimensions to the soil characteristics and the numerical simulation parameters, including volume fraction, packing limit, and angle of internal friction.

The main objective of the simulation was to obtain the numerical results as close to the experimental results as possible. After several simulating test runs, the results showed that packing limit and the angle of internal friction are the two critical and dominant factors in the simulations. Our work included

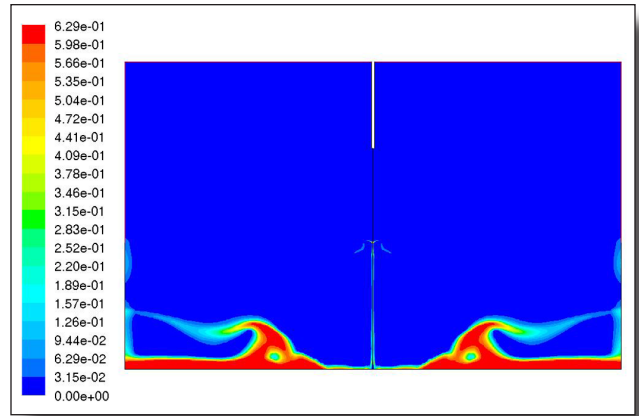
- reviewing numerical and experimental studies related to multiphase, supersonic flow,
- performing axisymmetric and 3-D supersonic flow impingement,
- comparing two-phase flow numerical results with experimental data,
- implementing a new user-defined function to model the nozzle boundary condition,
- presenting the study at the AIAA Fluid Dynamics conference, and
- delivering validated numerical solutions with a final report.

Contact: Dr. Bruce T. Vu <Bruce.T.Vu@nasa.gov>, NASA-KSC, (321) 867-2376

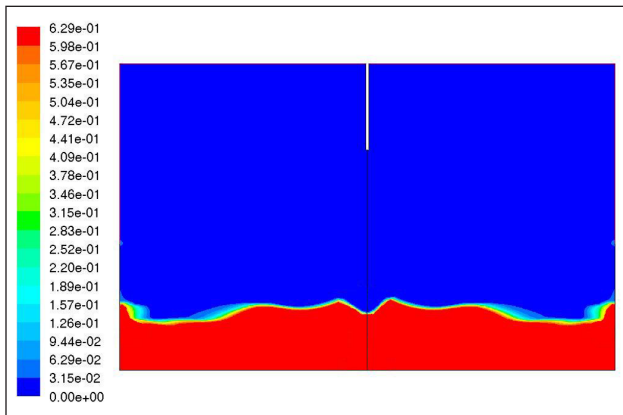
Participating Organization: Florida Institute of Technology (Dr. Pei-feng Hsu)



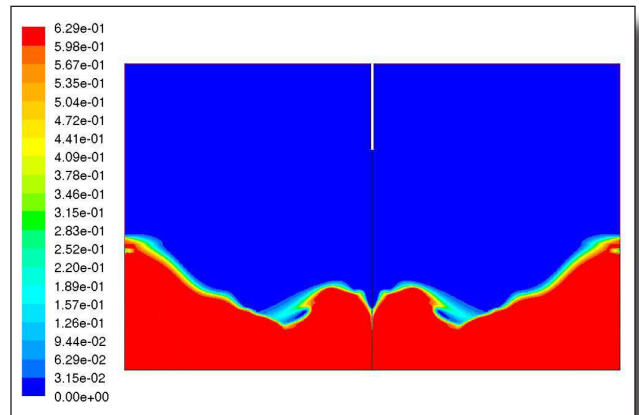
Sand volume fraction contour at $t = 0.5$ s Packing limit is 0.63.



Sand volume fraction contour at $t = 1.0$ s Packing limit is 0.63.



Sand volume fraction contour at $t = 0.5$ s Packing limit is 0.7.



Sand volume fraction contour at $t = 1.0$ s Packing limit is 0.7.

RESOLVE Projects: Lunar Water Resource Demonstration and Regolith Volatile Characterization



*In Situ Resource
Utilization (ISRU)
Oxygen Production*

To sustain affordable human and robotic space exploration, the ability to live off the land at the exploration site will be essential. NASA calls this ability *in situ* resource utilization (ISRU) and is focusing on finding ways to sustain missions first on the Moon and then on Mars.

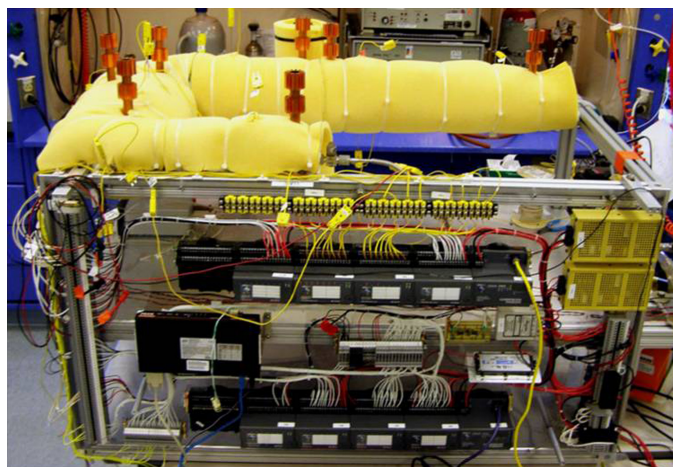
The ISRU project aims to develop capabilities to technology readiness level 6 for the Robotic Lunar Exploration Program and early human missions returning to the Moon. NASA is concentrating on three primary areas of ISRU: (1) excavating, handling, and moving lunar regolith, (2) extracting oxygen from lunar regolith, and (3) finding, characterizing, extracting, separating, and storing volatile lunar resources, especially in the permanently shadowed polar craters.

To meet the challenges related to technology development for these three primary focus areas, the Regolith and Environment Science and Oxygen and Lunar Volatile Extraction (RESOLVE) project was initiated in February 2005, through funding by the Exploration Systems Mission Directorate. RESOLVE's objectives are to develop requirements and conceptual designs and to perform breadboard concept verification testing of each experiment module. The final goal is to deliver a flight prototype unit that has been tested in a relevant lunar polar environment.

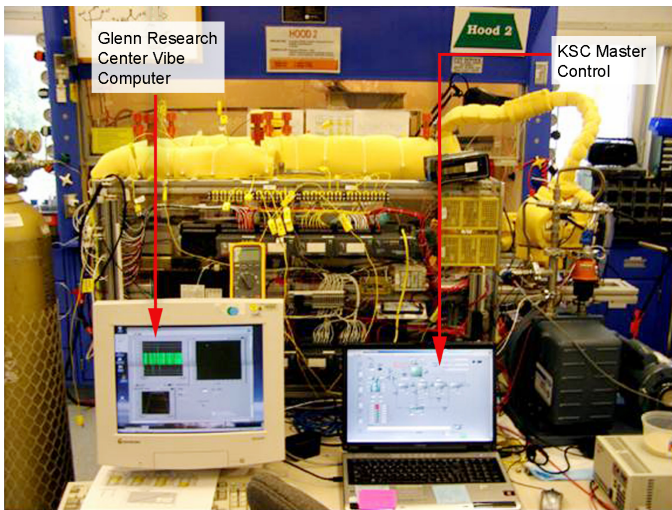
Here we report progress toward the third primary area—creating ways to find, characterize, extract, separate, and store volatile lunar resources. The tasks include studying thermal, chemical, and electrical ways to collect such volatile resources as hydrogen, water, nitrogen, methane, and ammonia. We approached this effort through two subtasks: lunar water resource demonstration (LWRD) and regolith volatile characterization (RVC).

For the LWRD, we

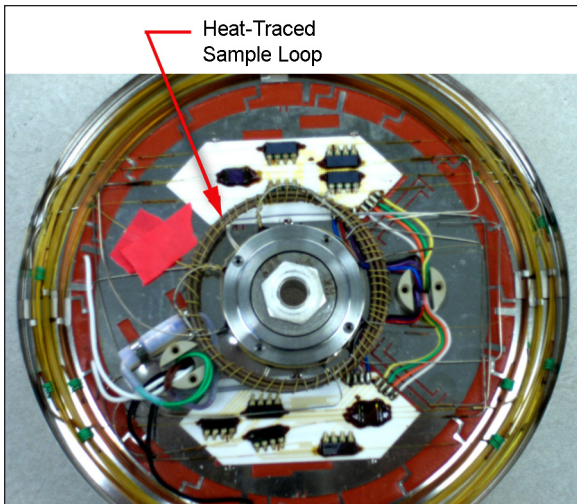
- developed methods for capturing and releasing hydrogen and water from a representative sample consisting of lunar simulant and representative gas mixtures,
- produced a water droplet from the captured water,
- reacted the water from the droplet in an electrolyzer to form hydrogen and oxygen,
- designed and built an engineering breadboard unit to demonstrate hydrogen and water capture from a representative sample, and
- performed a successful integrated test with RVC, demonstrating hydrogen and water capture, as well as electrolysis of water to form hydrogen and oxygen.



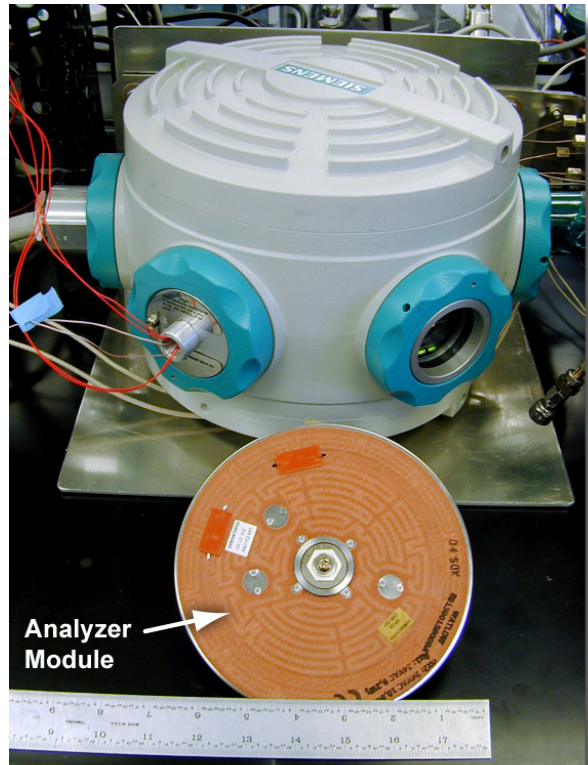
Final LWRD module.



Integrated LWRD/RVC engineering breadboard unit, showing computer controls.



Nichrome wire heat tracing for Siemens MicroSAM GC sample loop.



Siemens MicroSAM GC and Analyzer Module.

For the RVC, we

- identified a commercially available, process-control gas chromatography (GC) system of unusually small size, with extensive microelectromechanical systems technology capable of separating and quantifying gases of interest in short analysis times,
- modified the GC system to enable better quantification of water,
- optimized the GC system for water, hydrogen, and helium analysis, and
- developed an analysis method to successfully separate and quantify all permanent gases used in the representative samples (hydrogen, nitrogen, carbon dioxide, and carbon monoxide), including water.

Contacts: Dr. Janine E. Captain <Janine.E.Captain@nasa.gov>, NASA-KSC, (321) 867-6970; and Dr. Dale E. Lueck <Dale.E.Lueck@nasa.gov>, NASA-KSC, (321) 867-8764

Participating Organizations: NASA-KSC (Thomas J. Moss, Curtis M. Ihlefeld, and Dr. Jacqueline W. Quinn) and ASRC Aerospace (Dr. Tracy L. Gibson, Dr. Stephen A. Perusich, Steven L. Parks, Kevin A. Murland, and Walter B. Turner)

Tribocharging Lunar Soil for Electrostatic Beneficiation

2006 Center Director's Discretionary Fund Project



In Situ Resource
Utilization (ISRU)
Oxygen Production

Future human lunar habitation requires using *in situ* materials for both structural components and oxygen production. Lunar bases must be constructed from thermal- and radiation-shielding materials that will provide significant protection from the harmful cosmic energy which normally bombards the lunar surface. In addition, shipping oxygen from Earth is weight-prohibitive, and therefore investigating the production of breathable oxygen from oxidized mineral components is a major ongoing NASA research initiative. Lunar regolith may meet the needs for both structural protection and oxygen production. Already a number of oxygen production technologies are being tested, and full-scale bricks made of lunar stimulant have been sintered. The beneficiation, or separation, of lunar minerals into a refined industrial feedstock could make production processes more efficient, requiring less energy to operate and maintain and producing higher-performance end products.

The method of electrostatic beneficiation used in this research charges mineral powders (lunar simulant) by contact with materials of a different composition. The simulant acquires either a positive or negative charge depending upon its composition relative to the charging material. The charged particles can then undergo electrostatic separation in an electric field based upon their charge-to-mass ratio (Q/M). Characteristics such as bulk, surface composition, and particle size influence the ability of the material to garner a charge and separate under the influence of the electric field. The lunar regolith grains and the lunar environment are ideal for triboelectrification and electrostatic separation because the lack of moisture prevents the grains from sticking together and the lower gravitational pull permits longer contact times during charging and increased particle separation.

After successful beneficiation experiments had shown proof-of-concept with JSC-1 lunar simulant, an application to use lunar regolith was accepted by the lunar curator at Johnson Space Center. All the beneficiation experiments performed with JSC-1 lunar simulant were then repeated with Apollo 14163 lunar soil samples.

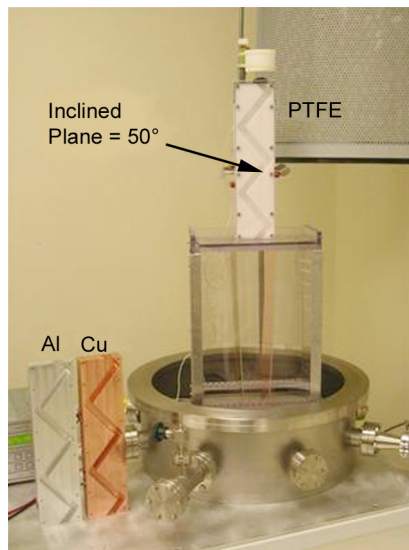


Figure 1. Inclined-plane charger and charge separator experimental setup.

Three inclined-plane tribochargers were constructed of copper, aluminum, and polytetrafluoroethylene (PTFE). These materials were selected because they offer different charging capabilities, and consequently separate the soil differently. The inclined-plane charger (Figure 1) was made from a block of material with a zigzag pathway (at an optimum angle of 50° as determined by friction studies performed prior to construction) cut the length of the block from top to bottom. Simulant was fed directly from the inclined-plane charger into an electrostatic separator between two charged plates (one positive and one negative) and collected as separate fractions.

X-ray photoelectron spectroscopy (XPS) was performed for the purpose of characterizing chemical composition before and after beneficiation. The XPS data (see the table) shows a change in the chemical composition of a number of elements in each of the beneficiated fractions.

Mean relative percentage change in elemental concentration compared with starting sample for Apollo 14163 lunar regolith, using aluminum charger (particle size = 50 to 75 μm).

Sample	Na	Fe	O	Ti	Ca	C	Si	Al
Positive plate	23	15	8	70	–*	–20	8	–*
Negative plate	7	–8	–10	–20	–7	7	–*	–*
Unseparated	–*	31	16	210	21	–44	15	17

* Relative changes are within error.

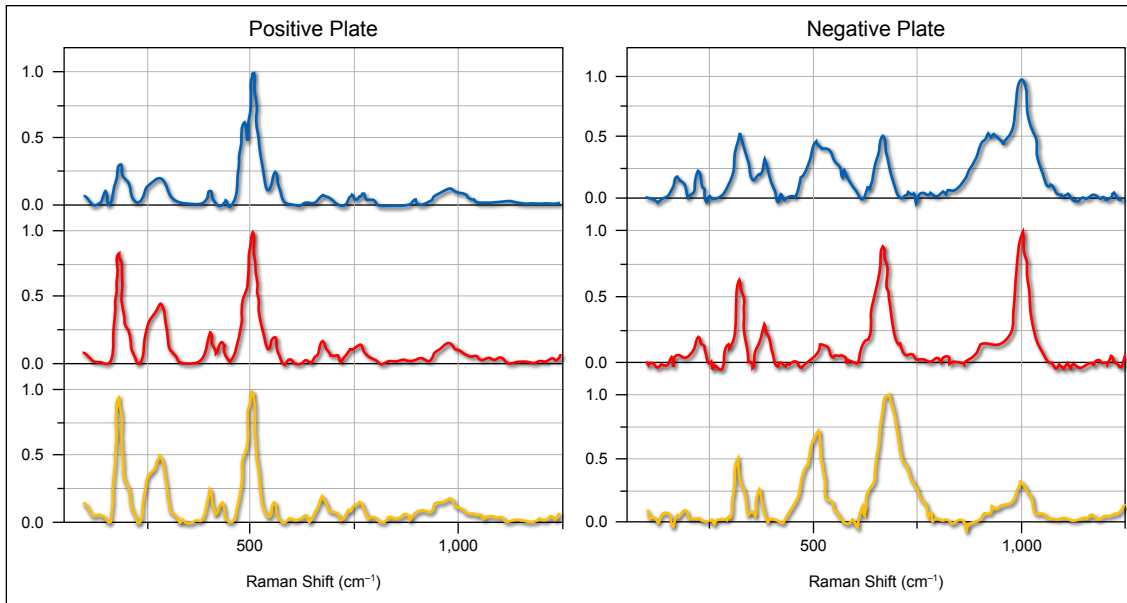


Figure 2. Raman spectra of beneficiated Apollo 14 samples, using an aluminum tribocharger.

Raman spectroscopy was performed for the purpose of characterizing the mineralogy of the samples before and after beneficiation. The Raman data (Figure 2) shows the difference in spectra between the different beneficiated fractions that result from the different mineral compositions. The positive plate is composed mostly of plagioclase. A few extra minerals are present, but their corresponding peaks are of low intensity. The negative plate is a mixture of solid solution α $\text{Fe}_2\text{O}_3/\text{FeTiO}_3$ (226 cm^{-1}), Pseudobrookite – FeTiO_5 (323 cm^{-1}), plagioclase, ilmenite (FeTiO_3), and pyroxene ($997, 1,000\text{ cm}^{-1}$).

The newly designed tribocharging setup successfully charged and separated JSC-1 lunar simulant and Apollo 14 lunar soil. It also provided preliminary data indicating enrichment of iron- and titanium-rich minerals in a vacuum. This technique may prove to be a viable tool for specific mineral enrichment of regolith prior to oxygen production processing or other structural-material processing. Future work will focus on optimizing the length of the tribocharger and the charge separator, as well as possible integration into the *In Situ* Resource Utilization project's engineering breadboard unit.

Contacts: Dr. Jacqueline W. Quinn <Jacqueline.W.Quinn@nasa.gov>, NASA-KSC, (321) 867-8410; and Dr. Steve Trigwell <Steven.Trigwell-1@nasa.gov>, ASRC Aerospace, (321) 867-1222

Participating Organizations: University of Central Florida (James G. Captain); University of Arkansas (Dr. Alex S. Biris); and NASA-KSC (Dr. Carlos I. Calle, Ellen E. Arens, and Dr. Janine E. Captain)

Numerically Modeling the Erosion of Lunar Soil by Rocket Exhaust Plumes

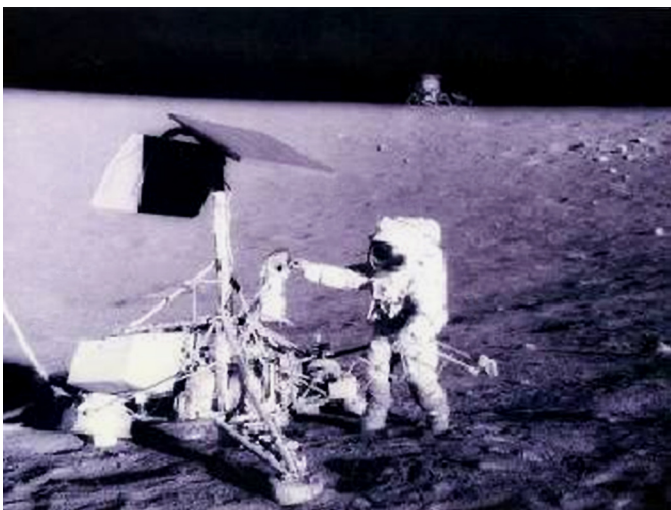
2006 Center Director's Discretionary Fund Project



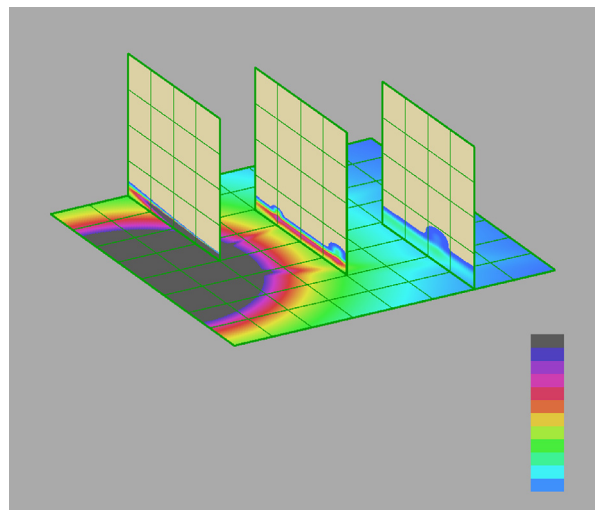
Site Preparation
and Excavation

In preparation for the Apollo program, Leonard Roberts of the NASA Langley Research Center developed a remarkable analytical theory that predicts the blowing of lunar soil and dust beneath a rocket exhaust plume. Roberts assumed that the erosion rate was determined by the excess shear stress in the gas (the amount of shear stress greater than what causes grains to roll). The acceleration of particles to their final velocity in the gas consumes a portion of the shear stress. The erosion rate continues to increase until the excess shear stress is exactly consumed, thus determining the erosion rate. Roberts calculated the largest and smallest particles that could be eroded based on forces at the particle scale, but the erosion rate equation assumed that only one particle size existed in the soil. He assumed that particle ejection angles were determined entirely by the shape of the terrain, which acts like a ballistic ramp, with the particle aerodynamics being negligible. The predicted erosion rate and the upper limit of particle size appeared to be within an order of magnitude of small-scale terrestrial experiments but could not be tested more quantitatively at the time. The lower limit of particle size and the predictions of ejection angle were not tested.

We observed in the Apollo landing videos that the ejection angles of particles streaming out from individual craters were time-varying and correlated to the Lunar Module thrust, thus implying that particle aerodynamics dominate. We modified Roberts' theory in two ways. First, we used ad hoc the ejection angles measured in the Apollo landing videos, in lieu of developing a more sophisticated method. Second, we integrated Roberts' equations over the lunar-particle size distribution and obtained a compact expression that could be implemented in a numerical code. We also added a material damage model that predicts the number and size of divots which the impinging particles will cause in hardware surrounding the landing rocket. Then, we performed a long-range ballistics analysis for the ejected particulates.



The Apollo 12 Lunar Module landed approximately 160 m from the deactivated Surveyor III spacecraft. Blowing sand grains pitted Surveyor's surface with microscopic craters, and the blowing dust particles eroded a thin layer of material from its surface.

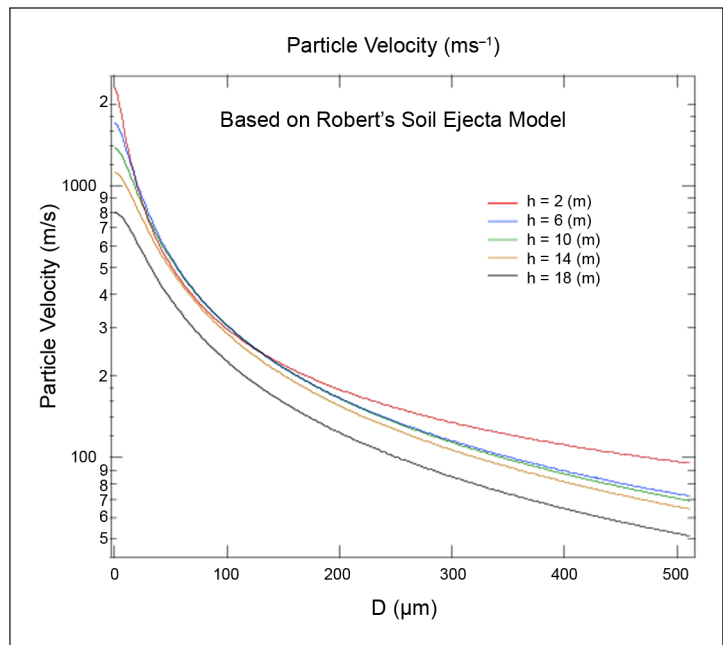


Output of modified Roberts' model showing mass flux in a 3-D map. Particles ejected from surface craters at higher angles create inhomogeneities.

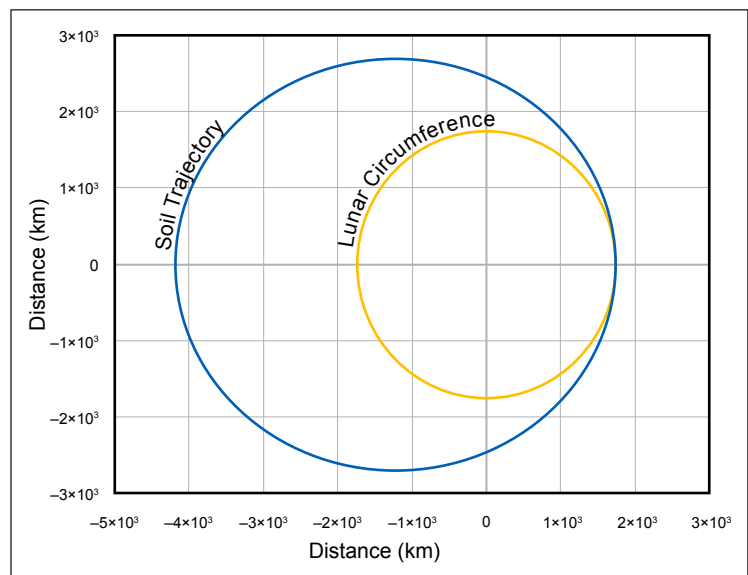
We compared the model's predictions with the divots observed in the Surveyor III hardware returned by the Apollo 12 astronauts. The model predicted about three divots per square centimeter compared to the one-half to five divots per square centimeter measured on the Surveyor. We compared the model's predictions for entrained-particle concentration with the concentration implied by the optical density in the Apollo landing videos. The model predicts 10^6 particles per cubic meter in the dust cloud. The Apollo landing videos indicate the true number was closer to 10^8 . This large error is almost certainly due to the form of Roberts' cohesion force equation, which apparently overestimates the lower limit of particle size. The ballistics indicate that the particles travel the circumference of the Moon, nearly reaching escape velocity, although Roberts' model may be overestimating the velocities. In ongoing work, we are correcting the cohesive force and lower limit of particle size, coupling the model to modern gas flow codes, including particle collisions in the erosion rate equation, and making other necessary improvements.

Contact: Dr. Philip T. Metzger
 <Philip.T.Metzger@nasa.gov>, NASA-KSC,
 (321) 867-6052

Participating Organization: ASRC Aerospace
 (Dr. Christopher D. Immer and Dr. John E. Lane)



Predicted particle velocities as a function of particle diameter and lander height.



Ballistic trajectory for particles traveling at predicted velocities transverse nearly the circumference of the Moon.

Trajectory Model of Lunar Dust Particles



Site Preparation
and Excavation

The goal of this work was to predict the trajectories of blowing lunar regolith (soil) particles when a spacecraft lands on or launches from the Moon. The blown regolith is known to travel at very high velocity and to damage any hardware located nearby on the Moon. It is important to understand the trajectories so we can develop technologies to mitigate the blast effects for the launch and landing zones at a lunar outpost. A mathematical model was implemented in software to predict the trajectory of a single spherical mass acted on by the gas jet from the nozzle of a lunar lander. As initial conditions, the trajectory calculation uses the particle diameter D and initial position of the particle $r_0 = (x_0, y_0, z_0)$, where the vertical direction x is positive up and equal to zero at the surface. Typically, the user sets the particle's starting position above the surface as $x_0 = D/2$.

The model uses an input file that contains data for the forces created by high-velocity gas flow. The model can use data in either of the following formats:

Two-dimensional: Based on cylindrical symmetry, in this format, the problem is set up to be independent of the azimuth angle. The two-dimensional data used in this project was created by computational fluid dynamics (CFD) software.

Three-dimensional: The full three-dimensional case makes no assumption of symmetries. Three-dimensional data was created with Direct Simulation Monte Carlo (DSMC) software, which uses probabilistic simulation to solve the Boltzmann equation for fluid flows. Individual molecules are moved through a simulation of physical space in a realistic manner that is directly coupled to physical time such that unsteady flow characteristics can be modeled. Intermolecular collisions and molecule-surface collisions are calculated by means of probabilistic, phenomenological models. The DSMC method assumes that the molecular movement and collision phases can be decoupled over periods shorter than the mean collision time. Figures 1 and 2 show simulation model geometry on the lunar surface with corresponding simulated craters.

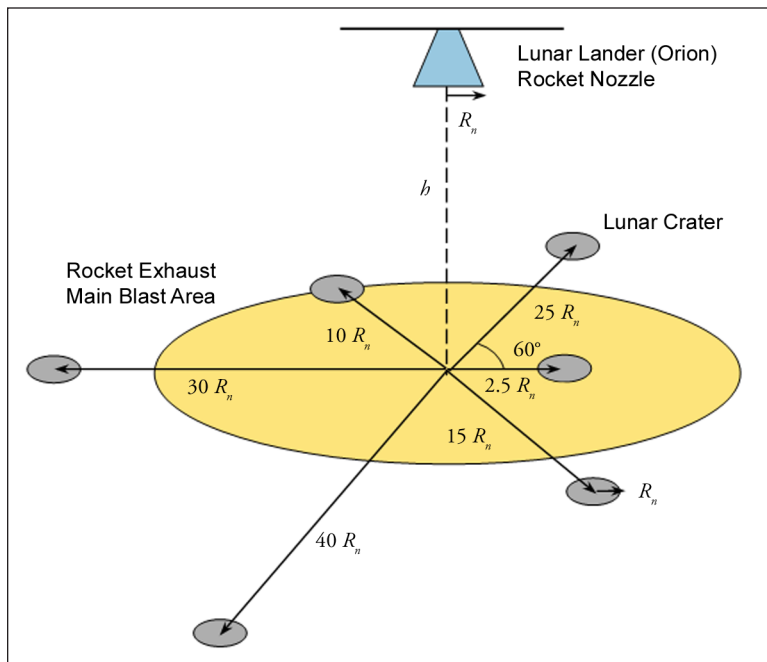


Figure 1. Three-dimensional simulation geometry with equal-size craters at varying distances from the rocket blast center.

For a particle of diameter D and mass m , the trajectory from drag can be estimated by a Taylor series expansion about time point k , resulting in a set of discrete-difference equations for position and velocity, using constant lunar gravity g_L and lunar soil particle density ρ_L . The CFD/DSMC output provides estimates of gas density $\rho(\mathbf{r})$ and gas velocity $\mathbf{u}(\mathbf{r})$. These values are interpolated from the CFD/DSMC grid by the identification of the nearest grid neighbors around the k th trajectory point and the application of an N-dimensional interpolation algorithm. See Figure 3.

The coefficient of drag, C_D , is a function of the computed Reynolds number, R_e . Lift acceleration caused by the vertical gradient of the horizontal component of gas flow is also computed, with the use of an estimated coefficient of lift, C_L . Since particle lift and drag coefficients (especially lift) are unknown at these high Mach and rarefied flow

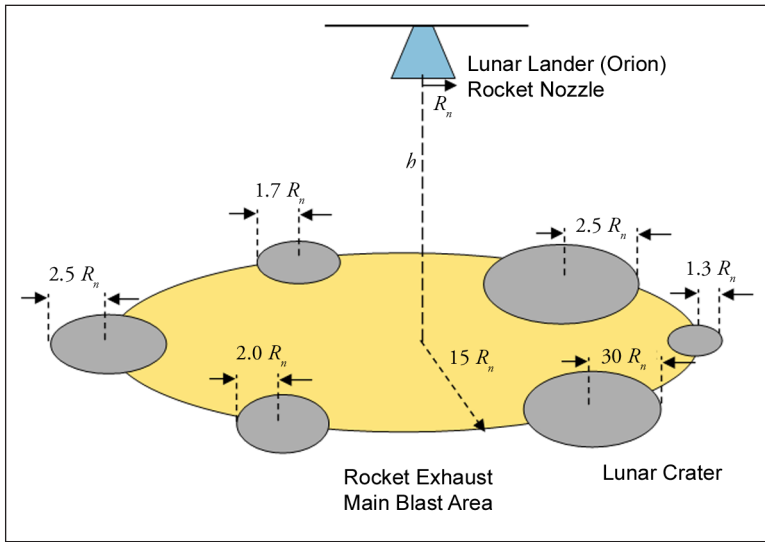


Figure 2. Three-dimensional simulation geometry with varying crater sizes at equal distances from the rocket blast center.

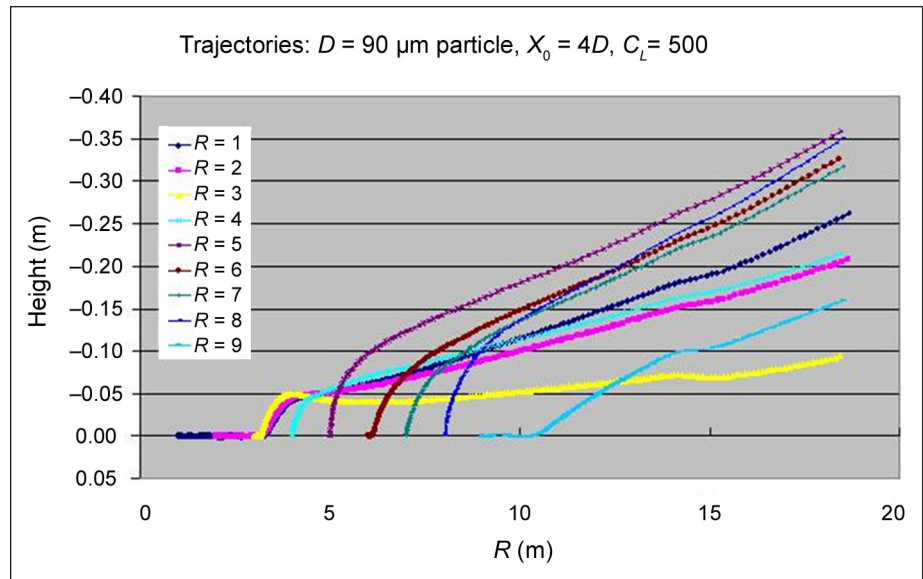


Figure 3. Trajectory plots of 90- μm lunar dust particles initialized to varying distances from the rocket blast center.

conditions, the simulation results for various particle sizes and trajectory angles are adjusted ad hoc to match Apollo video photogrammetry.

The gas properties, density, velocity vector, and temperature predicted by the CFD/DSMC simulations allow us to compute the forces on a single particle of regolith. Once these forces are known, the trajectory path and velocity of the particle are computed. Note that all calculations of trajectory assume that the duration of particle flight is much shorter than the change in gas properties. In other words, the particle trajectory calculations take into account the spatial variation of the gas jet, but not the temporal variation. This is a reasonable first-order assumption.

Contact: Dr. Philip T. Metzger <Philip.T.Metzger@nasa.gov>, NASA-KSC, (321) 867-6052

Participating Organization: ASRC Aerospace (Dr. Christopher D. Immer and Dr. John E. Lane)

Using Lunar Module Shadows To Scale the Effects of Rocket Exhaust Plumes



Site Preparation
and Excavation

Excavating granular materials beneath a vertical jet of gas involves several physical mechanisms. These occur, for example, beneath the exhaust plume of a rocket landing on the soil of the Moon or Mars. We performed a series of experiments and simulations (Figure 1) to provide a detailed view of the complex gas-soil interactions. Measurements taken from the Apollo lunar landing videos (Figure 2) and from photographs of the resulting terrain helped demonstrate how the interactions extrapolate into the lunar environment. It is important to understand these processes at a fundamental level to support the ongoing design of higher-fidelity numerical simulations and larger-scale experiments. These are needed to enable future lunar exploration wherein multiple hardware assets will be placed on the Moon within short distances of one another. The high-velocity spray of soil from the landing spacecraft must be accurately predicted and controlled or it could erode the surfaces of nearby hardware. This analysis indicated that the lunar dust is ejected at an angle of less than 3 degrees above the surface, the results of which can be mitigated by a modest berm of lunar soil. These results assume that future lunar landers will use a single engine. The analysis would need to be adjusted for a multiengine lander.

Figure 3 is a detailed schematic of the Lunar Module camera calibration math model. In this chart, formulas relating the known quantities, such as sun angle and Lunar Module dimensions, to the unknown quantities are depicted. The camera angle Ψ is determined by measurement of the imaged aspect ratio of a crater, where the crater is assumed to be circular. The final solution is the determination of the camera calibration factor, α .

Figure 4 is a detailed schematic of the dust angle math model, which again relates known to unknown parameters. The known parameters now include the camera calibration factor and Lunar Module dimensions. The final computation is the ejected dust angle, as a function of Lunar Module altitude.

Contact: Dr. Philip T. Metzger <Philip.T.Metzger@nasa.gov>, NASA-KSC, (321) 867-6052

Participating Organization: ASRC Aerospace (Dr. Christopher D. Immer and Dr. John E. Lane)

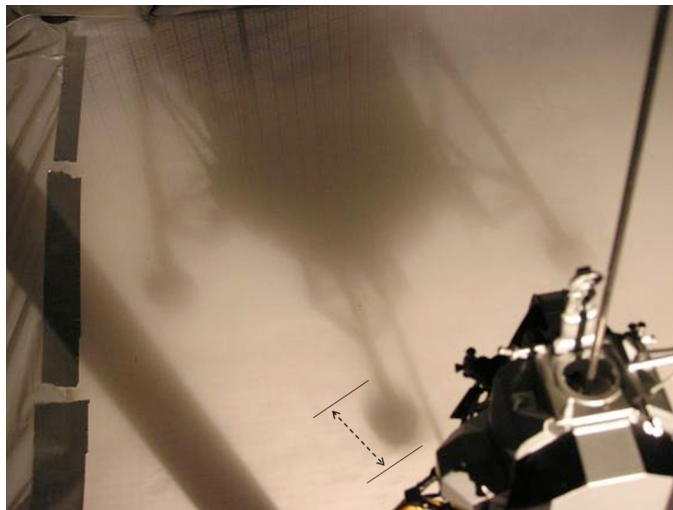


Figure 1. Scale model with “dust” beneath the angled transparent sheet.

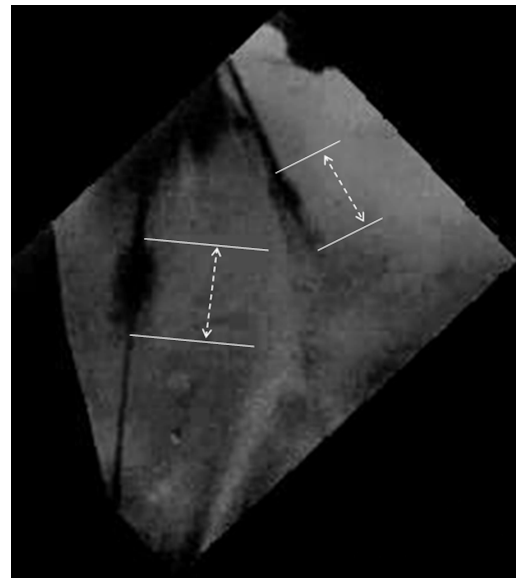


Figure 2. Video frame of Apollo 17 descent shadow, showing foot pad elongation resulting from the dust layer.

Predicting the Acoustic Environment Induced by the Launch of the Ares I Vehicle



Decision/Data
Models and
Analysis

The exhaust plumes of launch vehicles impose severe heating rates, pressures, and vibroacoustic loads on ground support equipment (GSE) on the Mobile Launcher (ML), as well as on the vehicle itself. The vibroacoustic environment must be predicted before the criteria for the acceptance and qualification testing of GSE components and their installations can be determined.

Near-field launch noise levels are traditionally computed as described in NASA SP-8072, "Acoustic Loads Generated by the Propulsion System," published in 1971. Figure 1 illustrates the method for determining the noise load on the vehicle. The rocket exhaust plume is a distribution of acoustic sources, each of which propagates to a point on the vehicle. The report contains empirical models for determining the strength and distribution of the noise and includes simple factors for various types of deflectors (Figure 1).

Since SP-8072 was published, there has been considerable research in jet and rocket noise modeling and sound propagation. For example, the overall sound power model in SP-8072 was based on a simple acoustic efficiency factor and is not consistent with Lighthill's well-established jet noise theory. Consistent rocket noise models, more recent research on source distributions and characteristics, and a much better understanding of the shielding of noise by parts of the launcher itself are now available.

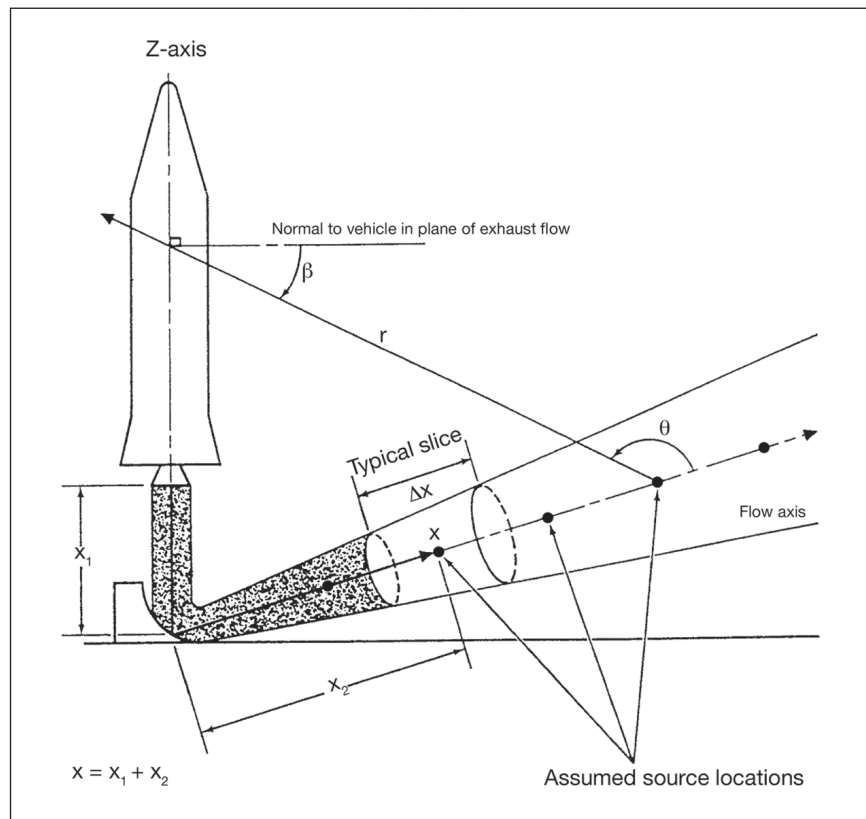


Figure 1. Noise modeling sketch from NASA SP-8072 shows the predominant angle of maximum noise generation.

The sketch in Figure 2 shows a launcher deck and general location of the receivers along the launch tower. Figure 3 shows the vehicle rising past the tower. Various propagation paths are indicated, including those in areas where the launcher deck provides shielding.

This project updates launch noise modeling in the following ways:

- It provides the overall sound power emission of the rocket with the Lighthill-consistent method developed by Sutherland.
- It updates distributions of noise along the plume with the empirical work of Sutherland, McNerny, et al., and by the recent theoretical and laboratory work of Harper-Bourne and others.
- It computes the shielding of propagation paths by the launcher deck via Maekawa's thin screen diffraction model.
- It uses the modern ground impedance model of Chien and Soroka to address how ground reflection affects propagation, and it uses current ANSI/ISO standards to determine the effects of absorption by air.

Key accomplishments were reviewing SP-8072 methodology and identifying components requiring update, generalizing the methodology for off-vehicle locations (in particular, locations on the launch tower), and identifying current technology to be used in updating predictions.

Contact: Dr. Bruce T. Vu <Bruce.T.Vu@nasa.gov>, NASA-KSC, (321) 867-2376

Participating Organization: Wyle Laboratories (Dr. Kenneth J. Plotkin)

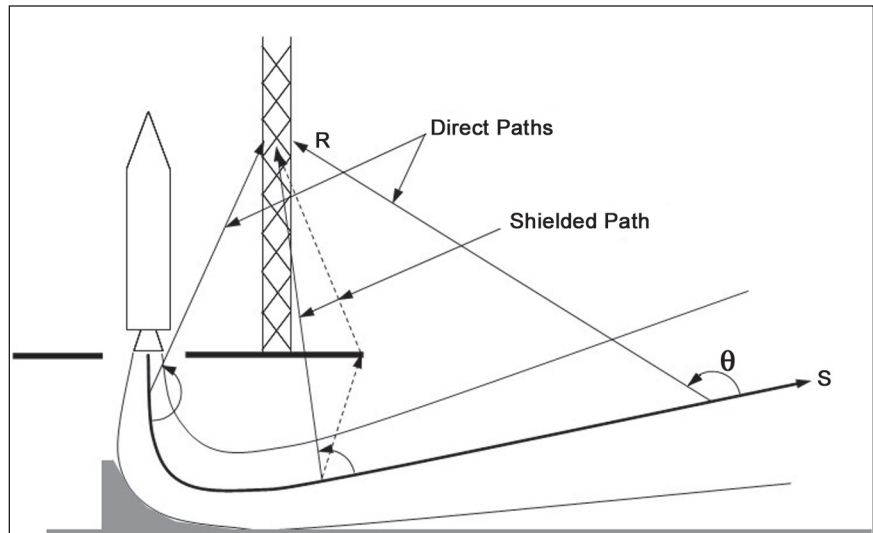


Figure 2. Noise modeling is shown for a mobile launcher with a rocket on the pad.

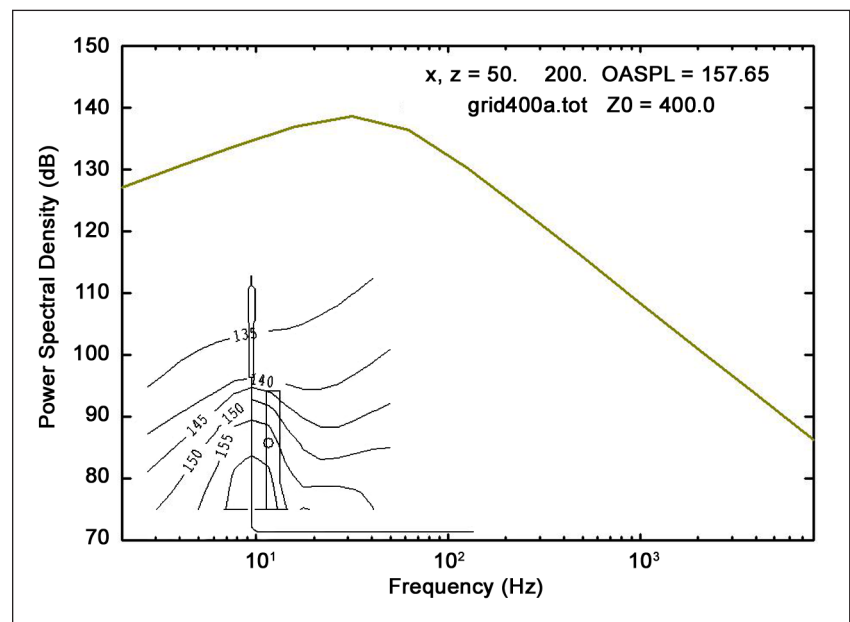


Figure 3. Noise contours and spectrum shown for a mobile launcher with a vehicle rising past the tower.

Measuring Ultrasonic Acoustic Velocity in a Thin Sheet of Graphite Epoxy Composite



Spaceport/Range
Situational
Awareness

A method for measuring the acoustic velocity in a thin sheet of a graphite epoxy composite (GEC) material was investigated. This method uses two identical acoustic-emission (AE) sensors, one to transmit and one to receive. The delay time as a function of distance between sensors determines a bulk velocity. A lightweight fixture (balsa wood in the current implementation) provides a consistent method of positioning the sensors, thus providing multiple measurements of the time delay between sensors at different known distances. A linear fit to separation, x , versus delay time, t , will yield an estimate of the velocity from the slope of the line.

Figure 1 shows the test jig used to align the AE transducers for the velocity measurements. The transmitting and receiving sensors are identical. The transducer on the left is the excitation transducer (transmitter) and the transducer on the right is the receiver. Both transducers are model WD wideband AE sensors manufactured by Physical Acoustics Corporation. A small amount of vacuum grease couples the AE sensors to the GEC surface. Removing the jig before a measurement is recorded minimizes the effect of test fixture loading and coupling. After each set of measurements, the grease is removed with an industrial wipe soaked in isopropyl alcohol.

The excitation signal is generated from a 5-V, peak-to-peak, 360-kHz, sinusoidal pulse composed of eight full cycles. The oscilloscope top trace, on the left of Figure 2, shows the transmitted signal and a typical received signal on the bottom. Pulse data for six distances (2, 4, 6, 8, 10, and 12 cm) is recorded, with the oscilloscope sampling average set to eight sweeps in order to remove the majority of the random noise from the AE sensor signal. Figure 3 shows an example of all received pulses for two sets of runs of a GEC sample material. When the delay times, as a function of Δx are plotted (shown in Figure 4), a linear fit yields an estimate of the acoustic velocity as the slope of the curve.

Contacts: Dr. John E. Lane <John.E.Lane@nasa.gov>, ASRC Aerospace, (321) 867-6939; and Stanley O. Starr <Stanley.O.Starr@nasa.gov>, NASA-KSC, (321) 861-2262

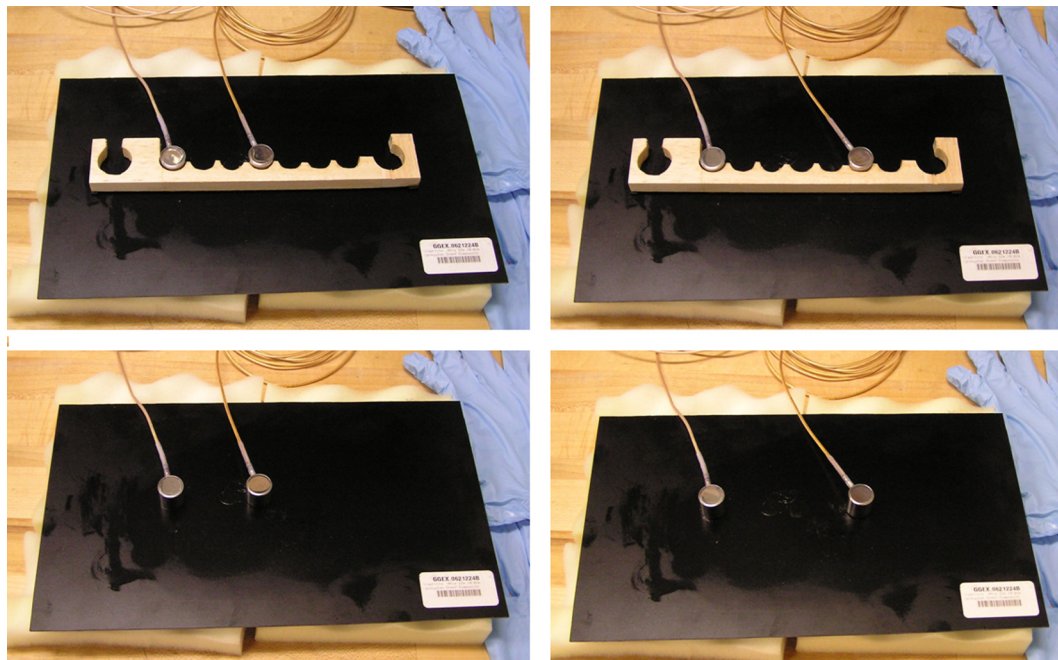


Figure 1. Ultrasonic Acoustic-Velocity Test: 6-cm separation (left); 10-cm separation (right). Top shows alignment with jig; bottom is signal measurement configuration.

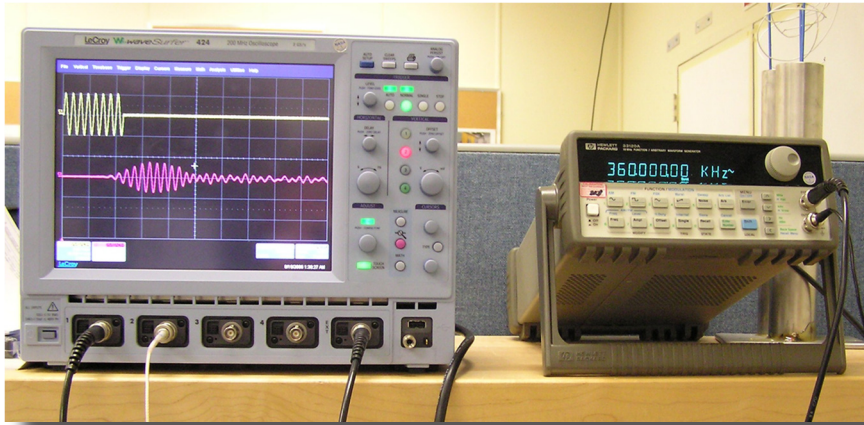


Figure 2. Signal generator (right) and oscilloscope (left): excitation signal (yellow trace) and received signal (pink trace).

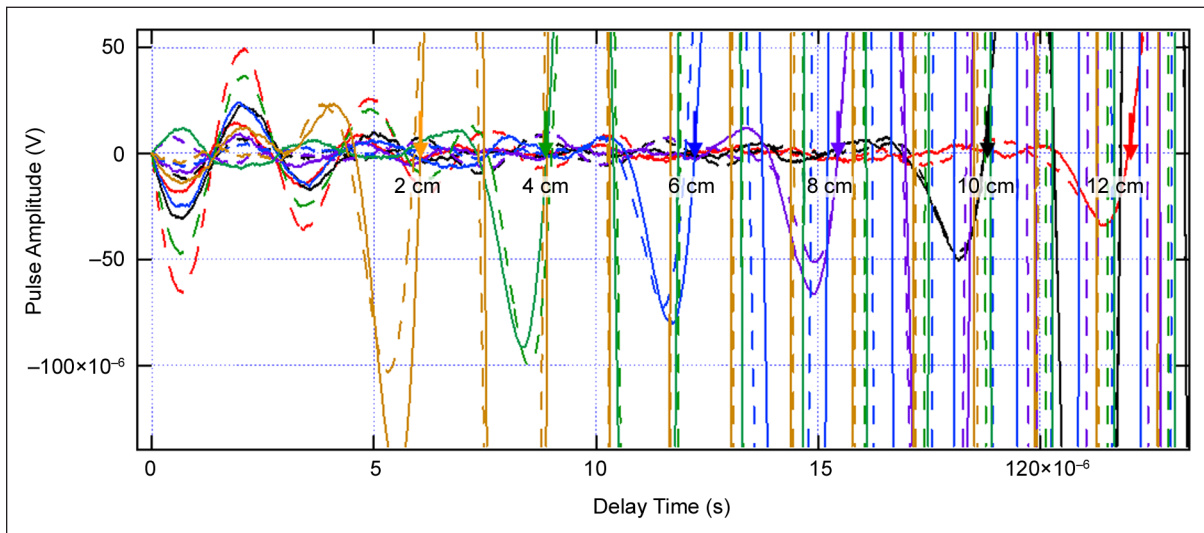


Figure 3. The first major zero crossing from negative to positive provides the delay time of the received signal. Each color represents a different separation of transmitter and receiver. Solid line is the first run; dotted line is a second run.

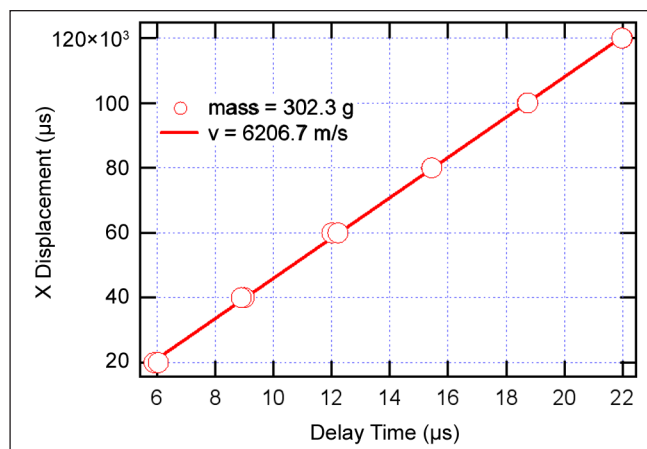
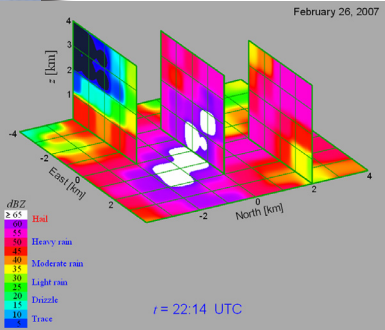
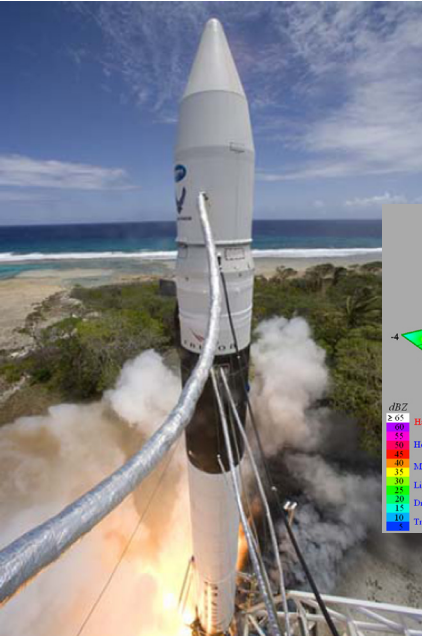
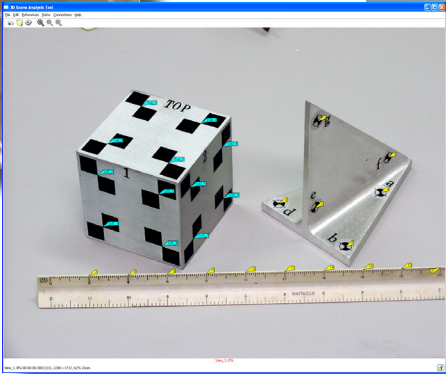
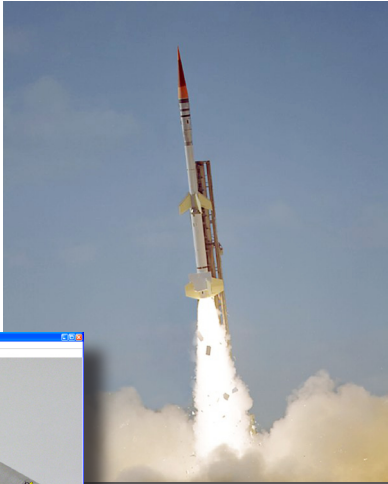
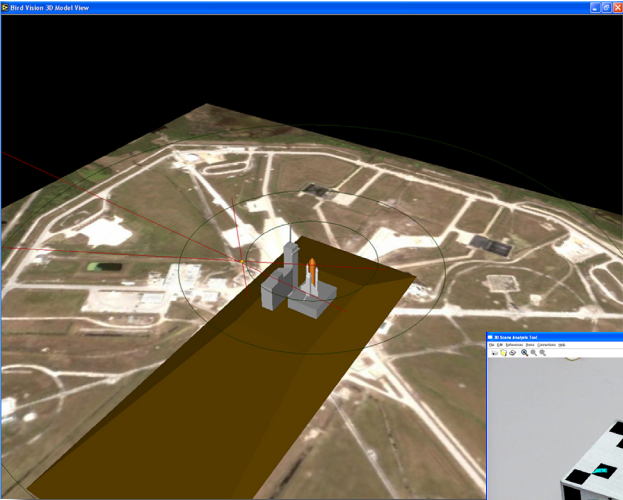


Figure 4. Delay times from Figure 3. Slope of x versus t provides an estimate of acoustic velocity.

Range Technologies



Hail Size Distribution Mapping



Localized-Weather
Forecasting and
Measurement

A 3-D weather radar visualization software program was developed and implemented as part of an experimental Launch Pad 39 Hail Monitor System. 3DRadPlot, a radar-plotting program, is one of several software modules that form building blocks of the hail data processing and analysis system (the complete software processing system under development). The spatial and temporal mapping algorithms were originally developed through research at the University of Central Florida, funded by NASA's Tropical Rainfall Measurement Mission (TRMM), where the goal was to merge National Weather Service (NWS) Next-Generation Weather Radar (NEXRAD) volume reflectivity data with drop size distribution data acquired from a cluster of raindrop disdrometers. In this current work, we adapted these algorithms to process data from a cluster of hail disdrometers positioned around Launch Pads 39A or 39B, along with the corresponding NWS radar data. Radar data from all NWS NEXRAD sites is archived at the National Climatic Data Center (NCDC). That data can be readily accessed at <http://www.ncdc.noaa.gov/nexradin/>.

3DRadPlot plots Level III reflectivity data at four scan elevations (this software is available at Open Channel Software, <http://www.openchannelfoundation.org/projects/3DRadPlot>). By using spatial and temporal interpolation/extrapolation based on hydrometeor fall dynamics, we can merge the hail disdrometer array data coupled with local Weather Surveillance Radar-1988, Doppler (WSR-88D) radial velocity and reflectivity data into a 4-D (3-D space and time) picture of hail size distributions. Hail flux maps can then be generated and used for damage prediction and assessment over specific surfaces corresponding to structures within the disdrometer array volume. Immediately following a hail storm, specific damage areas and degree of damage can be identified for inspection crews.

Contact: Dr. John E. Lane John.E.Lane@nasa.gov, ASRC Aerospace, (321) 867-6939

Participating Organization: NASA-KSC (Dr. Robert C. Youngquist)

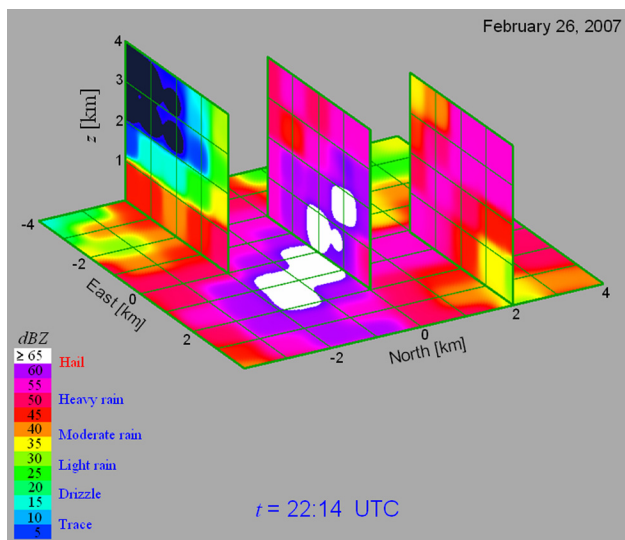


Figure 1a. Three-dimensional radar display plot, 8 km × 8 km × 4 km, centered on Pad 39A. Each grid line is 1 km. This reflectivity data corresponds to the severe hail event of February 26, 2007, which resulted in a 3-month delay of the launch of STS-117.

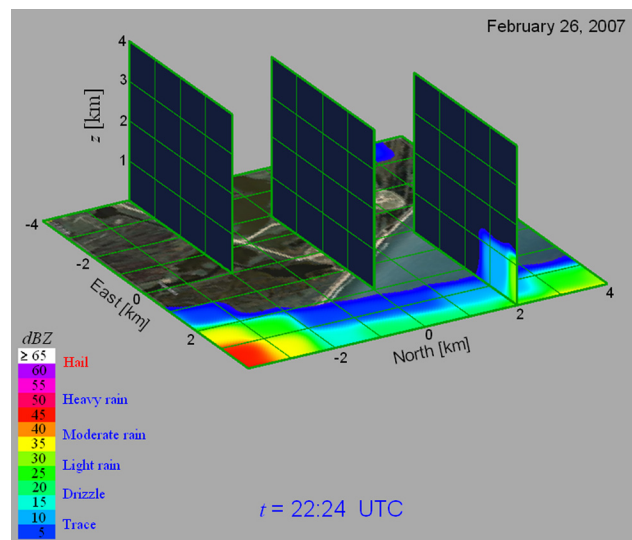


Figure 1b. Same 8-km × 8-km × 4-km view shown in Figure 1a but 10 minutes later, when Pad 39A was clear of hail and rain.

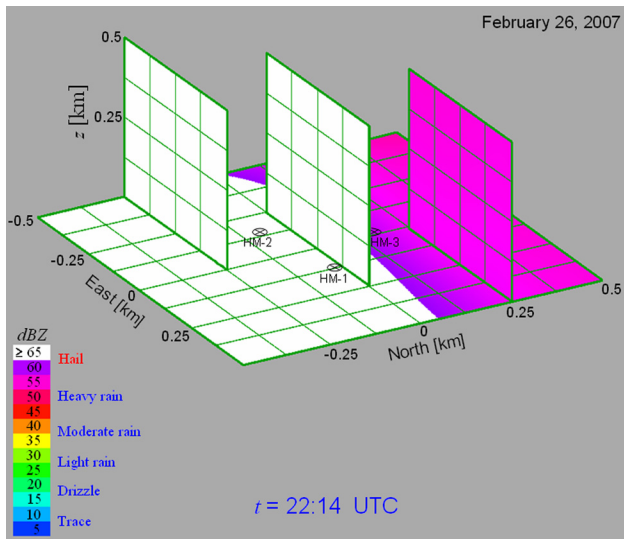


Figure 2a. Three-dimensional radar display plot, 1 km × 1 km × 0.5 km, centered on Pad 39A. Each grid line is 125 m. This NWS radar reflectivity data corresponds to the same time shown in Figure 1a.

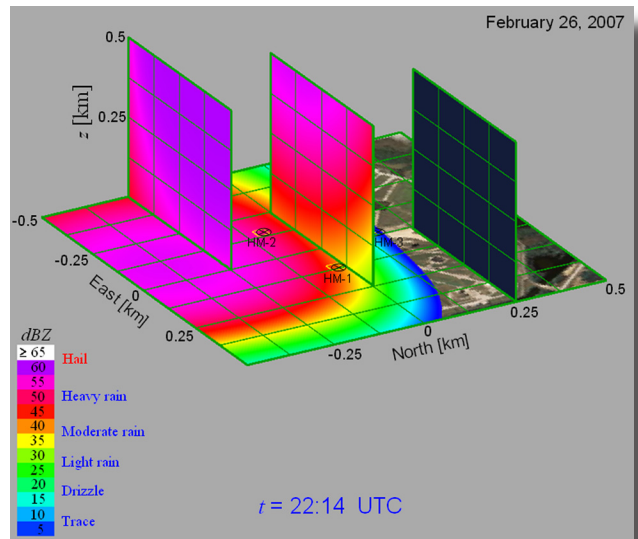


Figure 2b. Same 1-km × 1-km × 0.5-km 3-D view as shown in Figure 2a. This data is generated by the three hail monitor stations and is the equivalent hail reflectivity (minus rainfall background) that would be seen by radar if only hail were in the air.

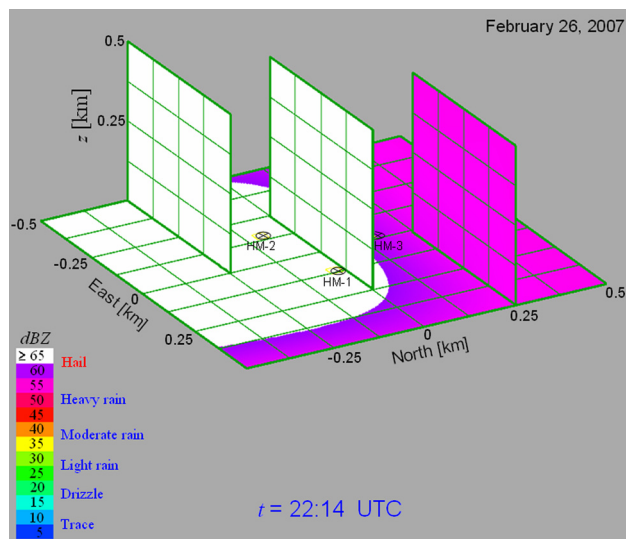


Figure 2c. Same plot as shown in Figure 2b, with a constant rain background added to the hail monitor data. The rain background is an estimate of what radar would see if only rain were in the air.

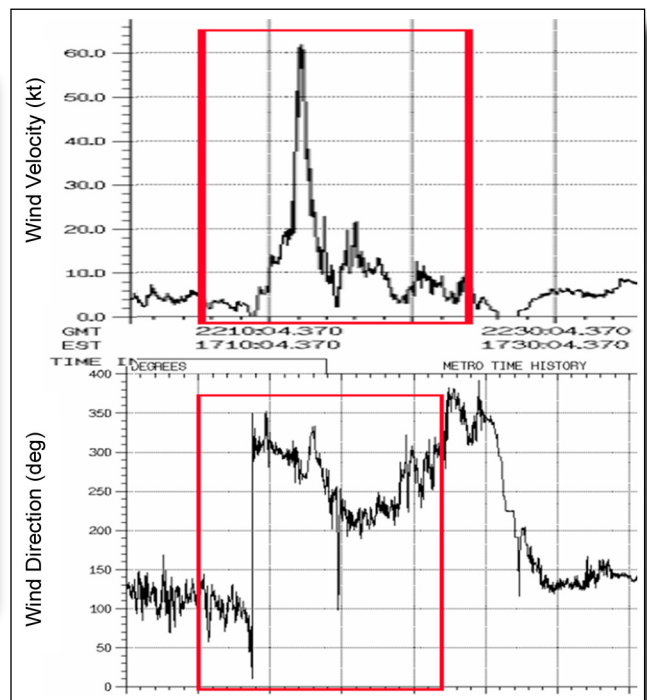


Figure 3. Wind tower data near Pad 39A, showing wind speed and direction. The wind speed peaked at over 60 kt during the hail event. The wind peak was very short (on the order of a minute). The entire hail event was on the order of 10 minutes, whereas the entire rain event was less than 1 hour.

Launch Pad 39 Hail Monitor Array System



Localized-Weather
Forecasting and
Measurement

Weather conditions at Kennedy Space Center are extremely dynamic, and they greatly affect the safety of the Space Shuttles sitting on the launch pads. For example, on May 13, 1999, the foam on the External Tank (ET) of STS-96 was significantly damaged by hail at the launch pad, requiring rollback to the Vehicle Assembly Building.

The loss of ET foam on STS-114 in 2005 intensified interest in monitoring and measuring damage to ET foam, especially from hail. But hail can be difficult to detect and monitor because it is often localized and obscured by heavy rain. Furthermore, the hot Florida climate usually melts the hail even before the rainfall subsides.

In response, the hail monitor array (HMA) system, a joint effort of the Applied Physics Laboratory operated by NASA and ASRC Aerospace at KSC, was deployed for operational testing in the fall of 2006. Volunteers from the Community Collaborative Rain, Hail, and Snow (CoCoRaHS) network, in conjunction with Colorado State University, continue to test duplicate hail monitor systems deployed in the high plains of Colorado.



Shuttle Launch Pads 39A and 39B.



Location of hail monitor stations, HM-1, HM-2, and HM-3, at Launch Pad 39A.

The HMA system consists of three stations approximately 500 ft from the launch pad. The hail monitor sensor is basically a metal plate in the shape of a shallow pyramid. It deflects hail from the sensor surface after one hit, thus preventing multiple bounces from the same hail stone. A microphone pickup is mounted beneath the center of the metal plate. The output of this microphone is connected to an electronic circuit that digitizes and processes the microphone signal and then transmits a trigger pulse to one of six output channels. Each output channel represents a signal that is twice as large as the previous channel, thereby categorizing the hail stone into one of six sizes, from diameters of about 10 to 20 mm, in 2-mm steps. The six output channels are connected to six liquid-crystal diode (LCD) counters, which create a permanent record of all hail hitting the sensor. The counters are manually reset after a hail storm.

The HMA system was first deployed to Launch Pad 39B for support of STS-115 in September 2006 and then to Pad 39A for support of STS-116 in December 2006. The system's deployment in support of STS-117 collected and analyzed data of foam damage from a freak hail storm on February 26, 2007, that delayed the launch of Atlantis for nearly two months (also see "Hail Size Distribution Mapping," page 52).

Support of STS-118 showed another important use of the hail monitor system. On July 13, 2007, hail was observed on the ground at the Vehicle Assembly Building, but no hail was recorded at the pad occupied by Endeavour. United Space Alliance Ground Operations personnel check the hail monitors every morning when a vehicle is on the pad and after any storm suspected of containing hail. If no hail is recorded by the hail monitors, the vehicle and pad inspection team has no need to conduct a thorough

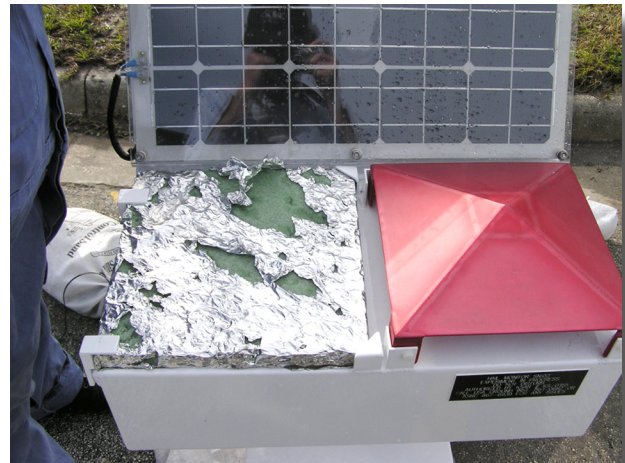


Hail monitor station 3 (HM-3) at Launch Pad 39A.

inspection of the vehicle immediately following a storm. During one week while Endeavour was on the pad, numerous hail storms occurred all around KSC. The HMA showed no detections, indicating that the Shuttle had not been damaged by hail at any time during those frequent local hail storms.

Contact: Dr. John E. Lane <John.E.Lane@nasa.gov>, ASRC Aerospace, (321) 867-6939

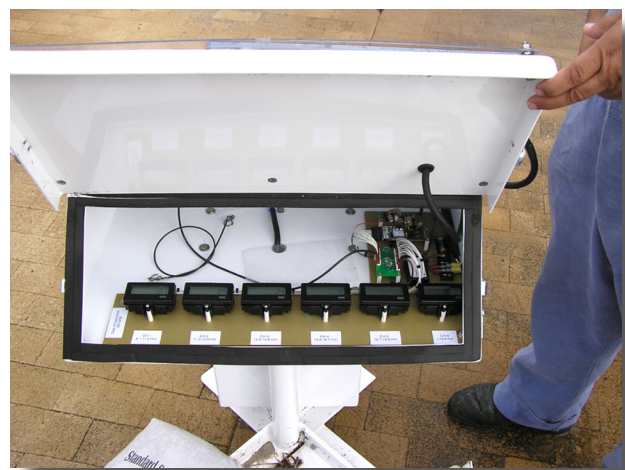
Participating Organizations: NASA-KSC (Dr. Robert C. Youngquist), ASRC Aerospace (William D. Haskell, Mark C. Minich, Joseph N. Dean, and Michael W. Csonka), CoCoRaHS, and Colorado State University



Close-up of HM-2 after February 26, 2007, hail event, showing ripping of the passive hail pad surface from 60-knot horizontal winds.



HM-2 after the February 26, 2007, severe hail event at Launch Pad 39A.



Under-the-hood view of HM-2, showing LCD counters and digital-signal-processing electronics.

Autonomous Flight Safety System – Phase III



Decision/Data
Models and
Analysis

The Autonomous Flight Safety System (AFSS) is a joint KSC and Wallops Flight Facility project that uses tracking and attitude data from onboard Global Positioning System (GPS) and inertial measurement unit (IMU) sensors and configurable rule-based algorithms to make flight termination decisions. AFSS objectives are to increase launch capabilities by permitting launches from locations without range safety infrastructure, reduce costs by eliminating some downrange tracking and communication assets, and reduce the reaction time for flight termination decisions.

The AFSS flew on a Terrier Improved-Orion two-stage sounding rocket at White Sands Missile Range on April 5, 2006. Two GPS sensors and two independently programmed processors were used, each with a different set of mission rules. The mission rules set for one processor were configured so that a nominal flight would not result in any flight termination actions. The mission for the other processor included three additional rules so that multiple destruct activations would occur during a nominal flight. Because the AFSS was not connected to a flight termination system, it could not initiate any destruct actions.

Preflight loading and verification went smoothly. However, the Ashtec G12 GPS receiver lost lock on liftoff and did not regain it until after the flight was over. The Javad GPS receiver maintained lock throughout the flight. The rocket behaved nominally, the nominal processor did not execute any unplanned destruct actions, and the errant processor successfully initiated three destruct actions as planned. Both processors provided navigation and status messages to observers via the vehicle telemetry stream. These messages were also stored in the nominal processor's nonvolatile (flash) memory for the entire operation. The errant processor's flash memory chip became partially dislodged during the flight and stopped recording at T+335 s. Otherwise, the system performed as expected.

An improved AFSS test article flew on the SpaceX Falcon 1 from the Kwajalein/Reagan Test Site on March 21, 2007. The test item consisted of a single chassis with redundant flight processors, a custom-built voting circuit, a power supply module, and a GPS receiver. An externally mounted GPS receiver and a 10-W Low-Cost Tracking and Data Relay System (TDRS) Transceiver (LCT2) for a

space-based range demonstration were also flown. The LCT2 was to transmit the status messages from one of the processors and the messages from the other processor were transmitted in the vehicle telemetry stream. Unfortunately, a concern was raised on launch day that the LCT2 might interfere with the vehicle GPS, and the Falcon 1 launch management team decided to fly with the LCT2 powered off. This meant that data from only one of the processors was available for postflight analysis.

Even with the loss of the LCT2 data, the AFSS met all the minimum success criteria. These included performing properly before the launch, maintaining at least one GPS solution, transmitting valid navigation data from at least one GPS receiver, transmitting mission rule evaluation status from at least one processor for the entire flight, and evaluating the full set of mission rules on at least one processor from launch to orbit insertion (or end of flight).



First AFSS sounding rocket test flight.



Falcon 1 launch vehicle at liftoff.

An anomaly in the navigation solution of the externally housed GPS receiver, caused when marginal satellites swapped in and out of track, led one processor to improperly flag first-stage burnout and second-stage ignition events. Because of a setup error, the system used the elapsed time from second-stage ignition as the time reference for tabulated, moving-gate coordinates instead of time from launch. These errors caused the two processors to issue ARM/FIRE commands at different times. In the future, acceleration data from one or more IMUs will be used for in-flight ignition and burnout event detection. Despite these anomalies, the inability to use the LCT2, and the rocket's failure to reach its desired orbit, the testing was a valuable experience and will lead to an improved AFSS.

Continuing efforts to improve the AFSS include making the chassis more rugged, formalizing the requirements and design, and adding a loosely coupled GPS/Inertial Navigation Solution (INS) to improve the reliability of the AFSS sensor suite. A prototype of this GPS/INS was flown on an F-104 at Kennedy Space Center on November 8, 2007. The equipment was integrated on the F-104 and recovered undamaged, but the GPS receiver did not function properly for reasons still being investigated. Consequently, the data collected was not sufficient to determine how the GPS/INS system performed. A second set of flights is planned for 2008.

Contacts: Dr. James C. Simpson <James.C.Simpson@nasa.gov>, NASA-KSC, (321) 867-6937; and Roger D. Zoerner <Roger.D.Zoerner@nasa.gov>, ASRC Aerospace, (321) 861-2960

The Photogrammetry Cube



Spaceport/Range
Situational
Awareness

We can determine distances between objects and points of interest in 3-D space to a useful degree of accuracy from a set of camera images by using multiple camera views and reference targets in the camera's field of view (FOV). The core of the software processing is based on the previously developed foreign-object debris vision trajectory software (see *KSC Research and Technology 2004 Annual Report*, pp. 2–5).

The current version of this photogrammetry software includes

- the ability to calculate distances between any specified point pairs,
- the ability to process any number of reference targets and any number of camera images,
- user-friendly editing features, including zoom in/out, translate, and load/unload,
- routines to help mark reference points with a “Find” function, while comparing them with the reference point database file, and
- a comprehensive output report in HTML format.

In this system, scene reference targets are replaced by a photogrammetry cube whose exterior surface contains multiple predetermined precision 2-D targets. Precise measurement of the cube's 2-D targets during the fabrication phase eliminates the need for measuring 3-D coordinates of reference target positions in the camera's FOV, using for example a survey theodolite or a Faroarm.

Placing the 2-D targets on the cube's surface required the development of precise machining methods. In response, 2-D targets were embedded into the surface of the cube and then painted black for high contrast. A 12-inch collapsible cube was developed for room-size scenes. A 3-inch, solid, stainless-steel photogrammetry cube was also fabricated for photogrammetry analysis of small objects.

Contacts: Dr. Robert C. Youngquist <Robert.C.Youngquist@nasa.gov>, NASA-KSC, (321) 867-1829; and Dr. John E. Lane <John.E.Lane@nasa.gov>, ASRC Aerospace, (321) 867-6939

Participating Organization: ASRC Aerospace (Robert B. Cox, Charles H. Curley, David P. Floyd, and Steven J. Klinko)

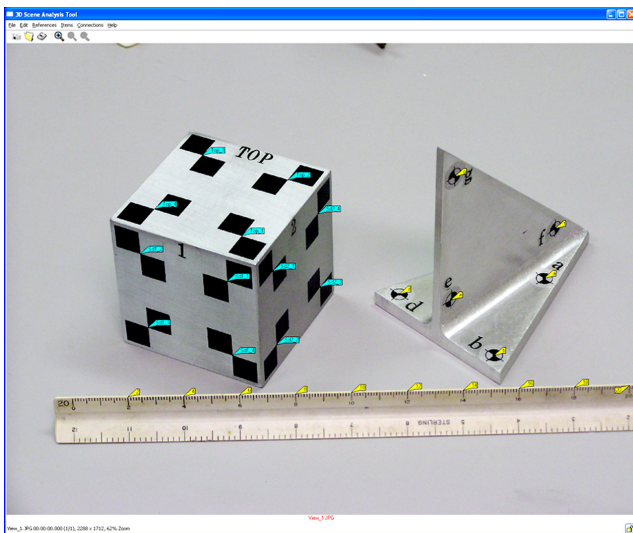


Figure 1a. A 3-in by 3-in photogrammetry cube and test object. The ruler is used to estimate the degree of lens distortion.

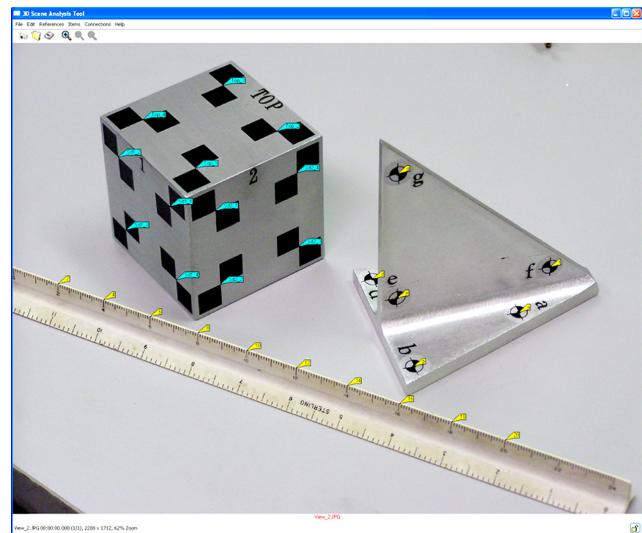


Figure 1b. The 3-in by 3-in photogrammetry cube and a test object, from a different viewpoint.

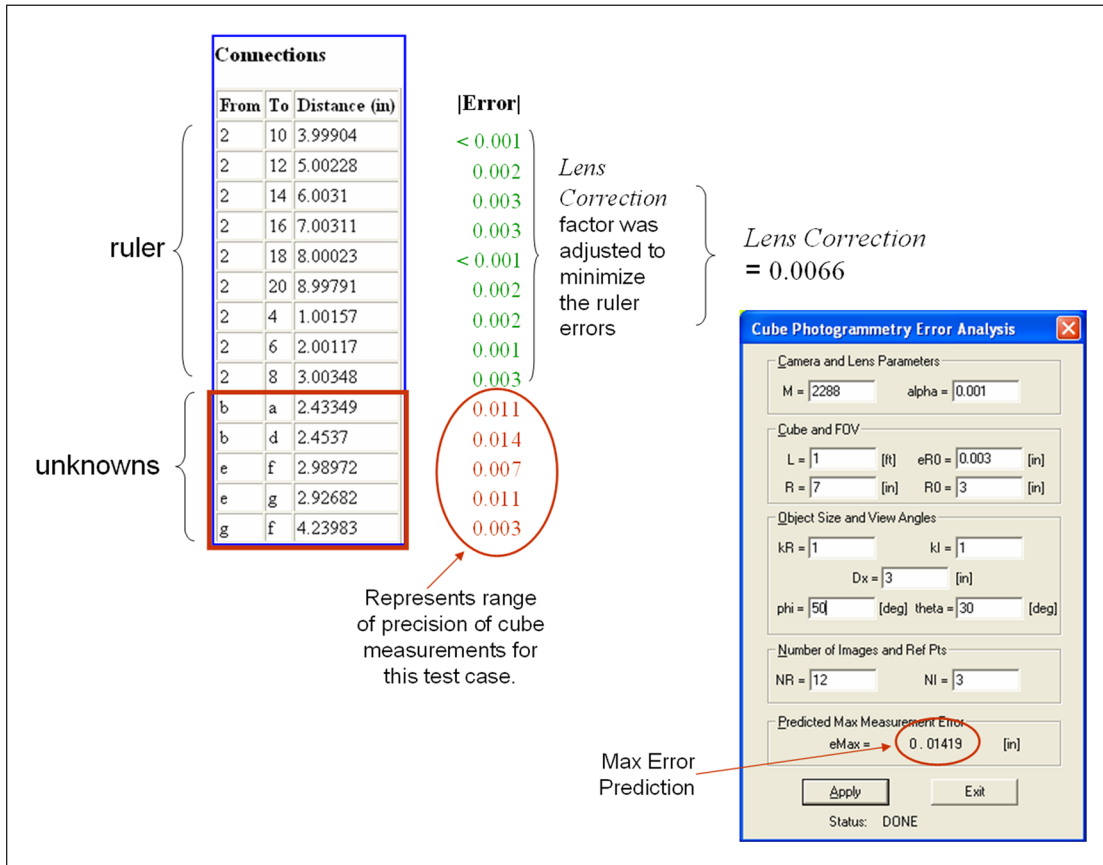


Figure 2. A demonstration of accuracy using the test images from Figures 1a and 1b. In this case, a lens correction factor was used to improve the results. The errors are compared to the Cube Photogrammetry Error Analysis model.

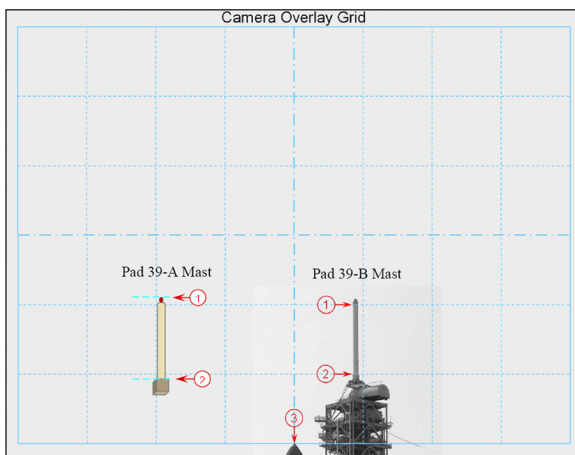
Bird Vision System



Spaceport/Range
Situational
Awareness

The Bird Vision system is a multicamera photogrammetry software application that runs on a Microsoft Windows XP platform and was developed at Kennedy Space Center by ASRC Aerospace. This software system collects data about the locations of birds within a volume centered on the Space Shuttle and transmits it in real time to the laptop computer of a test director in the Launch Control Center (LCC) Firing Room. The quality-controlled bird location data is also transmitted to the Firing Room bird tracking console, starting at the end of the T-9-minute hold. This data is available until T-60 seconds, when the tracker operators take control of the cameras and the Bird Vision application is terminated. This system uses the pad tracking cameras at three camera sites located about 1,200 feet from the pad, near the inside of the pad perimeter. The Bird Vision system backs up the Bird Radar system and includes the following features:

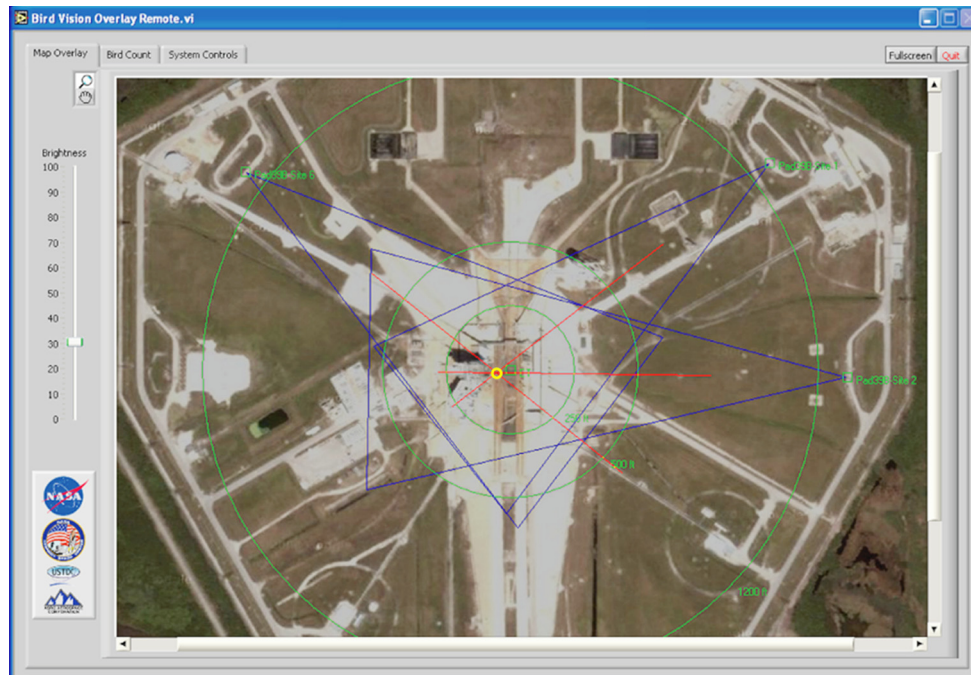
- 3-D Model Plot Mode (both local and remote overlay displays) provides real-time rotation, zoom, and translation of the 3-D view, using the mouse controls against a 3-D CAD model background and terrain map. There are several views for this display, including top view, side view, perspective view, and flyby view (rotating perspective view), which can be set via the 3-D Model Settings Tab.
- 3-D Overlay Plot Mode (both local and remote overlay displays) provides real-time rotation, zoom, and translation of the 3-D view, using the mouse controls.
- Triangulation (both local and remote overlay displays): For every pair of cameras set to Broadcast Mode, a circle is plotted on the 2-D overlay if the intersecting camera view lines pass within a maximum distance threshold, thus indicating a high probability of a bird at that location in 3-D space. The user may select the maximum distance threshold (the default is 2.5 m). A solid sphere is plotted in the 3-D Plot Mode where two camera view lines pass within this maximum distance threshold.
- The Bird Track (local overlay display only) generates a pseudo bird track by plotting a history of triangulated positions and then applying a fading-color function to the plot symbol. This feature is enabled when the number of history plots equals a nonzero value under the Bird Vision system control panel. The default value is 1.
- The system has the ability to record all processed data (camera view lines as well as triangulated positions) sent to the LCC Bird Vision remote display. This feature allows the test director to review all bird tracking data immediately following a launch or a scrub.



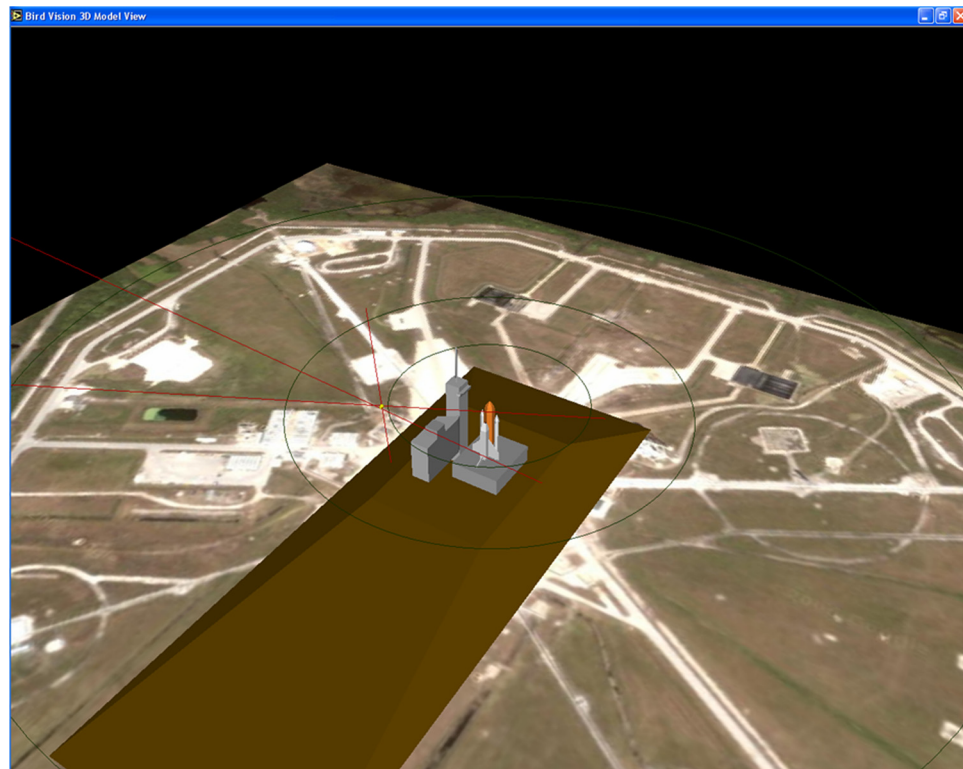
Vision system calibration is accomplished by marking the top and bottom positions of the pad lightning mast structure.



Manually drawing exclusive regions of interest helps mitigate false detections from background noise.



Plot Overlay Mode, where a yellow circle represents the 3-D intersection of all pairs of two-camera view lines to a detected object (bird).



3-D Model Plot Mode.

Contact: Dr. John E. Lane <John.E.Lane@nasa.gov>, ASRC Aerospace, (321) 867-6939

Participating Organizations: NASA-KSC (Dr. Robert C. Youngquist, Charles G. Stevenson, and Stephen J. Payne) and ASRC Aerospace (Dr. Christopher D. Immer, Jesus A. Dominguez, and Herbert W. Oleen)

Automating Range Surveillance Through Radio Interferometry and Field Strength Mapping Techniques



Spaceport/Range
Situational
Awareness

Space vehicle launches are often delayed because of the challenge of verifying that the range is clear, and such delays are likely to become more prevalent as more and more new spaceports are built. Range surveillance is one of the primary focuses of Range Safety for launches and often drives costs and schedules. As NASA's primary launch operation center, Kennedy Space Center is very interested in new technologies that increase the responsiveness of radio frequency (RF) surveillance systems. These systems help Range Safety personnel clear the range by identifying, pinpointing, and resolving any unknown sources of RF emissions prior to each launch.

Through the Small Business Innovative Research (SBIR) program, Soneticom, Inc., was awarded two Phase I contracts and has demonstrated an RF surveillance system that dramatically increases the ability to quickly locate and identify RF emitters. The system uses a small network of nodes (Figure 1), radio interferometry (RI) algorithms, time difference of arrival (TDOA) algorithms, and field strength mapping techniques to provide the quick response.

In their first Phase I SBIR project, Soneticom showed that the RI/TDOA techniques are feasible for locating RF emitters and met three technical objectives. The first objective was to demonstrate RI algorithms that can produce an image of an area and map specific RF activity within that area. The RI algorithms consistently located RF emitters within 100 meters. The computational complexity of these RI algorithms, or more specifically, group delay interferometry algorithms, exceeds that of similar TDOA techniques by orders of magnitude. The second objective was to demonstrate RF algorithms that can identify image differences based on a set of established criteria. The third objective was to demonstrate TDOA algorithms to help capture an RF image of an area and geolocate targeted RF emitters. However, the TDOA algorithms proved to be unsuitable for the automated background subtraction techniques used to distinguish the unknown emitters.

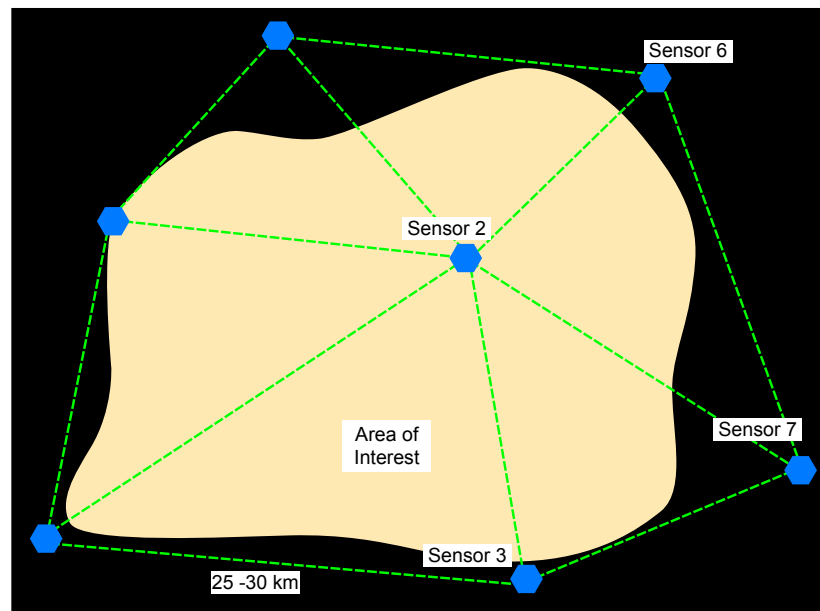


Figure 1. Example of an RF surveillance system network of nodes/sensors.



Figure 2. Conceptual EMI field strength map.

In their second Phase I SBIR project, Soneticom showed that electromagnetic-interference (EMI) field strength mapping techniques are feasible for computing signal strength contour maps of RF emitters, using radio propagation models and the company's Lynx geolocation system (Figure 2). Within the limited investigation, Soneticom's techniques reliably located the RF emitters and determined the transmitted power to within 3 dBm. Because the transmitted power is back-propagated, the accuracy of the field strength map's energy contours was largely limited to the accuracy of the topographical data provided to the propagation models. The accuracy is also affected by the assumptions made about the RF emitter's antenna patterns. This Phase I effort (1) enabled Soneticom's Lynx geolocation system to record and time-stamp the received-signal strength indication (RSSI), (2) developed and demonstrated a transmitted-power computation (TPC) algorithm for estimating the RF emitter's transmitted power, and (3) developed and demonstrated a back-propagation algorithm for estimating the RF emitter's field strength at any point in the range. The TPC algorithm computes the RF emitter's power at its location by using the RSSI and the distance to the node and by using least means squares (LMS) to fit a propagation model, such as COST231, Longley-Rice, or HATA, to the data. Reradiating or back-propagating the RF emission onto the range algorithmically through the use of the RF emitter's estimated power, computed antenna directivity, and a propagation model allowed the RF emitter's field strength to be computed at any point in the range.

Besides increasing the efficiency and effectiveness of Range Safety operations, other potential NASA applications include mitigating the effects of EMI, reducing interruptions in communication between flight and ground systems, and validating and mapping coverage areas of communication equipment. The potential non-NASA applications for the RF surveillance system include interference mitigation around commercial airports, cellular provider coverage mapping to identify poor reception areas and potential cross-cell interferences, and interference mitigation for the Federal Communications Commission (FCC) to efficiently enforce license spectrum regulations.

Contacts: Emilio Valencia <J.Emilio.Valencia@nasa.gov>, NASA-KSC, (321) 861-9074; and Richard A. Nelson <Richard.A.Nelson@nasa.gov>, NASA-KSC, (321) 867-3332

Participating Organization: Soneticom, Inc. (Alton Keel, Ronald Cobb, and William Anderson)

Next-Generation Telemetry Workstation



Global Positioning
System (GPS)
Metric Tracking

A next-generation telemetry workstation has been developed to replace the one currently used to test and control Range Safety systems. Improving upon the performance of the original system, the new telemetry workstation uses dual-channel telemetry boards for better synchronization of the two uplink telemetry streams. The new workstation also includes an Interrange Instrumentation Group/Global Positioning System (IRIG/GPS) time code receiver board for independent, local time stamping of return-link data. The next-generation system will also record and play back return-link data for postlaunch analysis.

The telemetry workstation software is based on C++ and was designed with the Microsoft Visual Studio 2005 development environment. Display screens were designed with National Instruments LabVIEW professional graphics development tools. The figures show examples of typical LabVIEW display screens. The C++ software sends display data to the LabVIEW software and receives button control commands from the LabVIEW software, using a Transmission Control Protocol/Internet Protocol (TCP/IP) communication scheme. The LabVIEW software does not control any hardware; rather it functions as a slaved smart graphical user interface.

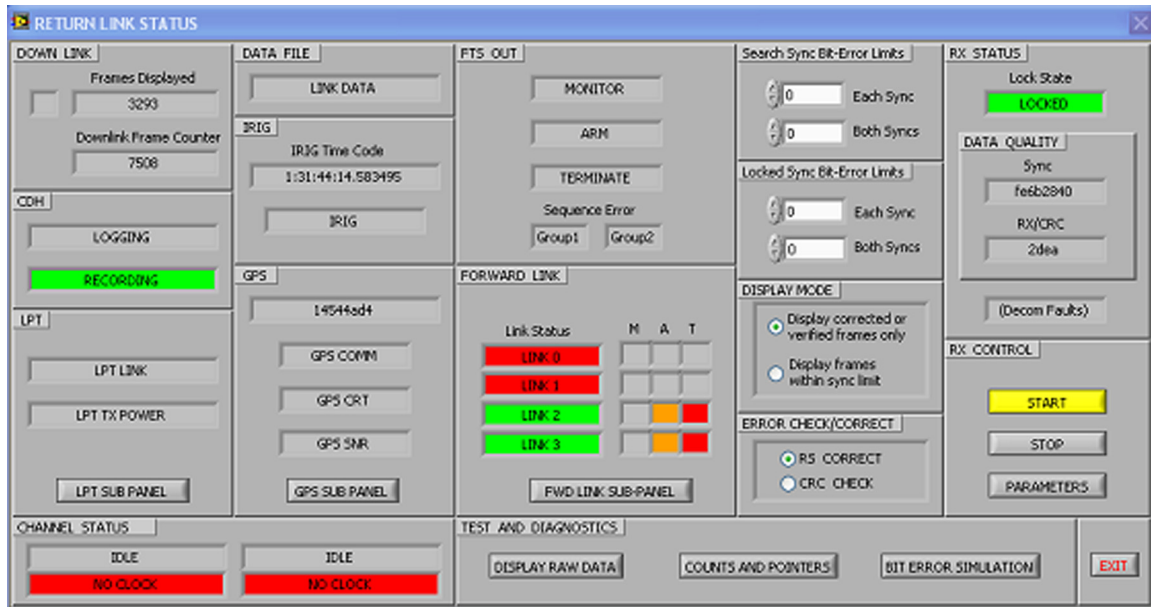
The workstation was designed to support various ongoing NASA and Air Force projects. The workstation can send and receive RS-422 telemetry data at a rate of up to 10 Mb/s over two uplink channels and two downlink channels simultaneously. When configured in record and playback mode, the workstation can record or play back up to four channels simultaneously. It can work with clocked or unclocked data using almost any return-to-zero (RZ) or non-return-to-zero (NRZ) data format. The workstation implements a clock recovery algorithm for unclocked data streams. It performs a software data decommutation operation on the incoming telemetry streams, and the data is processed for display and archiving according to the requirements of the particular telemetry system being supported.

The workstation can encrypt forward-link data, using triple Data Encryption Standard (DES) techniques, as well as encode and decode Reed Solomon error correction codes for forward- and return-link data and perform cyclical redundancy checks on return-link data.

The next phase in the development is to design and conduct comprehensive test procedures for the telemetry workstation. The tests will verify operation of the workstation hardware and the user interface software. Failure modes will be simulated, and the workstation's ability to detect, correct, and recover will be studied. Simulation software will need to be developed, and further software changes and enhancements will probably be necessary, based on the results of these tests. A final certification test will be developed and conducted to validate the workstation.

Contacts: Emilio Valencia <J.Emilio.Valencia@nasa.gov>, NASA-KSC, (321) 861-9074; and Christopher S. Forney <Christopher.S.Forney@nasa.gov>, NASA-KSC, (321) 867-6672

Participating Organization: ASRC Aerospace (Steven J. Klinko and Jesus A. Dominguez)



Telemetry workstation return-link status display.



Telemetry workstation forward-link status display.

GPS Metric Tracking Unit



Global Positioning
System (GPS)
Metric Tracking

As Global Positioning Satellite (GPS) applications become more prevalent for land- and air-based vehicles, GPS applications for space vehicles will also increase. The Applied Technology Directorate of Kennedy Space Center (KSC) has developed a lightweight, low-cost GPS Metric Tracking Unit (GMTU), the first of two steps in developing a lightweight, low-cost Space-Based Tracking and Command Subsystem (STACS) designed to meet Range Safety's link margin and latency requirements for vehicle command and telemetry data. The goals of STACS are to improve Range Safety operations and expand tracking capabilities for space vehicles. STACS will track the vehicle, receive commands, and send telemetry data through the space-based asset, which will dramatically reduce dependence on ground-based assets. The other step was the Low-Cost Tracking and Data Relay Satellite System (TDRSS) Transceiver (LCT2), developed by the Wallops Flight Facility (WFF), which allows the vehicle to communicate with a geosynchronous relay satellite. Although the GMTU and LCT2 were independently implemented and tested, the design collaboration of KSC and WFF engineers allowed GMTU and LCT2 to be integrated into one enclosure, leading to the final STACS.

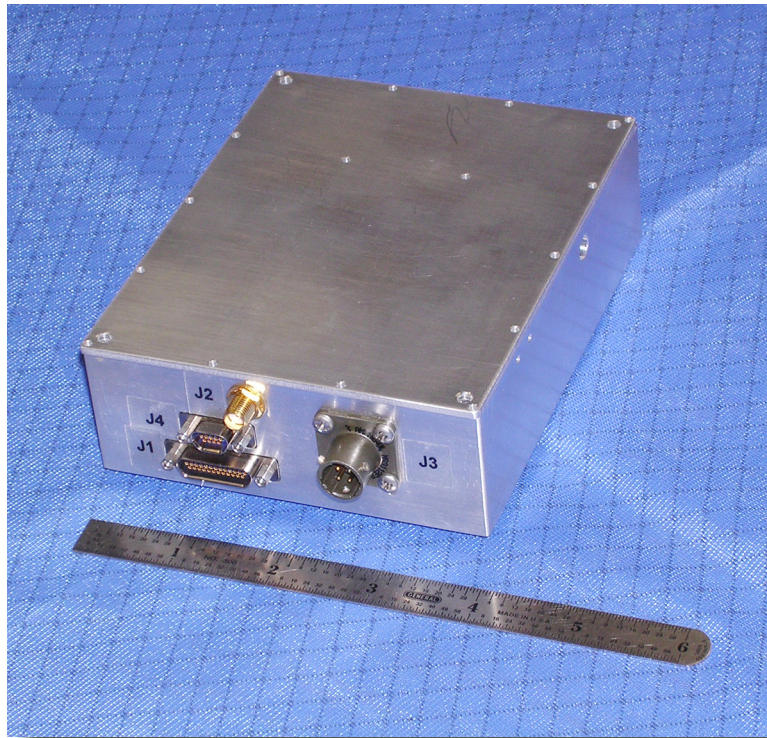
In operation, GMTU needs only a radio frequency (RF) input from a GPS antenna and outputs position and velocity data to the vehicle through a serial or pulse code modulation (PCM) interface. GMTU includes one commercial GPS receiver board and a custom board, the Command and Telemetry Processor (CTP) developed by KSC. The CTP design is based on a field-programmable gate array (FPGA) with embedded processors to support GPS functions. The programmability of the CTP allows designs to be changed and functions to be added without the need to modify the hardware. GMTU is well suited for applications requiring highly reliable metric tracking, such as robotics, autonomous air and ground vehicles, and manned vehicles. GMTU offers two command-receive channels, one output telemetry channel, and Ethernet, serial, and RS-422 interfaces. The unit is conduction-cooled, weighs less than 2 lb, and measures 1.5 by 5.0 by 4.0 inches.

GMTU has passed functional, vibration, and electromagnetic interference testing and is scheduled for flight testing in 2008 aboard a suborbital sounding rocket flight to be launched from WFF. The main objective of the test is to demonstrate the reliability of GMTU to track the rocket and the operational reliability of the hardware.

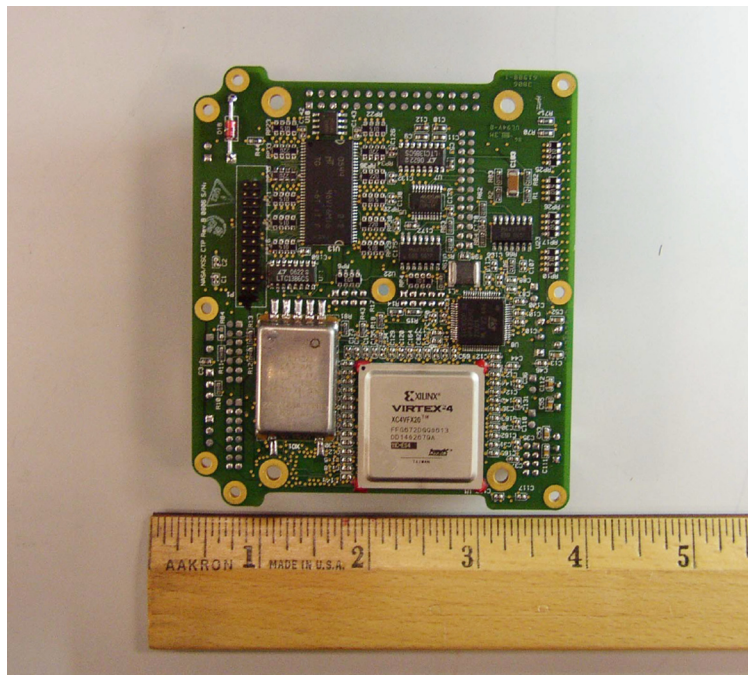
The final step in developing STACS will be to integrate and test the hardware and functional components of GMTU and LCT2.

Contacts: Emilio Valencia <J.Emilio.Valencia@nasa.gov>, NASA-KSC, (321) 861-9074; Christopher S. Forney <Christopher.S.Forney@nasa.gov>, NASA-KSC, (321) 867-6825; Robert L. Morrison <Robert.L.Morrison@nasa.gov>, NASA-KSC, (321) 867-6687; and Richard B. Birr <Richard.B.Birr@nasa.gov>, NASA-KSC, (312) 867-6301

Participating Organizations: NASA-KSC (Brian C. Cheshire) and ASRC Aerospace (Temel Erdogen, William D. Haskell, Michael A. Bertucci, Carlos E. Zavala, and Theresa G. Overcash)



GPS Metric Tracking Unit (GMTU).



Command and Telemetry Processor (CTP) board developed at KSC.

Space-Based Range



Global Positioning
System (GPS)
Metric Tracking

Space-Based Range (SBR), previously known as Space-Based Telemetry and Range Safety (STARS), is a multicenter NASA proof-of-concept project to determine if space-based communications using NASA's Tracking and Data Relay Satellite System (TDRSS) can support the Range Safety functions of acquiring tracking data and generating flight termination signals, while also providing broadband Range User data such as voice, video, and vehicle/payload data.

There was a successful test of the Range Safety system at Wallops Flight Facility (WFF) on December 20, 2005, on a two-stage Terrier-Orion spin-stabilized sounding rocket. SBR transmitted GPS tracking data and maintained links with two TDRSS satellites simultaneously during the 10-min flight. The payload section deployed a parachute, landed in the Atlantic Ocean about 90 miles downrange from the launch site, and was successfully recovered.

During the Terrier-Orion tests flights, more than 99 percent of all forward commands and more than 95 percent of all return frames were successfully received and processed. The time latency necessary for a command to travel from WFF over landlines to White Sands Complex and then to the vehicle via TDRSS, be processed onboard, and then be sent back to WFF was between 1.0 s and 1.1 s. The forward-link margins for TDRS-10 (TDRS East [TDE]) were 11 dB to 12 dB \pm 2 dB, and for TDRS-4 (TDRS Spare [TDS]) were 9 dB to 10 dB \pm 1.5 dB. The return-link margins for both TDE and TDS were 6 dB to 8 dB \pm 3 dB.

There were 11 flights on an F-15B at Dryden Flight Research Center (DFRC) between November 2006 and February 2007. The Range User system tested a 184-element TDRSS Ku-band (15 GHz) phased-array antenna with data rates of 5 Mbps and 10 Mbps. This data was a combination of black-and-white cockpit video, Range Safety tracking and transceiver data, and aircraft and antenna controller data streams. IP data formatting was used. The Range Safety system used the previously flown S-band transceiver to validate the forward and return links. Several "flyaway" maneuvers tested the transition from launch-head to satellite for the forward links.



Figure 1. Sounding rocket launch.

Figures 1 through 3 show the phased-array antenna mounted on the F-15 and architecture of the sounding rocket. Figure 4 shows the Range User return link margins as functions of antenna elevation for 5-Mbps and 10-Mbps flights. Link margins greater than 9 dB could not be measured, so it can only be said that the link margins were greater than 9 dB for elevations above 30°.

During the F-15 test flights, custom algorithms used the vehicle position and attitude to steer the phased-array antenna toward TDRSS West (TDW) at 174° W longitude with a pointing error typically much less than 1°. The measured data and video latency for the Range User system was about 0.4 s. More than 99 percent of the Range User frames were locked for both 5 Mbps and 10 Mbps when the antenna azimuth performance was within nominal operating parameters and more than 98 percent when these parameters were intentionally exceeded. There was a reasonably smooth transition between the Range Safety launch-head and satellite

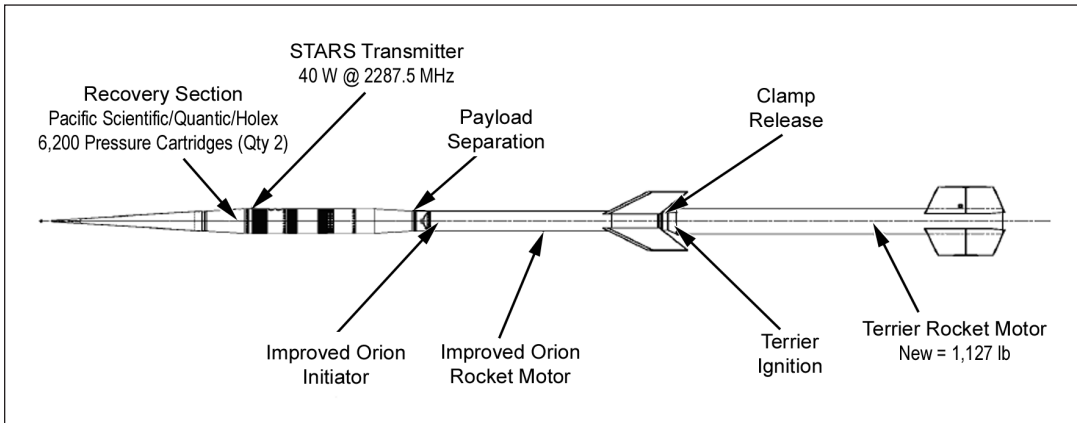


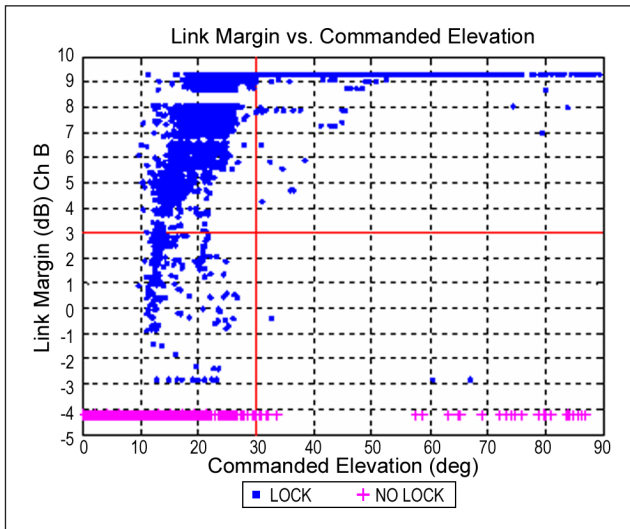
Figure 2. Sounding rocket.

forward links within 10 km to 20 km of the launch-head for a launch-head power level of -84 dBm. The antenna pattern of the four S-band telemetry Range Safety antennas on the F-15 (two forward and two return, with one set of each on the top and bottom of the F-15) was measured at the Benefield Anechoic Facility at DFRC.

Contact: Dr. James C. Simpson <James.C.Simpson@nasa.gov>, NASA-KSC, (321) 867-6937

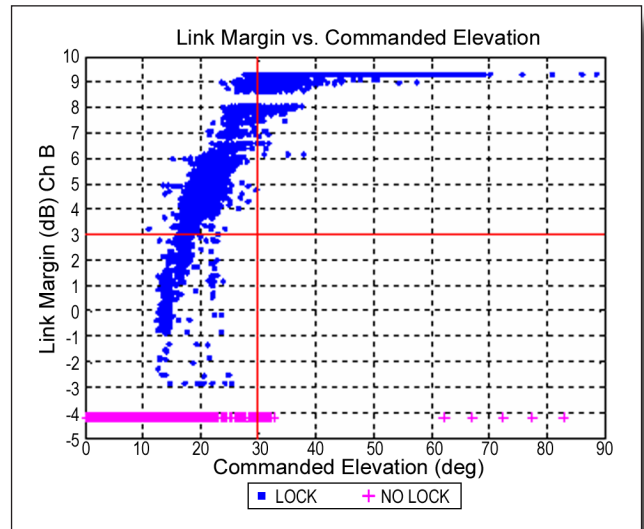


Figure 3. Phased-array antenna on the F15.



5-Mbps Flight

5-Mbps Flight No-lock conditions caused when TDRS passed through the antenna zenith and the aircraft dynamics exceeded azimuth performance.

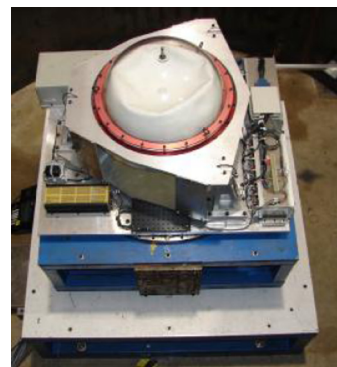
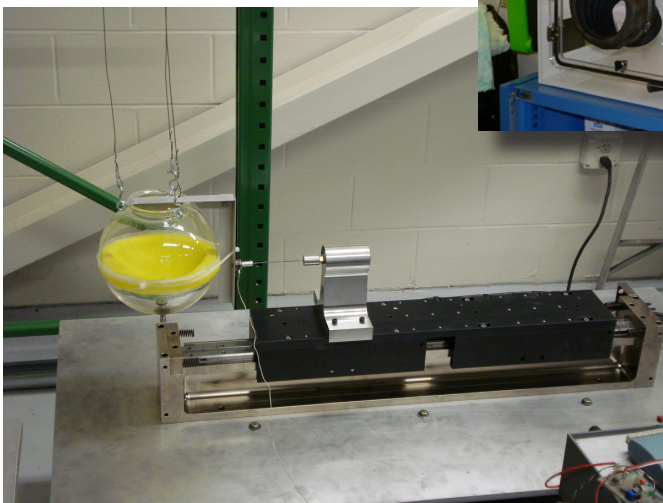
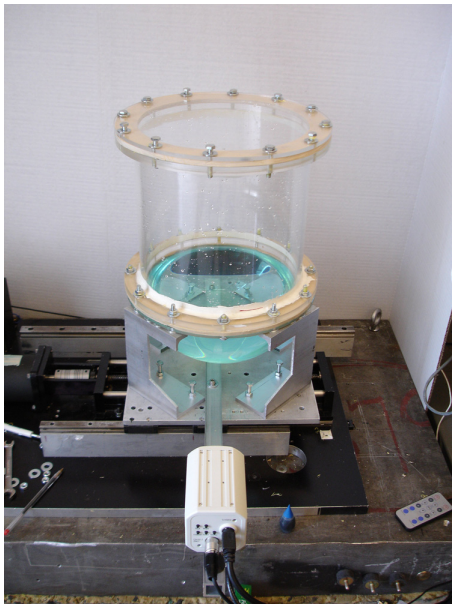


10-Mbps Flight

No-lock conditions caused when TDRS passed through the antenna zenith and signal reacquisition was delayed at the beginning of the test maneuver.

Figure 4. Link margin results for 5- and 10-Mbps flights. Note: No coverage was guaranteed by the manufacturer below 30° elevation.

Fluid System Technologies



Calibrating the Helium Pressurization System for the Space Shuttle Liquid-Hydrogen Tank



Hazardous-Leak
Detection and
Isolation

Analysis of the results from the STS-114 tanking tests and subsequent launch called into question existing thermal and mass models of helium pressurization of the liquid-hydrogen tank. This hydrogen tank, which makes up the bottom two-thirds of the External Tank, is pressurized prior to launch to avoid cavitation in the Shuttle Main Engine pumps. At about 2 minutes prior to launch, the main vent valve is closed, and pressurized helium flows into the tank ullage space to achieve set point pressure. As the helium gas cools, its pressure drops, calling for additional helium. Subsequent helium flows are provided in short, timed pulses. The number of pulses is taken as a rough leak indicator. An analysis of thermal models by Marshall Space Flight Center showed considerable uncertainty in the pressure-versus-time behavior of the helium ullage space and the ability to predict the number of pulses normally expected.

Kennedy Space Center proposed to calibrate the dime-sized orifice, which together with valves, controls the helium flow quantity (Figure 1). Pressure and temperature sensors were installed to provide upstream and downstream measurements necessary to compute flow rate based on the orifice discharge coefficient. An assessment of flow testing with helium indicated an extremely costly use of this critical resource. In order to reduce costs, we proposed removing the orifices from each Mobile Launcher Platform (MLP) and asking Colorado Engineering Experiment Station Inc. (CEESI) to calibrate the flow. CEESI has a high-pressure air flow system with traceable flow meters capable of handling the large flow rates. However, literature research indicated that square-edged orifices of small diameters often exhibit significant hysteresis and nonrepeatability in the vicinity of choked or sonic flow. Fortunately, the MLP orifices behaved relatively well in testing (Figure 2). Using

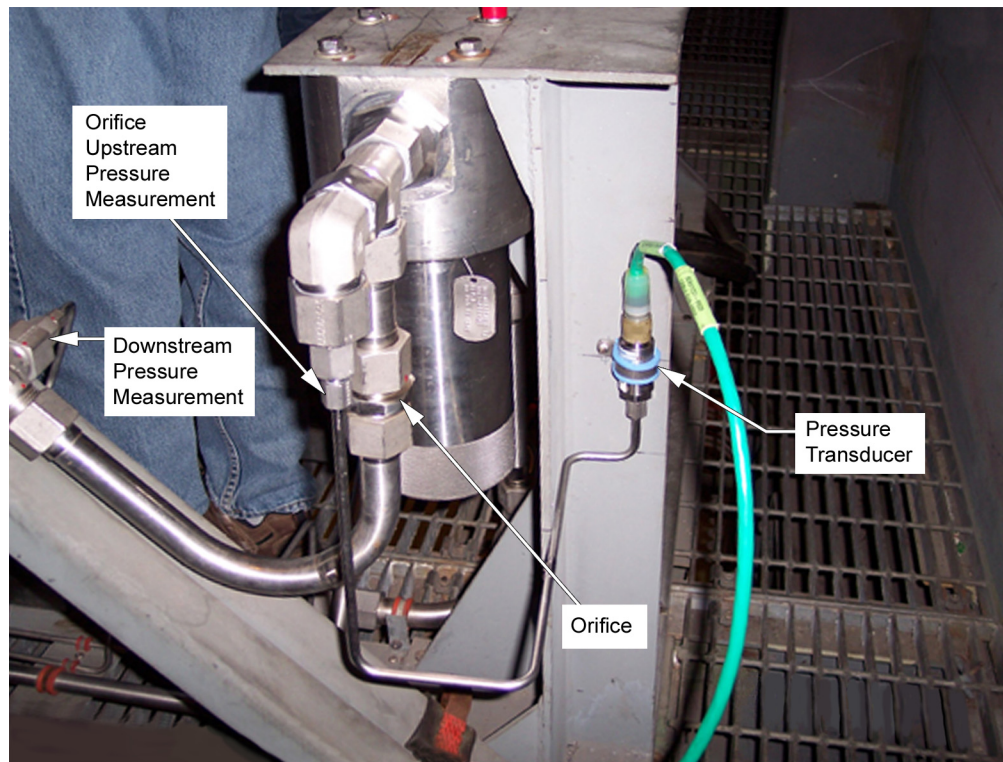


Figure 1. The helium flow control orifice and associated instrumentation.

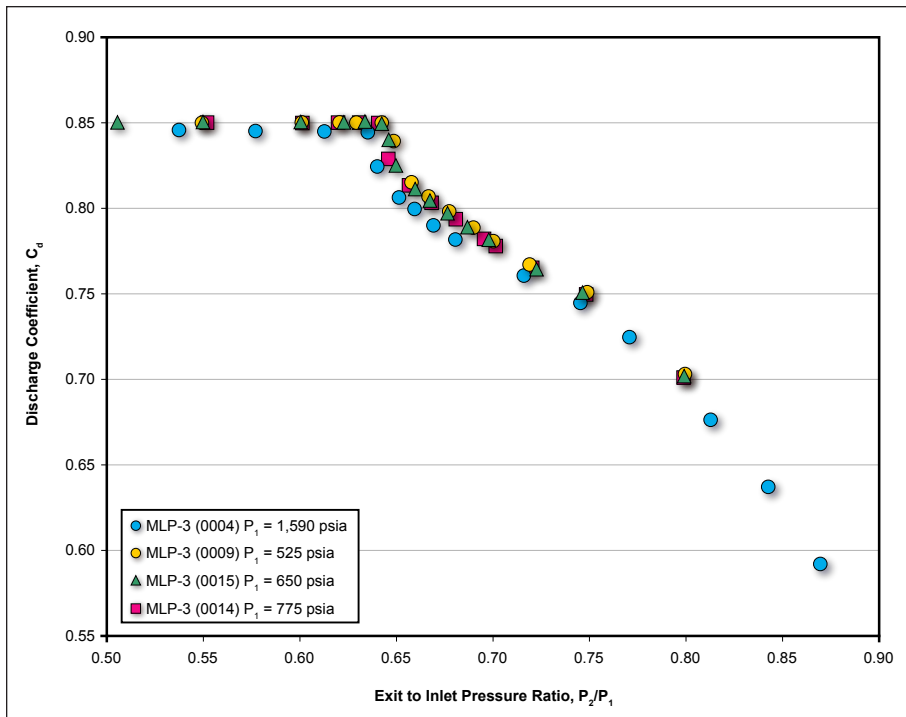


Figure 2. Typical flow-versus-pressure ratio curve, as measured in air by CEESI.

curve fitting of the air-flow data, in conjunction with ASME orifice modeling equations, a method of relating the helium mass flow to measured air flow data was obtained. This analysis showed that the highest uncertainty in flow occurred in the vicinity of the choking pressure ratio, as would be expected. In addition, analysis of typical flow pulses showed that most of the helium flow occurred either well below or well above this uncertain area. The final result is the ability to provide postlaunch estimates of helium mass flows that are within 1.5 percent of the actual value.

Contact: Stanley O. Starr <Stanley.O.Starr@nasa.gov>, NASA-KSC, (321) 861-2262

Participating Organization: United Space Alliance (Thomas J. Clark and Thomas A. Trovillion)

Composite Materials for Low-Temperature Applications

2006 Center Director's Discretionary Fund Project



Propellant Loading/
Servicing/Storage

Composite materials with improved thermal conductivity and good mechanical-strength properties should allow for the design and construction of more thermally efficient components (such as pipes and valves) for use in fluid-processing systems.

These materials should have wide application in any number of systems, including ground support equipment (GSE), lunar systems, and flight hardware that need reduced heat transfer. Researchers from the Polymer Science and Technology Laboratory and the Cryogenics Laboratory at Kennedy Space Center were able to develop a new series of composite materials that can meet NASA's needs for lightweight materials/composites for use in fluid systems and also expand the plastic-additive markets. With respect to thermal conductivity and physical properties, these materials are excellent alternatives to prior composite materials and can be used in the aerospace, automotive, military, electronics, food-packaging, and textile markets. One specific application of the polymeric composition is for use in tanks, pipes, valves, structural supports, and components for hot or cold fluid-processing systems where heat flow through materials is a problem to be avoided. These materials can also substitute for metals in cryogenic and other low-temperature applications.

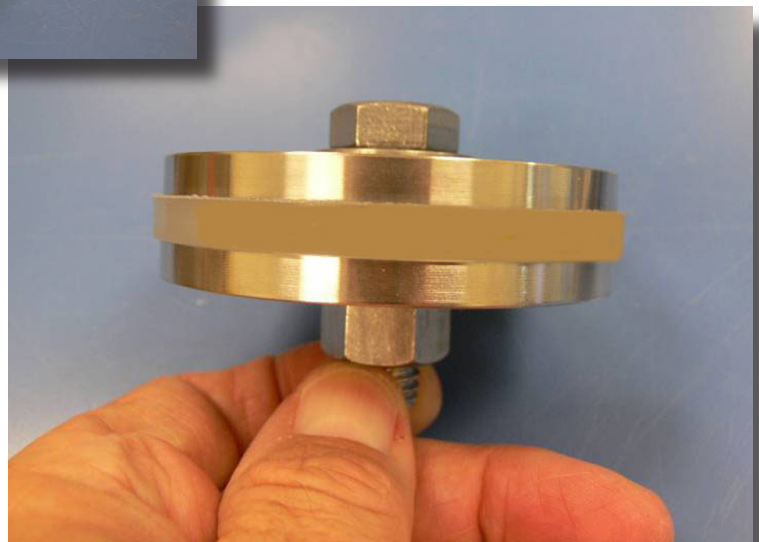
These organic/inorganic polymeric composite materials were invented with significant reduction in heat transfer properties. Decreases of 20 to 50 percent in thermal conductivity versus that of the unmodified polymer matrix were measured. These novel composite materials also maintain mechanical properties of the unmodified polymer matrix.

These composite materials consist of an inorganic additive combined with a thermoplastic polymer material. The intrinsic, low thermal conductivity of the additive is imparted into the thermoplastic, resulting in a significant reduction in heat transfer over that of the base polymer itself, yet maintaining most of the polymer's original properties. Normal polymer processing techniques can turn these composite materials into unique, custom parts for ground support, Shuttle, and Constellation needs.

We fabricated test specimens of the composite and base materials for thermal and mechanical characterization and found that the strength of the composite material at nominal-percentage loading remained relatively unchanged from the base material. In some polymer materials, the composite was noticeably more flexible at lower and cryogenic temperatures. In all cases, the heat transfer of test articles was reduced compared to the parent polymer.

Prototype GSE test articles were manufactured for use as seals and gaskets in cryogenic piping applications (see the figure). These articles are being evaluated on a proof-of-concept basis as candidate replacement materials for current polymer materials found to crack upon repeated thermal cycling. Additional testing will be required to raise the technology readiness level for continual GSE use. Future relevant environmental testing will prove the feasibility of composite materials in space and commercial applications.

By incorporating a hydrogen-sensing pigment, we developed and fabricated another composite technology. This composite can sense hydrogen at cryogenic temperatures and was demonstrated in a tape form on Launch Pad 39A in the Orbiter Midbody Umbilical Unit deployment for STS-117, STS-118, STS-120, and STS-122.



Composite seals for performance evaluation at low temperatures.

Contacts: NASA-KSC: Dr. Martha K. Williams <Martha.K.Williams@nasa.gov>, (321) 867-4554; Dr. Luke B. Roberson <Luke.B.Roberson@nasa.gov>, (321) 867-1542; James E. Fesmire <James.E.Fesmire@nasa.gov>, (321) 867-755; Trent M. Smith <Trent.M.Smith@nasa.gov>, (321) 867-7492; and Dr. LaNetra C. Tate <LaNetra.C.Tate@nasa.gov>, (321) 867-3789

Participating Organizations: NASA-KSC (Dr. Janine E. Captain, Jared P. Sass, and Stephen W. Huff) and ASRC Aerospace (Dr. Barry J. Meneghelli, Walter H. Hatfield, and Gary L. Wall)

Mitigating Problems in Measuring Hypergolic Fuels



Propellant Loading/
Servicing/Storage

To monitor hydrazine concentrations accurately and safely, hydrazine is converted into a stable derivative that will be monitored and correlated to the actual hydrazine concentration. The hydrazine's reactivity is harnessed to produce a chemical reaction that will form a stable gas-phase derivative which will not react or decompose before it reaches the detector.

Hydrazine, monomethylhydrazine, and unsymmetrical dimethylhydrazine belong to a class of compounds known as hypergolic fuels. These fuels self-ignite upon mixing with hypergolic oxidizer (dinitrogen tetroxide), without need of a spark or other ignition source. The resulting reaction produces thrust with exceptionally high energy, making these compounds particularly useful as rocket propellants.

Hydrazines are also highly toxic and corrosive. The combined properties of reactivity, corrosivity, and toxicity present the potential for a leak, a disastrous situation in a hypergol-loaded system. Consequently, leak detection is of the utmost importance in protecting equipment and personnel.

Hydrazine vapor quantification presents many challenges in addition to the safety concerns. The reactivity of these compounds causes thermal and catalytic decomposition, which results in significant losses. Further complications arise from the “sticky” nature of hydrazine. Molecules adsorb irreversibly to virtually any surface they make contact with before detection, which results in instrument drift. These properties make it difficult to accurately quantify hydrazines. Current analytical methods seek to minimize these interactions.

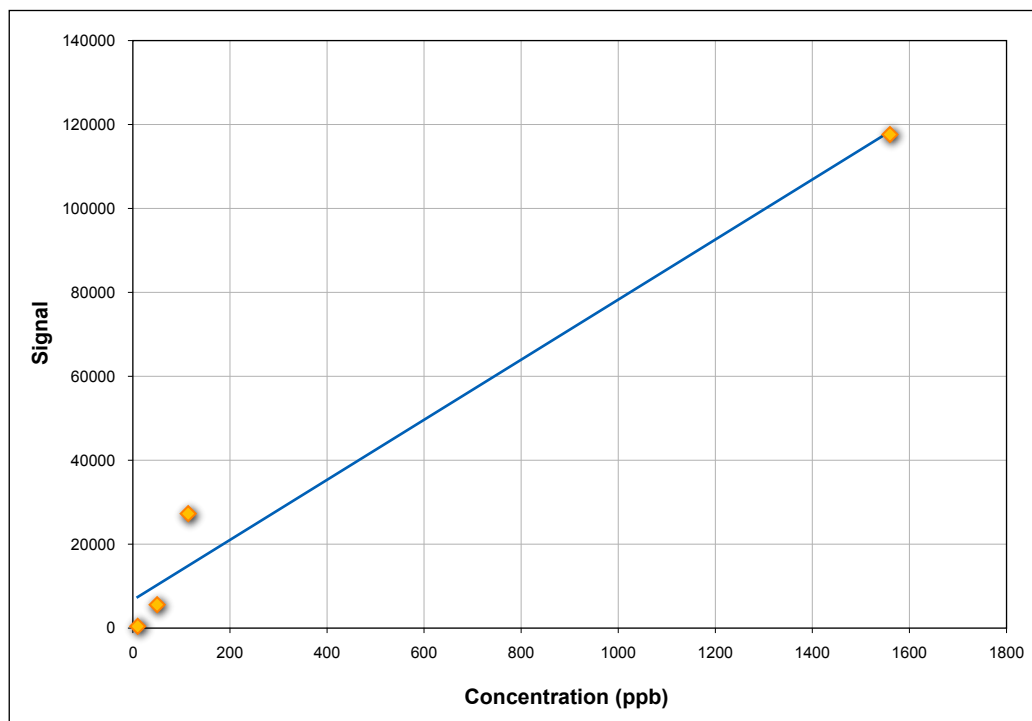
After an extensive literature search to determine appropriate chemical reactions, a method was devised to quantify hydrazines, without the limitations of monitoring hydrazines. In these experiments, we used the recently developed Desorption Electrospray Ionization (DESI) to ionize at ambient pressure a stabilized hydrazine derivative formed on a surface. To form the stabilized derivative, we exposed glass wool impregnated with a complexing reagent to hydrazine vapors at varying concentrations. We then used DESI to analyze the surface derivative, providing an indirect avenue for quantifying hydrazines. This approach harnesses, rather than limits, the reactivity of these hydrazines for more accurate quantification.

Our work successfully identified and characterized a gas-phase hydrazine reaction that formed a stabilized gas-phase hydrazine derivative which could be detected in place of the hydrazine. The work included using DESI to demonstrate the concept. The figure shows the results of the experiments.

Work continues in investigating and characterizing the current chemical reaction and in examining different chemical reactions and monitoring techniques. These tasks will be geared toward improving detection limits and producing a working prototype.

Contact: Dr. Timothy P. Griffin <Timothy.P.Griffin@nasa.gov>, NASA-KSC, (321) 867-6755

Participating Organization: ASRC Aerospace (Cristina M. Berger)



DESI response to hydrazine derivative.

Cryogenic Moisture Analysis of Spray-On Foam Insulation (SOFI)



Thermal Protection
System (TPS)
Enhancements

The NASA Cryogenics Test Laboratory at Kennedy Space Center conducted long-term testing of SOFI materials under actual-use cryogenic conditions. The lab tested NCFI 24-124 (acreage foam), BX-265 (close-out foam, including intertank flange and bipod areas), and a potential alternate material, NCFI 27-68 (acreage foam with the flame retardant removed).

Specimens of all three materials were placed at a site that simulated aging (the Vehicle Assembly Building [VAB]) and a site that simulated weathering (Atmospheric Exposure Test Site [beach site]). After aging/weathering intervals of 3, 6, and 12 months, the samples were retrieved and tested for their ability to absorb moisture under conditions similar to those experienced by the Space Shuttle External Tank (ET) during the loading of cryogenic propellants.

The Cryogenic Moisture Apparatus (CMA) is designed to determine the amount of water or ice taken into the specimen under actual-use cryogenic conditions. To simulate actual-use conditions, the top of the specimen is fixed at the temperature at which nitrogen remains liquid, while the bottom (outside) face is exposed to moist air at a constant humidity (90 percent) inside an environmental chamber. In order to keep the air quiet and the convection currents minimized, fans are not used. The surface temperatures of the specimen are also monitored by thermocouples and recorded by a LabVIEW data acquisition system. The edges of the CMA are guarded from moisture intrusion and from substantial heat leakage. The moisture uptake is measured by the water or ice taken into the specimen vertically (i.e., through the thickness of the specimen). Figure 1 shows the CMA and test setup.

All tests were conducted at ambient pressure (760 torr). The typical run time was 8 hours from start of cooldown to simulate the timeline for loading the Space Shuttle ET with cryogenic propellants. The warm boundary temperature (WBT) was approximately 293 K and the cold boundary temperature (CBT) was approximately 78 K. The specimen, including its edge guard ring, was quickly removed and replaced every hour to measure the weight gain.

Some results for the weathering case are shown in the table. These typical results are averaged values for a number of test runs and are given in percentage weight gains, using a 7-inch effective heat transfer area (between the 6-inch-diameter cold chamber and the 7-inch-diameter exposed face) for an 8-hour cold soak. Figures 2 and 3 compare the weight change for specimens of NCFI 24-124 at the aging (VAB) and at the weathering (beach) sites.

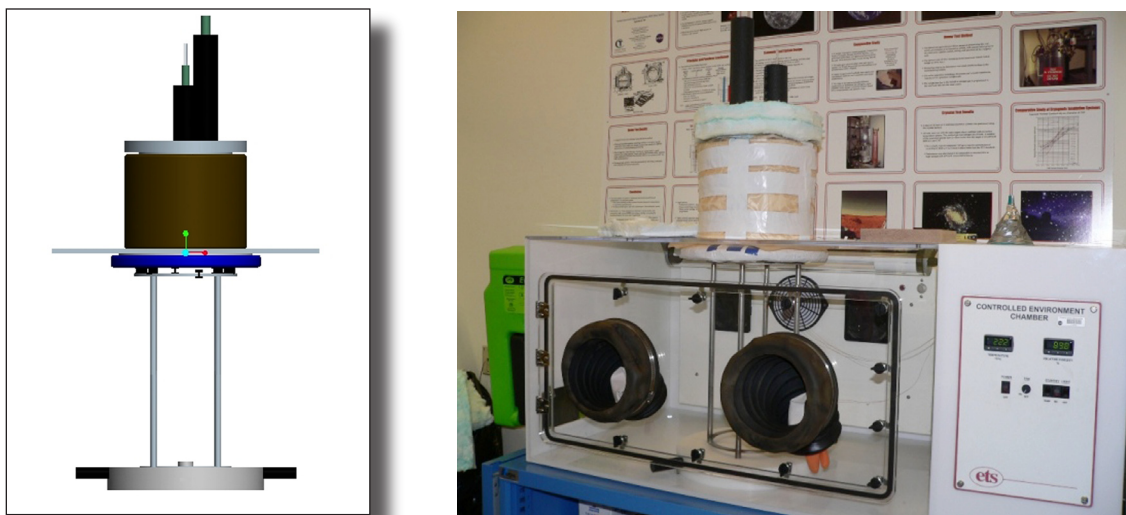


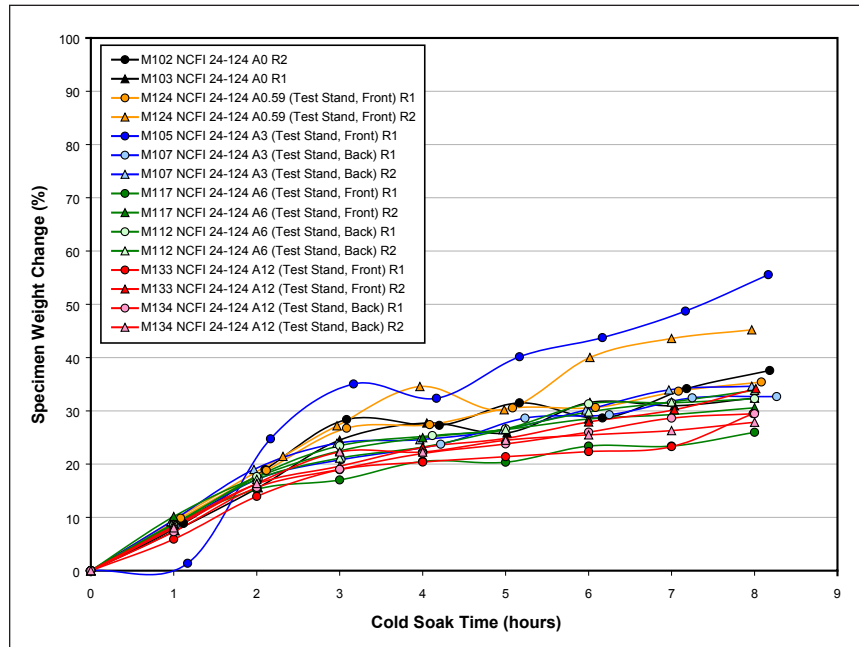
Figure 1. Cryogenic Moisture Apparatus: schematic (left) and overall view, including environmental control chamber (right).

Contacts: Dr. Barry J. Meneghelli <Barry.J.Meneghelli@nasa.gov>, ASRC Aerospace, (321) 867-4011; and James E. Fesmire <James.E.Fesmire@nasa.gov>, NASA-KSC, (321) 867-7557

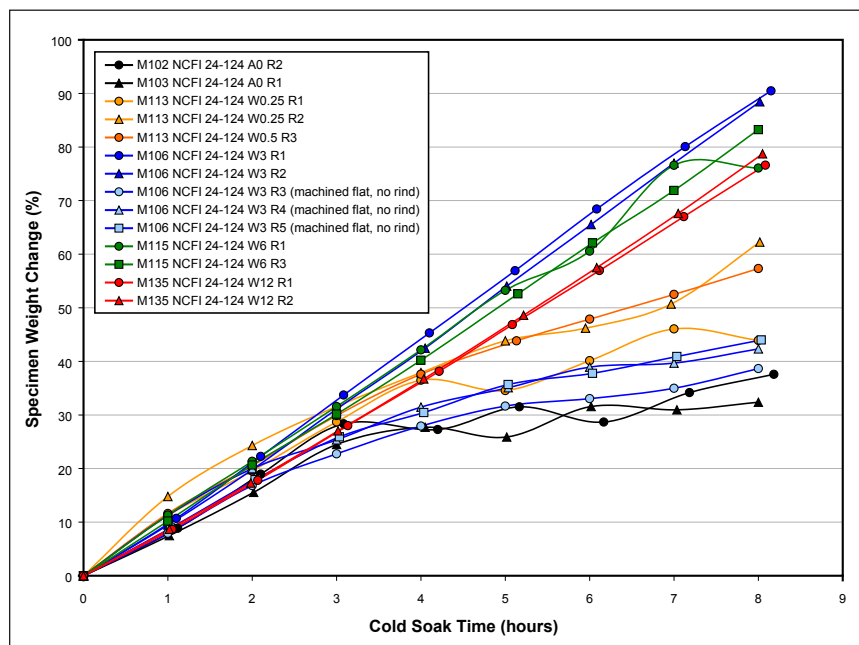
Participating Organization: ASRC Aerospace (Walter H. Hatfield and Kenneth W. Heckle, Sr.)

Weight gain results of SOFI weathering tests.

Material	Baseline (%)	3 Month (%)	6 Month (%)
NCFI 24-124	30	78	74
NCFI 27-68	32	72	72
BX-265	30	70	95



Figures 2. Uptake of cryogenic moisture in aged NCFI 24-124 samples (12-month data).



Figures 3. Uptake of cryogenic moisture in weathered NCFI 24-124 samples (12-month data).

Thermal Performance of Aged and Weathered Spray-On Foam Insulation (SOFI) Materials Under Cryogenic Vacuum Conditions (Cryostat-4)



Thermal Protection System (TPS) Enhancements

The NASA Cryogenics Test Laboratory at Kennedy Space Center conducted long-term testing of SOFI materials under actual-use cryogenic conditions with Cryostat-4. The materials included in the testing were NCFI 24-124 (acreage foam), BX-265 (close-out foam, including intertank flange and bipod areas), and a potential alternate material, NCFI 27-68, (acreage foam with the flame retardant removed). Specimens of these materials were placed at two locations: a site that simulated aging (the Vehicle Assembly Building [VAB]) and a site that simulated weathering (the Atmospheric Exposure Test Site [beach site]). After aging/weathering intervals of 3, 6, and 12 months, the samples were retrieved and tested for their thermal performance under cryogenic vacuum conditions with test apparatus Cryostat-4.

Cryostat-4 is a liquid-nitrogen boiloff calorimeter designed to determine the apparent thermal conductivity (k-value) of thermal insulation systems under actual-use cryogenic vacuum conditions. The method is comparative in that the total heat load to the test chamber includes a minor but repeatable parasitic heat leakage rate. The residual gas supplied to the vacuum chamber is nitrogen. The boiloff flow from the test chamber is in direct proportion to the total heat transfer rate through the thickness of the test article. Flow rate is typically averaged over the liquid level from 4 to 0 percent (near empty) to calculate the comparative k-value.

The SOFI test articles were 203 mm in diameter, with a nominal thickness of 25.4 mm. Tests were conducted starting at ambient pressure (760 torr) and working down, decade by decade of vacuum-pressure increments, to high vacuum (below 1×10^{-3} torr). At least eight cold vacuum pressure tests were performed for each test series. The warm boundary temperature (WBT) was approximately 293 K and the cold boundary temperature (CBT) was approximately 78 K. Figure 1 shows the installation of a SOFI test article.

The foams were tested in the baseline, aged, and weathered conditions. Here *baseline* means that the specimens were not weathered and only slightly aged. Specimens with rind were necessarily sanded down to a flat surface finish for good thermal contact with the warm and cold sides of the cryostat.

Surface Temperature Measurement	
Sensor	Location
T1, T3	Cold Boundary Temperature (CBT)
T2	Top of Cold Mass
T4, T5	Warm Boundary Temperature (WBT)
VC1, VC2, VC3	Vacuum Chamber Exterior
VC4, VC5, VC6	Heater Temperature

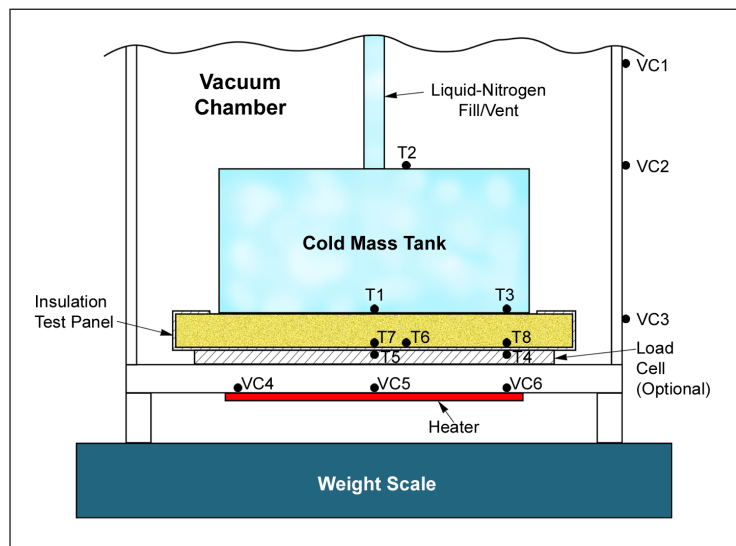


Figure 1. The SOFI test specimen is installed between the cold mass tank and the warm boundary of insulation in Cryostat-4.

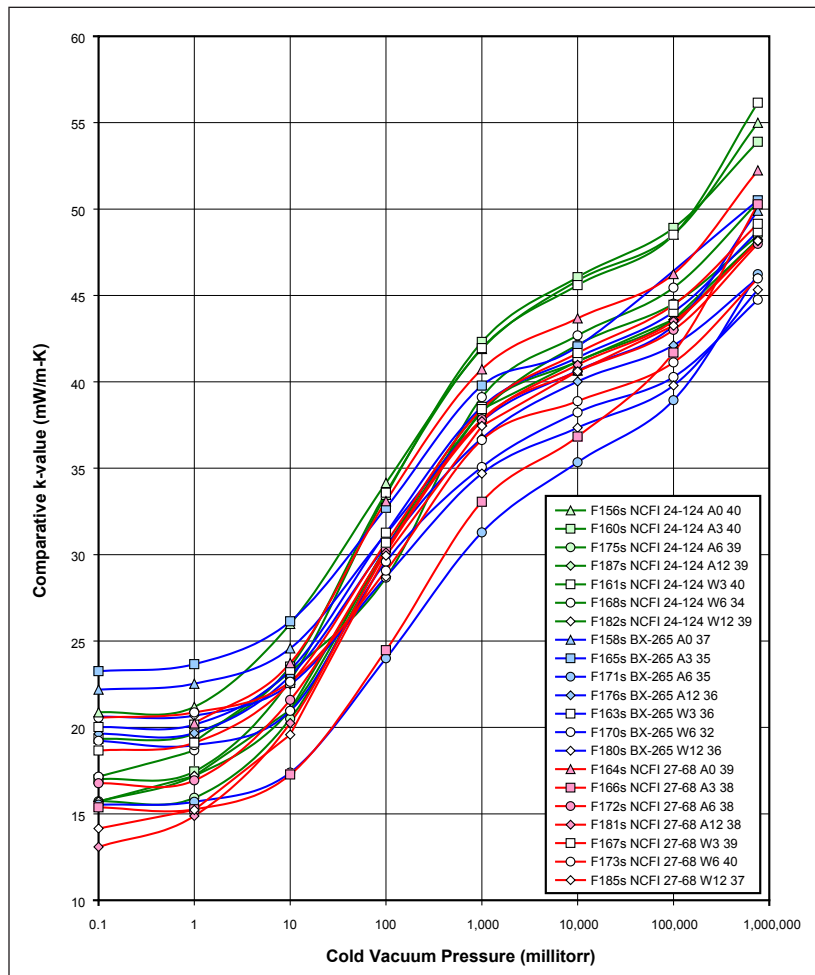


Figure 2. The variation of comparative k-value with cold vacuum pressure for all Cryostat-4 SOFI test specimens. The boundary temperatures are 293 K and 78 K. The residual gas is nitrogen.

Figure 2 shows the results for the cryogenic thermal-performance testing of the aged and weathered SOFI materials. The apparent thermal conductivity (k-value) is reported in the standard SI units (milliwatts per meter Kelvin), but these numbers are comparative and may only be applied among the test specimens listed in this report.

Contacts: Dr. Barry J. Meneghelli <Barry.J.Meneghelli@nasa.gov>, ASRC Aerospace, (321) 867-4011; and James E. Fesmire <James.E.Fesmire@nasa.gov>, NASA-KSC, (321) 867-7557

Participating Organization: ASRC Aerospace (Walter H. Hatfield and Kenneth W. Heckle, Sr.)

Automated Method for Estimating Nutation Time Constant Model Parameters for Spacecraft Spinning on Axis



Spacecraft
Nutation
Models

Calculating an accurate nutation time constant (NTC), or nutation rate of growth, for a spinning upper stage is important for ensuring mission success. Spacecraft

nutation, or wobble, is caused by energy dissipation anywhere in the system. Propellant slosh in the spacecraft fuel tanks is the primary source for this dissipation and, if it is in a state of resonance, the NTC can become short enough to violate mission constraints. The Spinning Slosh Test Rig (SSTR), developed by NASA and Southwest Research Institute (SwRI), is a forced-motion spin table where fluid dynamic effects in full-scale fuel tanks can be tested in order to obtain key parameters used to calculate the NTC. We accomplish this by independently varying nutation frequency versus the spin rate and measuring force and torque responses on the tank. This method was used to predict parameters for the Genesis, Contour, and Stereo missions, whose tanks were mounted outboard from the spin axis. These parameters are incorporated into a mathematical model that uses mechanical analogs, such as pendulums and rotors, to simulate the force and torque resonances associated with fluid slosh.

Most recently, the SSTR was modified to simulate the on-axis spin motions of the centerline-mounted tanks used in the Pluto New Horizons (PNH) and Deep Impact (DI) spacecraft (Figures 1 and 2). We varied diaphragm shapes (Figure 3), nutation frequencies (ratio of upper-motor to

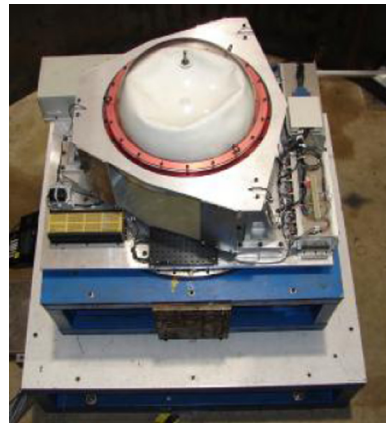


Figure 2. PNH configuration (without stand-off).

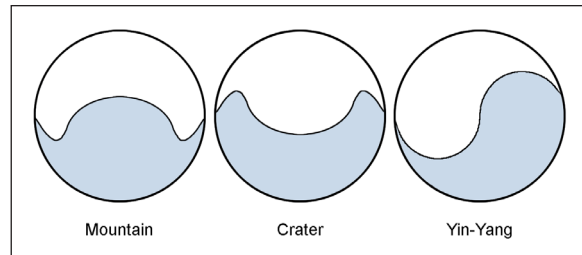


Figure 3. Diaphragm shapes tested by SwRI.

total revolutions per minute [RPM]), and fill levels at a constant spin rate of nearly 60.5 RPM to examine how the various force and torque activity would influence the mechanical analog parameters. Data was recorded while each fill level/diaphragm shape combination underwent a nutation sweep where specific nutation frequencies ranged from 10 to 90 percent of the total spin rate. After testing, it was determined that the pendulum analog parameters could be set to zero because very little resonance activity was observed in the force response along the tank wall, leaving the rotor analog available to be the sole influencer of the torque response. These ideal, or massless, rotors have inertia only about their primary axis of spin. Their associated parameters include inertia and spring/damping constants.

The current method for identifying model parameters involves laboriously hand-deriving equations of motion for both the SSTR and mechanical analogs and, by trial and error,

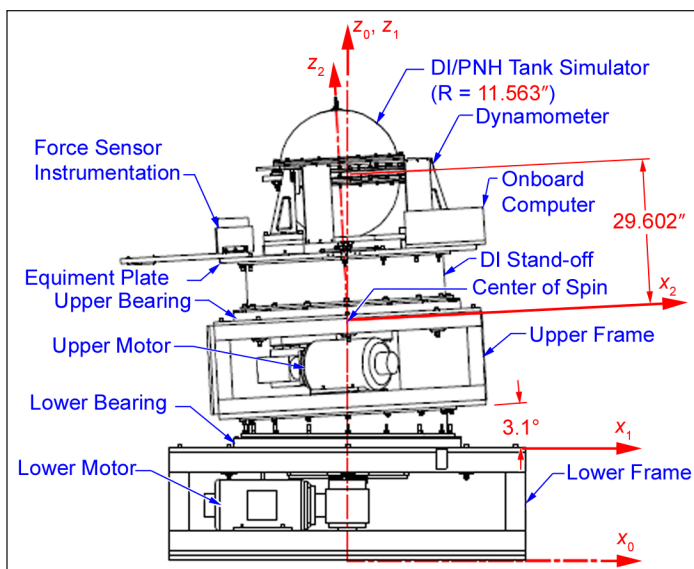


Figure 1. DI configuration (with stand-off).

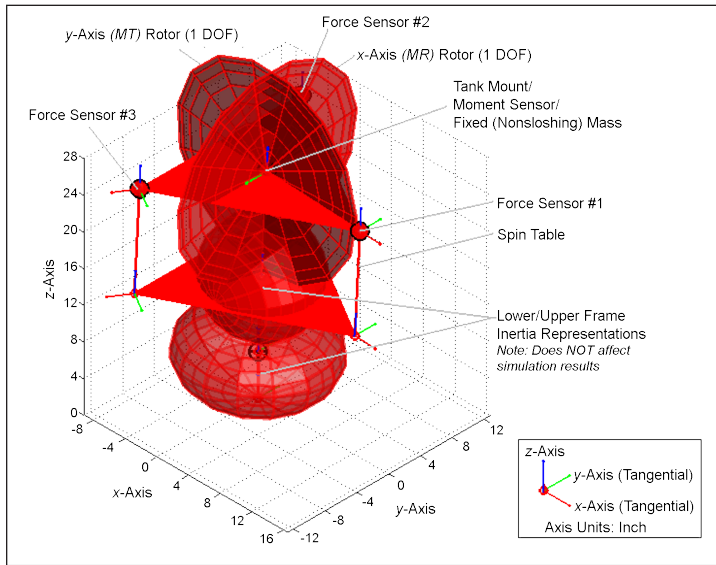


Figure 4. Overall layout of on-axis SSTR SimMechanics model.

comparing their results with experimental results. A strong desire exists to automate this method so different analogs can be tested quickly and the results can be compared with measured data.

The method presented accomplishes this task by using a MATLAB Simulink/SimMechanics-based simulation where the parameters are identified by the Parameter Estimation tool. Simulink Parameter Estimation provides a graphical interface where several optimization algorithms can be selected. The simulation incorporates the same slosh analog used by SwRI, two torque rotors about the radial (x) and tangential (y) axes (Figure 4), allowing direct comparisons between the hand-derived and automated methods. Six sets of measured data can be supplied to the simulation for parameter estimation. These include forces (F_x/F_y) along the tank wall and torques (MR/MT) resolved to the tank center of gravity (CG) (Figure 5), as well as the angular velocities of the tank CG (Ω_x/Ω_y) about each axis. Each nutation sweep test, usually consisting of 9 to 11 individual nutation frequencies, is supplied to the Estimator, where its multiple dataset estimation feature can be used. Estimating to the entire set of measured data allows the rotor parameters to be optimized for reproduction of the torque resonance response over the entire range of tested nutation frequencies (Figure 6).

Current research efforts focus on identifying and recording the differences between the hand-derived and SimMechanics methods, such as the effects of larger rotor inertias. Once complete, the same SimMechanics analog used in the SSTR model will be incorporated into

a compatible spacecraft model where the NTC can be calculated and compared with flight data. This proven process will be a valuable tool for quickly examining both traditional and novel mechanical fuel slosh analogs and for allowing spacecraft designers to build accurate slosh models early in the design phase, when potential NTC violations can be avoided.

Contacts: James E. Sudermann <James.E.Sudermann@nasa.gov>, NASA-KSC, (321) 867-8447; and Keith L. Schlee <Keith.L.Schlee@nasa.gov>, Analex Corporation, (321) 867-4186

Participating Organization: Southwest Research Institute (Dr. Steve Green and Russell C. Burkey)

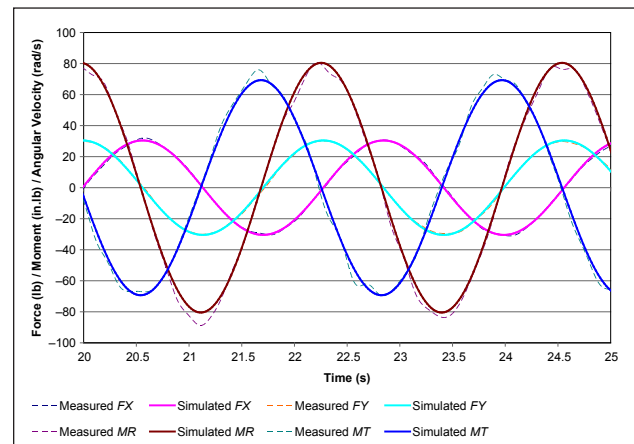


Figure 5. Comparison between measured and simulation data at a nutation rate of 0.44 for typical PNH test (upper-motor RPM = 26.26, lower-motor RPM = 34.30).

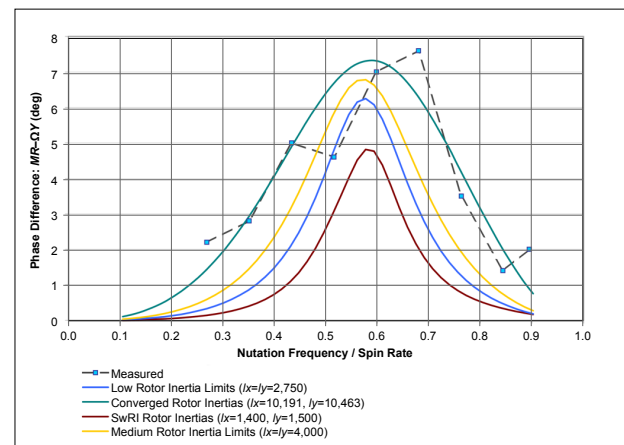


Figure 6. MT-to- ΩY phase comparison using various estimated parameters (inertia unit: lb.in²).

Parameter Estimation of Lateral Spacecraft Fuel Slosh



Spacecraft
Nutation
Models

Predicting the effect of fuel slosh on the attitude control system of a spacecraft or launch vehicle is a very important and challenging task. Whether the spacecraft is spinning or moving laterally, the dynamic effect of the fuel slosh helps determine whether the spacecraft will remain on its intended trajectory. Three categories of slosh can be caused by launch vehicle or spacecraft maneuvers when the fuel is in the presence of an acceleration field.

These are bulk-fluid motion, subsurface wave motion (currents), and free-surface slosh. Each of these slosh types has a periodic component defined by either a spinning or a lateral motion. For spinning spacecraft, all three types of slosh can greatly affect stability. Bulk-fluid motion and free-surface slosh can affect the lateral-slosh characteristics. For either condition, an unpredicted coupled resonance between the spacecraft and its onboard fuel could threaten a mission. This ongoing research effort seeks to improve the accuracy and efficiency of modeling techniques used to predict these types of fluid motions for lateral motion. Particular efforts focus on analyzing the effects of viscoelastic diaphragms on slosh dynamics.

Previous research used MATLAB SimMechanics to model free-surface fuel slosh with a simple one-degree-of-freedom (DOF) pendulum analog. The pendulum analog modeled a spherical tank undergoing free-surface slosh created by oscillating the tank via an electric motor attached to a locomotive arm assembly. A SimMechanics model incorporating the analog of the experiment was developed and tested. Parameters describing the simple pendulum models, such as spring and damping constants at the pendulum hinge location and pendulum length, characterized the modal frequency of the free-surface sloshing motion. The one-DOF model offered insights into free-surface fuel slosh and served as a stepping stone for the present research. Using the previous experimental setup, we tested different liquids undergoing free-surface slosh and estimated the various pendulum parameters using MATLAB's Parameter Estimator Toolbox.

The first step was to experiment with several liquids with different viscosities in order to better understand how that liquid property affects lateral fuel slosh and the resulting pendulum analog parameters. Liquids of varying viscosities and physical characteristics different from water were used. It was assumed that for higher viscosities, the peak amplitude of the reaction force on the tank

would be lower than the values measured when using water. As predicted, pendulum damping, which determines the stiffness of the pendulum, was the critical parameter when comparing the liquids with different viscosities. The more damped the pendulum hinge, the less peak force there was at resonance. Parameters (such as the slosh frequency and pendulum length) remained the same for all liquids, regardless of their viscosities. The SimMechanics model was updated and adjusted for the simulation using different liquids. After obtaining experimental data at three different fill levels (60, 70, and 80 percent) for both glycerine and corn syrup, the data was imported into SimMechanics, where free-surface slosh conditions were simulated. Figures 1 and 2 compare the experimental data and the simulated data for glycerine and corn syrup at the 60-percent fill level.

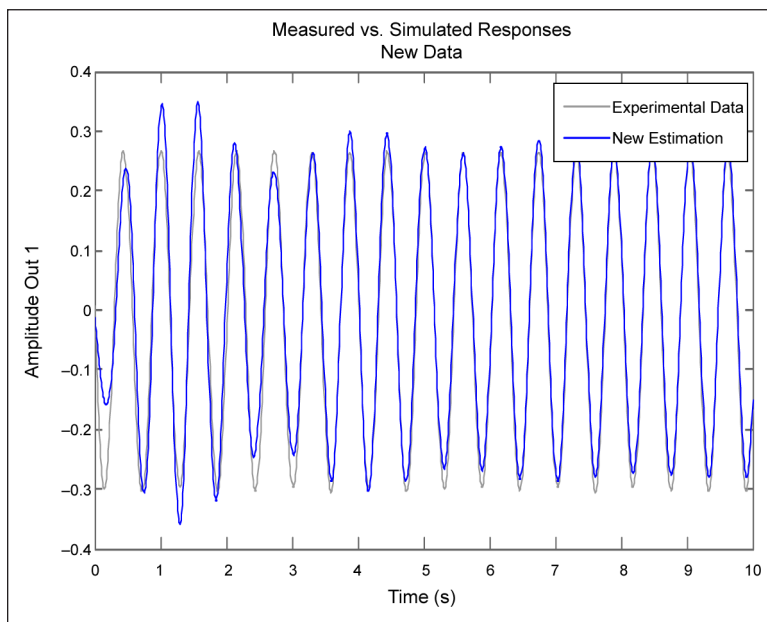


Figure 1. Glycerine: 60-percent fill level, oscillating at 1.75 Hz (unit = lbf).

In an ongoing effort for improvement, the locomotive assembly was replaced by a state-of-the-art shaker assembly. Four diaphragms, each with a different stiffness, were attached to the periphery of their tanks so that the effects of slosh on each could be studied (Figure 3). These new transparent spherical fuel tanks with diaphragms will be mounted on a fixture and linearly oscillated by the shaker. The forces at the tank wall, along the axis of lateral motion, will be measured by a force transducer mounted on the fixture, similar to what was done with the locomotive assembly.

Diaphragms provide a substantial level of slosh damping as a result of the combination of viscoelastic flexing of the diaphragm and the increased viscous effects at the liquid-diaphragm interface. It is assumed that, as the stiffness of the diaphragm increases, the pendulum damping parameter will increase, as was observed on free-surface tests of fluids with higher viscosities. The presence of a diaphragm in the fuel tank should also increase the natural frequency of the slosh because of the constraints imposed on the free-surface shape. In addition, the effective mass of liquid participating in the sloshing will most likely be smaller than that for a tank of the same shape and fill level without a diaphragm. That is, a greater percentage of fluid will behave as if it were attached to the tank. Figure 4 shows the new slosh test facility designed, fabricated, and installed at Embry-Riddle Aeronautical University to investigate the lateral sloshing of spacecraft propellant tanks.

Contacts: James E. Sudermann <James.E.Sudermann@nasa.gov>, NASA-KSC, (321) 867-8447; and Keith L. Schlee <Keith.L.Schlee@nasa.gov>, Analex Corporation, (321) 867-4186

Participating Organizations: Embry-Riddle Aeronautical University (Dr. Sathya Gangadharan, Yadira Chatman, and Brandon Marsell) and Hubert Astronautics, Inc. (Dr. Carl Hubert)

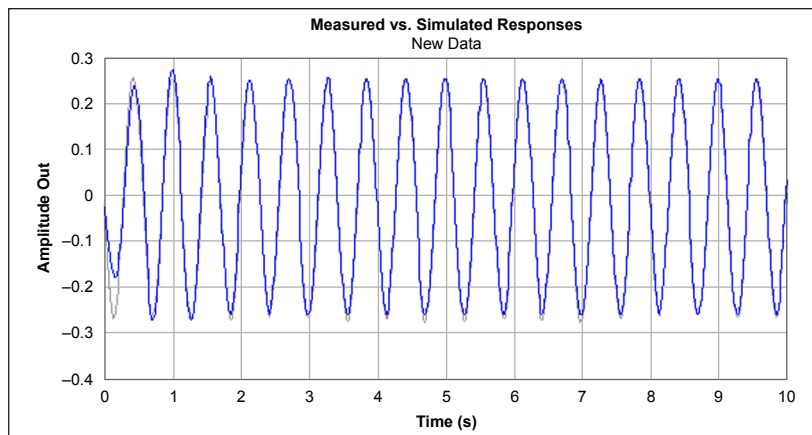


Figure 2. Corn syrup: 60-percent fill level, oscillating at 1.75 Hz (unit = lbf).

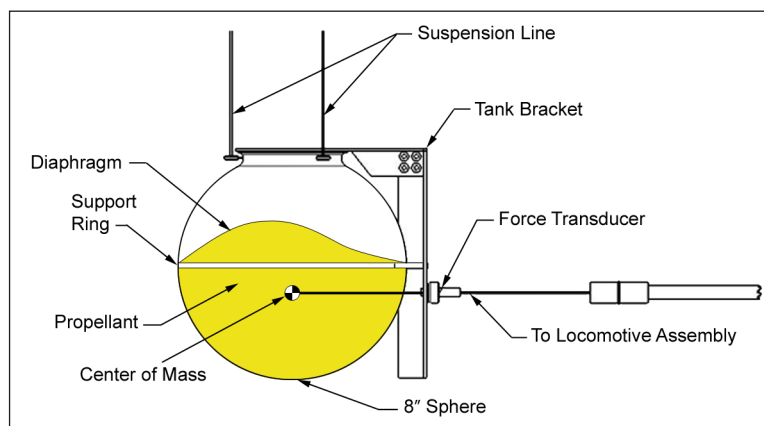


Figure 3. Experimental setup with the diaphragm.

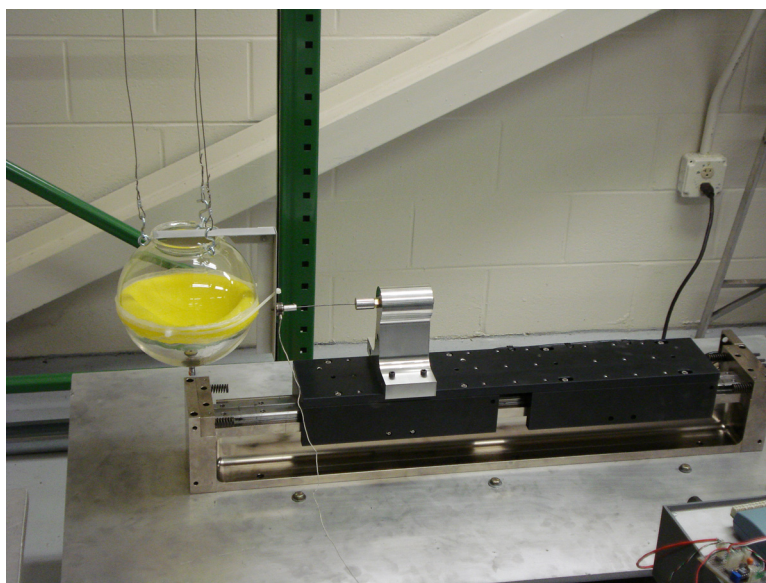


Figure 4. New slosh test facility at Embry-Riddle Aeronautical University.

Modeling of Slosh Dynamics in Cryogenic Propellant Tanks in Microgravity Environments



Mission Data
Feedback and
Analysis

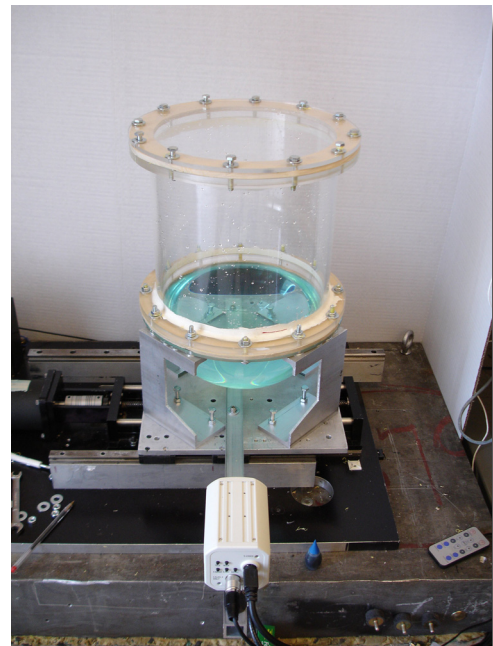
The slosh dynamics in cryogenic fuel tanks under microgravity is a pressing problem that severely affects the reliability of launching spacecraft. After reaching low Earth orbit, the propellant in a multistage rocket experiences large and cyclic changes in temperature as a result of solar heating. Tank wall heating can induce thermal stratification and propellant boiloff, particularly during slosh-inducing vehicle maneuvers. Precise understanding of the dynamic and thermodynamic effects of propellant slosh caused by these maneuvers is critical to mission performance and success. Computational fluid dynamics (CFD) analysis is used extensively within the space vehicle industry in an attempt to characterize the behavior of liquids in microgravity, yet experimental data to quantify these predictions is very limited and reduces confidence in the analytical predictions.

A novel approach designed to produce high-fidelity data for correlation to CFD model predictions is being developed with the assistance of Florida Institute of Technology (FIT) and Sierra Lobo, Inc. With few exceptions, previous work in slosh dynamics was theoretical or treated the mass of fuel as a variable of inertia only; such models did not consider the viscosity, surface tension, or other important fluid effects. The challenges in this research are in the development of instrumentation able to measure the required parameters, the computational ability to quantify the fluid behaviors, and the means to assess both the measurements and predictions.

The design of this experiment bridges the understanding of slosh dynamics in microgravity by a comprehensive approach that combines CFD tools, dynamic simulation tools, semianalytical models of the predominant fluid effects, and an experimental framework that includes measurement and characterization of liquid slosh in one-degree-of-freedom (DOF) and two-DOF experiments, and ultimately experiments in a NASA low-gravity aircraft.

A one-DOF ground test tank and visualization system was developed by FIT to capture slosh images. Software was developed (1) for image processing, surface extraction, and wall-wetting behavior, (2) for ground verification of the CFD modeling, and (3) for the test and checkout of the flight instrumentation in development.

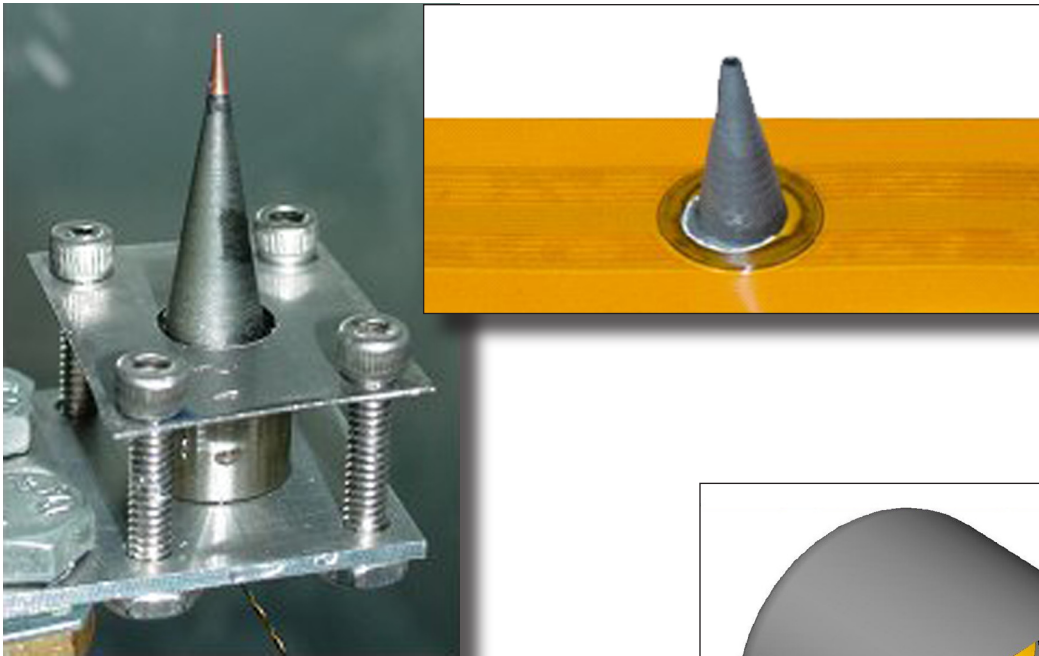
The reduced-gravity propellant-sensing system is based upon the Cryo-Tracker[®] system developed by Sierra Lobo, Inc., with NASA sponsorship, for cryogenic tank fill and drain operations. The system detects fluid levels and temperature by measuring



One-DOF ground test tank.



Slosh induced in test tank.



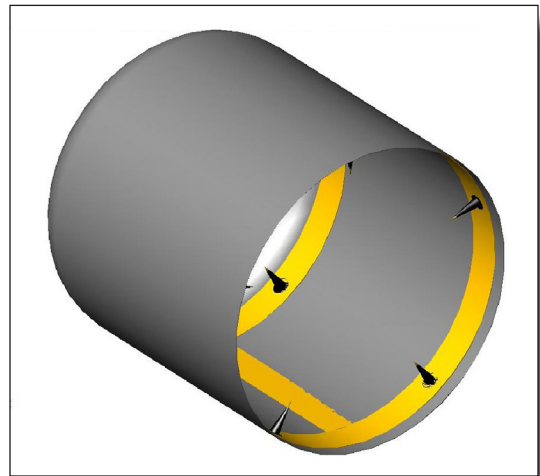
Low-gravity probe prototype test.

the change in impedance in a diode junction as a result of the heat transfer in the vicinity of the sensing element. Characterization of slosh dynamics in microgravity, however, requires an instrument whose accuracy is also independent of the gravity field in which it operates. The innovation in this development is a sensor that exploits certain aspects of low-gravity fluid physics to allow the sensing area to be exposed to liquid only when bulk liquid is present.

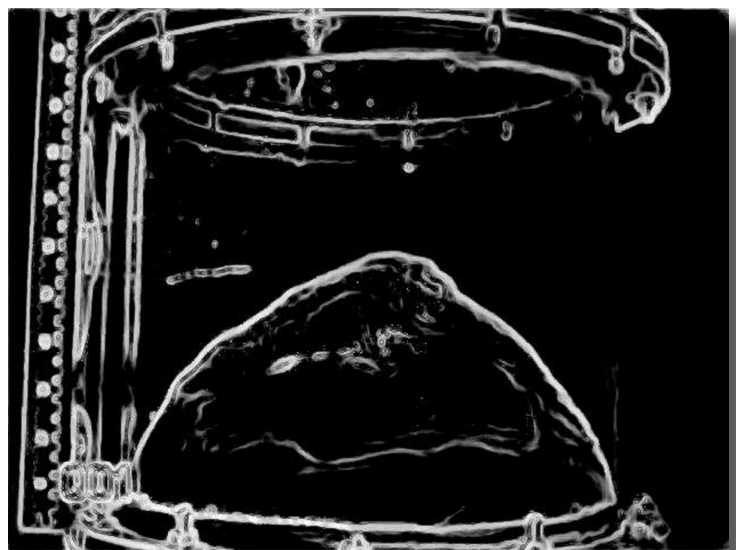
The technologies developed in support of these experiments will be of great benefit to launch vehicles and spacecraft, and the microgravity data will be of considerable interest throughout the space exploration community.

Contact: Laurie K. Walls <Laurie.K.Walls@nasa.gov>, NASA-KSC, (321) 867-1968

Participating Organizations: NASA-KSC (Paul A. Schallhorn), Florida Institute of Technology (Daniel Kirk), and Sierra Lobo, Inc. (Mark Habermusch)

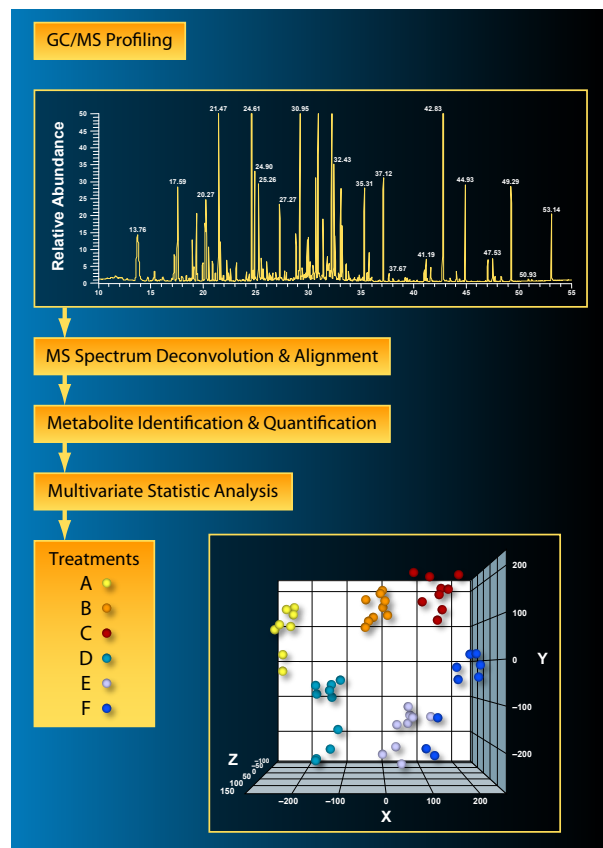
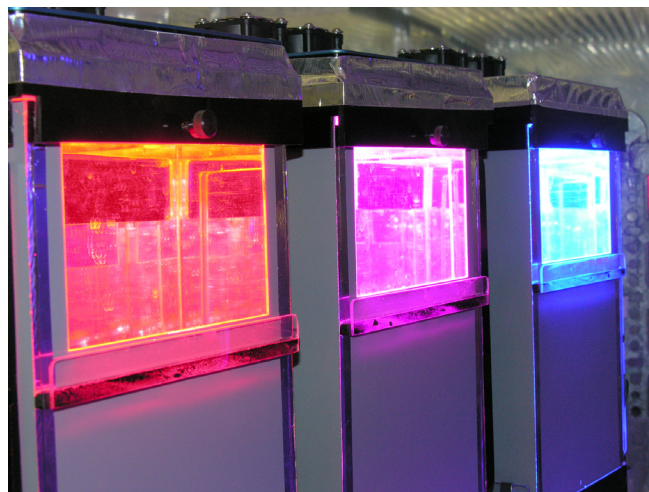
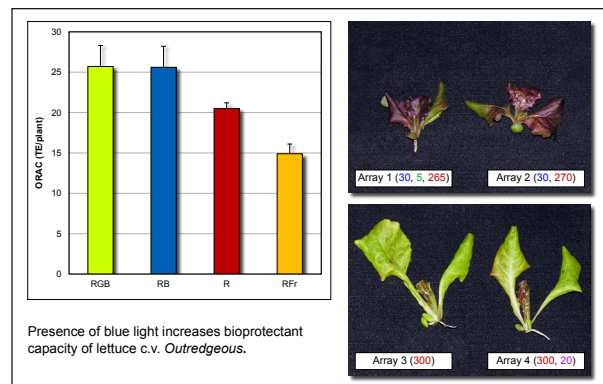
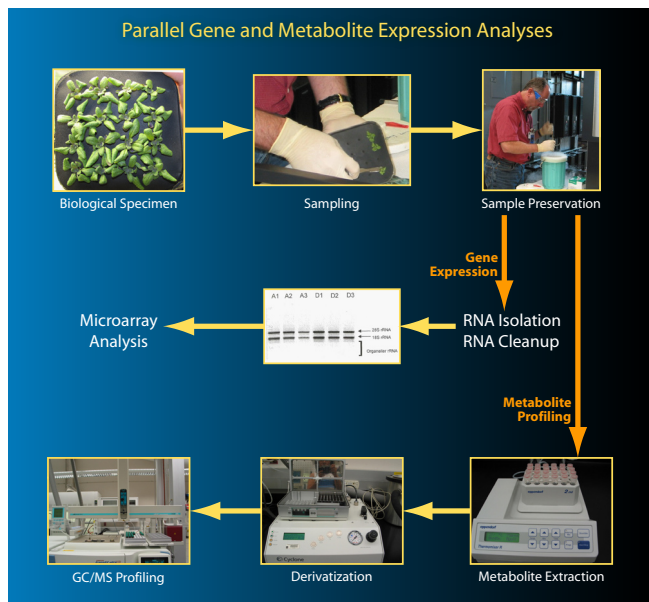


Tank instrumented with low-gravity probes.



Binary stage of data extraction process.

Biological Sciences



Countermeasure for Radiation Protection and Repair



Energy-Efficient
Lighting Systems

Exposure to ionizing radiation during long-duration space missions is expected to cause short-term illness and increase long-term risk of cancer for astronauts. Radiation-induced free radicals overload the antioxidant defense mechanisms and lead to cellular damage at the membrane, enzyme, and chromosome levels. A large number of radioprotective agents were screened, but most had significant side effects. But there is increasing evidence that significant radioprotective benefit is achieved by increasing the dietary intake of foods with high antioxidant potential.

Early plant-growing systems for space missions will be limited in both size and volume to minimize power and mass requirements. These systems will be well suited to producing plants containing high concentrations of bioprotective antioxidants. This project explored whether the production of bioprotective compounds could be increased by altering the lighting system, without increasing the space or power requirements for production, and evaluated the effects of environmental conditions (light quantity, light quality, and carbon dioxide [CO₂] concentration) on the production of bioprotective compounds in lettuce, which provide a biological countermeasure for radiation exposure.

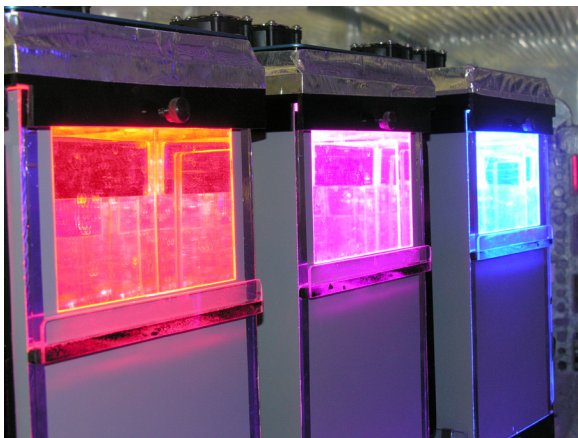
The specific deliverables were to

- develop a database of bioprotectant compounds in plants that are suitable for use on long-duration space missions,
- develop protocols for maintaining and increasing bioprotectant production under light-emitting diodes (LEDs),
- recommend lighting requirements to produce dietary countermeasures of radiation, and
- publish results in the *Journal of the American Society for Horticultural Science*.

Red leaf lettuce contains relatively high concentrations of bioactive pigments known as anthocyanins. These pigments, as well as other antioxidant molecules, have radioprotective properties. To determine if the concentration of these compounds could be increased, several red leaf lettuce cultivars were grown under either fluorescent lamps or LEDs at 300 $\mu\text{mol m}^{-2} \text{s}^{-1}$ of photosynthetically active radiation (PAR) of light intensity, 1,200 $\mu\text{mol mol}^{-1} \text{CO}_2$, 23 °C, and an 18-hr light/6-hr dark photoperiod in controlled-environment chambers. The LED treatments were selected to provide different amounts of red (640-nm), blue (440-nm), green (530-nm), and far red (730-nm) light in the spectra. Total anthocyanin content and the oxygen radical absorbance capacity (ORAC) of the tissue were measured at harvest. The results were compared

with effects of light intensity under fluorescent lamps from 100 to 450 $\mu\text{mol m}^{-2} \text{s}^{-1}$ PAR and CO₂ concentrations of 400, 1,200, and 3,000 $\mu\text{mol mol}^{-1}$. Bioprotectant concentration of red lettuce grown under red (640-nm) and blue (440-nm) light was comparable to plants grown under fluorescent lamps.

The source of light had a dramatic effect on both plant growth and production of radioprotective compounds. LEDs produced 50 percent more bioprotectant content per plant at the same light level than did conventional fluorescent lamps. The use of LEDs containing blue (440-nm) light in particular appeared to activate the pathways leading to increased concentration of bioprotective compounds in leaf tissue. LEDs provided a number of indirect effects that increased the bioprotective content. LEDs also allowed the ability to



High-output LED arrays provide the capability to define spectra to increase the concentration of radioprotective compounds.

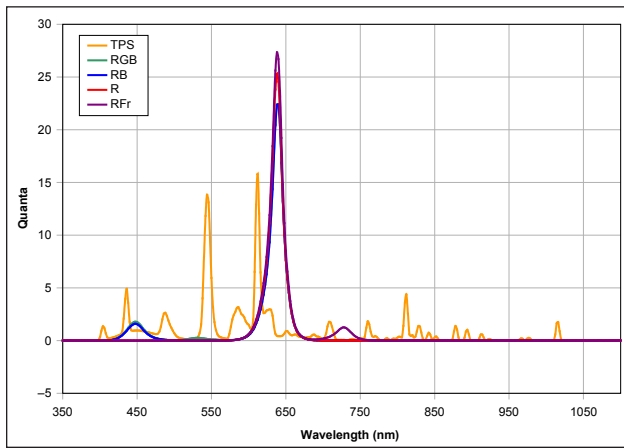
alter the spectral quality that can enhance leaf expansion and maximizes light interception. In addition, LED lighting systems minimized the use of nonphotosynthetic light and increased the photosynthetic efficiency of the lighting system.

Related research demonstrated photochemical regulation of the biochemical processes associated with the synthesis of bioprotective compounds in lettuce. These experiments showed the development of the bioprotective pigments (anthocyanin) and antioxidants (ORAC) is strongly affected by both light intensity and light quality. In particular, blue (440-nm) light seems to be necessary in order to maintain the bioprotective properties in lettuce.

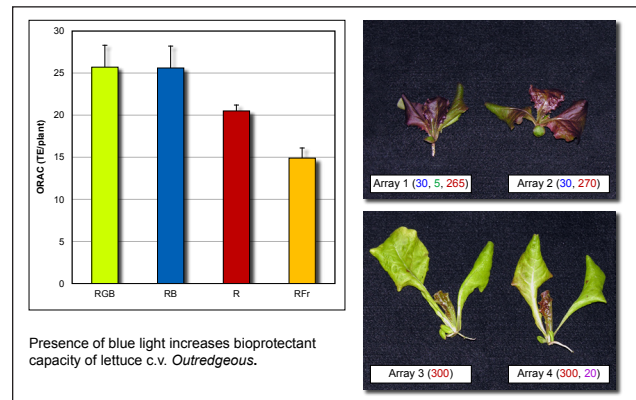
CO₂ enrichment had no direct effect on the regulation of the biochemical processes associated with synthesis of bioprotective compounds in lettuce. However, there was an indirect effect of increased growth rate at elevated CO₂ and thus greater bioproduction per plant.

Contacts: Dr. Gary W. Stutte <Gary.W.Stutte@nasa.gov>, Dynamac Corporation, (321) 861-3493; and Dr. Raymond M. Wheeler <Raymond.M.Wheeler@nasa.gov>, NASA-KSC, (321) 861-2950

Participating Organizations: Dynamac Corporation (Ignacio Erasó) and NASA-KSC (Dr. John C. Sager)

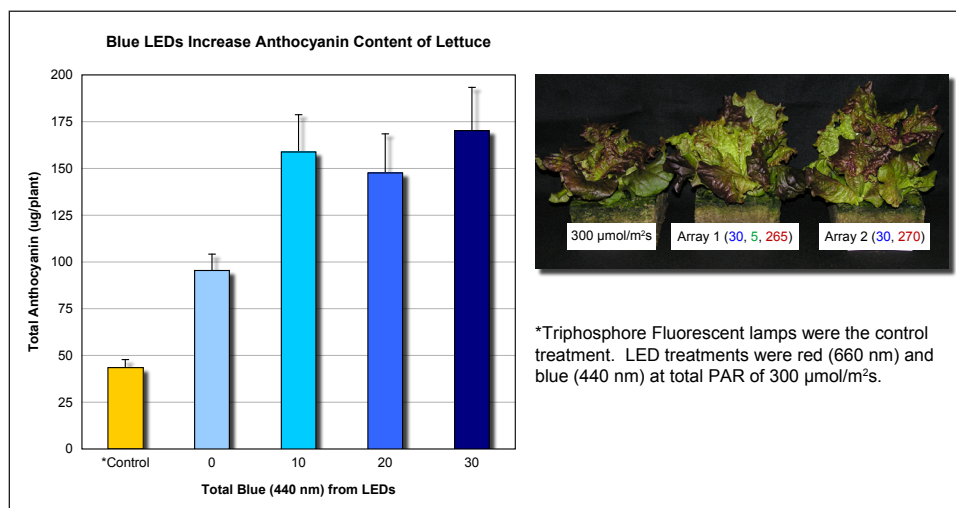


Spectroradiometric scans were used to set the light quantity and quality for growth of red leaf lettuce.



Presence of blue light increases bioprotectant capacity of lettuce c.v. *Outredgeous*.

Blue light was necessary in the spectra for anthocyanin production and to maximize antioxidant-potential tissue.



*Triphosphore Fluorescent lamps were the control treatment. LED treatments were red (660 nm) and blue (440 nm) at total PAR of 300 μmol/m²s.

Plants grown under LEDs were 30 to 40 percent larger than plants grown at the same light under fluorescent lamps (see inset). The addition of 10 μmol m⁻² s⁻¹ of blue (440-nm) light nearly doubled the concentration of anthocyanin in the leaves.

Focused Metabolite Profiling for Dissecting Cellular and Molecular Processes of Living Organisms in Space Environments

2006 Center Director's Discretionary Fund Project



Water and
Air Recovery/
Purification

Regulatory control in biological systems is exerted at all levels within the central dogma of biology: DNA→mRNA→Enzyme_{inactive}→Enzyme_{active}→Metabolites (Figure 1). Metabolites are the end products of all cellular regulatory processes and reflect the ultimate outcome of potential changes suggested by genomics and proteomics caused by an environmental stimulus or genetic modification. Following on the heels of genomics, transcriptomics, and proteomics, metabolomics has become an inevitable part of complete-system biology because none of the lower “-omics” alone provide direct information about how changes in mRNA or protein are coupled to changes in biological function. Analogous to the precedent “omics,” metabolomics is the systematic study of collections of small molecules (i.e., metabolites) in a biological system (a cell, organ, or organism). In contrast to the traditional biochemistry approach in which specific metabolites and enzymes are studied, metabolomics takes a holistic view of the entire suite of metabolites (the metabolome) in an organism to capture the coordinated regulation of biological systems. Thus, metabolomics, coupled with other “omics” such as transcriptomics and proteomics, holds great promise for deciphering the functions of genes, predicting novel metabolic pathways, and providing insights to the regulation of a biological event, as well as for directing metabolic engineering of plants for human benefit. However, the challenges are much greater than those encountered in genomics because of the greater number of metabolites and the greater diversity of their chemical structures and properties. To meet these challenges, much developmental work is needed, including (1) methodologies for unbiased extraction of metabolites and subsequent quantification, (2) algorithms for systematic identification of metabolites, (3) expertise and competency in handling a large amount of information (data set), and (4) integration of metabolomics with other “omics” and data mining (implication of the information).

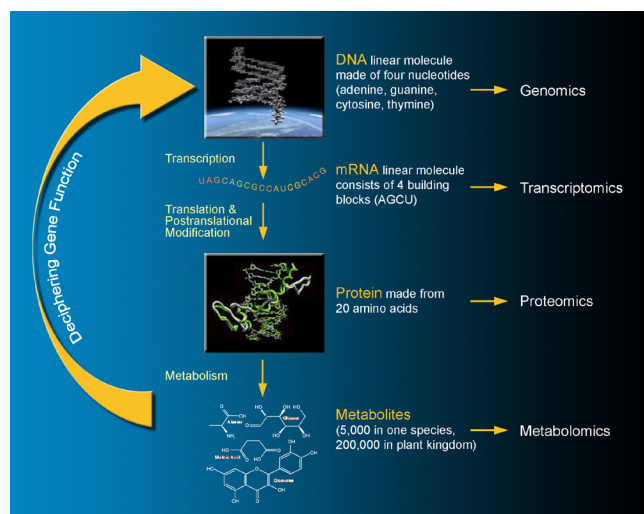


Figure 1. The central dogma of biology and the “omics” revolution.

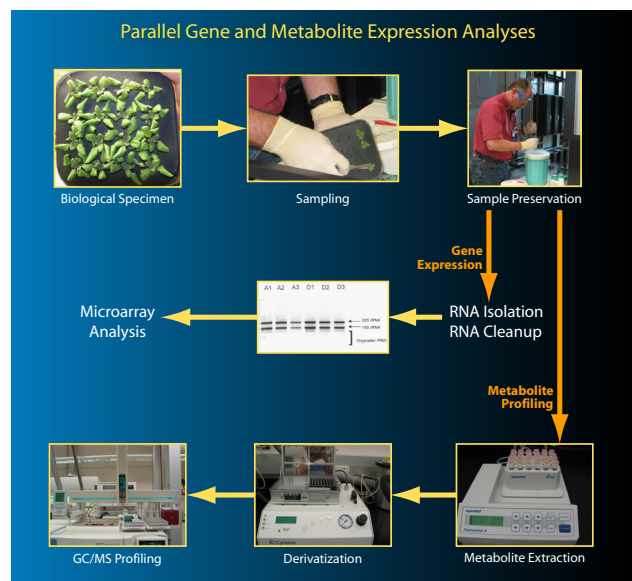


Figure 2. Analytical platform for metabolite profiling.

Project accomplishments include the following:

- A gas chromatography/mass spectrometry (GC/MS)-based analytical platform was developed and optimized (encompassing essential hardware [Figure 2]) for profiling small polar molecules. Procedures, software, and technical competency in metabolite profiling were also developed (also see “Development and Coupling of Metabolomics Capability With Transcriptomics To Dissect Cellular and Molecular Processes of Living Organisms” in *KSC Technology Development and Application 2005 Annual Report*).
- Metabolite profiling was completed for 54 samples generated in FY 2005 experiments.
- Microarray analysis for gene expression (about 22,000 transcripts) and data processing platform was completed.
- The Automated Mass Spectral Deconvolution and Identification System (AMDIS) was implemented and enabled to analyze the GC/MS raw data files for the purification of mixed spectra and the identification and quantification of target components (Figure 3). With the help of Bionetics, an Excel macro was developed to extract and format AMDIS outputs.
- A targeted mass spectra and retention index library was constructed for *Arabidopsis* metabolome and quantitative and qualitative information was extracted from the GC/MS metabolite profiles (70 unique mass tags are statistically responsive to carbon dioxide [CO₂] treatment).
- Competency was increased in statistics and bioinformatics to extract biological meaning from transcriptional and metabolite profiles, and work to interpret data continued in an effort to understand the differential effect of normally elevated CO₂ and super-elevated CO₂ on plant growth and stomatal function.
- Four additional elevated-CO₂ experiments were conducted to obtain complementary information on transpiration (indicative of stomatal function), growth, and morphology.
- The occurrence in this plant model of previous observations from other plant species was confirmed, thus offering opportunities to use molecular tools to reveal the mechanism underlying the biphasic response of growth and stomatal function to increasing atmospheric CO₂ concentration.
- A manuscript focusing on stomatal function under normally elevated CO₂ and super-elevated CO₂ was initiated.

Contact: Dr. Raymond M. Wheeler
<Raymond.M.Wheeler@nasa.gov>,
NASA-KSC, (321) 861-2950

Participating Organizations: Dynamac Corporation
(Dr. Lanfang H. Levine and Jeffrey T. Richards), University of
Florida (Dr. Charles Guy), and Bionetics Corporation
(Kevin A. Burtness)

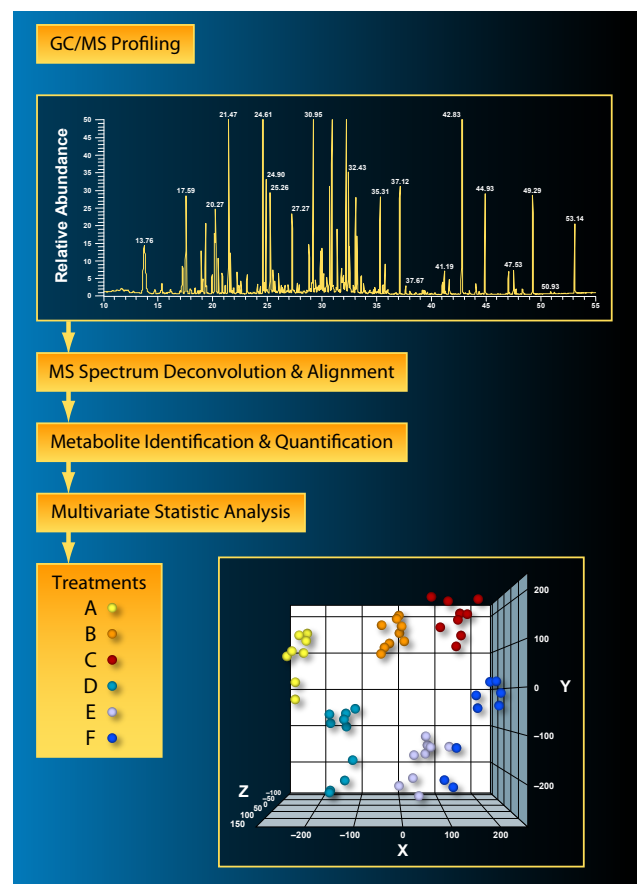
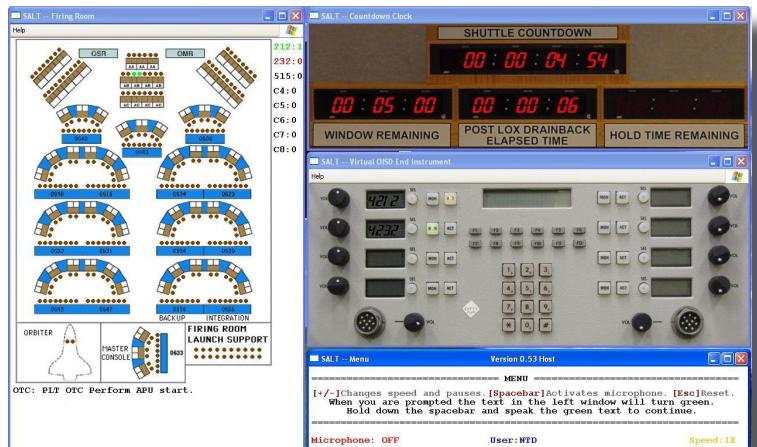
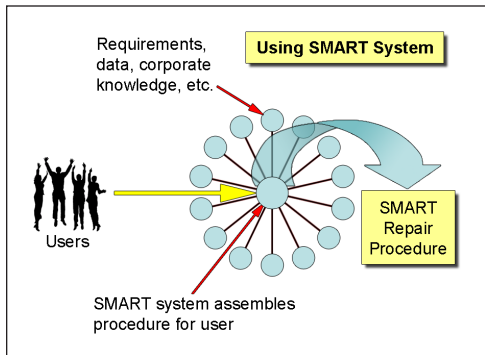


Figure 3. Data analysis and information extraction framework.

Process and Human Factors Engineering Technologies



Distributed Observer Network



Task/Process
Modeling and
Simulation

NASA's advanced visual simulations are essential for analyses associated with life cycle planning, design, training, testing, operations, and evaluation. Kennedy Space Center, in particular, uses simulations for ground services and space exploration planning in an effort to reduce risk and costs while improving safety and performance. However, it has been difficult to circulate and share the results of simulation tools among the field centers, and distance and travel expenses have made timely collaboration even harder.

In response, NASA joined with Valador Inc. to develop the Distributed Observer Network (DON), a collaborative environment that leverages game technology to bring 3-D simulations to conventional desktop and laptop computers. DON enables teams of engineers working on design and operations to view and collaborate on 3-D representations of data generated by authoritative tools, such as Delmia Envision, Pro/ENGINEER, or Maya. DON takes models and telemetry from these sources and, using commercial game engine technology, displays the simulation results in a 3-D visual environment. Multiple widely dispersed users, working individually or in groups, can view and analyze simulation results on desktop and laptop computers in real time.

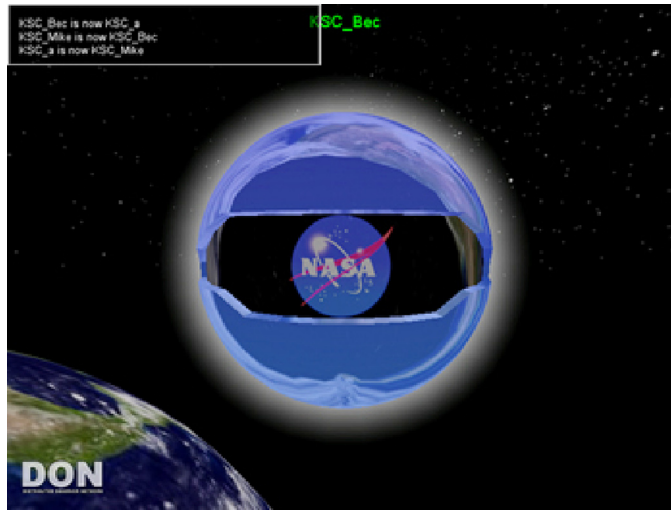
The development team experimented with a variety of NASA mission segment simulations, including Synergistic Engineering Environment (SEE) data, NASA Enterprise Visualization Analysis (NEVA) ground processing simulations, the Dynamic Simulation Suite (DSS) simulation for lunar operations, and the Johnson Space Center TRICK tool for guidance, navigation, and control analysis.

Users connect to DON through a client that runs on their own PCs or Mac computers. They can move freely within its virtual world and can preset camera points that let them jump to specific views. DON allows users to communicate textually or via Voice over Internet Protocol (VoIP); to write and save notes; and to replay, forward, fast-forward, pause, and loop simulations. Through DON, team members can share data, coordinate their work efficiently, and create a digital repository of their simulations and related information.

DON is slated for a 2008 release to support simulations for the Constellation Program. Plans for further development include improving DON's interaction with existing systems. Beyond NASA applications, DON offers opportunities in education and a myriad of other industries, particularly for overcoming the challenges that face dispersed teams collaborating on complex problems.

Contacts: William L. Little <William.L.Little@nasa.gov>, NASA-KSC, (321) 861-8938; and Rick Brubaker, Valador Inc., (703) 435-9155

Participating Organizations: NASA-KSC (Michael P. Conroy and Rebecca A. Mazzone), ASRC Aerospace (Dr. David K. Mann, Phillip B. Michael, and Michelle S. Ruder), and Valador Inc. (Tom Cuddy and Fred Spiker)



DON uses game technology to enable its geographically dispersed engineers to view and collaborate on the results of their complex simulations.



DON lets users replay, forward, fast-forward, reverse, pause, and loop simulations.

Influence Map Methodology for Evaluating Systemic Safety Issues

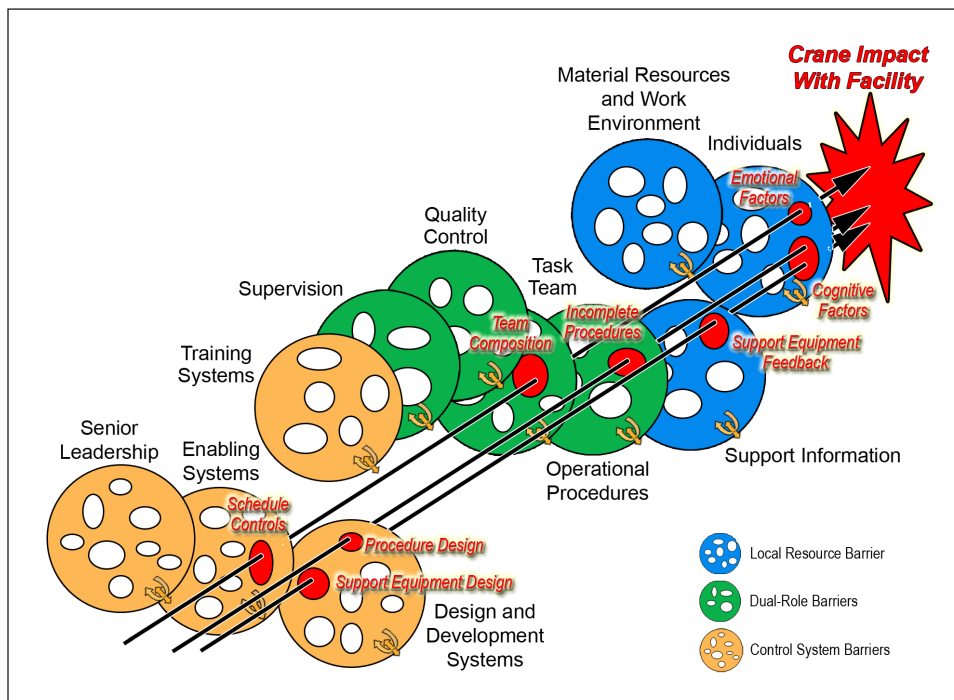


Task/Process
Modeling and
Simulation

“Raising the bar” in safety performance is a critical challenge for many organizations, including Kennedy Space Center. Contributing-factor taxonomies organize information about the reasons accidents occur and therefore are essential elements of accident investigations and safety reporting systems. Organizations must balance efforts to identify causes of specific accidents with efforts to evaluate systemic safety issues in order to become more proactive about improving safety.

This project successfully addressed the following two problems: (1) methods and metrics to support the design of effective taxonomies are limited and (2) influence relationships among contributing factors are not explicitly modeled within a taxonomy. The primary result of the taxonomic-relationship modeling efforts was an innovative “dual-role” taxonomy that is more comprehensive and has better diagnostics than existing contributing-factor taxonomies. The influence map methodology graphically and analytically combines the dual-role taxonomy and influence relationship models.

Influence maps were developed for an initial sample of safety incidents at Kennedy Space Center. A team of experts used the new dual-role taxonomy and influence chain methodology to evaluate the accuracy and completeness of contributing factors identified during formal incident investigations. Using the influence map methodology, the team identified 116 contributing factors. Only 16 percent of these events or conditions were identified as contributing factors, contributing causes, or root causes with traditional tools during the formal incident investigations, and over half of the 116 contributing factors were not addressed by the findings and recommendations in the formal incident reports.



Influence chains of contributing factors in mobile crane mishap.



Type of mobile crane that impacted the crossover between the KSC Vehicle Assembly Building and a utility annex.



Location and close-up of damage to the crossover between the KSC Vehicle Assembly Building and a utility annex.

Accomplishments of this ongoing project include the following:

- comparatively analyzing industry and government contributing factor taxonomies (2002),
- developing the dual-role taxonomy (2003),
- developing the influence chain methodology (2004),
- initially testing and evaluating the influence map methodology with incident data from Shuttle Ground Operations and applying taxonomy analysis results to the efforts of the NASA Engineering and Safety Center's taxonomy working group (2005),
- refining the influence map methodology and documenting the approach (2006),
- analyzing a representative sample of Shuttle processing incidents occurring since February 2003 with the influence map methodology (2007),
- delivering recommendations to (1) address the most significant systemic safety issues in Shuttle Ground Operations, (2) prevent recurrence of specific mishap types, (3) address design considerations that will benefit Constellation systems, and (4) improve the quality of incident investigations (2008), and
- applying the influence map tool to Orion processing, historical NASA events, and additional safety domains (2008).

Contact: Timothy S. Barth <Timothy.S.Barth@nasa.gov>, NASA Engineering and Safety Center, (321) 867-6230

Participating Organizations: United Space Alliance (Donna M. Blankmann-Alexander and Blake Parker) and NASA Ames Research Center (Dr. Barbara Kanki)

Simulation and Analysis of Launch Teams (SALT)



Task/Process
Modeling and
Simulation

A SALT effort was initiated in late 2005 with seed funding from the Office of Safety and Mission Assurance Human Factors organization. Its objectives included demonstrating human behavior and performance modeling and simulation technologies for launch team analysis, training, and evaluation. The goal of the research is to improve future NASA operations and training. The project employed an iterative approach, with the first iteration focusing on the last 70 minutes of a nominal-case Space Shuttle countdown, the second iteration focusing on aborts and launch commit criteria violations, the third iteration focusing on Ares I-X communications, and the fourth iteration focusing on Ares I-X Firing Room configurations. SALT applied new commercial off-the-shelf technologies from industry and the Department of Defense in the spaceport domain.

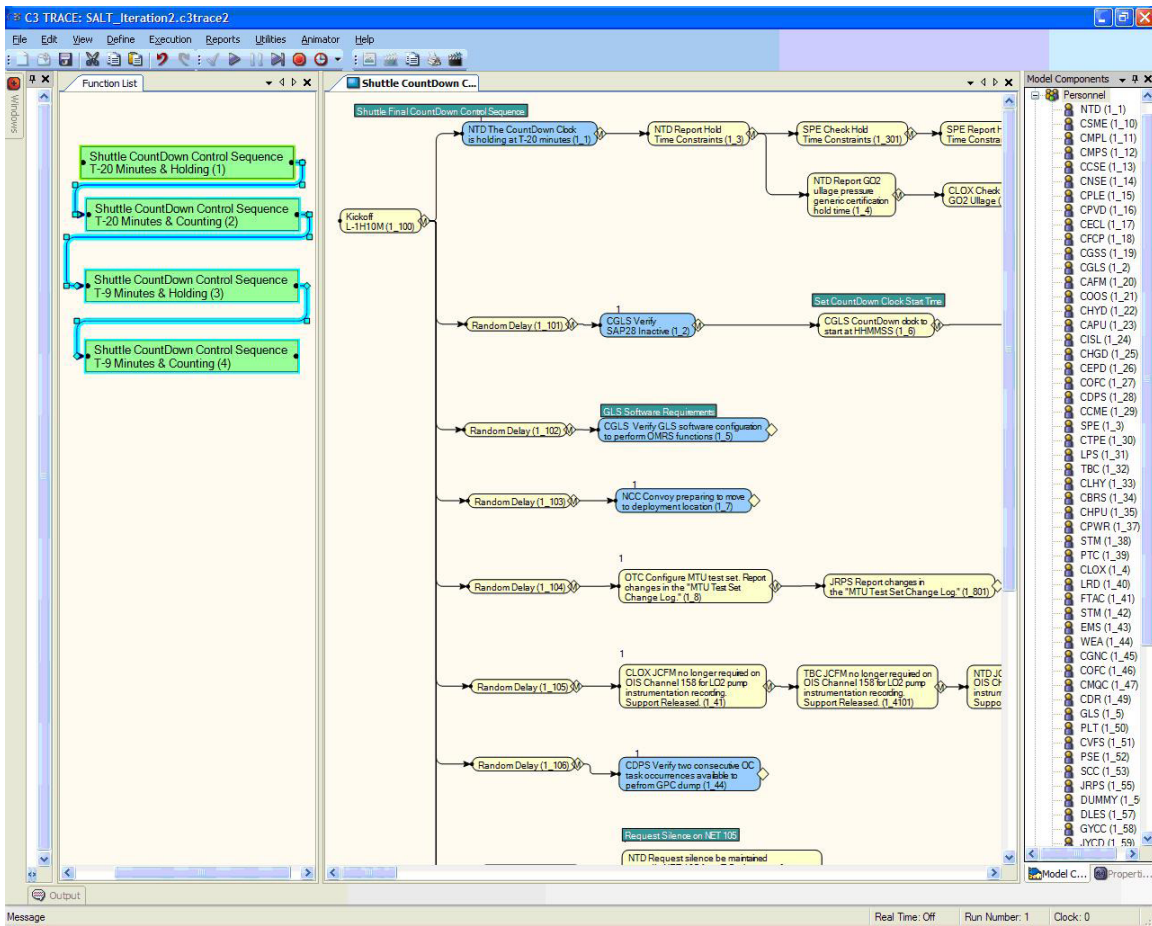
One of the first iteratively developed products was a task analysis. Data was gathered by reviewing documentation (including real and simulated launch procedures), observing training simulations, listening to audio recordings of operations, and interviewing launch domain experts. The task analysis included functions, tasks, call signs, call words, and as-run transcriptions. For each task, the analysis included step number, kickoff time, predecessors, initiating call sign, involved call signs, required communication channels, mean time and standard deviation, and description. The analysis was stored in spreadsheets and is a foundation on which other elements were built.

A second iteratively developed product was a human-performance simulation of the launch team's activities. It used the task analysis data and the Army Research Lab's Command, Control, and Communications – Techniques for the Reliable Assessment of Concept Execution (C3TRACE) tool. C3TRACE is owned by the U.S. Government, is free for NASA use, and is one of a family of proven tools targeted at human-performance modeling. The tool efficiently simulates communications, operations, utilization, availability, and shared situational awareness for tradeoff analysis. It can help organizations improve information quality and reduce workload peaks, communication bottlenecks, and decisionmaking vulnerabilities. The final iteration examined the effects of colocation and the number of key personnel on team performance during a nominal Ares I-X launch.

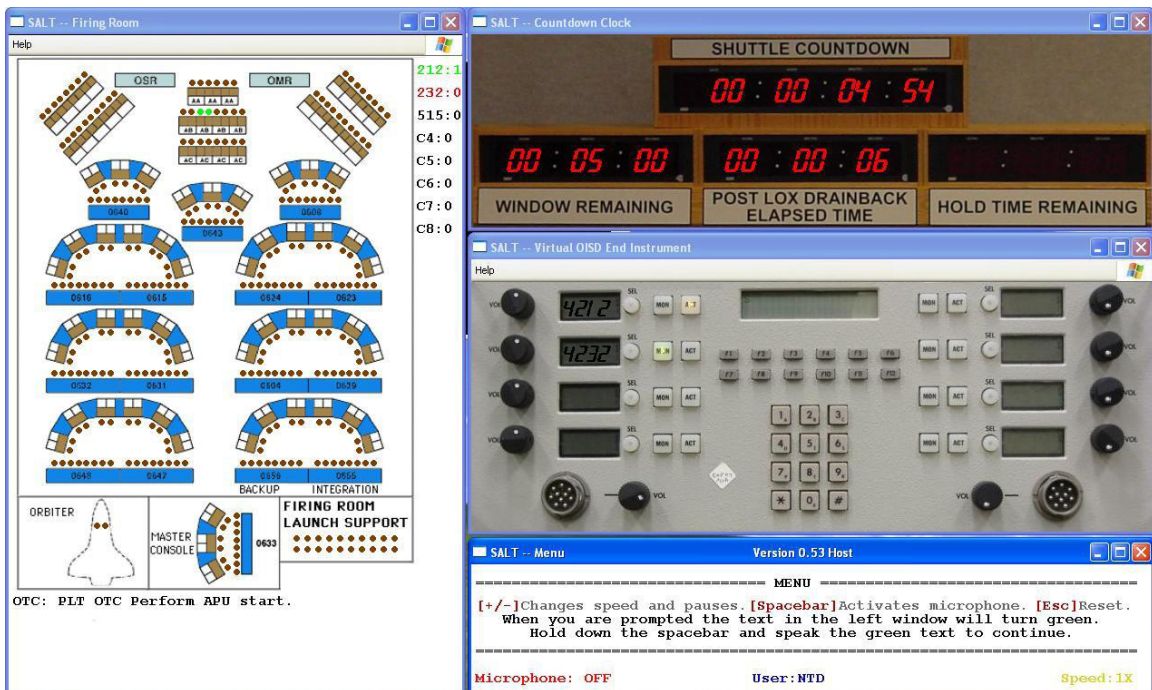
A third iteratively developed product was a proof-of-concept communication training application. The application was developed with Visual C++, OpenGL, the Microsoft Speech Software Development Kit and Speech Application Programming Interface, and for distributed small-team training, either Winsock or the High Level Architecture for simulation integration. The communication training application allows one or more trainees to play any launch team role while the computer plays the roles of all other virtual teammates. The application plays wave file utterances, provides prompts, and uses voice recognition to help teach trainees launch team communications and test team discipline. The application responds to the user's voice commands, so if a trainee says for example, "CGLS <trainee's call sign> give cutoff," then the simulation takes a launch abort path. NASA could use programs such as this to run individual or small-team lower-fidelity launch training rehearsals at the trainee's desk or other convenient location prior to conducting higher-fidelity training with the launch team in the Firing Room.

Contact: Cary J. Peaden <Cary.J.Peaden@nasa.gov>, NASA-KSC, (321) 867-9296

Participating Organizations: Alion Science and Technology (Nils D. LaVine and Timothy M. Bagnall), ASRC Aerospace (Luis M. Bares), and NASA-KSC (Stephen J. Payne and Richard M. Hoblitzell, Jr.)



SALT proof-of-concept communication training application.



SALT human-performance discrete-event simulation.

Solid-State Lighting Module (SSLM)



Energy-Efficient
Lighting System

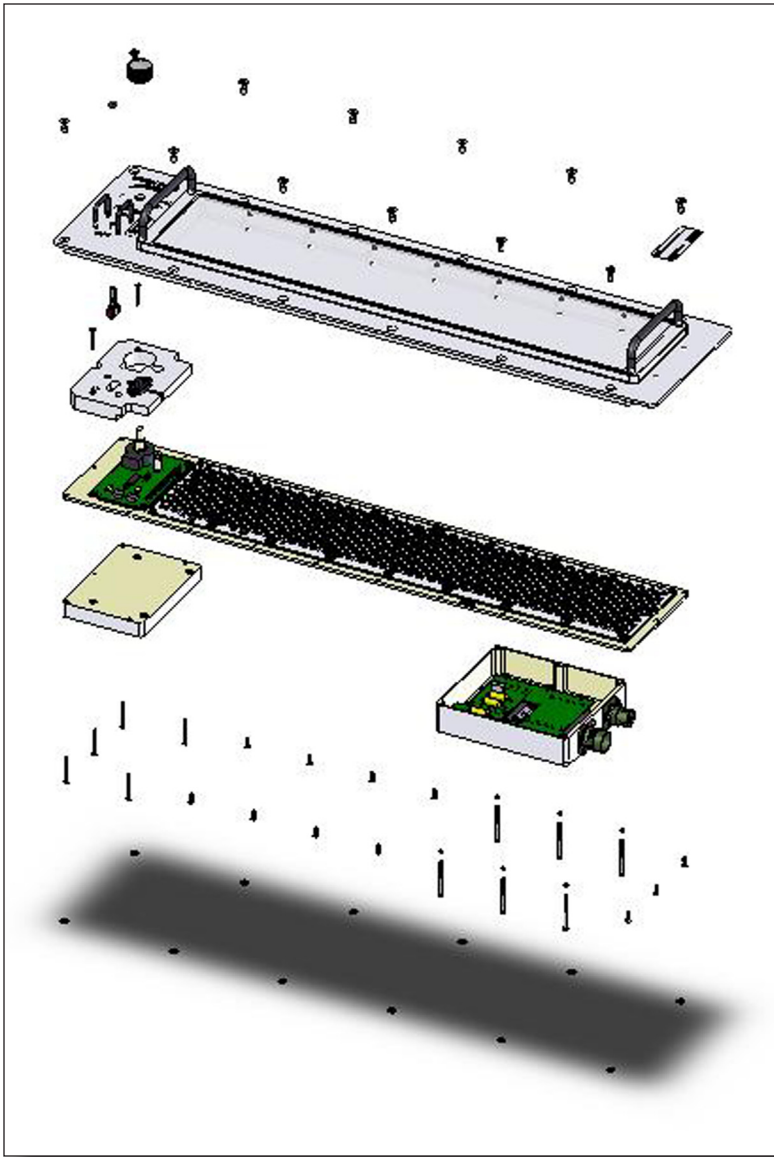
The project's goal was to build a light-emitting-diode (LED)-based light fixture that is identical in fit, form, and function to the existing International Space Station (ISS) General Luminaire Assembly (GLA) light fixture and fly it on the ISS in early FY 2008 as a Station Detailed Test Objective (SDTO).

Comparison of GLA and SSLM

Specification	GLA	SSLM	SSLM Benefits to ISS/Future Spacecraft
Power	30 W	30 W	n/a
Photo-optic Luminous Flux	449 lm	479 lm	Better illumination = safer operation
Mass	4.0 kg	3.6 kg	Less up-mass = more flexibility for manifesting
Input Voltage	120 VDC	120 VDC	n/a
Dimmability	flickering	0–100%	No flicker = less eye strain
Planned Life	~5,000 hr	~50,000 hr	Less maintenance = less up-mass and crew time



SSLM.



SSLM CAD model.

Our design offers the following strengths:

- proven component hardware: Our design uses components flown in other KSC-developed hardware;
- “heat path” thermal pad: LED array heat is transferred from the circuit board by silicon pad, negating the need for a cooling fan;
- variable colorimetry: The output light color can be changed by inserting different LED combinations.

Contact: Daniel C. Shultz <Daniel.C.Shultz@nasa.gov>, NASA-KSC, (321) 861-2896

Participating Organization: Bionetics Corporation (Trevor Murdoch, April C. Spinale, and Howard W. Wells)

Systems Maintenance Automated Repair Tasks (SMART)



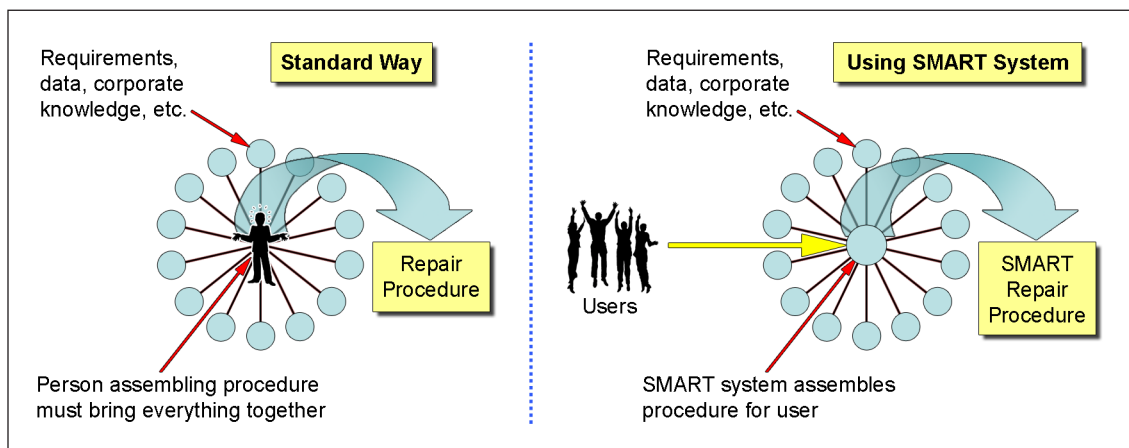
Decision/Data
Models and
Analysis

SMART is an interactive decision analysis and refinement software system that uses evaluation criteria for discrepant conditions to automatically provide and populate a document/procedure with predefined steps necessary to repair a discrepancy safely, effectively, and efficiently. SMART can store the tacit (corporate) knowledge merging the hardware specification requirements with the actual “how to” repair methods, sequences, and required equipment, all within a user-friendly interface. Besides helping organizations retain repair knowledge in streamlined procedures and sequences, SMART can also help them in saving processing time and expense, increasing productivity, improving quality, and adhering more closely to safety and other guidelines. Though SMART was developed for Space Shuttle applications, its interface is easily adaptable to any hardware that can be broken down by component, subcomponent, discrepancy, and repair.

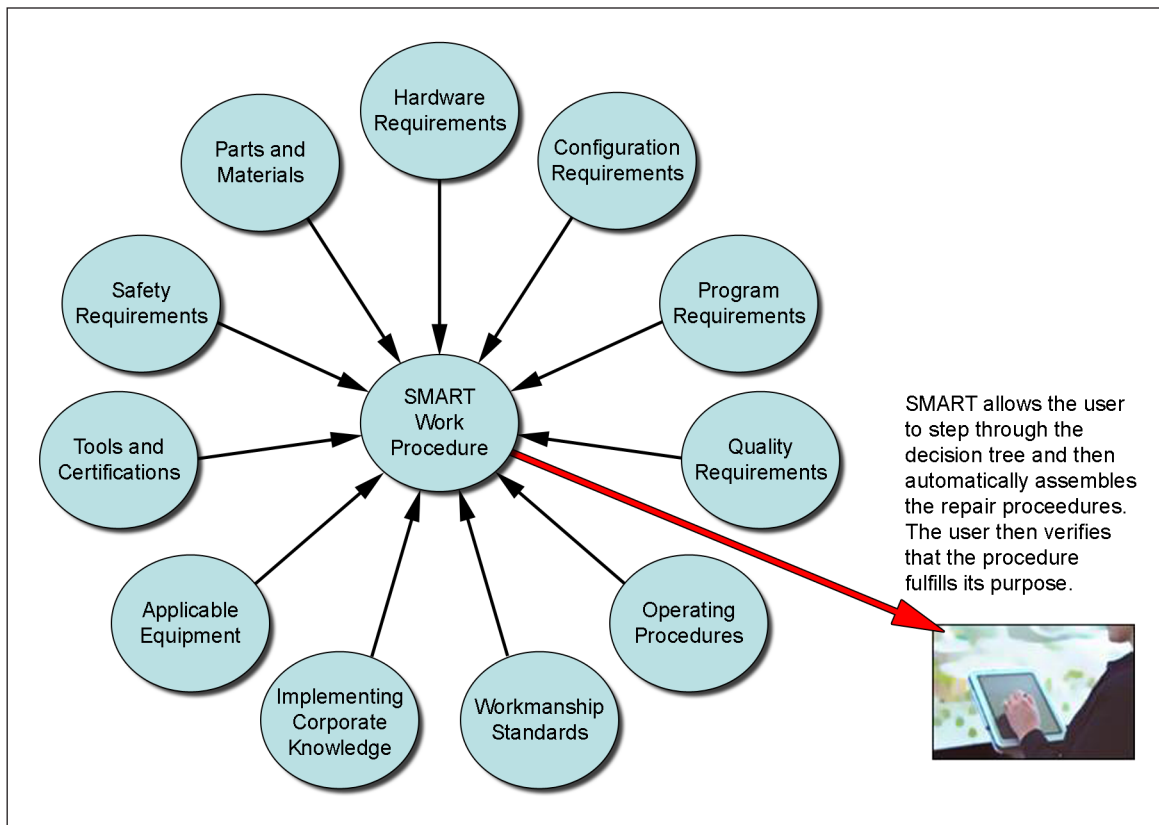
Through SMART’s decision analysis tree, all the permutations among the hardware’s components, subcomponents, possible discrepancies, and corresponding repairs can be identified. SMART’s repair matrix allows the user to define the specific steps and sequences required for any repair identified in the decision tree and to select specific steps from multivariable steps. SMART can interface with external databases and identify information to be inserted into the repair procedure document and will have the ability to automatically select which multivariable step is appropriate.

The user will log onto SMART, then through various levels of the predefined decision tree, identify a hardware discrepancy and refine its description. While navigating through the decision tree, the user can see not only the decision path but the breakdown of the hardware. Backing through decisions or changing a path is extremely easy. After the discrepancy is fully described, SMART will present a set of predefined steps for the user to verify and to tailor or qualify as necessary. The output can be sent to a database for quick retrieval or to a work authoring system in the form of a predefined sequence of steps identifying actions, tools, parts, materials, certifications, and specific requirements.

SMART’s backbone is its ability to create and manipulate interactive decision trees for single-variable and multivariable repair sequences. The user is always presented with the options of the correct hardware configuration and best repair methods. SMART is quick and easy to learn. No special loads are required, and SMART’s security and stability are ensured because the program is Oracle-based and exists on a maintained network server. This reduces the maintenance required for proper functioning and saves time, money, and operational steps. The software itself can be expanded and



Old process versus SMART process.

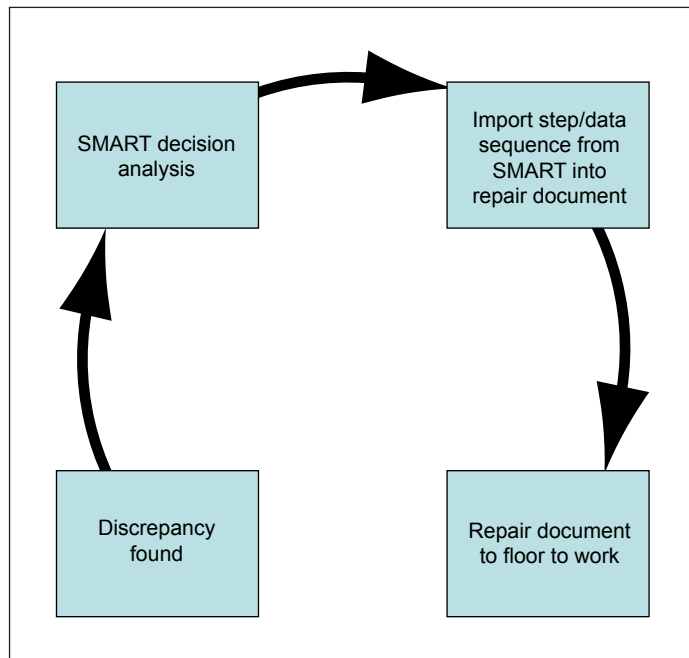


Variables that can be integrated by SMART.

tailored easily. In the scope of its use, SMART has cut process time by about 50 percent, reduced human error, and increased the consistency of hardware evaluation and repair.

Contact: Joseph M. Schuh <Joseph.M.Schuh@nasa.gov>, NASA-KSC, (321) 861-0662

Participating Organization: United Space Alliance (MaryJo Y. Al-Shihabi, Martin A. Belson, Derek A. Hardin, Nadean L. King, Louis W. Locklear, Brent H. Mitchell, and Elkin F. Norena)



Where SMART fits within the repair process.

Launch and Landing Effects Ground Operations (LLEGO) Model



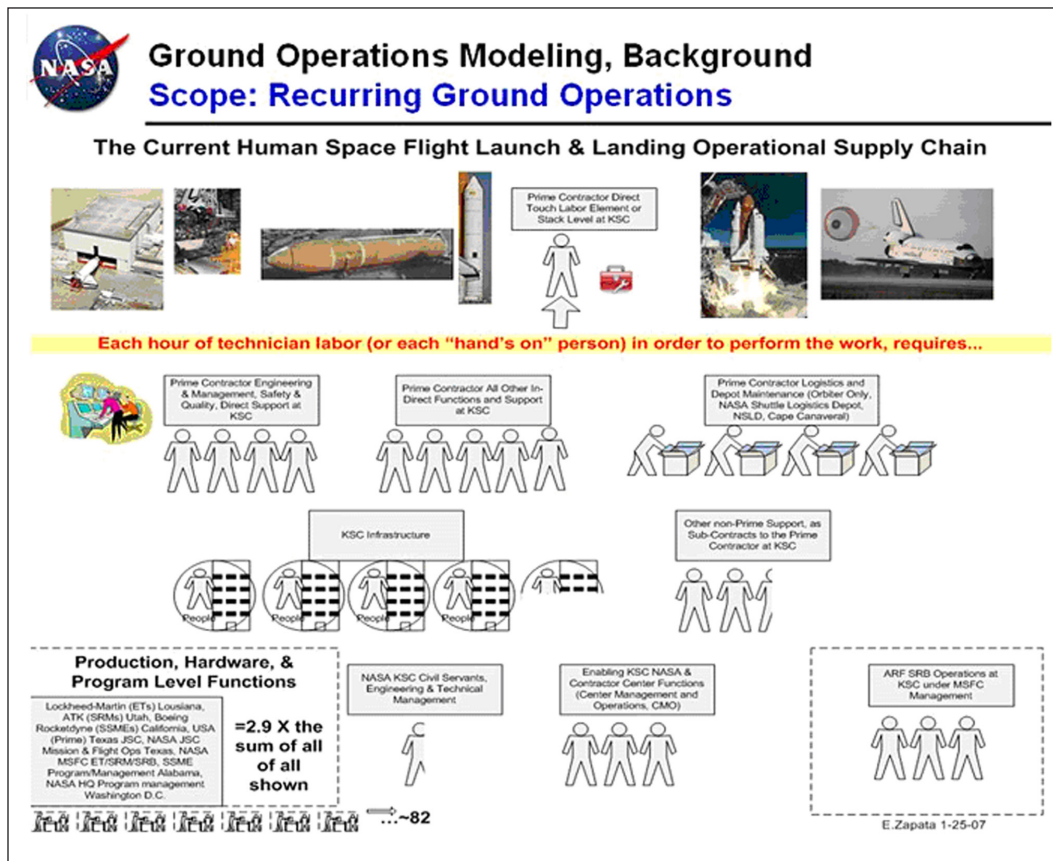
Decision/Data
Models and
Analysis

LLEGO is a model for understanding recurring launch and landing operations costs at Kennedy Space Center for human space flight. Launch and landing operations are often referred to as “ground processing,” or “ground operations.” Currently, this function is specific to the ground operations for the Space Shuttle Space Transportation System within the Space Shuttle Program.

The Constellation system to follow the Space Shuttle consists of the crewed Orion spacecraft atop an Ares I launch vehicle and the uncrewed Ares V cargo launch vehicle. The Constellation flight and ground systems build upon many elements of the existing Shuttle flight and ground hardware, as well as upon existing organizations and processes. In turn, the LLEGO model builds upon past ground operations research, modeling, data, and experience in estimating for future programs. Rather than to simply provide estimates, the LLEGO model’s main purpose is to improve expenses by relating complex relationships among functions (ground operations contractor, subcontractors, civil service technical, center management, operations, etc.) to tangible drivers. Drivers include flight system complexity and reliability, as well as operations and supply chain management processes and technology. Together these factors define the operability and potential improvements for any future system, from the most direct to the least direct expenses.

Contact: Edgar Zapata <Edgar.Zapata@nasa.gov>, NASA-KSC, (321) 867-6234

Participating Organization: Blue Frog Technologies, Inc. (Dr. Alex J. Ruiz-Torres)



The human space flight supply chain at Kennedy Space Center and beyond.

Exploration Supply Chain Simulation




Decision/Data
Models and
Analysis

The Exploration Supply Chain Simulation project was chartered by the NASA Exploration Systems Mission Directorate to develop a software tool, with proper data, to quantitatively analyze supply chains for future program planning. This tool is a discrete-event simulation that uses the basic supply chain concepts of planning, sourcing, making, delivering, and returning. This supply chain perspective is combined with other discrete or continuous simulation factors. Discrete resource events (such as launch or delivery reviews) are represented as organizational functional units. Continuous resources (such as civil service or contractor program functions) are defined as enabling functional units. Concepts of fixed and variable costs are included in the model to allow the discrete events to interact with cost calculations. The definition file is intrinsic to the model, but a blank start can be initiated at any time. The current definition file is an Orion Ares I crew launch vehicle. Parameters stretch from Kennedy Space Center across and into other program entities (Michaud Assembly Facility, Aliant Techsystems, Stennis Space Center, Johnson Space Center, etc.) though these will only gain detail as the file continues to evolve.

The Orion Ares I file definition in the tool continues to evolve, and analysis from this tool is expected in 2008. This is the first application of such business-driven modeling to a NASA/government-aerospace contractor endeavor.


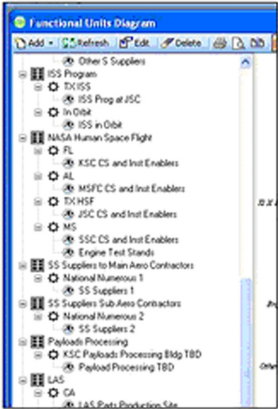
Contacts: Michael C. Galluzzi <Michael.C.Galluzzi@nasa.gov>, NASA-KSC, (321) 867-4796; and Edgar Zapata <Edgar.Zapata@nasa.gov>, NASA-KSC, (321) 867-6234

Participating Organization: Productivity Apex, Inc. (Dr. Mansooreh Mollaghasemi and Dr. Mohamed S. Fayez)



Software

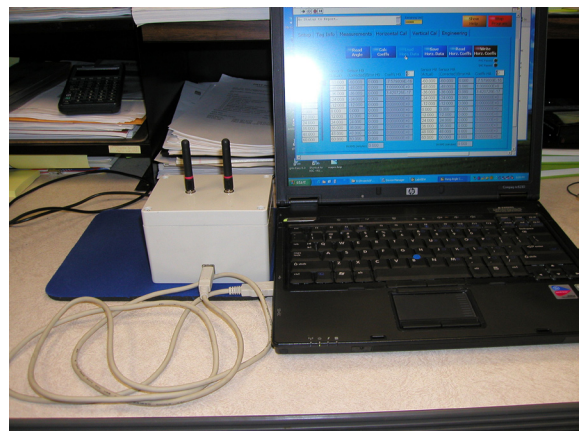
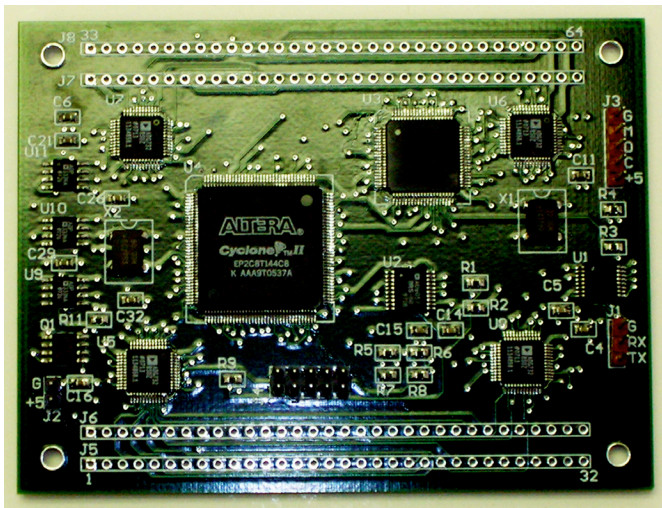
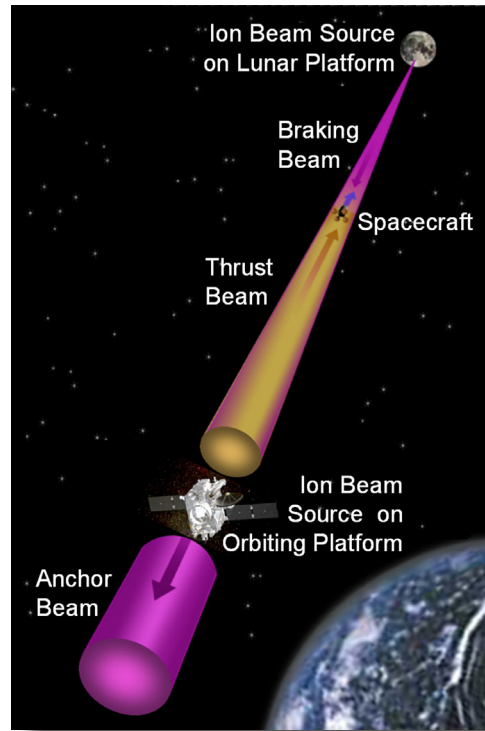
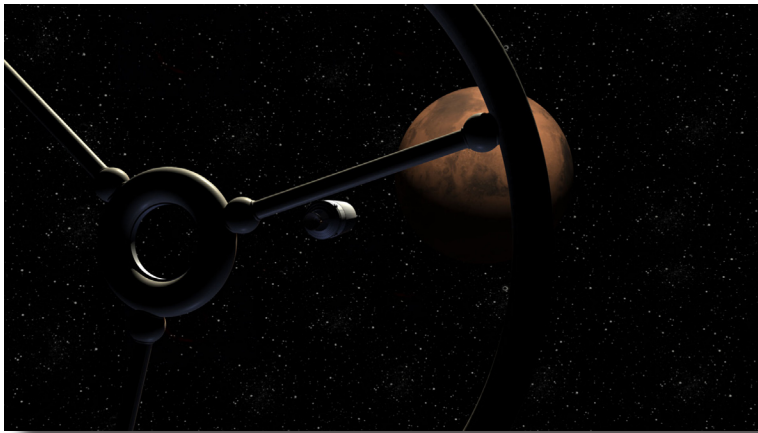
- ◆ Software consists of 4 basic pieces
 - Graphic user interface – Visual Basic
 - Underlying Data **As xml, xml schema**
 - Simulation in Arena
 - **A file the user creates that contains the system being represented, which can be saved or “save as” such as Shuttle or Orion / Ares and which can be altered in “what-if” exercises.**



```
<EnterpriseID>44</EnterpriseID>  
<Name>Rocketdyne at CA</Name>  
<Description />  
</Enterprise>  
- <Enterprise>  
  <EnterpriseID>45</EnterpriseID>  
  <Name>SRB Fwd Assy Suppliers</Name>  
  <Description />  
</Enterprise>  
- <Enterprise>  
  <EnterpriseID>46</EnterpriseID>  
  <Name>ATK at UT</Name>  
  <Description />  
</Enterprise>  
- <Enterprise>  
  <EnterpriseID>47</EnterpriseID>  
  <Name>Lockheed Martin CEV Prod at KSC</Name>  
  <Description />  
</Enterprise>  
- <Enterprise>  
  <EnterpriseID>48</EnterpriseID>  
  <Name>Other Suppliers Infrass Grnd Ops and Log</Name>  
  <Description />  
</Enterprise>  
- <Enterprise>  
  <EnterpriseID>51</EnterpriseID>  
  <Name>CLV 2nd Stage at TBD</Name>  
  <Description />  
</Enterprise>  
- <Enterprise>  
  <EnterpriseID>65</EnterpriseID>  
  <Name>Other S Suppliers</Name>
```

Representing the exploration supply chain: a collection of entities that partner together to achieve specific goals.

Command, Control, and Monitoring Technologies



Nanosensors for Evaluating Hazardous Environments



Hazardous-Leak
Detection and
Isolation

Personnel working in a confined environment can be exposed to hazardous gases, and certain gases can be extremely dangerous even in concentrations as low as a few parts per billion.

Nanosensors can be placed in multiple locations over a large area, thus allowing for more precise and timely detection of gas leaks. ASRC Aerospace and its research partners are developing nanosensors to detect various gases, including hydrogen, ammonia, nitrogen tetroxide, and hydrazine. Initial laboratory testing demonstrated the capability to detect these gases in concentrations lower than parts per million, and current testing is evaluating sensitivity at concentration levels three orders of magnitude lower. Testing and development continue to improve the response and recovery times and to increase the sensitivity of the devices. The development team is evaluating different coatings and electrodes to determine the optimum configuration for detecting and identifying a variety of gases.

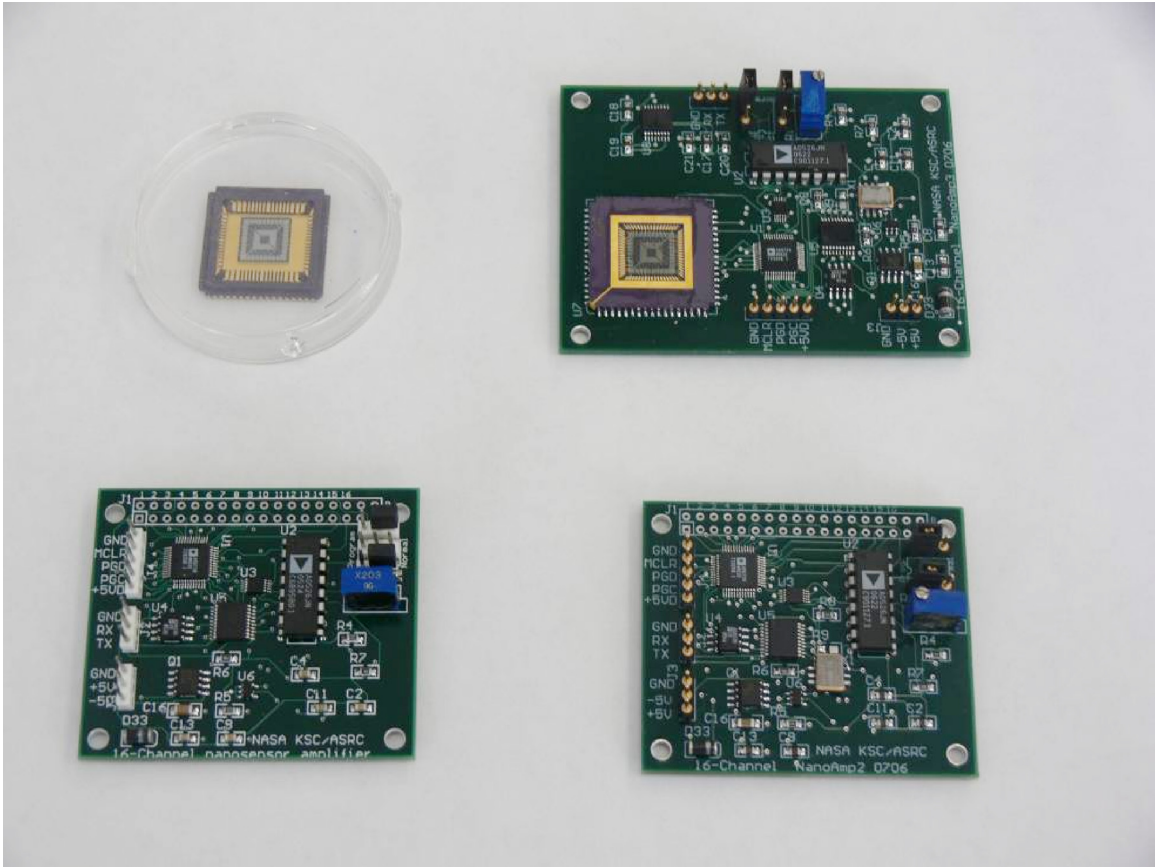
The small footprint of the nanosensors allows several devices to be placed into a single substrate. Each sensor is responsive in a different way to different gases. Embedding multiple devices into a single substrate results in better reliability and less frequent calibrations. The use of different coatings for individual elements of a multichannel sensor allows different gases to be identified. The sensor system is implemented by the use of a custom multichannel signal conditioner amplifier built on a small multichip module. This device processes the output of the sensors and transmits a signal that can be monitored and analyzed remotely. All the data is digitized and transmitted over the same cable pair used to power the amplifier. Connecting multiple outputs to a single cable pair will reduce the weight and expense associated with cabling in a spacecraft.

Although the initial work concentrated on the detection of nitrogen dioxide and nitrogen tetroxide, sensors are being developed and tested for detection of hydrogen, ammonia, hypergolic fuel (hydrazine), hypergolic oxidizer (nitrogen tetroxide, which is analyzed as nitrogen dioxide), and monomethylhydrazine. The sensors are being evaluated under a wide variety of environmental conditions, including various temperatures, humidities, and gas concentrations. The initial test evaluates the sensor's ability to identify and analyze three concentrations of hydrazine at constant temperature and humidity. The final objectives will be to optimize individual responses to various gases and to integrate the sensors onto a single substrate.

Monitoring of the environment is not limited to the detection of gas leaks, and monitoring will become increasingly important as longer-duration space missions are planned and executed. A wide array of nanosensors needs to be developed and qualified for space flight under realistic operating conditions, and this activity will continue for years to come.

Contact: Dr. Pedro J. Medelius <Pedro.J.Medelius@nasa.gov>, ASRC Aerospace, (321) 867-6335

Participating Organizations: ASRC Aerospace (Dr. Tracy L. Gibson and Dr. Barry J. Meneghelli), NASA-KSC (Michael E. Vinje and Jose M. Perotti), and NASA Ames Research Center (Dr. Jing Li)



Sensor and signal-conditioning amplifier.

Sixty-four-Channel Inline Cable Tester



Wire/Cable
Inspection and
Repair

Faults in wiring are a serious concern for the aerospace and aeronautics (commercial, military, and civil) industries. A number of accidents have occurred because faulty wiring created shorts or opens that resulted in the loss of control of the aircraft or because arcing led to fires and explosions. Some of these accidents have resulted in the massive loss of lives (such as in the TWA Flight 800 accident). Circuits on the Space Shuttle have also failed because of faulty insulation on wiring. STS-93 lost power when a primary power circuit in one engine failed and a second engine had a backup power circuit fault. Cables are usually tested on the ground after the crew reports a fault encountered during flight. Often such failures result from vibration and cannot be replicated while the aircraft is stationary. It is therefore important to monitor faults while the aircraft is in operation, when cables are more likely to fail.

Work is in progress to develop a cable fault tester capable of monitoring up to 64 individual wires simultaneously. Faults can be monitored either inline or offline. In the inline mode of operation, the monitoring is performed without disturbing the normal operation of the wires under test. That is, the operations are performed unintrusively and are essentially undetectable for the test signal levels are below the noise floor. A cable can be monitored several times per second in the offline mode and once a second in the inline mode. The 64-channel inline cable tester not only detects the occurrence of a fault, but also determines the type of fault (short/open) and the location of the fault. This will enable the detection of intermittent faults that can be repaired before they become serious problems.

The operation of the fault detector is based on time domain reflectometry (TDR). TDR techniques have been used to locate faults on cables since the advent of the telegraph. However, new technologies and signal processing techniques developed for the fault detector described here have significantly improved the operation and applicability of the TDR principle.

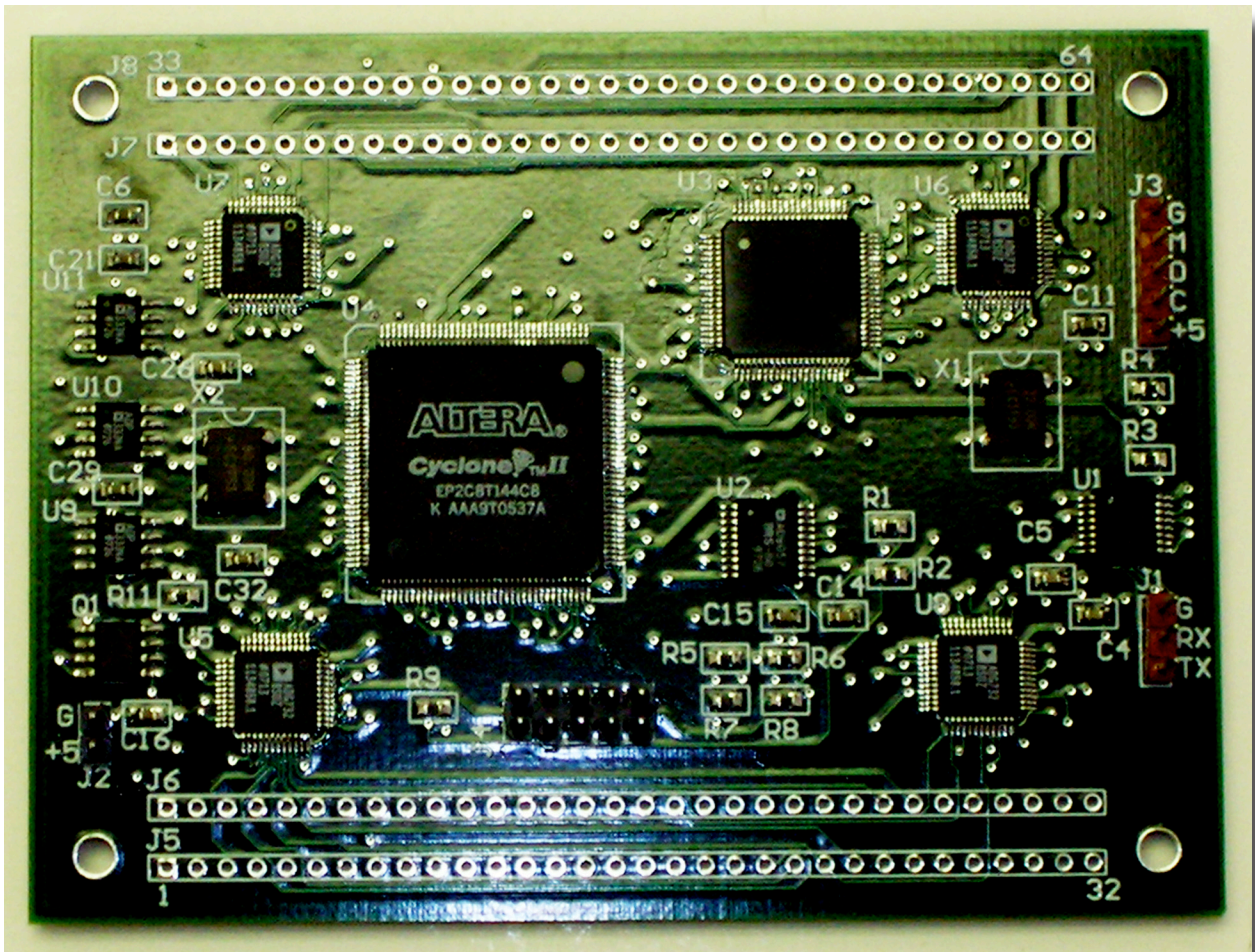
The 64-channel inline cable tester incorporates the following innovations:

- The amplitude of the fast-rising test pulse injected into the cable under test can be selected. The amplitude can be set to a few volts for testing wires offline and to a few millivolts when used in a live circuit.
- The reflections originating from any short- or open-cable condition can be detected, even when the amplitude of the test pulse is significantly smaller than the amplitude of other signals present in the cable. This is accomplished by synchronous detection of successive pulses, which removes the effect of any signals since they are uncorrelated with the test pulse.

The design incorporates over 8,000 logical gates and is based on a field-programmable gate array (FPGA). The FPGA allows for custom logic to be designed and embedded into a single chip and results in significant savings in printed circuit board space.

Contact: Dr. Pedro J. Medelius <Pedro.J.Medelius@nasa.gov>, ASRC Aerospace, (321) 867-6335

Participating Organizations: ASRC Aerospace (Dr. Tracy L. Gibson) and NASA-KSC (Dr. Martha K. Williams)



Circuit board from 64-channel inline cable tester.

Wireless Inclinometer Calibration System



Digital-Communication
Technology Upgrades

A special system was fabricated to properly calibrate the wireless inclinometer, a new device that will measure the Orbiter's hang angle. The wireless inclinometer has a unique design and method of attachment to the Orbiter that will improve the accuracy of the measurements, as well as the safety and ease of the operation. The system properly calibrates the four attached inclinometers, in both the horizontal and vertical axes, without needing to remove any of the component parts.

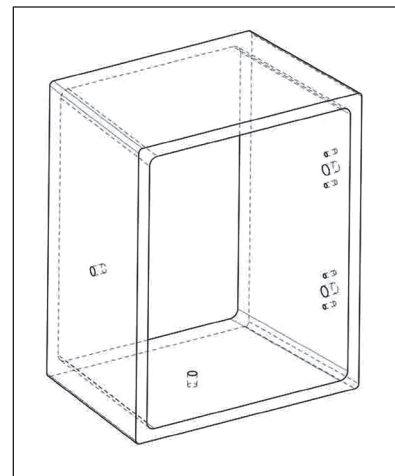
The Wireless Inclinometer Calibration System combines (1) a calibration fixture that emulates the point of attachment to the Orbiter in both the horizontal and vertical axes and the measurement surfaces, (2) an application-specific software program that accepts calibration data such as dates, zero functions, or offsets and tables, and (3) a wireless interface module that enables the wireless inclinometer to communicate with a calibration PC.

The stainless-steel mounting fixture emulates a mount to the Orbiter ground support equipment (GSE) door frame on the aft fuselage compartment. This design accounts for the 8-degree offset from the fuselage parallel to the Orbiter when the inclinometer is mounted in the horizontal position. The outside walls of the fixture can accommodate mounting to the Calibration Laboratory measurement tilt table in the proper axes, and the open-box design is self-supporting both in the upright position (equivalent to Orbiter horizontal) and when rotated 90 degrees (Orbiter in the vertical position). The mounting location side of the fixture is designed to ensure that the inner walls and the outer walls are parallel. The opposite wall of the fixture is characterized to account for the 8-degree (plus/minus the fabrication offset) difference between the mounting edge and the centerline of the Orbiter to the mounting wall. The wall adjacent to the mounting wall is characterized as 90 degrees (plus/minus the fabrication offset) off the mounting wall. The wall opposite the mounting wall has the outside surface as flat as possible. Since it is impossible to fabricate a perfect fixture, the device lends itself to characterization of known values.

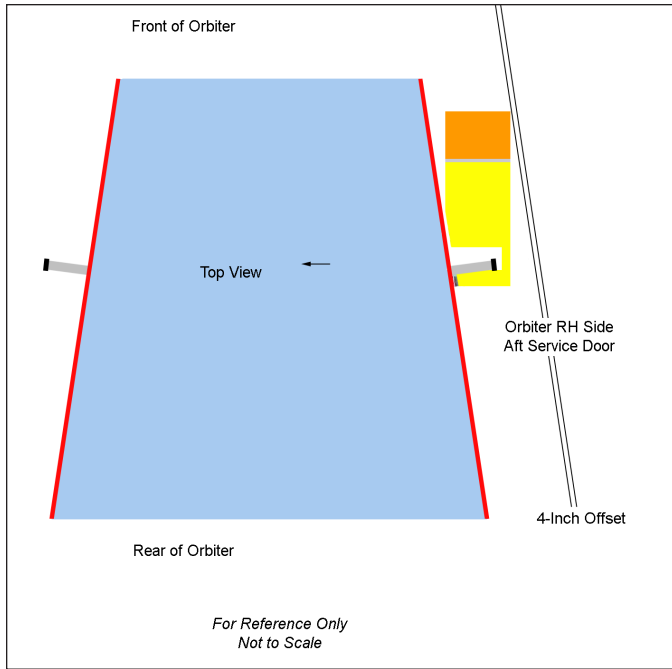
The software application consists of a LabVIEW runtime program with a user-friendly interface for a desktop or laptop in a Windows XP environment. The operator can download previous calibration data and upload new calibration dates, special notes, and offsets. Both old and new data can be saved in text format for use in spreadsheets. In addition, the software attempts to find coefficients that will convert the readings from the sensor into values that will match the real angle values. The operator can choose the number of coefficients to be used.

The wireless interface module is powered directly from the PC or desktop USB port. Wireless communication permits the entire remote wireless inclinometer to be calibrated as a unit.

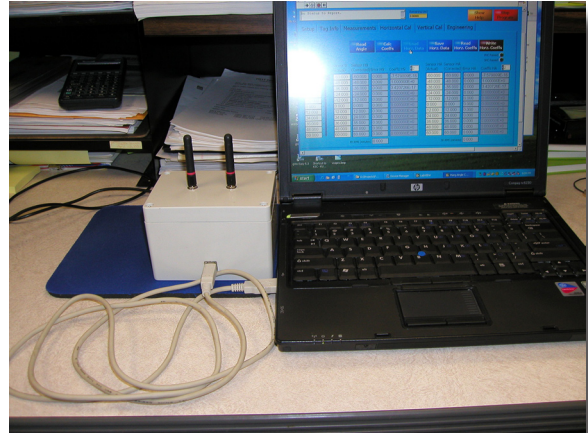
Though the wireless inclinometer calibration system was designed exclusively to support Orbiter processing operations, the system requires only minor hardware and software modifications to be ready for aircraft, military, industrial and construction applications. The benefits are much simpler calibration procedures, more reliable measurements, and lower maintenance costs.



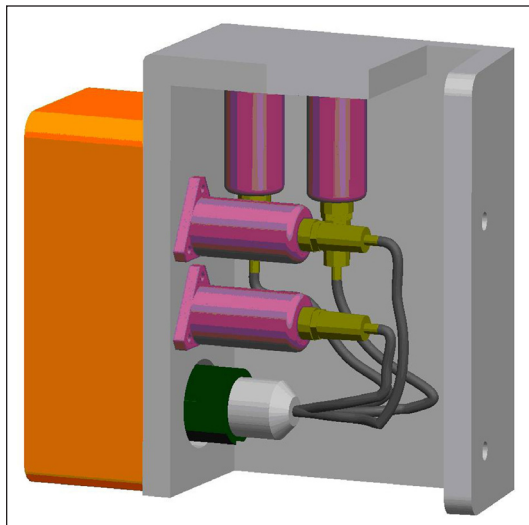
Calibration fixture.



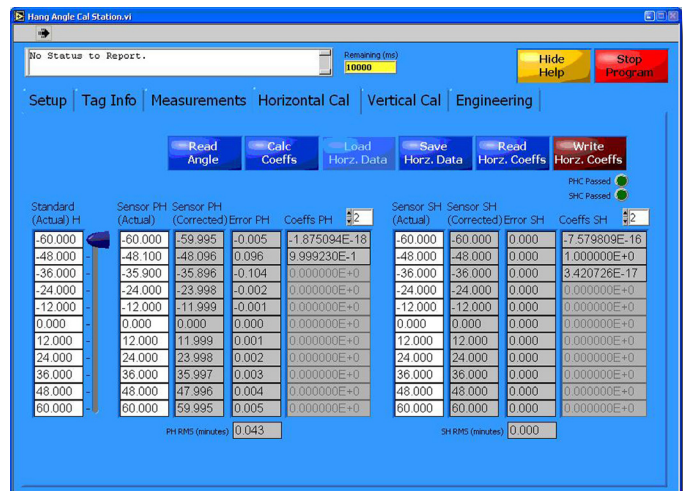
Mounting location and critical dimensions.



Calibration system interface module.



Wireless inclinometer concept.



Application software.

Generating Safety-Critical PLC Code From a High-Level Application Software Specification



Seamless Command and Control Coordination

The benefits of automatic-application code generation are widely accepted within the software engineering community. These benefits include raised abstraction level of application programming, shorter product development time, lower maintenance costs, and increased code quality and consistency. Surprisingly, code generation concepts have not yet found wide acceptance and use in the field of programmable logic controller (PLC) software development. Software engineers at Kennedy Space Center recognized the need for PLC code generation while developing the new ground checkout and launch processing system, called the Launch Control System (LCS). Engineers developed a process and a prototype software tool that automatically translates a high-level representation or specification of application software into ladder logic that executes on a PLC.

All the computer hardware in the LCS is planned to be commercial off the shelf (COTS), including industrial controllers or PLCs that are connected to the sensors and end items out in the field. Most of the software in LCS is also planned to be COTS, with only small adapter software modules that must be developed in order to interface between the various COTS software products.

A domain-specific language (DSL) is a programming language designed to perform tasks and to solve problems in a particular domain, such as ground processing of launch vehicles. The LCS engineers created a DSL for developing test sequences of ground checkout and launch operations of future launch vehicle and spacecraft elements, and they are developing a tabular specification format that uses the DSL keywords and functions familiar to the ground and flight system users. The tabular specification format, or tabular spec, allows most ground and flight system users to document how the application software is intended to function and requires little or no software programming knowledge or experience. A small sample from a prototype tabular spec application is shown in Figure 1.

LINE	ROUTINE	DSL API	OBJECT(S)	DESCRIPTION/MESSAGE	LO/VAL	HI	VOTING	DURATION	REACTION
1	# Routine sends primary OPEN command and waits for appropriate indicators								
2	OpenValve1Primary	# Send primary OPEN command							
3		send_command	VLV1_PRI_OPEN_CMD	Valve1 Primary Open Command	ON				
4									
5		# Verify both primary indicators change appropriately within appropriate time durations, on failure call another routine to perform Secondary Open Command							
6		verify_within	VLV1_PRI_CLOSED_IND	Valve1 Primary Closed Indicator	OFF		2 of 2	8 sec	
7		verify_within	VLV1_PRI_OPEN_IND	Valve1 Primary Open Indicator	ON		2 of 2	26 sec	OpenValve1Secondary
8	end								
9									

Figure 1. Sample of tabular spec formatted application.

The LCS developers needed a mechanism or tool to translate application software from tabular spec format into PLC code to execute on the PLC platforms out in the field. The functionality of some representative samples of tabular spec was manually coded into PLC ladder logic and tested with a field item simulator to verify the proper operation of the manually coded ladder logic. This manual process of conversion or translation from tabular spec representation to PLC ladder logic demonstrated that translation points or patterns existed between portions of the tabular spec and portions of the PLC ladder logic.

With the aid of these translation points, a few representative samples of the manually coded PLC ladder logic were exported from the PLC coding Integrated Development Environment (IDE) as plain text. This exported text was then converted by hand into plain-text PLC code “libraries” with the intent that a future automatic utility to translate tabular spec to ladder logic would use these PLC code libraries. After some representative samples were translated from tabular spec to PLC ladder

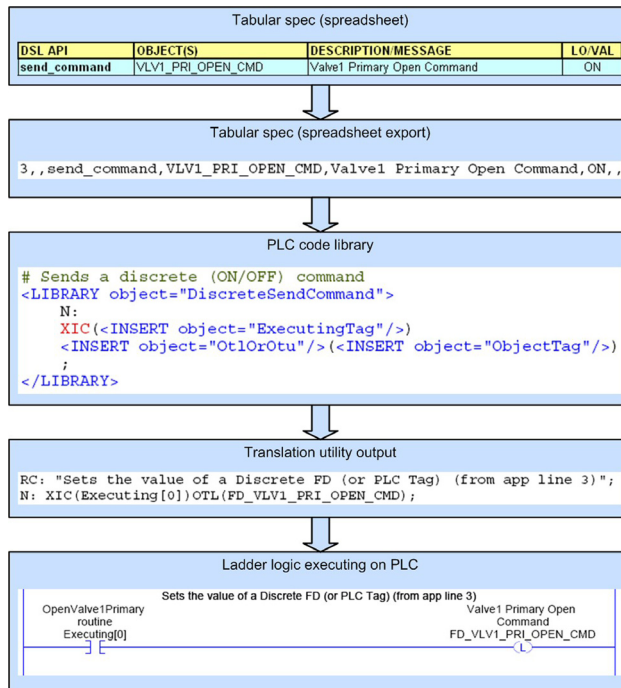


Figure 2. Transition process flow.

logic and after a PLC code library was manually created for each of the translation points contained in the samples, a prototype automatic translation utility was developed and demonstrated. The translation capabilities of the utility will be expanded upon as more and more translation points are identified, translated manually, and then turned into additional PLC code libraries.

Figure 2 shows the simplified process flow for translating a single “send_command” line from tabular spec to PLC code. The spreadsheet that contains the application software in tabular spec format is exported to plain text and is used as input to the translation utility, along with the PLC code library. The translation utility processes these input files, using program transformation steps. This creates an output file that can be imported by the PLC coding IDE.

This work successfully demonstrated that a process and a software tool can generate executable PLC code from a high-level specification representation of a safety-critical control system. This process includes some manual work to find translation points and to create PLC code libraries, but that up-front and one-time manual effort is overshadowed in the end by the automatic generation of repetitious and tedious functionality that would be difficult and error-prone to perform manually. Such a process

and tool increase the quality, reliability, maintainability, and verification/validation pedigree of the PLC code over code that is generated manually. It also provides a high level of PLC code consistency and could even reduce operations and maintenance costs for the control system after it is deployed.

Follow-on phases of development of the automatic translation utility should include most, if not all, of the following tasks:

- represent as much LCS application software in the tabular spec format as possible without overcomplicating the tabular spec format,
- manually implement the remaining translation points and any newly discovered translation points, along with the matching PLC code libraries,
- add code to the translation utility to recognize and handle the new translation points, along with the new PLC code libraries, and
- test and certify the translation utility for automatic generation of safety-critical PLC control logic in the LCS at KSC.

Contacts: Kurt W. Leucht <Kurt.W.Leucht@nasa.gov>, NASA-KSC, (321) 861-7594; and Glenn S. Semmel <Glenn.S.Semmel@nasa.gov>, NASA-KSC, (321) 861-2267

Spacecraft Electrostatic Radiation Shielding



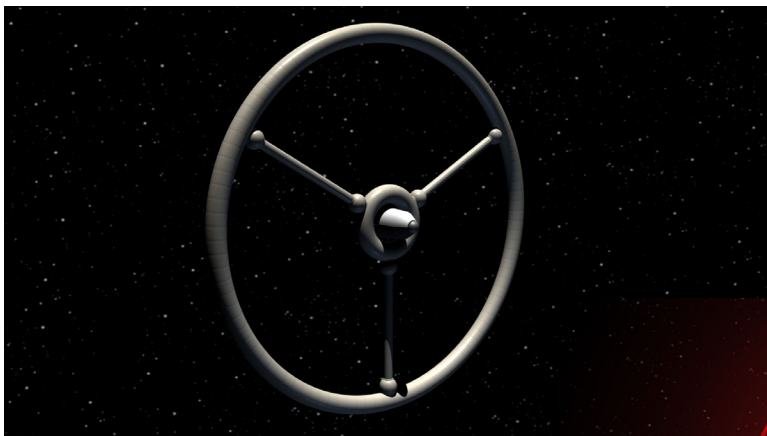
Flight
Environment
Measurement

This project analyzed the feasibility of placing an electrostatic field around a spacecraft to provide a shield against radiation. The concept was originally proposed in the 1960s and tested on a spacecraft by the Soviet Union in the 1970s. Such tests and analyses showed that this concept is not only feasible but operational. The problem though is that most of this work was aimed at protection from 10- to 100-MeV radiation. We now appreciate that the real problem is 1- to 2-GeV radiation. So, the question is one of scaling, in both energy and size. Can electrostatic shielding be made to work at these high energy levels and can it protect an entire vehicle?

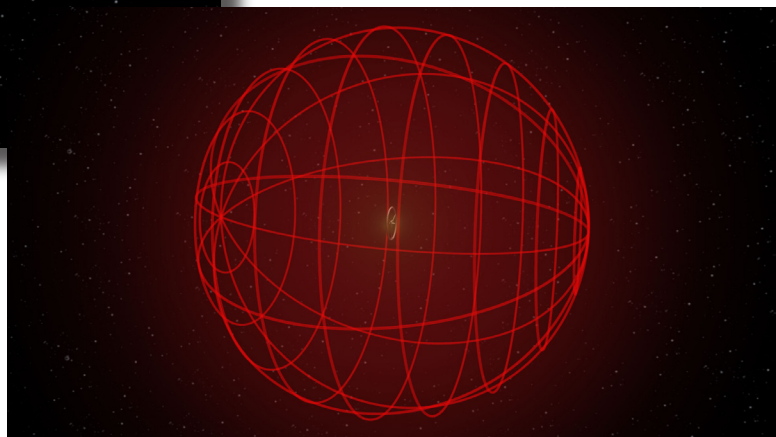
After significant analysis and consideration, an electrostatic shield configuration was proposed. The selected architecture was a torus, charged to a high negative voltage, surrounding the vehicle, and a set of positively charged spheres. Van de Graaff generators were proposed as the mechanism to move charge from the vehicle to the torus to generate the fields necessary to protect the spacecraft. This design minimized complexity, residual charge, and structural forces and resolved several concerns raised during the internal critical review. But, it still is not clear if such a system is cost-effective or feasible, even though several studies have indicated usefulness for radiation protection at energies lower than that of the galactic cosmic rays. Constructing such a system will require power supplies that can generate voltages 10 times that of the state of the art. Of more concern is the difficulty of maintaining the proper net charge on the entire structure and ensuring that its interaction with solar wind will not cause rapid discharge. Yet, if these concerns can be resolved, such a scheme may provide significant radiation shielding to future vehicles, without the excessive weight or complexity of other active shielding techniques.

Contact: Dr. Robert C. Youngquist <Robert.C.Youngquist@nasa.gov>, NASA-KSC, (321) 867-1829

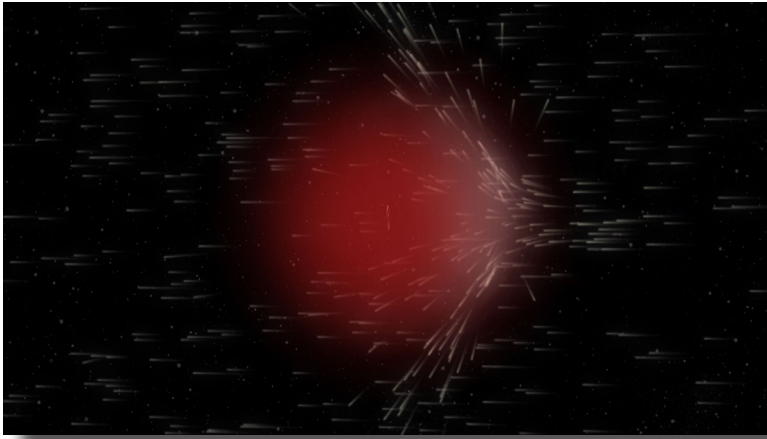
Participating Organization: ASRC Aerospace (Dr. John E. Lane and Irving E. Bushnell)



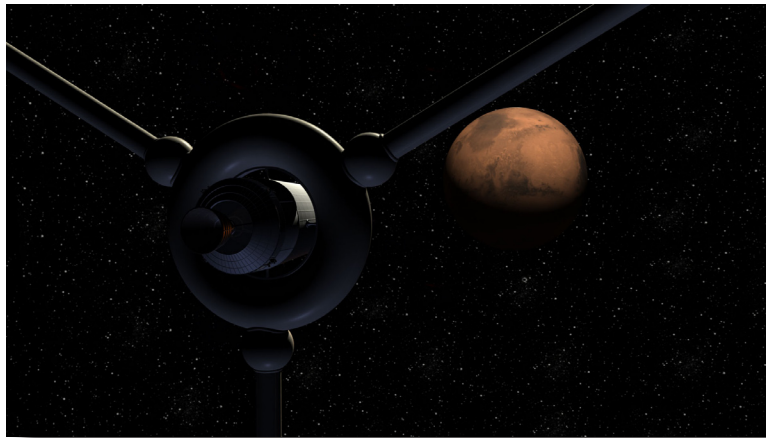
"Spokes" house belts of large Van de Graaff generators.



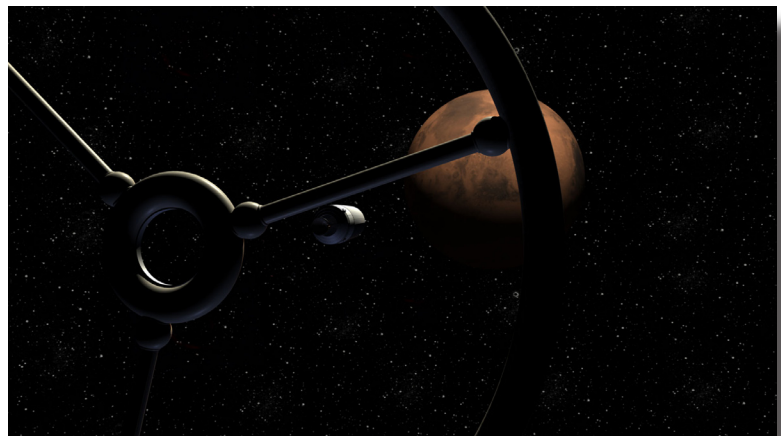
An equipotential electric-field surface at a far-field distance from the shield.



The electrostatic force field in action, repelling charged-particle radiation.



Spacecraft with shield, approaching Mars orbit.



Spacecraft jettisons shield before entering Mars orbit. Shield may be picked up on the return to Earth.

Ion Beam Propulsion Study



Spacecraft
Nutation Models

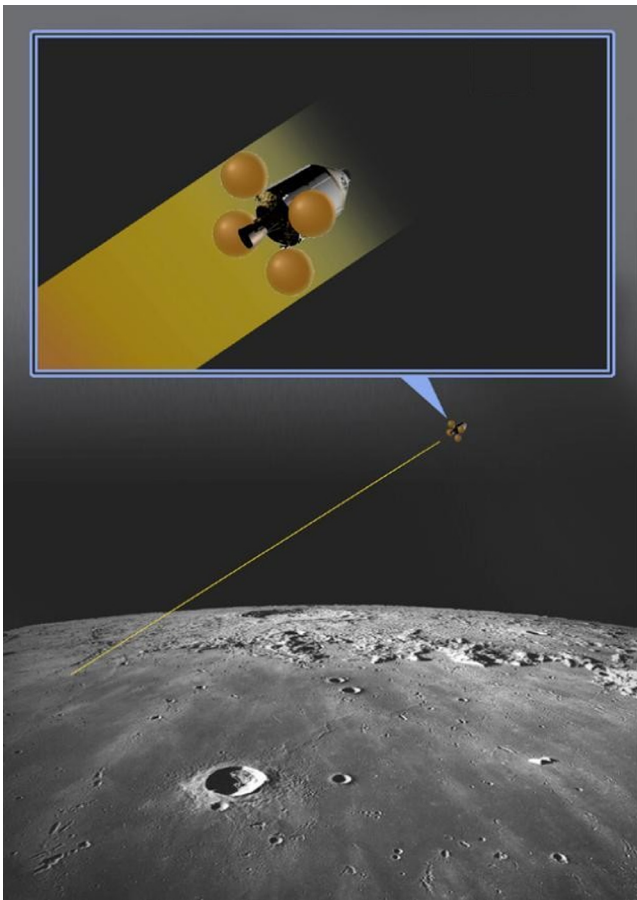
The Ion Beam Propulsion Study was a joint high-level study between the Applied Physics Laboratory operated by NASA and ASRC Aerospace at Kennedy Space Center, Florida, and Berkeley Scientific, Berkeley, California. The results were promising and suggested that work should continue if future funding becomes available.

The application of ion thrusters for spacecraft propulsion is limited to quite modest ion sources with similarly modest ion beam parameters because of the mass penalty associated with the ion source and its power supply system. Also, the ion source technology has not been able to provide very high-power ion beams. Small ion beam propulsion systems were used with considerable success. Ion propulsion systems brought into practice use an onboard ion source to form an energetic ion beam, typically Xe^+ ions, as the propellant. Such systems were used for steering and correction of telecommunication satellites and as the main thruster for the Deep Space 1 demonstration mission. In recent years, “giant” ion sources were developed for the controlled-fusion research effort worldwide, with beam parameters many orders of magnitude greater than the tiny ones of conventional space thruster application. The advent of such huge ion beam sources and the need for advanced propulsion systems for exploration of the solar system suggest a fresh look at ion beam propulsion, now with the giant fusion sources in mind.

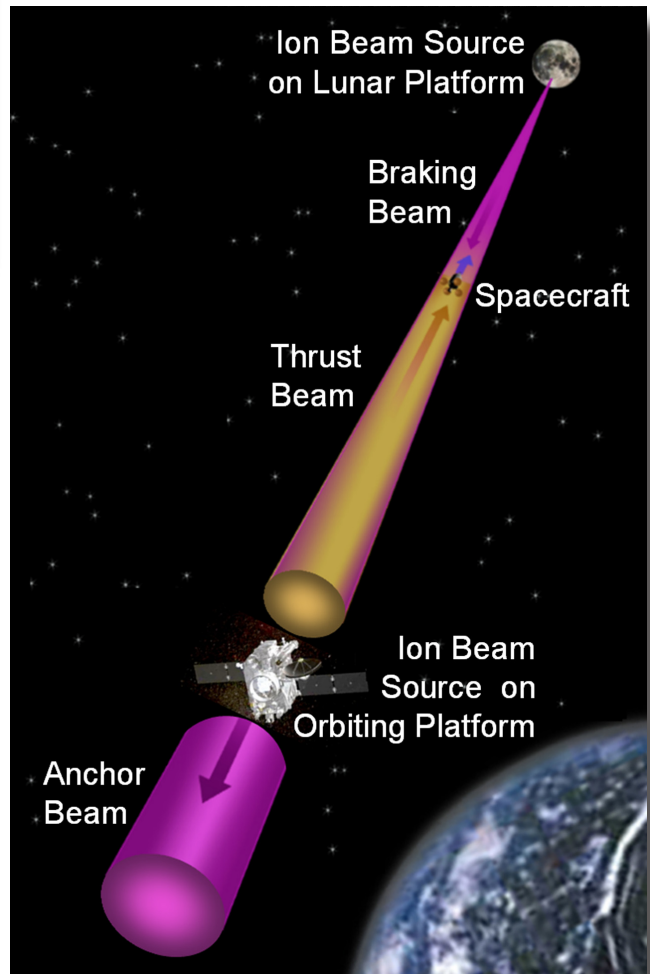
At the same time, the severe mass penalty associated with such huge ion sources and their power supply systems calls for innovative approaches that could avoid this substantial drawback. The giant ion source and its power supply system are located not onboard the spacecraft but at a fixed location, with the powerful ion beam directed toward an “ion beam sail,” which collects the beam and transfers momentum to the spacecraft, thus providing thrust. Several related but different embodiments of this approach are envisioned. The ion source cumulative power supply system could be located on the lunar surface (but not on the Earth’s surface because the ion beam will not propagate through the atmosphere) or in space (e.g., Earth orbit), with the reaction force from the driving ion beam balanced by another identical ion beam that provides equal and opposite reaction force and thus anchors the beam generator system. Further, the ion beam sail might be passive, simply collecting the beam and transferring momentum to the vessel, with the thrust vector aligned with the incident ion beam; or it might be active (electrostatically biased) so as to reflect some of the incident beam in a controllable way, thus providing the possibility of steering the spacecraft. Alternatively, the sail might be a system of a number of sail segments, perhaps spherical appendages that could be independently positioned and electrically biased. In this way, the incident ion beam, rather than being absorbed by a passive collector, could be deflected in a chosen direction, adding a new thrust vector to the system and thereby allowing momentum to be transferred in a direction other than toward the incident ion beam.

Contact: Dr. Robert C. Youngquist <Robert.C.Youngquist@nasa.gov>, NASA-KSC, (321) 867-1829

Participating Organizations: ASRC Aerospace (Dr. John E. Lane) and Berkeley Scientific (Dr. Ian G. Brown)



Ion beam generator located on the surface of the Moon.



Dual ion beam generator positioned in Earth orbit.

RT-MATRIX: Measuring Total Organic Carbon by Photocatalytic Oxidation of Volatile Organic Compounds



Elemental and
Gas Composition
Sensors

Volatile organic compounds (VOCs) inevitably accumulate in enclosed habitats such as the International Space Station and the Crew Exploration Vehicle (CEV) as a result of human metabolism, material off-gassing, and leaking equipment. Some VOCs can negatively affect the quality of the crew's life, health, and performance; and consequently, the success of the mission. Air quality must be closely monitored to ensure a safe living and working environment. Currently, there is no reliable air quality monitoring system that meets NASA's stringent requirements for power, mass, volume, or performance. The ultimate objective of the project—the development of a Real-Time, Miniaturized, Autonomous Total Risk Indicator System (RT-MATRIX)—is to provide a portable, dual-function sensing system that simultaneously determines total organic carbon (TOC) and individual contaminants in air streams.

TOC is often used as an indicator of organic contaminants in both liquid and vapor phases. On Earth-bound applications, TOC is analyzed in liquid samples either by catalyst or ultraviolet (UV)-promoted persulfate oxidation or by catalyst-assisted high-temperature combustion of organics. TOC in the gas phase is analyzed by flaming ionization of organics, followed by nondispersive infrared detection. Several types of flame ionization detector-based hydrocarbon analyzers are commercially available. They have been used for real-time monitoring of the effluent of volatile-contaminant reduction equipment for environmental compliance, lower-exposure-limit monitoring, and fugitive-emission monitoring. Unfortunately, the smallest available system weighs 55 to 65 pounds and measures 19×21×9 inches. Such TOC analyzers require carrier and fuel gases (hydrogen, air, or oxygen) for operation and have high power consumption (750 watts), which make them unsuitable for application in a space environment.

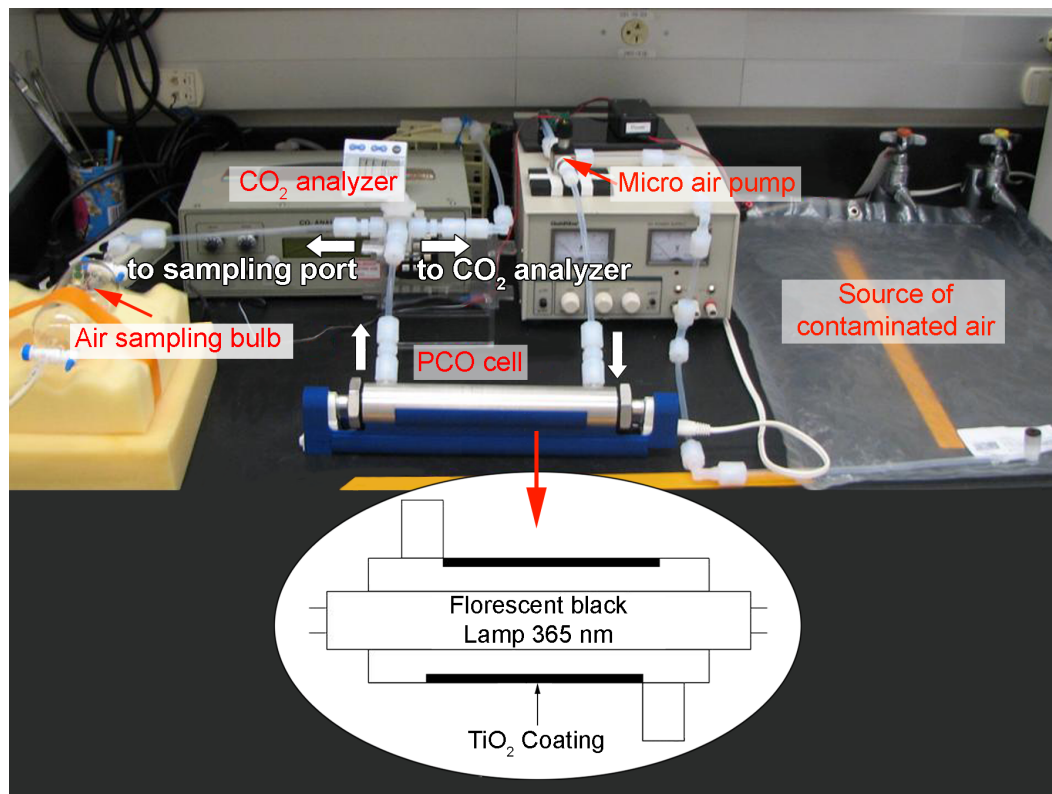


Figure 1. Experimental setup for evaluation of PCO cell performance.

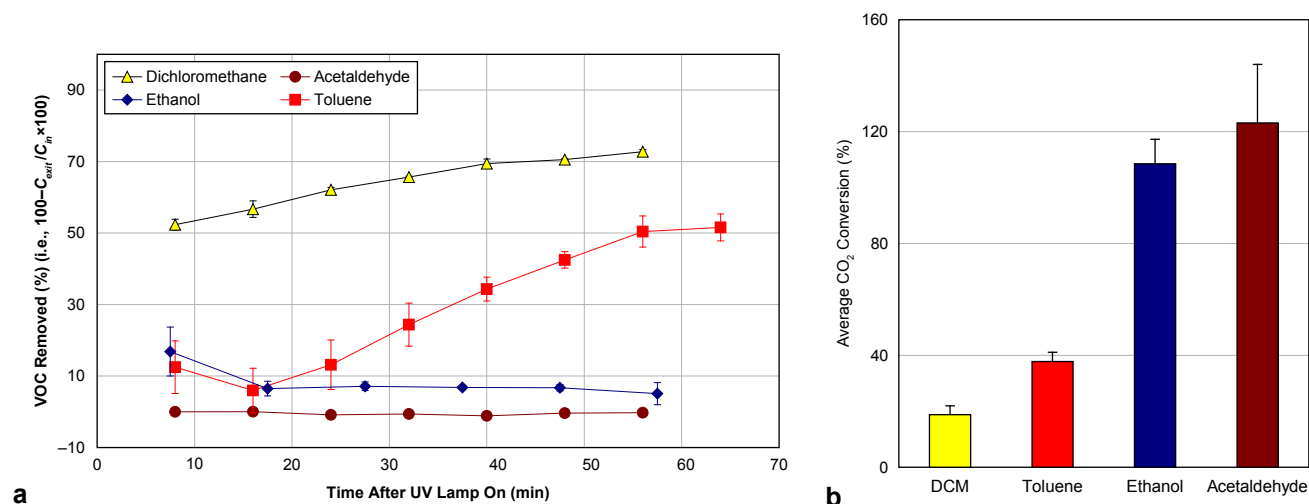


Figure 2. Photocatalytic oxidation of a constant flow (0.2 L/min) of 100 ppm toluene, dichloromethane, acetaldehyde, and 500 ppm ethanol; (a) VOC removed upon single pass through PCO cell; and (b) corresponding CO₂ formation.

Photocatalytic oxidation (PCO) of organic pollutants consumes less power, uses a nontoxic catalyst, and can destroy most organic pollutants. This technology has been employed in air revitalization systems. However, it is not known whether organic compounds are stoichiometrically oxidized into carbon dioxide. The concept of using PCO for TOC determination was tested. A prototype PCO cell (Figure 1) was constructed and evaluated against four VOCs representing alcohol, aldehyde, aromatic, and halogenic compounds. Representative results are summarized in Figure 2. Ethanol and acetaldehyde were oxidized almost completely upon single pass through the PCO cell, as is evident by the low level of starting material in PCO cell effluent and the formation of carbon dioxide at 100 percent of the theoretical conversion. However, the percentages of toluene and dichloromethane oxidized were about 80 and 50 percent initially and declined over time. This decreased oxidation may be attributed to the formation of intermediates that compete for the active site on the titanium dioxide catalyst. Over 50 minutes, the carbon dioxide conversion efficiency (i.e., actual [carbon dioxide]/expected [carbon dioxide] × 100) was about 40 and 20 percent for toluene and dichloromethane, respectively. The effect of linear velocity and surface area on the oxidation efficiency was also examined. Based on these preliminary results, a new PCO cell with improved performance was designed and is under construction.

We plan to couple this PCO cell with a commercial off-the-shelf (COTS) encoded photometric infrared (EP-IR) spectrometer to provide early detection of harmful VOCs and equipment leaks and to monitor the efficacy of air revitalization and solid-waste management systems. This dual-function sensor is portable and reagent-free, has no consumables, and is ideal for field application.

The project demonstrated stoichiometric conversion of select VOCs (e.g., ethanol and acetaldehyde) into carbon dioxide, implying the feasibility for PCO of VOCs as an alternative means for TOC measurement. Furthermore, a COTS EP-IR was acquired as our sensing component.

Contact: Dr. John C. Sager <John.C.Sager@nasa.gov>, NASA-KSC, (321) 861-2949

Participating Organizations: Dynamac Corporation (Dr. Lanfang H. Levine, William A. Rigdon, and Patricia A. Bisbee), NASA-KSC (Dr. Paul E. Hintze), and University of Delaware (Dr. Karl S. Booksh and Dr. Yoon-Chang Kim)

Appendix A



KSC High-Priority Technology Needs

Articles from the KSC Technology Development and Application 2006-2007 Report are listed under the applicable technology need.

Hazardous-Leak Detection and Isolation

- Reversible Chemochromic Hydrogen Detectors (p. 2)
- Calibrating of the Helium Pressurization System for the Space Shuttle Liquid-Hydrogen Tank (p. 72)
- Nanosensors for Evaluating Hazardous Environments (p. 110)

Contamination Control

- Determining Trajectory of Triboelectrically Charged Particles, Using Discrete Element Modeling (p. 4)
- Using Indium Tin Oxide To Mitigate Dust on Viewing Ports (p. 6)

Integrated System Health Management (ISHM) Technologies

Corrosion Control

- High-Performance Polyimide Powder Coatings (p. 8)
- Controlled-Release Microcapsules for Smart Coatings for Corrosion Applications (p. 10)
- Aerocoat 7 Replacement Coatings (p. 12)
- Photocatalytic Coatings for Exploration and Spaceport Design (p. 14)

Task/Process Modeling and Simulation

- Distributed Observer Network (p. 96)
- Influence Map Methodology for Evaluating Systemic Safety Issues (p. 98)
- Simulation and Analysis of Launch Teams (SALT) (p. 100)

Wire/Cable Inspection and Repair

- New Materials for the Repair of Polyimide Electrical Wire Insulation (p. 16)
- Sixty-four-Channel Inline Cable Tester (p. 112)

Advanced Work Instruction/Work Control/Planning and Scheduling Systems

Propellant Loading/Service/Storage

- Commodity-Free Calibration (p. 18)
- Novel Ice Mitigation Methods (p. 20)
- Composite Materials for Low-Temperature Applications (p. 74)
- Mitigating Problems in Measuring Hypergolic Fuels (p. 76)

Resource, Personnel, or Foreign-Object Debris (FOD) Identification and Tracking

Digital-Communication Technology Upgrades

- Wireless Inclinometer Calibration System (p. 114)

Localized-Weather Forecasting and Measurement

- Hail Size Distribution Mapping (p. 52)
- Launch Pad 39 Hail Monitor Array System (p. 54)

Self-Contained Atmosphere Protective Ensemble (SCAPE) Suit Upgrades

Nondestructive Evaluation/Nonintrusive Inspection Technologies

Seamless Command and Control Coordination

- Generating Safety-Critical PLC Code From a High-Level Application Software Specification (p. 116)

Thermal Protection System (TPS) Enhancements

- Cryogenic Moisture Analysis of Spray-On Foam Insulation (SOFI) (p. 78)
- Thermal Performance of Aged and Weathered Spray-On Foam Insulation (SOFI) Materials Under Cryogenic Vacuum Conditions (Cryostat-4) (p. 80)

Minimally Intrusive Repair and Self-Healing Systems

Window Inspection

Improved Gaseous-Nitrogen (GN₂) Pipeline Gas Filtration

Defect/Damage Location

- Crack Offset Measurement With the Projected Laser Target Device (p. 22)
- New Materials for Structural Composites and Protective Coatings (p. 24)

Tracking and Evaluation

Spacecraft Transportation, Handling, and Alignment Systems

Hydrogen Vent Recovery

Improved Helium Delivery System

Payload Environment Models

Flight Environment Measurement

- Fire Chemistry Testing of Spray-On Foam Insulation (SOFI) (p. 26)
- Using Aerogel-Based Insulation Material To Prevent Foam Loss on the Liquid-Hydrogen Intertank (p. 28)
- Spacecraft Electrostatic Radiation Shielding (p. 118)

Spacecraft Nutation Models

- Automated Method for Estimating Nutation Time Constant Model Parameters for Spacecraft Spinning on Axis (p. 82)
- Parameter Estimation of Lateral Spacecraft Fuel Slosh (p. 84)
- Ion Beam Propulsion Study (p. 120)

Risk Assessment Tool

Mission Data Feedback and Analysis

- Modeling of Slosh Dynamics in Cryogenic Propellant Tanks in Microgravity Environments (p. 86)

Lunar Launch/Landing Site Ejecta Mitigation

- Particle Ejection and Levitation Technology (PELT) (p. 30)
- Electrostatic Characterization of Lunar Dust (p. 32)
- Numerical Analysis of Rocket Exhaust Cratering (p. 34)

Modular Support Equipment

***In Situ* Resource Utilization (ISRU) Oxygen Production**

- RESOLVE Projects: Lunar Water Resource Demonstration and Regolith Volatile Characterization (p. 36)
- Tribocharging Lunar Soil for Electrostatic Beneficiation (p. 38)

Site Preparation and Excavation

- Numerically Modeling the Erosion of Lunar Soil by Rocket Exhaust Plumes (p. 40)
- Trajectory Model of Lunar Dust Particles (p. 42)
- Using Lunar Module Shadows To Scale the Effects of Rocket Exhaust Plumes (p. 44)

Energy-Efficient Lighting Systems

- Countermeasure for Radiation Protection and Repair (p. 90)
- Solid-State Lighting Module (SSLM) (p. 102)

Water and Air Recovery/Purification

- Focused Metabolite Profiling for Dissecting Cellular and Molecular Processes of Living Organisms in Space Environments (p. 92)

Elemental and Gas Composition Sensors

- RT-MATRIX: Measuring Total Organic Carbon by Photocatalytic Oxidation of Volatile Organic Compounds (p. 122)

Decision/Data Models and Analysis

- Predicting the Acoustic Environment Induced by the Launch of the Ares I Vehicle (p. 46)
- Autonomous Flight Safety System – Phase III (p. 56)
- Systems Maintenance Automated Repair Tasks (SMART) (p. 104)
- Launch and Landing Effects Ground Operations (LLEGO) Model (p. 106)
- Exploration Supply Chain Simulation (p. 107)

Spaceport/Range Situational Awareness

- Measuring Ultrasonic Acoustic Velocity in a Thin Sheet of Graphite Epoxy Composite (p. 48)
- The Photogrammetry Cube (p. 58)
- Bird Vision System (p. 60)
- Automating Range Surveillance Through Radio Interferometry and Field Strength Mapping Techniques (p. 62)

Water Detection and Removal

Bird Abatement System

Quantum Computers

Autonomous/Robotic Inspections

Helium Measurement, Recovery, and Purge Gas Substitution

Global Positioning System (GPS) Metric Tracking

- Next-Generation Telemetry Workstation (p. 64)
- GPS Metric Tracking Unit (p. 66)
- Space-Based Range (p. 68)

Appendix B

Innovative Partnership Program

Kennedy Space Center (KSC) is NASA's lead center for developing technologies in support of launch/landing and vehicle/payload processing. NASA's Innovative Partnership Program (IPP) was established to provide leveraged technologies for NASA's mission directorates, programs, and projects through investments and technology partnerships with industry, academia, Government agencies, and national laboratories. Within the Technology Programs and Partnerships Branch of KSC's Applied Technology Directorate's, the IPP Office performs the following key program functions.

Intellectual-Property Management

Home to world-class researchers, KSC offers a number of inventions and discoveries to the outside world through our Technology Programs and Partnerships Branch. When discoveries or inventions are conceived at KSC, the inventors promptly report them as innovative technologies to the Technology Programs and Partnerships Branch in order to protect the Government's interest and to obtain the widest practicable and appropriate dissemination for the benefit of the general public and the scientific, industrial, and commercial communities. In FY 2006, 136 innovations were reported to the Technology Programs and Partnerships Branch by KSC innovators. There were 2 patent licenses and 10 partnerships. In FY 2007, 141 new technologies were reported, together with 12 partnerships and 1 patent license.

Technology Commercialization

Liquid Galvanic Coating

KSC developed a sacrificial coating for application to the outer surface of reinforced concrete to protect the embedded rebar from corrosion. The coating contains one of several types of metallic particles—magnesium, zinc, and indium. An electrical current that is established between metallic particles in the applied coating and the surface of the steel rebar produces cathodic protection of the rebar. The current forces a flow of electrons from the coating (anode) to the rebar along a separate metallic connection; this surplus of electrons at the rebar (cathode) prevents the loss of metal ions that would normally occur as part of the natural corrosion process. The technology is innovative because it can be applied (1) to the outside surface of reinforced concrete (most rebar corrosion prevention must be applied directly to the rebar) and (2) with a conventional brush or sprayer.

The high salinity of the Atlantic and the prevalent high temperatures and humidity at Kennedy Space Center accelerate the corrosion of the steel inside reinforced concrete structures, reducing their life. Liquid galvanic coating has been deployed successfully at the KSC to increase the life of concrete structures and reduce their associated maintenance costs.

NASA applied for a U.S. patent on the Liquid Galvanic Coating System[®], and the Technology Programs and Partnerships Branch marketed the technology to the corrosion prevention industry. Several companies expressed interest in commercializing the technology, including Surtreat Holdings, LLC, headquartered in Pittsburgh, Pennsylvania. Surtreat provides full-service, innovative, technical solutions for restoring corroded materials and preventing deterioration and corrosion in steel-reinforced concrete structures.

Surtreat licensed the patent in late 2006. The company used the technology under a contract with the U.S. Army to conduct tests on new technologies to preserve Army structures around the world, including those in Okinawa, Japan. Okinawa has a severely corrosive environment because of its highly corrosive soil and its hot, humid weather. The concrete walls of the warehouse there that stores supplies for all of the U.S. armed forces in the Pacific Theater have severely deteriorated as a result of rebar corrosion. If not given proper attention, the rebar will continue to corrode, cracking the concrete, weakening the walls, and ultimately requiring large-scale structural repair.

Surtreat has installed the Liquid Galvanic Coating System® at the U.S. Army NaHa Port, Okinawa, Japan, and NASA is currently awaiting final results of the testing.

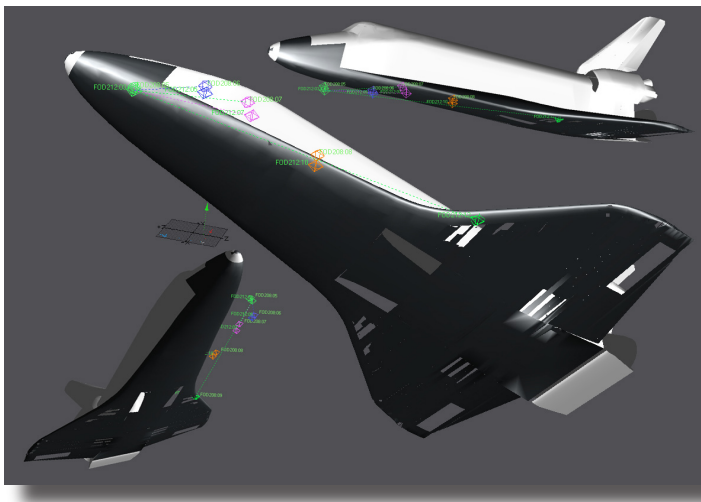
Scene Analysis Software

Routine analysis of launch video images is critical to Space Shuttle operations at KSC. During every launch, large amounts of foreign-object debris (FOD) could strike the Shuttle during its ascent. Thus, it is critical to identify and locate FOD in the vicinity of the spacecraft and to measure the speed and direction of the FOD during the first few minutes of flight.

Innovators from ASRC Aerospace developed a Microsoft Windows-compatible program for 3-D-scene photogrammetry systems for the purpose of tracking FOD or measuring objects within a digital image. With a minimum of two cameras viewing an event from different perspectives, the software can estimate the x , y , and z coordinates of an object against a fixed background, as well as estimate the object's velocity and acceleration.

This software package was initially funded and developed as part of the Columbia accident investigation in order to analyze the film and video data that showed a single chunk of External Tank foam debris falling from the bipod ramp area and colliding with the lower leading edge of Columbia's left wing. Image-processing methodologies were developed to derive the 3-D trajectory and velocity estimates for the 3-D modeling analysis of digitally scanned filmed and video images taken January 16, 2003, of STS-107.

This software is an invaluable tool to the Space Shuttle program in the search for FOD during the ascent phase. This helps to maintain an operational Shuttle fleet and helps to ensure the safety of the Shuttle and its crew.



Scene Analysis Software

The NASA Technology Programs and Partnerships Branch reviewed the Scene Analysis Software for commercial potential, acquired copyright assignment from ASRC Aerospace, and filed a provisional patent application. NASA marketed the software to companies in the forensics industry and to other Government agencies. KSC demonstrated the Scene Analysis Software for representatives of the U.S. Army and two of their contractors, Morgan Research and Camber Corporation, for possible application to new security systems under development.

On May 8, 2007, the KSC Technology Programs and Partnerships Branch completed a Software Usage Agreement with the U.S. Army for the Scene Analysis Software. The Army contracted with Camber Corporation to develop a security

system for the Government, using the new software. Camber envisions employing the Scene Analysis Software to enhance its Vigilant Sentinel security system. The software will allow a facility management system to perform more intelligent analysis of the data captured. The Scene Analysis Software will create a more intelligent video security system, which will be able to target and track traditional and nontraditional movement of objects approaching a building. The new system incorporating the Scene Analysis Software will be installed for the first time at McConnell Air Force Base in Kansas.

Research and Development Partnerships

Partners can collaborate on research and development efforts under a NASA Space Act Agreement. NASA and its partners contribute personnel, use of NASA facilities, expertise, or equipment, technology, etc., to perform the research and development. Four Space Act Agreements were signed this year with partners.

Ulyssix Technologies, Inc., a company that provides high-quality, innovative, digital-signal-processor (DSP)-based communication products to the telemetry and satellite communication markets, is developing an improved telemetry acquisition system with NASA's Communications and Telemetry Branch, under KSC's Launch Services Program.

BCS Life Support, LLC, signed a Space Act Agreement with NASA to develop two technologies: (1) a method for efficiently storing cryogenic liquid air by minimizing premature nitrogen boiloff and subsequent oxygen enrichment of the fluid, and (2) a method to extract cryogenic air from a portable storage vessel, regardless of physical attitude. Under this agreement, NASA and BCS intend to test and evaluate a system and/or method for efficient liquid-air storage and to fabricate and test a prototype device (i.e., a siphon) for supplying liquid air from a cryogenic vessel. This prototype will supply liquid air from a portable dewar while in any attitude other than upside down.

Evergreen Performance and Compliance is furthering the development of nonvolatile immobilized liquid membranes that are highly selective for carbon dioxide over carbon monoxide, nitrogen, or oxygen. Originally developed at KSC, this technology will have broad commercial applications if a low-power, high-efficiency method of removing carbon dioxide from flue gas can be found. Evergreen will conduct research and development on this patented technology for application to the fossil-fueled combustion industries.

Open Channel Foundation, a company that publishes software from academic and research institutions, entered into a Space Act Agreement to promote the availability, transfer, use, and collaborative development of KSC software to the public and private sector.

Technology Infusion

In 2006, NASA's IPP introduced its Partnership Seed Fund as a mechanism for selecting highly leveraged partnerships for the joint development of key, mission-related technologies. The ultimate goal of the program is to raise the readiness level of these key technologies sufficiently to allow for infusion into NASA's missions and programs. KSC was awarded three Seed Fund projects in 2006 totaling \$1.2M in combined development, and five Seed Fund projects in 2007 totaling \$6.2M in combined development.

As an example, KSC's IPP Office teamed with the Launch Services Program and Sierra Lobo, Inc., on the further development of the Cryo-Tracker® Mass Gauging System (MGS) to advance the flight readiness of this strategic technology for use as a propellant measurement system on NASA

and commercial launch vehicles. The MGS will provide much higher-fidelity data on the quantities and thermodynamic states of the propellants during launch and flight.

Significant progress has been made in this effort. Qualification verification plans have been developed for the Cryo-Tracker® MGS, which consists of the Cryo-Tracker® probe, avionics, and tank feedthrough. The probe has been tested to obtain material property data, including tensile yield stress, elastic modulus, and thermal expansion coefficients at ambient and cryogenic temperatures. These data are being used in a high-fidelity finite-element analysis on the probe to determine structural margins and resonance frequencies for worst-case in-tank loads and vibrations.

In addition, the MGS electronics box has been redesigned and fabricated for space-vacuum environments and will undergo qualification testing for flight environments. A continuous tank-feedthrough (containing no connectors) has been designed and fabricated and has passed extensive leak testing at both ambient and cryogenic temperatures. Operational tests of the feedthrough design are under way.

The project is expected to be completed on schedule, and the technology is expected to advance significantly in maturity and readiness for use as a propellant measurement system for launches and space vehicles.

SBIR/STTR

KSC's Innovative Partnership Program also encompasses the Small Business Innovation Research (SBIR) and Small Business Technology Transfer (STTR) Programs. SBIR and STTR play an integral role in fulfilling the missions and objectives of KSC. These programs provide small, high-tech companies and research institutions opportunities to participate in Government-sponsored research and development efforts in key technology areas, enabling innovations that also have potential commercial applications and thereby contributing to the overall NASA mission. As small businesses work to meet NASA's research and development needs, they stimulate growth in local economies and nearby business communities.

Successes

EM Photonics Solver for Image Enhancement

The quality of the images taken with long-range optical systems (more than 1 kilometer) is severely degraded by atmospheric movements in the path between the region under observation and the imaging system. Fortunately, image-processing algorithms have been developed to help compensate for these disturbances. However, these atmospheric compensation algorithms are computationally intensive, which prevents even top-of-the-line PCs from evaluating them in real time. EM Photonics is building a solver capable of enhancing long-range imagery in real time.

Range surveillance and launch tracking are critical components of space exploration because of their implications for safety, cost, and the overall mission timeline. Space vehicle launches are often delayed because of the challenge of verifying that the range is clear, and such delays are likely to become more prevalent as more and more spaceports are built. To expedite range clearance, it is vital to see through the atmosphere. Reduced visibility also makes it hard to track rockets throughout launch, when atmospheric effects can be even more pronounced. NASA collects massive amounts of long-range imagery for providing prelaunch range safety,

tracking objects after launch, and observing objects in space. Because these applications require imaging through the atmosphere at great distances, the images collected are often blurred and detail is often lost. Employing the device developed by EM Photonics to enhance images, NASA officials will have access to additional information to aid in key decisions. During launch, the added level of detail will provide the ability to make more informed “go” or “no go” decisions. For tracking rockets or the Shuttle, enhanced imagery will provide more detail on pieces that may fall from the craft during flight. Accounting for atmospheric effects will also improve the quality of all images taken of space-based objects from Earth. All applications at NASA that require long-range imagery can be improved by rapidly enhancing the collected data.

Range Surveillance

Radio interferometry (RI) and time-difference-of-arrival (TDOA) techniques developed by Soneticom of Melbourne, Florida, are applied to survey, identify, and locate radio frequency (RF) energy signatures within a launch range or other strategic area. When deployed with a TDOA system, the range surveillance technology will allow an operator to identify and locate the source of RF emissions more quickly and easily than can be accomplished today. This technology greatly improves range safety by quickly locating the presence of an unauthorized emitter or individual in a strategic area and by quickly providing graphic detail of potential RF threats that could interfere with operations and launch activities.

This technology was developed to assist the security team at KSC in finding intentional and unintentional intruders. The defined use for the technology is to increase security capabilities at the Center by identifying possible intrusion of inappropriate RF signals. The technology can also be used for identifying sources of RF interferences during launch activities and transport of payloads, as well as for asset and vehicle tracking. The technology works by taking RF spectrum “images” of an area, by means of the TDOA system, and then comparing the images over time to identify nominal and anomalous RF activity.

AWARDS

Kennedy Space Center continues to provide incentives to innovators through Space Act Awards. NASA’s Inventions and Contributions Board is authorized to recommend the granting of Space Act Awards. The objectives of the Space Act Award program are to provide official recognition of and to grant equitable monetary awards for those inventions and other scientific and technical contributions that have helped to achieve NASA’s aeronautical, commercial, and space goals; and to stimulate and encourage the creation and reporting of similar contributions in the future.

Monetary Summary of Space Act Awards for 2006 and 2007		
	2006	2007
Board Action Awards	\$153,650	\$69,350
Patent Application Awards	\$7,500	\$19,000
Software Awards	\$33,500	\$34,000
Tech Brief Awards	\$16,800	\$14,000
Total	\$211,450	\$136,350

Appendix C



Office of External Relations Export Control and Interagency Liaison Division

NASA Export Control Program

The Export Control Program at John F. Kennedy Space Center (KSC) is part of a NASA-wide system. The NASA Headquarters Office of External Relations disseminates export control policy and guidance to KSC.

KSC Export Control Program

The KSC Export Control Office (ECO) ensures that exports and transfers to foreign parties in international activities are consistent with NASA's international cooperative agreements and United States federal regulations: Export Administration Regulations (EAR), International Traffic in Arms Regulations (ITAR), Arms Export Control Act (AECA).

With the KSC focus on Space Shuttle, International Space Station, a new crew launch vehicle, and the technology development surrounding each, the ultimate goal of the KSC ECO is to maintain national security and limit access to our most sensitive space technologies.

KSC Export Control Office

Wayne Ranow	Center Export Administrator (CEA)	(321) 867-6066
Melanie Chan	Associate CEA	(321) 867-6367
Bill Collins	Export Control Specialist	(321) 867-9209

KSC Export Control Web Site

<http://exportcontrol.ksc.nasa.gov/>

Public Release of This Document

The content of this report has been reviewed for security, export control, and intellectual property. It has been released on NASA Form 1676, "Document Availability Authorization," via the NASA Scientific and Technical Information (STI) process (NPR 2200.2B), and is filed in the office of the KSC STI manager, phone (321) 867-6481.

REPORT DOCUMENTATION PAGE

*Form Approved
OMB No. 0704-0188*

The public reporting burden for this collection of information is estimated to average 1 hour per response, including the time for reviewing instructions, searching existing data sources, gathering and maintaining the data needed, and completing and reviewing the collection of information. Send comments regarding this burden estimate or any other aspect of this collection of information, including suggestions for reducing the burden, to Department of Defense, Washington Headquarters Services, Directorate for Information Operations and Reports (0704-0188), 1215 Jefferson Davis Highway, Suite 1204, Arlington, VA 22202-4302. Respondents should be aware that notwithstanding any other provision of law, no person shall be subject to any penalty for failing to comply with a collection of information if it does not display a currently valid OMB control number.

PLEASE DO NOT RETURN YOUR FORM TO THE ABOVE ADDRESS.

1. REPORT DATE (DD-MM-YYYY) 03-03-2008	2. REPORT TYPE Technical	3. DATES COVERED (From - To) January 1, 2006 – December 31, 2007
--	------------------------------------	--

4. TITLE AND SUBTITLE Technology Development and Application 2006–2007 Report	5a. CONTRACT NUMBER
	5b. GRANT NUMBER
	5c. PROGRAM ELEMENT NUMBER

6. AUTHOR(S)	5d. PROJECT NUMBER
	5e. TASK NUMBER
	5f. WORK UNIT NUMBER

7. PERFORMING ORGANIZATION NAME(S) AND ADDRESS(ES) NASA, John F. Kennedy Space Center Kennedy Space Center, Florida 32899	8. PERFORMING ORGANIZATION REPORT NUMBER NASA-TM 2008-214740
--	--

9. SPONSORING/MONITORING AGENCY NAME(S) AND ADDRESS(ES) National Aeronautics and Space Administration Washington, D.C. 20546	10. SPONSOR/MONITOR'S ACRONYM(S)
	11. SPONSOR/MONITOR'S REPORT NUMBER(S)

12. DISTRIBUTION/AVAILABILITY STATEMENT
Unclassified – Unlimited
Subject Category:
Availability: NASA CASI (301) 621-0390

13. SUPPLEMENTARY NOTES

14. ABSTRACT

Successful technology development and application projects are critical to maintaining and enhancing KSC capabilities. Advanced technologies are required to solve technical problems, resolve operational issues, and optimize designs of flight and ground systems. When new technologies are infused in KSC systems and processes, the outcomes are safer, more efficient, and more responsive spaceport and range operations for our customers.

The KSC technology development team includes a wide variety of partnerships among civil servants, contractors, academic institutions, and commercial industries. KSC focuses its advanced technology activities on a list of KSC high-priority technology needs defined by our primary stakeholders, including current operational programs, future programs, and institutional technical programs. We focus and align our technology investments, personnel investments, new project proposals, and strategic partnerships with the technology needs most important to the programs supporting our Nation’s exploration mission.

KSC Chief Technologist Dr. Dave Bartine, (321) 867-7069, is responsible for publication of this report and should be contacted for any desired information regarding KSC’s technology development and application activities.

15. SUBJECT TERMS
Technology Development and Application 2006–2007 Annual Report

16. SECURITY CLASSIFICATION OF:			17. LIMITATION OF ABSTRACT UU	18. NUMBER OF PAGES 148	19a. NAME OF RESPONSIBLE PERSON Dr. Dave Bartine
a. REPORT U	b. ABSTRACT U	c. THIS PAGE U			19b. TELEPHONE NUMBER (Include area code) (321) 867-7069

